Nanobiocatalytic Conversion of Agri-Food Waste into Biochemical Products

A thesis

submitted in partial fulfillment of the requirements for the award of degree of

DOCTOR OF PHILOSOPHY

IN

BIOTECHNOLOGY

THAPAR INSTITUTE
OF ENGINEERING & TECHNOLOGY
(Deemed to be University)

Submitted by

Devendra Sillu

(Reg. No. 901600015)

Under the supervision of

Dr. Shekhar Agnihotri

Dr. M.S. Reddy

Department of Biotechnology

THAPAR INSTITUTE OF ENGINEERING AND TECHNOLOGY

(Deemed to be University)

Patiala – 147004, Punjab, India

February 2023

CERTIFICATE

Certified that the thesis entitled "Nanobiocatalytic Conversion of Agri-Food Waste into Biochemical Products" submitted by Mr. Devendra Sillu, Reg. no. 901600015 in the partial fulfilment of the requirements for the award of the degree of Doctor of Philosophy in the Department of Biotechnology, Thapar Institute of Engineering and Technology, Patiala, Punjab is a record of candidate's own independent and original research work carried out by him under our supervision and guidance. The material embodied in this thesis has not been submitted in part or full to any other University or Institute for the award of any degree.

Dr. Shekhar Agnihotri
Assistant Professor
Department of Agriculture and
Environmental Sciences,
National Institute of Food Technology
Entrepreneurship and Management-Kundli,
(NIFTEM-K),
Sonepat-131028, Haryana, India

Dr. M.S. Reddy
Professor
Department of Biotechnology,
Thapar Institute of Engineering and
Technology (Deemed to be University),
Patiala-147004, Punjab, India

DECLARATION

I, hereby declare that the work presented in the thesis entitled "Nanobiocatalytic Conversion of Agri-Food Waste into Biochemical Products" in the partial fulfilment of the requirement for the award of the degree of Doctor of Philosophy in the Department of Biotechnology, Thapar Institute of Engineering and Technology (TIET), Patiala, Punjab is an authentic record of my work carried out under the supervision and guidance of Dr. Shekhar Agnihotri, Assistant Professor, Department of Agriculture and Environmental Sciences, NIFTEM, Sonepat, Haryana and Dr. M.S. Reddy, Professor, Department of Biotechnology, Thapar Institute of Engineering and Technology, Patiala, Punjab. This report has not been submitted for the award of any degree or certificate in any other university in India or abroad.

Place: Patiala
Date: 15/09/2022

Devendra Sillu
(Reg. No. 901600015)

ACKNOWLEDGEMENTS

"*No one who achieves success does so without acknowledging the help of others. The wise and confident acknowledge this help with gratitude*."

-Alfred North Whitehead

It feels surreal that I am at the end of my journey as a PhD scholar. The memorable voyage that lasted a little more than half a decade has been a roller coaster ride with lots of ups and downs. Compilation of this thesis would have been unimaginable without the immense help and support of many individuals. I have been fortunate enough to receive great inspiration, guidance, direction, cooperation, love and care, be it in scientific, emotional or any other means, paramount to complete this academic endeavour. Even though it seems almost impossible to acknowledge everyone involved in the process. However, this is a small effort from my end to remember and appreciate all the people who have supported me unconditionally throughout this long but fulfilling journey.

First and foremost, I take this cherished opportunity to express heartfelt gratitude to the person who undoubtedly made the biggest difference in my life, my respected supervisor ***Dr. Shekhar Agnihotri***, Assistant Professor, Department of Agriculture and Environmental Sciences, National Institute of Food Technology Entrepreneurship and Management (NIFTEM), Sonepat. Dr. Agnihotri's consistent guidance, precious advices, timely suggestions and immense patience throughout the period were vital for the successful completion of my work and PhD. His unique way of looking at the problems from various angles, encouraging me to take up new challenges and tackle them with determination and an optimistic attitude has imprinted an ever-lasting impact on my life. It was his support which made me thrive for excellence and nothing less; I shall carry this with me and try to the best of my limits to transmit it to the forthcoming research generation. He constantly motivated me to learn academic and administrative works in parallel with research works, flourishing me to the level I currently stand. I am also grateful to him for the freedom that he granted me in my research work, inculcating great self-confidence in me. I will always be seeking his blessings and valuable guidance throughout life.

I am beyond privileged to have received the co-supervision from ***Prof. M.S. Reddy***, Head, Department of Biotechnology, Thapar Institute of Engineering and Technology, Patiala. His critically pointed suggestions, thought provoking discussions, moral encouragement helped me overcome ups and downs and smoothly sail through this journey. I will forever be in debt

of him for showing faith in me; his association with this endeavour will remain a beacon light to me forever.

I express my sincere gratitude to visionary director of TIET, ***Prof. Prakash Gopalan***, for providing necessary infrastructure and excellent research environment. I extend my genuine word of thanks to ***Prof. Anil Kumar***, Co-ordinator, TIFAC-CORE, TIET, Patiala, for providing necessary equipment facilities to carry out this work and his encouragement and support during my research work in the Institute.

I am also thankful to the whole faculty of Department of Biotechnology for the constant encouragement, support, intellectual and material help that I have received from each one of them. My special word of thanks to members of my doctoral committee, ***Prof. Niranjan Das***, ***Prof. Dinesh Goyal***, BTD, TIET and ***Prof. Haripada Bhunia***, Department of Chemical Engineering, TIET for their valuable suggestions, constant support and encouragement during the course of my study.

This research was only possible due to the financial support of **Department of Science and Technology-Science and Engineering Research Board (DST-SERB), Government of India**, New Delhi provided as sponsored project **YSS/2015/001599**. I am grateful to the **Council of Scientific & Industrial Research (CSIR), New Delhi** for **Direct-Senior Research Fellow fellowship (09/677(0045)/2020-EMR-I)** during the hard hitting Covid-19 pandemic. I also appreciate the financial help received from **TIET, Patiala** in means of **Teaching Assistantship**.

The help and cooperation offered by the Department of Biotechnology and TIFAC CORE is gratefully acknowledged. I am grateful to ***Mrs. Manjula Kamra*** for her motivating words, timely help and moral support. I owe my sincere thanks to ***Mr. Avinash Kumar*** for his consistent support, encouragement and suggestions. Most of the work would have been incomplete without the sincere support of Lab assistants. I am thankful to ***Mr. Ram Newal (Babban ji)***, ***Mr. Surinder Pal, Mr. Prabhat***, ***Mr. Lallan***, ***Mr. Mohinder*** and ***Mr. Phoolchand*** for their invaluable assistance during the lab work. I am also thankful to ***Mr. Vijay Verma*** for his help and suggestion in financial matters which enabled smooth running of the sponsored research project.

I shall be failing in my duty if I do not acknowledge the corporation of my lab mates ***Ms. Navneet Kaur Dhiman*** and ***Ms. Anjali Chauhan***. All three of us joined the "SA nano-bio

lab" in the span of 6 months, we have been the longest companion in PhD and this companionship developed into a very good friendship. The experience acquired by Navneet during her master's dissertation with Dr. Agnihotri greatly helped me to understand overall dynamics of the lab during my initial time. Anjali has always been the helping hand in every matter I have come across. The professional as well as personal discussions regarding all aspects of life with the lab mates have certainly transformed me into a better person. I will forever cherish the bond we share.

Words fail me to express my appreciation for my loving friends ***Dr. Vagish Dwibedi***, ***Dr. Piyush Sharma***, ***Dr. Davinder Singh***, and ***Dr. Aadil Bathla*** for their constant support and motivation. I thank you all for being with me through thick and thin and I wish you best of luck, in all that life has to offer. Hostel friends are the individuals that let you be you, without any judgment or prejudice. I have been bestowed upon with best of them, ***Dr. Santosh Rath, Dr. Iqubal Singh***, ***Dr. Sukhveer Singh***, ***Dr. Nandan Sarkar***, ***Mr. Kaushlendra Pandey***, ***Mr. Arun Rana***, ***Mr. Kamal Anand***, and ***Mr. Amit Pandey***. I thank all of them for all fun filled and wonderful memories.

Ms. Prerna, ***Dr. Charu Behl***, ***Dr. Neha Kapoor***, ***Dr Saloni Sharma***, ***Dr. Ishtpreet***, and ***Ms. Simarpreet*** were very helpful seniors and made me feel at home when I joined the department. It is difficult to find words to thank ***Mr. Nirmalya Halder***, ***Mr. Ashok Rana*** and ***Mr. Atul Choudhary*** for their help in most critical situations. I am also thankful to all the (in past as well as in present) masters dissertation students ***Ms. Tamanna Mahajan***, ***Ms. Darshdeep Kaur***, ***Ms. Garima Sharma***, ***Mr. Yeshaswi Kaushik*** and ***Ms. Gaganjot Kaur*** for providing me a very conducive environment in the lab. These young researchers always kept me on my toes to match their energy and enthusiasm.

I am grateful to **SAI Lab, TIET**, **SAIF Punjab University**, and **CIL, NIFTEM** for the instrument facilities used during this work. I acknowledge the help of ***Dr. Balaram Sahoo*** and ***Dr. Rajeev Kumar***, Indian Institute of Science, Bangalore, India for HR-TEM analysis. I gratefully acknowledge the co-operation of ***Dr. Priyankar Dey***, DBT, TIET and ***Mr. Ankur Kumar***, CIL, NIFTEM for helping me understand the basics of HPLC. I am immensely thankful to ***Mr. Pardeep Bhatia*** and ***Mr. Ghanshyam Mourya***, SAI lab-TIET for providing timely assistance in SEM and XRD analyses. I am also grateful to ***Dr. Shagun Kainth*** for helping me with FTIR analysis.

I would like to place on record, a special mention of a wonderful person ***Ms. Gurleen Kaur Sodhi*** for placing her immense faith in me, even when I had the most doubts about my capabilities as a research scholar. She made her support available in infinite number of ways every time and anytime. The critical discussions with her certainly led to betterment in my approach towards science and more importantly towards life. I could not have asked for more than what I got from you as a partner and friend.

I find it hard to pen-down my deepest sense of indebtedness towards my parents ***Mr. Ranjeet Sillu*** and ***Mrs. Shakuntala Devi*** for their selfless support, encouragement, love, affection and immense patience throughout life including this period. Both of them were an unfathomable source of inspiration and support which held me strong even during the worst period, for what I cannot measure but treasure. To them, I owe my wonderful today and dream filled future. I would also like to extend my deep gratitude to my brother ***Mr. Kulwant Sillu*** and sister-in-law ***Mrs. Kavita Rani*** for always standing behind me, believing in me and pouring all their love and blessings. It is their efforts and perseverance that has resulted in the completion of my PhD. I will forever be in debt for all the sacrifices they have made and I hope to make them the proudest mini parents. My beautiful niece ***Ms. Harman Sillu*** and handsome nephew ***Mr. Tarun Sillu*** were the key source of happiness during my PhD. Their unconditional love has made this journey way smoother than it could have been.

Last but not the least, please accept my sincerest apology if I unintentionally missed any name. I wish to thank all the individuals who directly or indirectly helped me during my PhD work and thesis compilation.

Devendra Sillu

List of Publications

Publications

1. **Devendra Sillu**, M. Sudhakara Reddy and Shekhar Agnihotri* (2022). Magnetic Halloysite Nanotubes/α-amylase based Nanobiocatalytic Transformation of Food Processing Waste into an Active Fermentation Ingredient. ACS Sustainable Chemistry & Engineering. **(I.F. 9.22)**
2. **Devendra Sillu** and Shekhar Agnihotri* (2020). Cellulase immobilization onto magnetic halloysite nanotubes: enhanced enzyme activity and stability with high cellulose saccharification. ACS Sustainable Chemistry & Engineering, 8(2), 900-913. **(I.F. 9.22)**

Other Publications

1. Davinder Singh, **Devendra Sillu**, Anil Kumar and Shekhar Agnihotri* (2021). Dual nanozyme characteristics of iron oxide nanoparticles alleviate salinity stress and promote the growth of an agroforestry tree, *Eucalyptus tereticornis* Sm. Environmental Science: Nano, 8(5), 1308-1325. **(I.F. 9.47)**
2. Anjali Chauhan, **Devendra Sillu** and Shekhar Agnihotri* (2019). Removal of pharmaceutical contaminants in wastewater using nanomaterials: a comprehensive review. Current Drug Metabolism, 20(6), 483-505. **(I.F. 3.40)**
3. Shekhar Agnihotri*, **Devendra Sillu**, Garima Sharma and Raj Kumar Arya (2018). Photocatalytic and antibacterial potential of silver nanoparticles derived from pineapple waste: process optimization and modeling kinetics for dye removal. Applied Nanoscience, 8(8), 2077-2092. **(I.F. 3.87)**

Book chapters

1. **Devendra Sillu**, Charu Agnihotri, Shekhar Agnihotri (2022). Advances in industrial biocatalysis through immobilized extremozymes. In *Extremozymes and their Industrial Applications* Ch 14, pp. 375-404. Academic Press.
2. **Devendra Sillu**, Yeshaswi Kaushik, Shekhar Agnihotri (2021). Immobilization of enzymes onto silica-based nanomaterials for bioprocess applications. In *Immobilization Strategies* Ch 11, pp. 399-434. Springer, Singapore.

List of Papers in conferences (National/International)

1. **Devendra Sillu** and Shekhar Agnihotri (2018). Magnetic Halloysite Nanotubes as Support for Immobilization of α-Amylase with High Biocatalytic activity, Reusability and

Recovery. International Conference on “Drug Discovery: Biotechnology & Pharma at Cross Roads, TIET, Patiala, Punjab (India) (Poster).

2. **Devendra Sillu** and Shekhar Agnihotri (2018). Magnetic Cellulase/Halloysite Nanotubes as Biocatalytic System for Converting Agro-Waste into Value-Added Product. 20th International Research Conference on Biotechnology and Bioengineering, Bangkok (Thailand) (Poster).
3. **Devendra Sillu**, Navneet Kaur and Shekhar Agnihotri (2018). Improvement in nano-biocatalytic conversion of non-edible feedstock into high fructose corn syrup (HFCS) production. International Conference on Food Security: Challenges and Opportunities, TIET, Patiala, Punjab (India) (Poster).
4. **Devendra Sillu** and Shekhar Agnihotri (2018). Immobilization of glucose isomerase over magnetic nanotubes with improved stability and biocatalytic activity. 2nd International Conference on Nanobiotechnology for Agriculture: Detection, Conservation and Responsible Use of Natural Resources, The Energy and Resources Institute (TERI), Gurugram, Haryana (India) (Oral).
5. Davinder Singh, **Devendra Sillu**, Shekhar Agnihotri and Anil Kumar (2020). Impact of Iron oxide nanoparticles on growth and salt stress tolerance in the cultures of *Eucalyptus tereticornis* Sm. National Symposium on Trends in Plant Biotechnology and Agriculture (41st PTCA(I)), TIET, Patiala, Punjab (India) (Oral)

Workshops

1. Two-day workshop on “MATLAB for Beginners” organized by School of Mathematics, Thapar Institute of Engineering and Technology, Patiala, Punjab on 22-23 October, 2021.
2. One-day National workshop on “Intellectual Property Rights and Patenting” sponsored by Punjab Pollution board at Department of Biotechnology, Thapar Institute of Engineering and Technology, Patiala, Punjab on 17 February, 2018.

TABLE OF CONTENTS

LIST OF TABLES

LIST OF FIGURES

LIST OF SYMBOLS

%	Percentage
°	Degree
°C	Degree celsius
µL	Microliter
µg	Microgram
µm	Micrometre
µM	Micromolar
Å	Angstrom
cm^{-1}	Reciprocal centimetres
cm^3/g	Cubic centimetres per gram
E_d	Thermal denaturation
eV	Electron-volt
g	Gram
g/l	Gram per litre
h	Hour
IU	International unit of enzyme
J	Joule
k_d	Thermal deactivation rate constant
kJ	Kilo joule
k_M	Michaelis constant
Km^3	Cubic kilometre
kWh/t	Kilowatt hour per tonne
L	Litre
M	Molar
m^2/g	Square meter per gram
mA	Milli ampere
mg	Milligram
min	Minute
mL	Millilitre
mm	Millimetre
nm	Nanometre
Psi	Pounds per square inch

R^2	Correlation coefficients
rpm	Rotations per minute
S	Concentration of a substrate
$t_{1/2}$	Half-life
U/g	Units per gram
V	Velocity of reaction
v/v	Volume by volume
V_{max}	Maximum rate achieved
w/v	Weight by volume
w/w	Weight by weight
wt%	Weight percentage
ΔG	Gibbs free energy change
ΔH	Enthalpy change
ΔS	Entropy change
θ	Theta
λ	Lambda

LIST OF ABBREVIATIONS

([bmim][Cl]	1-Butyl-3-Methylimidazolium Chloride
ABE	Anaerobic Biological Fermentation
AFW	Agri-Food Waste
AIL	Acid Insoluble Lignin
Al-OH	Aluminol
ANOVA	Analysis of Variance
AOAC	Association of Official Analytical Chemists
APTES	3-Aminopropyl-Triethoxysilane
AS	Alkylsulfonic
ASL	Acid Soluble Lignin
BBD	Box-Behnken Design
Ca^{+2}	Calcium ion
$CaCO_3$	Calcium carbonate
CMC	Carboxymethyl cellulose
CNTs	Carbon nanotubes
CO_2	Carbon dioxide
CrI	Crystallinity Index
Cu^{+2}	Cupric ion
d-MHNTs	Dopamine Functionalized Magnetic halloysite nanotubes
DNA	Deoxyribonucleic acid
DNSA	3,5-Dinitrosalicylic acid
DW	Dry weight
EDS/EDX	Energy-Dispersive X-Ray Spectroscopy
EDTA	Ethylenediaminetetraacetic acid
FAO	Food And Agriculture Organization of The United Nations
Fe^{+2}	Ferrous ion
Fe^{+3}	Ferric ion
FE-SEM	Field Emission Scanning Electron Microscopy
FTIR	Fourier-Transform Infrared Spectroscopy
GAE	Gallic Acid Equivalents
HMF	Hydroxymethylfurfural
HNTs	Halloysite nanotubes
HPLC	High-Performance Liquid Chromatography
HR-TEM	High Resolution Transmission Electron Microscopy
IL	Ionic liquid
IONPs	Iron oxide nanoparticles
K^+	Potassium ion
KH_2PO_4	Monopotassium phosphate
LAPs	Laboratory Analytical Procedures
Mg^{+2}	Magnesium ion
$MgSO_4$	Magnesium sulfate
MHNTs	Magnetic halloysite nanotubes

MHNTs-SH	Mercapto Functionalized Magnetic halloysite nanotubes
MHNTs-SO_3H	Sulfonic acid-Functionalized Magnetic halloysite nanotubes
MPTMS	3-Mercaptopropyl-(Trimethoxy)Silane
Na^+	Sodium ion
NaOH	Sodium hydroxide
NBC	Nanobiocatalyst
NM	Nutrient media
PDB	Potato Dextrose Broth
PEG	Poly Ethylene Glycol
PFS	Perfluoroalkylsulfonic
PPW	Potato peel waste
PPW_{NCB}	Nanobiocatalyst treated potato peel waste
RSM	Response Surface Methodology
SCB	Sugarcane bagasse
SEM	Scanning Electron Microscope
SHF	Separate Hydrolysis and Fermentation
Si-OH	Silanol
Si-O-Si	Siloxane
SO_4^{2-}	Sulfate
SSA	Specific Surface Area
SSF	Simultaneous Saccharification and Fermentation
TCAC	Total carboxylic acid content
TGA	Thermogravimetric Analysis
VSM	Vibrating Sample Magnetometer
XPS	X-Ray Photoelectron Spectroscopy
XRD	X-Ray Powder Diffraction
Zn^{+2}	Zinc ion

ABSTRACT

Agri-food waste reduction is a huge priority for many nations including India to develop a resilient food ecosystem. The unavoidable agri-food waste is becoming a major threat to our efforts to alleviate global hunger along with safeguarding socio-economic and environmental interests. On contrary, such waste exhibits immense potential to be repurposed for industrial bioprocessing that could contribute to circular bioeconomy. It is critical to understand ways how we can utilize non-edible waste in generating value-added products via advanced transformation strategies that lead to a more sustainable and prosperous future. The present work thus demonstrates a viable 'waste-to-feed' strategy for valorizing agri-food waste using 'nanobiocatalyst' with potential benefits. Sugarcane bagasse and potato-peel waste were considered the model representatives of waste from agriculture and food–processing sectors, respectively. The work is broadly classified into three major sections; (i) developing a facile pre-treatment approach for agri-food waste, (ii) fabrication of individual nanobiocatalytic systems involving cellulase and α-amylase enzymes onto halloysite nanotubes (HNTs) as immobilizing template, and (iii) nanobiocatalyst-assisted valorization of agri-food waste to value-added products such as glucose, fructose syrup, and other hydrolysates. These products were employed as medium-alternative for industrial bioprocessing, fermentation and bio-cementation applications.

Developing an eco-friendly and facile pre-treatment process is essential for effective bioprocessing of lignocellulosic biomass. A two-step pretreatment approach was developed in this study, employing a solid acid catalyst, i.e., sulfonic acid functionalized magnetic halloysite nanotubes. Acid-functionalized magnetic halloysite nanotubes (MHNTs) were fabricated via mercaptosilane grafting and subsequent oxidation. The solid acid catalyst treatment followed by dilute alkaline treatment of sugarcane bagasse resulted in a more effective removal of hemicellulose (75.27%) and lignin (60.02%) contents from the biomass. The catalyst was easily recoverable using a magnet and could be reused over five consecutive cycles. The presence of high xylose (18.76 g/L) and low concentrations of inhibitory products in wash liquids indicated the effectiveness of the pretreatment approach employed. Sugarcane bagasse after solid-acid catalyst pre-treatments was more amenable towards enzymatic hydrolysis resulting in 60.32% cellulose saccharification and increased glucose yield/g biomass. A 2.63-fold higher ethanol production was achieved using pre-treated

sugarcane bagasse than its raw form, validating the effectiveness of the pre-treatment approach.

A quest for efficient biotransformation of cellulosic material into sustainable biochemical products for recent biotechnological interventions is currently under way. Herein, the fabrication of nanobiocatalyst (NBC) employing halloysite nanotubes (HNTs) as a template for immobilizing cellulase enzyme was attempted, which catalyzed the hydrolysis of cellulose into glucose. Magnetic character was imported to HNTs by *in situ* anchoring of iron oxide nanoparticles, onto which cellulase was immobilized using aminosilane surface functional chemistry. Characterization studies revealed nanobiocatalyst to be extremely stable during heterogeneous catalysis without compromising their catalytic activity. The optimization of process parameters yielded ~93.5% activity of cellulase with high enzyme loading (111.6 mg/g support) after immobilization. Immobilized cellulase displayed superior stability at elevated temperatures (≥60°C) and storage capability compared with their free forms. The NBC even retained ~68.2% of its original activity after seven consecutive uses with a minimum yield of 25.4 mg glucose/g cellulose and was 100% recoverable using a magnet. Displaying a high ionic-liquid tolerance ability is concurrent with superior catalytic potential against CMC and extracted cellulose (pretreated sugarcane bagasse), and achieving ~50.2% saccharification and 0.56 g glucose/g cellulose within 48 h of continuous operation establishes the commercial viability of using cellulase-immobilized HNTs for efficient cellulose hydrolysis. The glucose stream produced using pretreated sugarcane bagasse was further converted into fructose syrup employing a packed bed reactor with immobilized glucose isomerase. The parameters involved in isomerization reaction were optimized and a high glucose conversion (48.9%) into fructose was achieved. Overall, the nanobiocatalyst-assisted valorization of pretreated sugarcane bagasse for producing a clean glucose stream and fructose syrup was established.

The concept of 'nanobiocatalysis' creates exciting opportunities for improving enzyme performance via immobilization onto nanomaterials. A nanobiocatalyst consisting of magnetic halloysite nanotube (MHNT)/α-amylase was evaluated to transform food processing waste into an active fermentation medium formulation for low-cost bioprocessing. A high loading of α-amylase (185.5 mg (g of support)$^{-1}$) was achieved on the surface of MHNTs through polydopamine functionalization. We validated the establishment of an enzyme-support system retaining >89% catalytic activity (27332 IU (g of support)$^{-1}$) with

improved enzyme handling (>99.1% recovery) and reusability (>56% activity, 10 cycles). MHNTs remarkably improved the enzyme kinetics and thermodynamic characteristics along with operational and storage stabilities and mitigated the likely inhibitory effects of cellulose/metal ions as contaminants. In addition to facilitating a continuous production of reducing sugars from the extracted starch over 72 h, the nanobiocatalyst was equally effective in preparing a nutritive food waste hydrolysate as a fermentable medium substitute for batch culturing of *E. coli* and a single-cell protein (*A. niger*). The commercial relevance of waste hydrolysate was also investigated to promote calcite precipitation via *Bacillus* sp. induced biocementation. We evidenced that nanobiocatalyst-assisted "starch depolymerization" released more nutritional components into the hydrolysate suspension, easily accessible to growing microbial cultures.

Summarizing all, the natural abundance and low cost of support material (halloysite nanotubes), simple functionalization procedures, and excellent immobilization capability of our system warrants huge potential to be adopted for immobilizing other bio macromolecules beyond enzymes. The successful implementation of the current strategy at an industrial scale will also open new dimensions for transforming other agri-food wastes into biochemical products of commercial relevance.

Chapter 1

Introduction

1.1 Scientific Background

"*We cannot solve our problems with the same thinking we used when we created them*."

– Albert Einstein, Physicist

The generation of agri-food waste is inevitable. Be it land, processing activities, logistics/distribution, retail stores, restaurants, and even at home, edible food is discarded at every stage of the supply chain. The United Nations Environment Programme's food waste index report-2021 estimated that about 17% of global food production is wasted every year where a major proportion (45-60%) of food waste occurs at farm (postharvest operations) and industrial (manufacturing, processing) level alone (UNEP 2021). Intergovernmental bodies like Food and Agriculture Organization (FAO), World Food Programme, and World Health Organization are constantly enforcing nations to adopt suitable policies and strategic guidelines/frameworks and implement them in respective states to reduce food waste (FAO 2011). Strict implementation of food waste reduction policy however seems politically impractical to many nations as it may lead to an increase in food pricing, which eventually affects country's economy and to a larger extent, government credentials (Sinha and Tripathi 2021). Fortunately, India has taken a decisive step to reduce food wastage by introducing the compulsory food waste reduction bill-2018 in Rajya Sabha (The Compulsory Food Waste Reduction Bill 2018). The bill ambitiously targets to achieve 50% food waste reduction in supermarkets, food manufacturers, and food redistribution centers by 2030 adopting effective recovery, reuse, and recycling strategies. The growing problem of waste management however, calls for newer interventions to handle it with environmental and socioeconomic benefits (Makov et al. 2020).

The existing technologies for agri-food waste management mostly end up in landfills and incinerators, similar to other solid waste-disposal mechanisms. Converting them either as animal feed via recycling or biofertilizers through composting makes it at least more sustainable. However, the exploration of agri-food waste (AFW) for the generation of biochemical products has captured scientific attention in recent times (Kawaguchi et al. 2016; Patel et al. 2016; Carmona-Cabello et al. 2018; Bolaji et al. 2021; Sharma et al. 2021; Lee et al. 2022). The key factors driving this shift are increasing demand for renewable resources and the issues related to agri-food waste management (Carmona-Cabello et al. 2018). On other hand, utilizing edible feedstock in industrial sectors unreasonably escalates our burden and competition to fulfill food demand of the ever-growing population. Hence, it is desirable

to lessen our reliance on edible feedstock for industrial bioprocessing and emphasize its substitution with non-edible portion of agri-food waste. This is certainly a revolutionary step for a country like India to become self-sufficient to the extent possible, which is economically prudent, as well as socioeconomically sensible (Usmani et al. 2021; Klein et al. 2022).

On a global scale, a lack in technological breakthroughs has made policymakers completely ignorant of the inherent richness of agri-food waste to produce value-added products. For example, the sugarcane processing plants in India generate about 100 million tonnes of sugarcane bagasse annually (Konde et al. 2021). While 50% of sugarcane bagasse is inherently utilized as the source of heat and power to run sugar industries, the remaining is either disposed of directly or sent to thermal plants. After extracting soluble sugars, the bagasse still possesses many vital ingredients, which can strategically be valorized to produce various metabolites, biochemicals and enzymes through fermentation processes contributing to a circular economy (Singh et al. 2022). Similarly, potato peel waste, generated during food processing is merely utilized either as animal feed or low-value fertilizer despite having inherent potential to be transformed into valuable bio-products (Soltaninejad et al. 2022). An improper disposal of agri-food wastes marks negative impact on environment since it alone accounts for an estimated 4.4 billion metric tons of carbon dioxide emissions each year (Makanjuola et al. 2020b). Environmental problems like pollution of natural water bodies, toxicity to aquatic life, inferior soil quality and phytotoxicity are other major concerns. In contrast, the abundant agri-food waste can be harnessed as a low cost and ideal substrate for producing value-added products (Osorio et al. 2021). Developing effective valorization strategies may provide enormous opportunities for grossing additional revenues, while ensuring regional food security (Bhat 2017; Ben-Othman et al. 2020b; Panzella et al. 2020; Habashy et al. 2021). In this regard, advanced bio-based processing of waste biomass has emerged as a greener, more viable, and sustainable approach to manage and effectively valorize agri-food waste (Medina-Morales et al. 2021; Kumar et al. 2022).

Recent studies cite some exciting opportunities in utilizing agri-food waste to manufacture fortified foods, active pharmaceutical ingredients, and biodegradable packaging due to its diverse biochemical composition (Arshadi et al. 2016; Sun et al. 2018; Ben-Othman et al. 2020b; Torres-Valenzuela et al. 2020; Osorio et al. 2021; Saadoun et al. 2021). A few studies also witnessed the importance of polysaccharides content available in sugarcane bagasse and

potato peel waste, which must be utilized as an energy source for industrial fermentation and bioprocessing (Papaioannou et al. 2022). Without exception, transforming polysaccharides like, cellulose, hemicellulose, and starch into monosaccharides is a crucial step for valorizing such agri-food wastes (Kumar et al. 2021a). The inherent, recalcitrant nature of lignocellulosic biomass however limits its widespread utilization (Fitzgerald 2017; Niju and Swathika 2019; Dey et al. 2021a; Talan et al. 2021; Agarwal et al. 2022). The presence of lignin covering polysaccharide components, lignin carbohydrate complexes, and high cellulose crystallinity confer such recalcitrant properties in sugarcane bagasse. An alteration in structure assembly of the biomass is an essential step to make them bioprocessing-friendly (Arshadi et al. 2016). Selecting an appropriate pretreatment approach that could effectively solubilize hemicellulose components, minimizes lignin content and exposes the cellulose component is desired (Campo et al. 2006; Peguero et al. 2021). Additionally, pretreatments strategies offers a higher surface area and porosity to the biomass promoting enzyme-led digestion of its cellulose components (Torgbo et al. 2021).

A variety of pretreatments for lignocellulosic biomass have been explored in past (Zabed et al. 2019; Mankar et al. 2021). The conventional pretreatment involving physical and chemical approaches are energy-intensive and often discharge hazardous chemicals in environmental bodies (Tu and Hallett 2019). Furthermore, the formation of byproducts during pretreatment demands an additional purification step, increasing the overall cost (Mankar et al. 2021). On the other hand, biological approaches require longer time period (Sharma et al. 2019a). Furthermore, the recovery of catalyst (chemical or biological) used in these pretreatment processes is considerably hard. The economic and environmental concerns regarding prerequisite treatment steps before biomass bioprocessing undermine the commercial utilization of agri-food waste. The scientific community is consistently seeking reusable, eco-friendly, and proficient pretreatment approaches. One such pretreatment strategy using solid acid catalysts has demonstrated promising results (Tian et al. 2021; Xiong et al. 2021; Zhou et al. 2021).

Solid acid catalysts are considered as green alternatives to liquid acid catalysts in variety of applications (Liu et al. 2018b; Zeng and Pan 2022). Solid acid catalysts have been reported for high selectivity and admirable hemicellulose removal capability with minimal formation of inhibitory product(s) (Qi et al. 2019; Wang et al. 2022a). Solid acid catalysts though come with limitations viz. complex synthetic procedures, poor acid activity, and operational

stability. Some limitations can be minimized by selecting an appropriate support material with high surface area, amenable to undergo acid functionalization and subsequent superior catalytic (acidic) activity. Silica and carbon-based, solid acid catalysts have been studied extensively owing to their high catalytic activity (Gawande et al. 2014; Konwar et al. 2019; Liu et al. 2020). However, the separation capabilities of these solid acid catalysts are still lacking, a critical drawback for their practical application. The introduction of a segregative component such as magnetic nanoparticles could result in superior reusability of the solid acid catalyst. Considering the added advantages scientists have developed magnetic solid acid catalysts (Gardy et al. 2018; Chen et al. 2019; Wang et al. 2019b; Munyentwali et al. 2022).Further assessment of novel magnetic solid acid catalysts could provide cost-efficient substitution for concurrent lignocellulosic pretreatment approaches.

After pretreatment, the hydrolysis of polysaccharide components is an essential step for generating biochemical products. Enzyme-led hydrolysis of biomass into monomeric fermentable sugars has been widely accepted as a viable and eco-friendly approach (Sheldon and Woodley 2018; Intasian et al. 2021). The types of enzyme used in hydrolysis process depend on the composition of the agri-food waste used. For instance, cellulose is a major chemical component of lignocellulosic biomass, which provides structural stability and protection from external factors. It is the most abundant biopolymer on earth, composed of the linear chains of β (1–4) linked glucose monomers. This non-edible biopolymer is widely used in veterinary foods, paper making, construction, and textile industries. Owing to its easy availability at low prices and non-edible nature, cellulose can be established as a preferred substrate in bioprocessing industry to produce biochemical products instead of edible feedstock. The high cellulose content present in lignocellulosic waste biomass has immense potential for producing fermentable sugars through enzymatic hydrolysis. The hydrolytic enzyme, cellulase plays an important role to convert insoluble cellulose into soluble fermentable sugar, i.e., glucose. Cellulase includes three enzymes endoglucanase, cellobiohydrolase, and β-glucosidase, which synergistically operate to degrade cellulose (Payne et al. 2015). The sugars stream produced via cellulase-driven catalysis can be subsequently used into range of biochemical products using enzymatic or fermentation approaches.

Starch is another natural biopolymer, composed of glucose monomer units interlinked via alpha-glycosidic bonds. It is a common substrate while producing many biochemical products

especially biofuels (Marques et al. 2018). Being easily digestible than cellulose, starch rich edible feedstock often competes with food demand. The starch-rich waste and by-products in food processing sector are generated in large quantities and thus can be exploited as cheaply available substrate in industrial fermentation (Dutta et al. 2022). Hydrolysis and subsequent fermentation of starch component is a globally preferred bioprocessing method for starch-rich waste such as, potato peel waste. Alpha-amylase is an endoglucanase enzyme that catalyzes hydrolysis of endo α-(1,4) glycosidic bonds, resulting in the formation of dextrin, maltodextrin, maltose and glucose as the hydrolyzed products (Pinto et al. 2020). The wide scale potential applications of these products into industrial sector such as foods, health, textile, chemical and engineering results in immense growth in starch based bioprocessing sector.

Enzyme-led bioprocessing has numerous benefits as they are bestowed with exceptional substrate/product specificity and capacity undergoing transformation in mild reaction conditions. However, a high production cost, extreme-sensitivity towards harsh processing conditions and reusability are main obstacles that largely impeded the commercial relevance of enzymes. Recent advancements in enzyme immobilization has been quite effective in overcome these limitations (Liu et al. 2018a; Zdarta et al. 2018; Bilal et al. 2019). The heterogeneous nature of immobilized enzymes allows their easy recovery from the reaction mixture, continuous-flow processing and adaptability to existing bioreactor designs that could be readily implemented in industrial processes (DiCosimo et al. 2013). Concomitantly, use of nanoscale support matrices for immobilizing enzymes has provided new impetus to the field of biocatalysis (Aditya et al. 2018; Roy et al. 2021; Guisan et al. 2022). Nanomaterials adorned with high surface area/volume and minimal mass transfer limitations impart enough robustness to immobilized enzymes and exhibit enhanced stability and activity than their colloidal form (Mohammadi et al. 2022; Sriwong and Matsuda 2022). Such enzyme-nanostructure system is termed as 'nanobiocatalyst' (NBC). The nanobiocatalysts have numerous advantages over classical biocatalysts especially in bioprocessing sector, such as higher catalytic efficiency over other traditional materials, greater surface reaction activity, strong adsorption ability, and thermal stability (Rai et al. 2019; Najeeb et al. 2021; Razzaghi et al. 2021; Reshmy et al. 2021).

Several nanostructures such as silica, carbon nanotubes, graphene, iron oxide, zinc-oxide nanoparticles, and mesoporous materials have been used as matrices for enzyme

immobilization (Bilal et al. 2020; Gkantzou et al. 2021). Despite huge success in developing a nanobiocatalyst, the quest for generating an economically benign and easily modifiable support material is still underway. The cost of nanomaterial synthesis, complex functionalization procedure, and providing a compatible environment for enzyme-substrate interaction remain the key challenges to establish a compatible design for industrial relevance. In recent years, naturally occurring clay materials have emerged as a substitute to conventional nanomaterials for enzyme immobilization owing to their natural abundance, low cost, diverse functional sites and an extremely large specific-surface area (Almeida et al. 2022). Halloysite nanotubes (HNTs) is one such material with distinctive features (Yuan et al. 2015). The high surface area of halloysite nanotubes allows high enzyme loading while its curved surface eliminates the likely possibilities of steric hindrance which could affect its catalytic activity. The unique site-dependent surface chemistry of HNT enables easy functionalization based on the intended application (Massaro et al. 2020). A high biocompatibility and low cytotoxicity of HNTs also make it amenable for biotechnological applications, specifically while immobilizing macromolecules, including proteins and enzymes (Tully et al. 2016). The separation feature on HNTs can be easily induced by loading magnetic nanoparticles on its surface. The exploration of functionalized magnetic halloysite nanotube for enzyme immobilization in recent past has resulted in development of competent nanobiocatalysts for various applications with excellent stability and catalytic activity (Kadam et al. 2018; Katana et al. 2019; Kadam et al. 2020b; Zhu et al. 2021; Kim et al. 2022b). The inherent characteristics of magnetic halloysite nanotubes are equally employable to develop a solid acid catalyst. Though a few recent studies reported the acidic functionalization of HNTs (Silva et al. 2018; Mahajan and Gupta 2020; Kumar et al. 2021b; Gupta et al. 2022b; Xiang et al. 2022), its relevance for valorizing agri-food waste has not been attempted. The development of HNTs-based solid acid catalyst for biomass pretreatments would pave paths for establishing a more economical, reusable and eco-friendly catalysts for feasible bioprocessing.

1.2 Scope of Work and Objectives

Based on above discussion, it is imperative that an increased demand for bio-chemical products and depleting non-renewable resources calls a shift of our reliance from edible feedstock to non-edible feedstock. The environmental issues related to improper disposal of agri-food waste would further escalate the efforts made in this field. The study thus aimed to

establish nanobiocatalytic system as a tool for effectively transforming agri-food waste into biochemical products having greater utility and economic relevance. As a prerequisite, the solid-acid catalysis was employed during pretreatments of lignocellulosic biomass. Two independent nanobiocatalysts, comprising cellulase and α-amylase were immobilized onto magnetic halloysite nanotubes and subsequently used for converting the non-edible, agro-food waste (i.e., sugarcane bagasse and potato peel waste) into value-added biochemical products. The fundamental questions that were critically addressed in the current research work are;

Research Question-1: *Is it possible to convert a non-edible agri-food material into edible bioproducts for human consumption?*

Research Question-2: *Does transforming agri-food wastes into value-added biochemicals products via nano-biocatalysis is a feasible strategy that could be implemented at industrial scale.* Despite several odds and numerous advantages, it is equally important to witness as how these transformations can be tested at lab scale studies, which would broad our horizon to implement into pilot scale production.

Research Question-3: *Can we develop a more eco-friendly yet economical strategy for biomass treatments?*

Research Question-4: *Does immobilizing cellulase and α-amylase onto halloysite nanotubes will be effective in preserving or enhancing their catalytic activities as compared to their free counterparts?*

The questions mentioned above, coupled with extensive survey of the literature available followed by logical extrapolation may lead to the following objectives;

1. Development of a facile pretreatment method for efficient conversion of agri-food waste into hydrolysates.

2. Synthesis and characterization of halloysite nanotubes-based nanomaterials for immobilization of enzymes.

3. Evaluation of the kinetic parameters and optimization of process conditions for value-added products.

1.3 Organization of the Thesis

The doctoral research work in the current thesis is systematically organized in five chapters.

Chapter-1 addresses the scientific background and key challenges associated with agri-food waste management, industry-adaptable strategies and their implications on sustainability and the environment. A comprehensive discussion on emerging need of agri-food waste utilization and their possible transformation into bio-based products via enzyme-led bioprocessing, associated limitations and potential solutions are also presented. Nanotechnological interventions to further argument the process effectiveness at various stages in bioprocessing are elaborated.

Chapter-2 describes the current state-of-art literature review, starting with socio-environmental impact of agri-food wastes and generation of value-added products via bioprocessing. The conventional and concurrent pretreatment methodologies employed in industries are summarized in brief. The shortcomings of the process-flow employed, contemporary utilization of 'immobilized enzyme' and the limitations faced are evaluated through the lens of time. Recent advancements made in the concerned domains are mentioned. Latest nanotechnological progresses facilitating the process with eco-friendly attributes are also elaborated. The importance of naturally occurring halloysite nanotubes in currently investigated fields i.e., development of solid acid catalyst and the nanobiocatalysts are summarized by collating research studies in last five years.

Chapter-3 describes all materials and methods employed for synthesis and optimization of magnetic halloysite nanotubes, fabrication of solid acid catalyst, optimization of sugarcane bagasse pretreatment, production of biochemical product viz. bioethanol. The surface-functionalization protocols adopted for making magnetic halloysite nanotubes, the optimization process of enzyme immobilization, evaluation of catalytic process parameters of synthesized nanobiocatalyst(s) and their industrial applications are presented in detail.

Chapter-4 entails the results obtained using the methods described in Chapter-3, their scientific explanations, plausible mechanisms, and their futuristic implications.

Chapter-5 describes the key outcomes and important conclusions drawn from the current research work along with concurrent challenges and recommendations for future research. Finally, a bibliography is included at the end of thesis.

Chapter 2

Review of Literature

Modern life we relish revolves around thousands of products varying from baby feed to fuel used in rockets for space exploration. The primary step towards creation of these products involves the conversion of available “raw materials” into chemical blocks. These chemicals are then utilised as precursors by industrial sector such as pharmaceutical, personal care industry, food industry, and agrochemical industry etc. to generate commercial products for consumer’s use. The widely employed strategy for primary conversion step is chemical processing. Fossil fuels (coal, natural gas, and petroleum) are used as raw materials in the chemical processing and transformation is carried out using chemical catalysts or procedures. The critical drawback associated with chemical processing includes harsh conditions requirement, by-product formations etc. The chemical processing of non-renewable fossil fuels is one of the key sources of environmental pollution. On the other hand, bioprocessing approach utilises renewable biomass as raw material and biological catalysts (microorganisms, animal cells, plants cells or enzymes) are employed for their transformation into chemical products. Bioprocesses offer numerous advantages over chemical processing such as mild reaction conditions, specificity for products and substrates, efficient conversion, and by-products produced can be further used in other applications. The rapid depletion of fossil fuels and increasing green processing demand are driving forces behind shift from chemical processing to bioprocessing in industrial sectors. This shift leads to deviation from corrosive chemical substances and reduced greenhouse gas emission during industrial processing.

Although the bioprocessing sector is reasonably small as compared to the chemical processing sector, but the industrial engagement of this benign and greener approach is expanding swiftly. Considering the current trends, the global market size of bioprocessing technology is forecasted to be worth 46 billion USD by 2028. Edible feedstock has been widely used as precursors for bioprocessing sector; however, this competes with feed and food stocks. Continuously increasing human population and respective food demand calls for sustainable and renewable substitute of edible feedstock. To eliminate the negative environmental impacts of non-renewable resources and to attain food security, scientific community is continuously exploring other renewable resources as precursors for bioprocessing. The emerging circular bio-economy concept focuses on the efficient utilization and recycling of waste materials with renewable potential. Non-edible waste materials are explored as precursors for production of different biochemical products.

2.1 Agri-Food Waste (AFW)

The global population has quadrupled over the course of the 20th century and according to the recent trends, is expected to cross nine-billion mark by 2050 (FAO 2009). The apparent food demand has resulted in intensification of agricultural activities and food processing industries. The agri-food waste (AFW), produced throughout the food chain cycle during harvest, processing, and post-consumption has also increased reasonably (Figure 2.1). The worldwide waste generated from agricultural practices alone is estimated to be 140 Gt per year (Dtie 2009). Whereas, around 1.3-1.6 billion tons of food product is wasted annually during production chain or in the distribution and consumption sector (Esteban and Ladero 2018). The magnitude of the total waste generated can be visualised by the mere fact that this waste accounts for more than one-quarter of the global agricultural production (Amicarelli and Bux 2020). The dedicated utilization techniques for these wastes are limited, where some portions of the crop residues are used as organic substrate to improve soli quality and for mulching. Generation of heat by combustion is yet another common utilization along with consumption as cattle feed, however a large chunk is incinerated or disposed directly in landfills.

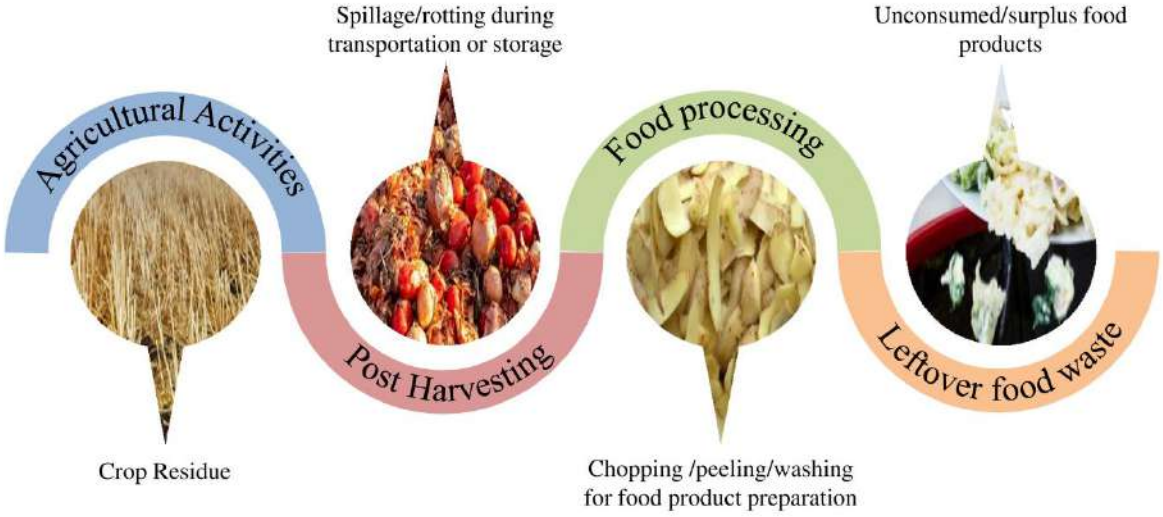

Figure 2.1 Agri-food wastes generated throughout the farm to fork cycle.

The current waste management practices of agri-food waste have considerable economic and environmental implications: air pollution, waste of valuable resources (land, water etc.), soil contamination and greenhouse gas emissions (Bhatia et al. 2018). For instance, dumping in landfills acquire approximately 1.4 billion hectares of land along with surface and groundwater resources equivalent to 250 km^3 (Amicarelli et al. 2021). Direct dumping into

landfills also results in release of about 4.4 billion metric tons of carbon dioxide each year (Makanjuola et al. 2020a), which is almost 6% of the global CO_2 emissions (Amicarelli et al. 2021). The highly biodegradable nature of the content present makes AFW an easily accessible substrate for microorganism growth, resulting in proliferation of pathogenic bacteria and fungi (Ng et al. 2020). The AFW in native form has low economic value, with incurred disposal costs and environmental issues (Kassim et al. 2022). Development of sustainable waste management strategies for agri-food waste is a major challenge faced by humanity in current time.

Agri-food wastes contain a wide range of macro and micro nutrients such as carbohydrates, proteins, polyphenolic compounds, etc. (Matei et al. 2021). The most common class of organic content present in agri-food waste are carbohydrates (Polysaccharides-cellulose, hemicellulose, starch, pectins and their oligo-saccharides, monosaccharides etc.). The amount of carbohydrates although fluctuates considerably with geographical location, a table demonstrating the approximate carbohydrate content is compiled based on recently published articles (Table 2.1).

Table 2.1 Compositions of common agri-food wastes.

Agri-food waste	Carbohydrate	Lignin	Protein	Ash	Reference (s)
Wheat straw	69.7	10.8	3.4	6.5	Froese and Sparling (2021)
Rice straw	53.9	10.34	3.31	16.15	Ambatkar et al. (2021)
Barley straw	81.4	6.7	4.4	-	Feng et al. (2019)
Rye straw	78.4	14.2	7.1	-	Molaverdi et al. (2019)
Oat straw	65.1	-	4.3	-	Sethy et al. (2015)
Flax straw	64	15	6	-	Zykova et al. (2021)
Corn stover	58.9	18.5	-	5	Zhao et al. (2018)
Cotton stalk	68	30	-	6.68	Gupta et al. (2020)
Sunflower Stalk	46.33	18.34	-	2.36	de Souza et al. (2020)
Wheat husk	54	16	6	6	Hýsek et al. (2018)
Rice husk	53.6	22.34	-	13.87	Kumar et al. (2010)
Cocoa pod husk	38.9	28	10	8.4	Lu et al. (2018)
Coffee husk	53.6	23.2	-	1.4	Collazo-Bigliardi et al. (2018)
Sugarcane bagasse	74.6	23.85	-	2.46	Ávila et al. (2018)
Orange peel	80.06	1.2	6.6	3.3	Kute et al. (2020); Tsouko

					et al. (2020)
Banana peel	60.2	2.9	8.1	9.8	Karthikeyan and Sivakumar (2010); Tibolla et al. (2018)
Cassava peel	66.6	12.30	5.50	4.5	Papathoti et al. (2021); Acheampong et al. (2022)
Pineapple peel	52.33	17.8	3.70	4.87	Zakaria et al. (2021); Dahunsi et al. (2022)
Potato peel	56.21	-	14.64	6.42	Sillu et al. (2022)
Onion skin	51.6	-	5.3	-	Piechowiak et al. (2020)
Soybean hulls	47.1	13.1	9.4	-	Bittencourt et al. (2021)

2.2 Value-added Products from Agri-Food Waste

The biodegradable organic composition of AFW along with abundance offers a possibility of utilizing them as cheap, sustainable and renewable resources for bioconversion into different value-added products. Developing novel strategies for production of value added biochemicals from agri-food waste would offer advantages such as sustainable waste management, generation of additional economic value and most importantly lower dependence on edible feedstock thus guarantying food security (McNutt and He 2019). The circular bio-economy relies on utilization of these AFW as feedstock in bio-refinery which can lead to the production of a wide range of intermediate bio-chemicals used in food, cosmetics, materials, biopolymers, and biofuels industries. This approach provides an opportunity to convert waste into product with higher economic value while keeping the carbon in its organic form, thus avoiding the emission of CO_2 (Ben-Othman et al. 2020a). The specific aim of this approach is to yield highest possible value product, while generating least processing waste and environmental issues (Bhavya and Hebbar 2019). The most common utilization of AFW as an energy source provides the lowest economic value, while adding significant burden on the environment. Highest value can be generated by utilizing AFW for production of biochemical products used in fuel, feed, food, cosmetic and pharmaceutical sectors (Berbel and Posadillo 2018; Yang et al. 2021).

The agri-food biomass can be utilized for production of different value-added biomolecules and platform chemicals. Biomolecules such as phytochemicals (phenolic compounds, flavonoids, carotene etc.) and natural biopolymers (cellulose, chitin, pectin, starch, xylan etc.) can be extracted directly from agri-food waste instead of synthesizing those using petroleum-based chemicals. A wide range of biological methods have been explored till date for

effective extraction of these molecules, including microorganism assisted extraction and enzyme-assisted extraction. Platform chemicals are basically building block chemicals that can be converted into wide range of products or commodities. They are produced through transformation of carbohydrate component present in the agri-food waste. Commonly produced platform chemicals are lactic acid, glycerol, furanics, ethanol, and xylitol. Biotechnological techniques such as anaerobic digestion, fermentation and composting have been studied widely for transformation of agri-food waste into value added biochemical products since they results in maximum utilization of biomass and least amount of waste generation (Kover et al. 2021). The low energy/water requirements and cost are added advantages (Hadj Saadoun et al. 2021). Enzymatic routes have also been explored for the production of these platform chemicals. Enzymatic hydrolysis of agri-food waste results in higher release of biomolecule products including antioxidants, protein hydrolysates, pigments, oligosaccharides, sugars, growth-promoting substrates, etc. (Torres-León et al. 2021). Integrated bio-refinery approach which uses different conversion technologies in combinations is currently being explored globally to produce value added products from agri-food waste. For effective bioprocessing transformation of agri-food waste into value added chemicals, soluble fermentable sugars are obtained by enzymatic hydrolysis, followed by fermentation to produce target chemicals. Following are the few classes of products produced from agri-food waste through bioprocessing techniques:

2.2.1 Bioactive Compounds

The different bioactive compounds (phenolic compounds, flavonoids compounds, tannins etc.) present in agri-food waste can be extracted from biomass using bioprocessing approach (Premjit et al. 2021). Solid-state fermentation, submerged fermentation, and enzyme assisted extraction methods are commonly used to extract bioactive compounds from waste biomass. These products have excellent antioxidant, anti-inflammatory, and antibacterial properties, which can be utilised in food and pharmaceutical industries (Mata et al. 2018; Rivero-Cruz et al. 2020). The current research worldwide focuses to improve the production capability along with making the process more economical for industrial scale (Sodhi et al. 2022). Various agri food waste including apple pomace, grape seeds, mango seeds, citrus peels have been used to obtain a range of bioactive compounds. Gallic acid, ferulic acid, quercetin, gallotannins, ellagic acid, limonene, chlorogenic acid, caffeic acid, neochlorogenic acid,

rutin, quercetin 3-acetyl- glucosideand, and γ-linoleic acid are some of the bioactive compounds produced from the agri-food waste.

2.2.2 Biopolymers

Several bacterial and fungal microorganisms have been explored for production of different biopolymers from agri-food waste as substrate. Cellulose, chitosan, collagen, pullulan, xylan, xanthan gum, are key biopolymers produced (Gautam et al. 2022). These biopolymers are used directly in industries like food and beverage, and biomedical industry, owing to their biocompatible and biodegradable nature (Moradali and Rehm 2020; Jethani and Hebbart 2021; Russo et al. 2021). Furthermore, the polysaccharides biopolymers obtained can be converted into sugars via enzymatic hydrolysis, and subsequently into platform chemicals via fermentation.

2.2.3 Single Cell Protein

The increasing demand of protein rich supplements/food items has been observed throughout the globe, considering the vital role of protein in human diet. The high cost and limited availability of protein sources gravely affects the accessibility of protein rich foods to ever increasing population. The protein availability can be enhanced by using novel techniques/resources for protein production. Single cell protein is a protein rich microbial biomass generated using algae, yeast, fungi or bacterial strains, which can be used as substitute of agricultural protein for animal or human consumption (Dey et al. 2021b). The microbial production of protein has distinctive advantages over conventional methods such as, high protein content, shorter growth cycles, and continuous production ability. The selection of microbial strain is based on their ability to grow on different raw materials (Matassa et al. 2016). The reduction in the cost of final product is a vital aspect for dealing with the problems related to protein scarcity, which can be achieved using agri-food waste as substrate for microorganisms' growth. Agri-food wastes such as corn stover, orange peel, potato peel waste etc. have been used in the past for single cell protein production.

2.2.4 Organic Acids

Organic acids are defined as organic compounds with acidic characteristics. Organic acid contains one or more carboxylic acid groups and can be easily attached to various functional moieties. Organic acids such as lactic, 3-hydroxy propionic, acetic, succinic, citric, butyric,

and oxalic acid have considerable applications in food, pharmaceutical and chemical industries (Panda et al. 2019). These acids either can be used individually as monomer units or in polymeric form compounds. Enzymatic hydrolysis and fermentation of agri-food waste has been explored for the production of these organic acids, which serves two purpose, reduction in the cost and recycling of the waste otherwise resulting in environmental threats (Costa et al. 2020). Agri-food wastes such as potato pomace, tomato pomace, wheat straw, sugarcane bagasse, kimchi cabbage, pineapple waste etc. have been used for organic acid production.

2.2.5 Pigments

The food industry relies heavily on use of additives for enhancing the colour and texture of the final product. The consumption of bio-derived food grade colour pigments is preferred over synthetic dyes, considering the associated impact on human health and environment. (Sen et al. 2019). Various microorganisms have been used for production of a wide range of pigments including carotenoids, prodigiosin, flavins, violacein, anthraquinones etc. The high growth rate of these microorganisms' matches well with the industrial production required. Utilization of agri-food waste can make the production both environmentally benign and cost effective (Panesar et al. 2015). The associated characteristics such as antioxidant activity, of these bio-derived pigments also results in overall improvement in nutritional profile of the food product. The broad colour spectrum exhibited by microbial pigments present them as potential substitute for synthetic dyes used in textile industry for colouring fabrics (Kumar et al. 2015). The medicinal properties of microbial pigments can be utilized in different pharmacological formulations. Microbial pigments demonstrating antioxidant, de-pigmentation and photoprotection potential are also used in cosmetic industry (Tuli et al. 2015). The low cost, sustainable and greener production of these pigments would reduce the overall adverse impact generated by the industries using chemically synthesised additives or dyes.

2.2.6 Biosurfactants

Biosurfactants are yet another class of bioproducts with immense industrial potential attributed to their biodegradable and highly selective nature (Ahamed and Prasad 2021). Bioprocessing approaches utilising agri-food waste have been explored for production of different biosurfactants such as surfactin, lauric acid ester, rhamnolipid, glycoprotein,

lipopeptide, glycolipopeptide, glycolipid, sophorolipid etc. Biosurfactants are used in food industry, medical, cosmetics soaps, cleansing products, petroleum process chain and bioremediation (Verma et al. 2020; Markande et al. 2021).

2.2.7 Enzymes

Enzymes are eco-friendly substitute of different chemical catalysts with high selectivity, high product formation, and can operate at ambient reaction conditions. Considering the features, enzymes are considered critical components for futuristic sustainable development and are currently consumed by various industries like pharmaceuticals, detergents, dairy products, agriculture products, and oil chemistry. The raw material makes up about 30% of the total production cost of enzymes (Ravindran and Jaiswal 2016). The increasing demand of these biocatalysts in coming future is foreseen, hence new and sustainable approaches for enzyme production are being investigated to bring down the overall cost of the enzyme production. The utilisation of agri-food waste as substrate for enzyme production would certainly help in cutting the production cost. Commercially important enzymes such as cellulases, pectinases, laccases, xylanases, proteases, α-galactosidases and lipases have been produced via bioprocessing of agri-food waste.

2.2.8 Biofuels

Considering the current global energy demands and depleting non-renewable resources scientists are exploring alternative renewable resources for production of energy sources. One of the leading research areas for agri-food waste valorization is production of second-generation biofuels. Biofuels can be produced in different states such as solid fuels (firewood, wood chips, and wood pallets), liquid fuels (bioethanol, biodiesel, bio-oil, and butanol) and gaseous fuels (biogas and syngas) (Salehi Jouzani et al. 2020). Bioprocessing route for production of liquid and gaseous fuels is preferred as compared to physicochemical method owing to its eco-friendly nature, high conversion rate, operation at ambient conditions, and energy efficient nature (Paul et al. 2021). Bioethanol is most common biofuel and is produced via fermentation process using microorganism able to transform sugars into ethanol. One of the commonly used fermentation approaches is simultaneous saccharification and fermentation (SSF), where enzymatic hydrolysis of polysaccharide content and fermentation is carried out in a single step to obtain bioethanol. Another approach relies on sequential enzymatic hydrolysis and fermentation steps also known as separate hydrolysis and

fermentation (SHF). Butanol is another promising biofuel with excellent characteristic such as high heat of combustion, and less volatility. Butanol can be mixed with gasolines in higher percentage which can be used to fuel different motor engines without any modification. Anaerobic biological fermentation also known as ABE fermentation (Acetone–butanol–ethanol fermentation) of agri-food waste using *Clostridia* genus is widely employed method for butanol production. ABE fermentation converts sugars into acetone-butanol-ethanol in ratio of 3:6:1, respectively.

Biodiesel is produced via transesterification reaction, where fatty acids react with alcohol and form alkyl esters in presence of a catalyst. Biodiesel can be obtained from agri-food wastes via using oleaginous microorganism, resulting in production of lipids also known as microbial oil (single cell oil) which is then transformed into biofuels. Biogases are produced via biomethanation of organic content under oxygen depleted conditions. Biogases can be produced via anaerobic digestion of agri-food waste, which results in production of a gas mixture consisting methane, carbon-dioxide as major part, and hydrogen sulfide, ammonia, hydrogen and carbon monoxide in trace amounts. Biohydrogen can also be produced from agro-waste by microbial action, which is used as fuel in combustion engines. The biomass remained after the digestion can be used as organic manure in different applications. Hydrogen, bioethanol, and biodiesel have been produced from agri-food waste using different bioprocessing methods (Gong et al. 2021). Some of the value-added products are mentioned in Table 2.2, along with bioprocessing approach, current market value and agri-food waste employed.

Table 2.2 A comprehensive analysis of value-added biochemical products derived from agri-food waste.

Product	Bioprocessing approach	Value (USD/kg)	Agri-food waste used	Industrial use	Reference
Bioactive compounds	Fermentation, Enzyme assisted extraction	23-25	AP, APP, KP, LP, MS, PFP, PP, RB, SCG	Food, Bakery, Pharmaceutical, Cosmetic	Ben-Othman et al. (2020b)
Aroma compounds	Fermentation	-	AP, CB, CH, MP, SCB, TP, WB	Food, Chemical, Pharmaceutical, Cosmetic	Hadj Saadoun et al. (2021)
Soluble sugars	Hydrolysis	0.9-5	BP, CB, PPW, RB, RS, SCB, SCG, WB, WS	Food, Chemical, Fuel	Gutierrez-Macias et al. (2015)
Lactic acid	Enzymatic hydrolysis and fermentation	1.3-1.8	CB, CS, PPW, RB, SCB, SCG, WB,	Food, Textile, Detergent, Paper, Pharmaceutical, Cosmetic	Dedenaro et al. (2016)
Citric acid	Enzymatic hydrolysis and fermentation	1-1.6	AP, BP, CP, GP PP, SCB, WB	Detergent, Electroplating, Leather, Pharmaceutical, Cosmetic	González-García et al. (2019)
Succinic acid	Enzymatic hydrolysis and fermentation	121-176	BP, CB, CH, PPW, SCB, TP, WB	Food and beverages, Pharmaceuticals, Polymers, Paints, Cosmetics	Morone et al. (2019)
Enzymes	Fermentation	20-98	AP, BP, CH, CP, GP, LP, MP, PP, PPW, RB, RS, WB, WS	Food and beverage, Pharmaceutical, Detergent, Dairy, Textile	Arya et al. (2022)
Methane	Anaerobic digestion	0.106/m^3	AP, BP, CB, CH, PPW, RS, SCB, SCG, TP, WS	Heat generation, Electricity, Transportation	Tamburini et al. (2020)
Ethanol	Enzymatic hydrolysis and fermentation	0.38	AP, APP, BP, CB, CH, RB, RS, SCB, SCG, WB, WS,	Petroleum, Chemical, Power generation	Ayodele et al. (2020)

*AP=Apple pomace; APP=Apricot pomace; BP=Banana peels; CB=Cassava bagasse; CH=Coffee husks; CP=Citrus peels; GP=Grape pomace; KP=Kiwifruit pomace; LP=Lime peel; MP=Mango peel; MS=Mango seed, PFP=Passion fruit peel; PP=Pomegranate peels; PPW=Potato peel waste; RB=Rice bran; RS=Rice straw; SCB=Sugarcane bagasse; SCG=Spent coffee grounds; TP=Tomato peel/pomace; WB=Wheat bran; WS=Wheat straw.

One of the key challenges of agri-food waste conversion into value-added biochemical products is their low bioconversion rate. The lignin-carbohydrate complexes are indigestible using most bioprocessing approaches, adversely affecting the affordability and sustainability of bioprocess route. Hence, effective methods to destroy the lignin-carbohydrate complexes thus making the carbohydrate content more accessible for enzymatic hydrolysis are essential for utilizing the agri-waste. Pretreatment has been used as an effective approach for utilising the full potential of lignocellulosic biomass.

2.3 Recalcitrance nature of Lignocellulosic Biomass

The unique physico-chemical features such as hardly accessible carbohydrate component, crystallinity of cellulose, and presence of lignin and hemicellulose impedes the efficient enzymatic hydrolysis of lignocellulosic biomass (Yoshida et al. 2008). The factors affecting the accessibility carbohydrate component for hydrolytic enzyme can be classified in two categories, chemical factors and physical factors.

2.3.1 Chemical Factors

Cellulose, the most abundant polysaccharide in lignocellulosic biomass, is made up of 1,4–β-d-glucopyranose units (Sharma et al. 2019a). Cellulose fibrils are present in form of closely packed linear microfibrils linked by β(1→4) glycosidic bonds in lignocellulosic biomass (Robak and Balcerek 2018). The location of cellulose makes it hard to access directly, as cellulose is embedded inmatrix formed by hemicellulose and lignin. Cellulose content has been directly linked with the hydrolysis yield. Moreover, the characteristic properties of cellulose such as size, crystallinity, degree of and polymerization have prominent impact on the hydrolysis, which is discussed in later part.

Hemicellulose, a heterogeneous group of biopolymer is second major abundant constituent of lignocellulose biomass after cellulose (Chandel et al. 2018). Owing to its amorphous structure and nominal physical strength, hemicellulose can be easily hydrolysed into hexoses and pentose sugars (monosaccharides) by hemicellulases enzymes (Isikgor and Becer 2015). Presence of hemicellulose limits the accessibility of cellulose, removal of hemicellulose has resulted in superior hydrolysis of cellulose content (de Oliveira Santos et al. 2018). Hemicellulose removal results in higher porosity and the accessible surface area available for enzyme interactions with substrate i.e., cellulose (Kruyeniski et al. 2019). The presence of

acetyl groups on the surface of hemicellulose also inhibit the catalytic activity of cellulase by interfering with catalytic domains of enzyme and restraining the formation of enzyme-substrate complexes (Pan et al. 2006; Zhao et al. 2012).

Lignin content has been widely associated with limiting the rate of enzymatic saccharification, as it forms a protective barrier around cellulose (Chang and Holtzapple 2000). Enzyme adsorption on the biomass surface is the initiation step for the of hydrolysis process, lignin covering the digestible parts of the biomass thus become the major factor. Additionally, cellulase adsorption on lignin is also reported to inhibit the catalytic activity of cellulase enzyme (Berlin et al. 2006). During pretreatment process the redistribution or removal of lignin occurs which provide more space for the enzyme to interact with the substrate directly (Raud et al. 2016; Dos Santos et al. 2019). The presence of lignin as well as the topographical features of the biomass has prevailing effect on the saccharification of the cellulosic content (Ju et al. 2013).

The interaction between basic constituents of lignocellulosic biomass i.e., cellulose, hemicellulose and lignin also plays a major role in recalcitrance nature of biomass (Zoghlami and Paës 2019). Polysaccharides cellulose and hemicellulose are attached together by hydrogen bonds, which are comparatively easy to break. On the other hand, hemicellulose and lignin are linked with stronger covalent bonds resulting in lignin-carbohydrate complex (Giummarella et al. 2019). These interactions provide basic strength and protective stealth to the biomass from external attacks. The basic aim of the pretreatment approaches is to diminish the compact biomass structure by breaking these interactions so that cellulose is easily available for enzymatic hydrolysis.

2.3.2 Physical Factors

Overall crystallinity of the lignocellulosic biomass influences the hydrolysis efficiency. Lignocellulosic biomasses with highly crystalline cellulose content are hard to hydrolyze, whereas presence of amorphous cellulose has been linked with higher hydrolysis yields using cellulase enzymes (Hall et al. 2010). Highly crystalline cellulose fibers are interlinked in close proximity by non-covalent bonds, and are almost 3-30 folds less hydrolysed as compared to the amorphous cellulose content (Zhao et al. 2012). However an exact relation has not yet been proven as there are studies, stating that there is less impact of crystallinity as compared to other factors (Meng et al. 2017; Zhang et al. 2018). Degree of polymerization

has been linked with presence of hemicellulose and lignin on cellulose fibres, strength of fibres, accessible surface area, and pore size (Zhang and Lynd 2005). The pretreatment process and hydrolysis both have been observed to result in in decreased degree of polymerization (Thielemans et al. 2022).

The accessible surface area of lignocellulosic biomass also has significant impact on the hydrolysis yield. The accessible surface area is directly related to porosity characteristics of biomass such as specific surface area (SSA) and pore volume (Liu et al. 2015). Reducing the biomass size has been associated with increased pore volume and high accessible surface area, subsequently resulting in higher hydrolysis (Torr et al. 2016). The high accessible surface area facilitates the hydrolytic enzyme and substrate interactions. Specific surface area is commonly used to determine the area available for enzyme interactions (Zhang et al. 2018; Lu et al. 2019). Along with surface area, overall accessible volume also affects the enzymatic hydrolysis of lignocellulosic biomass (Jeoh et al. 2007). Pore size of biomass structure is used to determine the accessible volume, biomass with pore size larger than the cellulase enzyme size are easily hydrolysed (Meng et al. 2013; Peciulyte et al. 2015). Recently, it was observed that interaction of enzyme with substrate is also biomass species dependant, where some biomasses were easily hydrolysed even at comparatively smaller pore size while others were not (Herbaut et al. 2018). On the other hand, studies have also been reported where no direct linkage between pore size and hydrolysis efficiency was found, however lignin and hemicellulose content were major reason behind limited hydrolysis (Vaidya et al. 2016; de Oliveira Santos et al. 2018).

Overall, it is a well-established fact that pretreatment of biomass facilitates higher enzymatic hydrolysis. The pretreatment step aims at altering the structural characteristics of the biomass along with chemical composition so that components (lignin and hemicellulose) limiting the cellulose hydrolysis can be removed and cellulose is easily accessible for the hydrolytic enzyme (cellulase) (Agbor et al. 2011).

2.4 Pretreatment Approaches

Pretreatment of lignocellulosic biomass before subjecting it to bioprocessing has significant influence on valorization effectiveness. The pretreatment process results in removal of rigid chemical content, reduction of biomass size, increase in available surface area, porosity and effective facile interaction of enzyme and substrate. A wide range of methods have been

examined for lignocellulosic biomass pretreatment in the past including, physical, chemical, hybrid physico-chemical, and biological pretreatments. For industrial scale applications the pretreatment method should be simple, effective in eliminating the factors limiting the enzymatic hydrolysis, economical, and must avoid production of inhibitory by-products. The advantages and limitations of major pretreatment methods used are summarized in Table 2.3. The following are the commonly employed pretreatment methods.

2.4.1 Physical Pretreatment

Physical methods are one of the widely employed approaches for biomass pretreatment. Physical pretreatment brings along changes in biomass structural factors such as size, crystallinity, surface area and porosity via mechanical, thermal or electromagnetic routes. Different physical pretreatment methods include extrusion, ultrasound, irradiation, milling and grinding, and thermal have been investigated for lignocellulosic biomass pretreatment. Extrusion, milling and grinding methods reduces the size of lignocellulosic biomass resulting in higher available surface for enzymatic interaction. While microwave and ultrasound pretreatment methods disrupt the biomass structure by formation of small cavitation bubbles thus increasing the accessibility of cellulose for the hydrolysing enzymes. Thermal treatment on other hand increases the solubility of hemicellulose and lignin and improves biodegradability. The high cost of instruments, and intensive energy requirements are the critical drawbacks of physical pretreatment methods despite their excellent pretreatment efficiency. The energy demand varies from 3 to 55 kWh/t depending upon the pretreatment approach selected and substrate type (Bhagwat et al. 2015).

2.4.2 Chemical Pretreatment

Oxidizing agents, acids, alkaline and other chemical catalysts are used in chemical pretreatment of biomass, to break down lignin and hemicellulose content (Kaur et al. 2020). The efficiency of chemical methods largely depends on type of chemical catalyst used and can be broadly divided in four major categories, acid, alkaline, oxidation, and ionic liquid pretreatment. Acidic catalysts mainly attack the hemicellulose content, hydrolyze it and expose the cellulose content for further processing. Alkali catalysts are responsible for the degradation of side chains of esters, glycosides and removal of lignin content, resulting in structural disorder of lignocellulosic biomass.

Oxidation and ionic liquid are based on the degradation of the lignin component, and reducing the crystallinity of cellulose content. The requirement of corrosion resistant equipments, use of environmentally hazardous chemicals, production of inhibitory by products, and complicated recovery of chemical catalysts are some of the key limitations.

2.4.3 Physicochemical Pretreatment

The physicochemical pretreatment methods are combinations of physical parameters like temperature, pressure, sonication with chemical catalysts (Kumar et al. 2021a). Steam explosion, oragnosolv, hot water and ammonia-based pretreatments are part of physicochemical pretreatment methods. The physicochemical methods provide distinctive features such as improving the overall digestibility of biomass along with superior recovery of lignin, which further can be used for different applications. The reusability of chemical catalysts used and formation of inhibitory products during pretreatment still restrict their wide spread applications.

2.4.4 Biological Pretreatment

Biological pretreatment methods utilize the biological cells or molecules to remove hemicellulose and lignin content, while leaving the cellulose content intact. The selection of appropriate microbial catalyst is the most critical step for this pretreatment approach (Sindhu et al. 2016). White rot, soft rot and brown rot fungi are most commonly used microbial catalyst for the degradation of hemicellulose and lignin. The low energy requirement, mild operation conditions, avoidance of corrosive chemicals presents this as eco-friendly pretreatment approach, which is preferred over physical and chemical pretreatment approaches (Kumar et al. 2021a). However, the long pretreatment time required owing to the slow activity of microbial catalysts hampers the industrial scale utilization of this method.

Considering the crucial advantages and drawbacks of the commonly used methods, chemical pretreatments combined with high temperature/pressure conditions are considered adequate for industrial scale biomass pretreatment, due to their homogeneous catalysis nature, and reaction efficiency. These methods work well with diluted acid and alkaline catalysts, thus minimizing the overall cost and environmental impacts. However, difficulty in product separation, catalyst recycling, production of by-products, and requirement of corrosion resistant equipment are major drawbacks limiting their wide scale applications.

Table 2.3 Critical analysis of various pretreatment approaches for biomass pretreatment.

Pretreatment approach	Method	Advantages	Drawbacks
Physical	Extrusion	✓ Low cost ✓ Better control over the process ✓ No sugar degradation products ✓ Decreased biomass moisture content ✓ High continuous throughput	• Energy-intensive process • Limited enzymatic digestibility • Not appropriate for all biomass samples
	Milling and grinding	✓ Reduced particle size ✓ High available surface area ✓ Decreased degree of polymerization and crystallinity of biomass	• High cost • Energy-intensive process
	Ultrasound	✓ Effective disruption of biomass structure ✓ Delignification	• High cost • Require specific vessels and facilities
	Irradiation	✓ Faster process ✓ Improved enzymatic hydrolysis	• High energy demand • Special equipment is required • Inhibitory/toxic by-product formation
Chemical	Acid	✓ Higher hemicellulose solubility ✓ High sugar recovery ✓ Superior cellulose accessibility	• Corrosive, hazardous chemicals • Inhibitor formation • Neutralization required • Difficult catalyst recycling
	Alkaline	✓ Cleaved lignin-carbohydrate complex ✓ Increased accessible surface area ✓ Decreased crystallinity and degree of polymerization	• Phenolic by-products • High cost of alkaline catalyst • Long resident time • Large amount of water required for washing • Modification in lignin structure
	Oxidation	✓ Efficient removal of lignin ✓ Low energy demand ✓ Improved cellulose digestibility	• High cost of chemicals • Alkaline condition required

	Ionic-liquid	✓ Low crystallinity of cellulose ✓ High accessible surface area ✓ Superior recovery of lignin	• High cost of chemicals • Additional process required for recovery of solubilized polysaccharide content • Toxicity of ionic liquid remained towards downstream processing
Physicochemical	Steam explosion	✓ Large pores and highly accessible cellulose ✓ Hemicellulose degradation and lignin transformation ✓ Cost effective	• Require expensive reactor system • Inhibitory compound formation • Uncontrolled disruption of biomass structure • Large amount of water required for washing
	Oragnosolv	✓ Superior lignin and hemicellulose removal ✓ Easy lignin recovery	• High cost of chemicals • Requires high pressure equipment • Inhibitory/toxic compound formation • Difficult solvent recovery cycle
	Hot water	✓ Cost effective ✓ High accessible surface area ✓ Low inhibitory compounds formation	• Degradation of monosaccharide sugars • Addition drying process required • Energy intensive
	Ammonia based	✓ Increased accessible surface area ✓ Low inhibitory compound formation	• High cost of ammonia and its recycling • Less hemicellulose solubilisation • Not appropriate for biomass with high lignin content
Biological		✓ Economical and eco-friendly ✓ No corrosion chemical required ✓ Low energy requirement ✓ Effective on all type of biomass samples	• Time consuming • Very few microorganisms are known • Recovery issues

A lot of scientific resources have been devoted in the quest for efficient catalysts, carrying the advantageous capabilities of homogenous chemical catalysts while dealing with the associated shortcomings. The use of solids having acidic capacities commonly known as solid acid catalysts has been explored in the recent past for effective pretreatment and hydrolysis of biomass. These heterogeneous catalysts are easy to separate from the reaction mixture, hence resolve the crucial issue of reusability.

2.4.5 Solid Acid Catalysts

Solid acid catalysts, basically defined as solids capable of donating protons or accepting electrons during catalytic reaction, have been investigated widely in the recent past as a potential substitute for the chemical catalysts (Gupta and Paul 2014; Körner et al. 2018). Acidic moieties present on the surface of solid acid catalysts acts as catalytic domains. The high specific activity, selectivity, ease in recovery, and minimal environmental discharge are some of the key advantages of these heterogeneous solid acid catalysts (Guo et al. 2012). The acidic strength, number of acidic sites on surface and nature of solid support are the major aspect considered for classification of solid acid catalysts. Solid acid catalysts can be broadly categorized in two classes based on the acidic moieties present on their surfaces, Brønsted-type and Lewis-type (Chouhan and Sarma 2011). A wide range of solid acid catalysts based on different support materials have been used for esterification, dehydration, and pretreatment of lignocellulosic biomass (Guo et al. 2012; Gupta and Paul 2014; Schwiderski et al. 2014).

Zeolites, metal oxide, resins, heteropoly compounds, and carbonaceous materials have been used for the synthesis of solid acid catalysts. Acidic functionalization has been employed to produce Brønsted-type and Lewis-type solid acid catalysts. The limitation associated with these macro materials such as nominal inherent acidic activity, limited surface area for acidic functionalization, and deactivation of acidic moieties in presence of water restricts their wider applications. Materials with higher surface area and easy recovery procedure are preferred over these conventional materials for use as support for fabrication and utilization as solid acid catalysts. Nanomaterials owing to their unique physiochemical features have been extensively explored for their acidic functionalization and engagement as nano solid acid catalyst for biomass pretreatment and hydrolysis (Peña Duque 2009; Feng and Fang 2013; Ingle et al. 2019).

Sulfonic acid and carboxylic acid functionalization are most commonly used strategy for preparing nano solid acid catalyst. Magnetic nanoparticles are preferred due to their easy recovery process. Wang et al. (2012) investigated perfluoroalkylsulfonic (PFS), and alkylsulfonic (AS) acid functionalized magnetic nanoparticles for pretreatment of wheat straw. The pretreatment reactions were carried out at 80 and 160 °C for 24 and 2 h, respectively. Highest hemicellulose solubilisation was observed using PFS at 160 °C (2 h), yielding 46.3% oligosaccharides while AS resulted in production of 45% oligosaccharides. The hemicellulose conversion was recorded at 66.3% and 61% under the mentioned condition. The high hemicellulose removal in case of PFS was attributed to the higher acidic power of perfluorosulfonic acids as compared to sulfuric acid. It was concluded that the acid-functionalized nanoparticles hydrolysed hemicellulose polysaccharide into oligomer forms. The easy recovery and reusability of these solid acid catalysts was also reported. Similarly, Propyl-sulfonic acid functionalized cobalt iron oxide nanoparticles have also been investigated for pretreatment of corn stover, and complete hydrolysis into glucose was achieved at 200 °C (Peña et al. 2014). Iron oxide nanoparticles (Fe_2O_3) functionalized with SO_4^{2-} consisting both Lewis and Brønsted acidity was used for hydrolysis of hemicellulose content from wheat straw (Zhong et al. 2015). The selectivity towards hemicellulose hydrolysis with hydrolysis yield of 63.5% was evident from this study as cellulose and lignin content were intact after the hydrolysis reaction.

Alkylsulfonic acid and butylcarboxylic acid functionalized magnetite nanoparticles were evaluated for sugarcane bagasse pretreatment (Ingle et al. 2020a; Ingle et al. 2020b). The pretreatment reaction was carried out at 120 °C with 15 psi pressure for 15 min using a conventional autoclave. A concentration depending impact of both solid acid catalysts was observed, an increase in pretreatment efficiency was evident with increasing the concentration of solid acid catalysts. The highest investigated concentration (500 mg/g sugarcane bagasse) of alkylsulfonic acid and butylcarboxylic acid functionalized nanoparticles resulted in liberation of 18.83 g/L and 18.67 g/L xylose, respectively. The obtained xylose yield was higher than that recorded in case of homogeneous acid pretreatment (15.40 g/L). Both solid acid catalysts demonstrated reusability up to total three cycles of sugarcane bagasse pretreatment with slight decrease in pretreatment efficiency. The decrease was ascribed to the loss of acidic groups present at surface of magnetic nanoparticles. The observed results demonstrated the potency of the acid-functionalized nanoparticles (solid acid catalyst) as economical and eco-friendly technology for effective

pretreatment of lignocellulosic biomass. In another report, alkylsulfonic acid, butylcarboxylic acid and sulfonic acid functionalized magnetic nanoparticles were investigated for their cellobiose hydrolysis capacity (Ingle et al. 2020c). Under optimum conditions 74.8% cellobiose conversion was reported using sulfonic acid functionalized magnetic nanoparticles, the conversion efficiency however reduced to 49.8% when the solid acid catalyst was reused for second cycle. Solid acid catalyst containing alkylsulfonic acid demonstrated almost similar hydrolysis capacity, while butylcarboxylic acid had the minimum hydrolysis capacity. Sulfonic acid functionalized carbon based materials have also been explored for cellobiose hydrolysis (Carlier and Hermans 2020). Activated coal, nanotubes, nanofibers, and graphene nanoplatelets were investigated and highest cellulose conversion of 84% was obtained using SO_3H/RGO solid acid catalyst, with 95% selectivity.

The overall acidity of the nano solid acid catalyst is the major factor affecting the hydrolysis potential, as for hemicellulose hydrolysis break down the C-O bonds interactions between adjacent sugar molecules is essential (Dhepe and Sahu 2010). On the other hand, β-1,4-glycosidic bond breakage is vital for cellulose hydrolysis, which requires comparatively higher acidic strength (Huang and Fu 2013). Development of nanomaterials based solid acid catalysts based for hemicellulose hydrolysis has received significant attention in the recent times. The nominal productions of inhibitory by-products as compared to homogeneous acid catalysts provide an environmentally critical edge to the heterogeneous nano solid acid catalysts (Ingle et al. 2020b). The combination with dilute alkaline pretreatment could be a feasible approach to remove the lignin components, and producing pretreated lignocellulosic biomass for enzymatic hydrolysis.

2.5 Enzymatic Hydrolysis

Hydrolysis of polysaccharide content into monosaccharide fermentable sugar is an important step for production of biochemical products from agri-food waste. Enzymatic hydrolysis is preferred due to its substrate/product specificity, minimal bio-product formation, high product yield and mild operation conditions. Cellulase enzyme with endoglucanase, exoglucanase or cellobiohydrolases and β-glucosidase activity has been widely employed to hydrolyze cellulosic biomass into glucose. Through a multi-step hydrolytic reaction, endoglucanases and cellobiohydrolases synergistically initiate the hydrolysis of cellulose chains into short intermediates i.e., short celluloligosaccharides and cellobiose, which

eventually get transformed into glucose units by the action of β-glucosidase enzyme (Figure 2.2). Similarly, α-amylase is commonly used for production of hydrolysate products from starch rich waste biomass. Enzyme α-amylase hydrolyzes internal α-1,4 glycosidic bonds present in the starch polysaccharide and liberates small-chain dextrins, low-molecular-weight products such as glucose, maltose, and maltodextrin units (Figure 2.3). The interesting fact about the starch-amylase reaction is that size of α-amylase (3-4 nm) is almost 3000 times smaller than the substrate (25 μm) (Payan et al. 1980). These hydrolytic enzymes have been used extensively in industries, such as food and beverages, cosmetics, pharmaceuticals, and chemical detergents, for greener and efficient catalytic reactions.

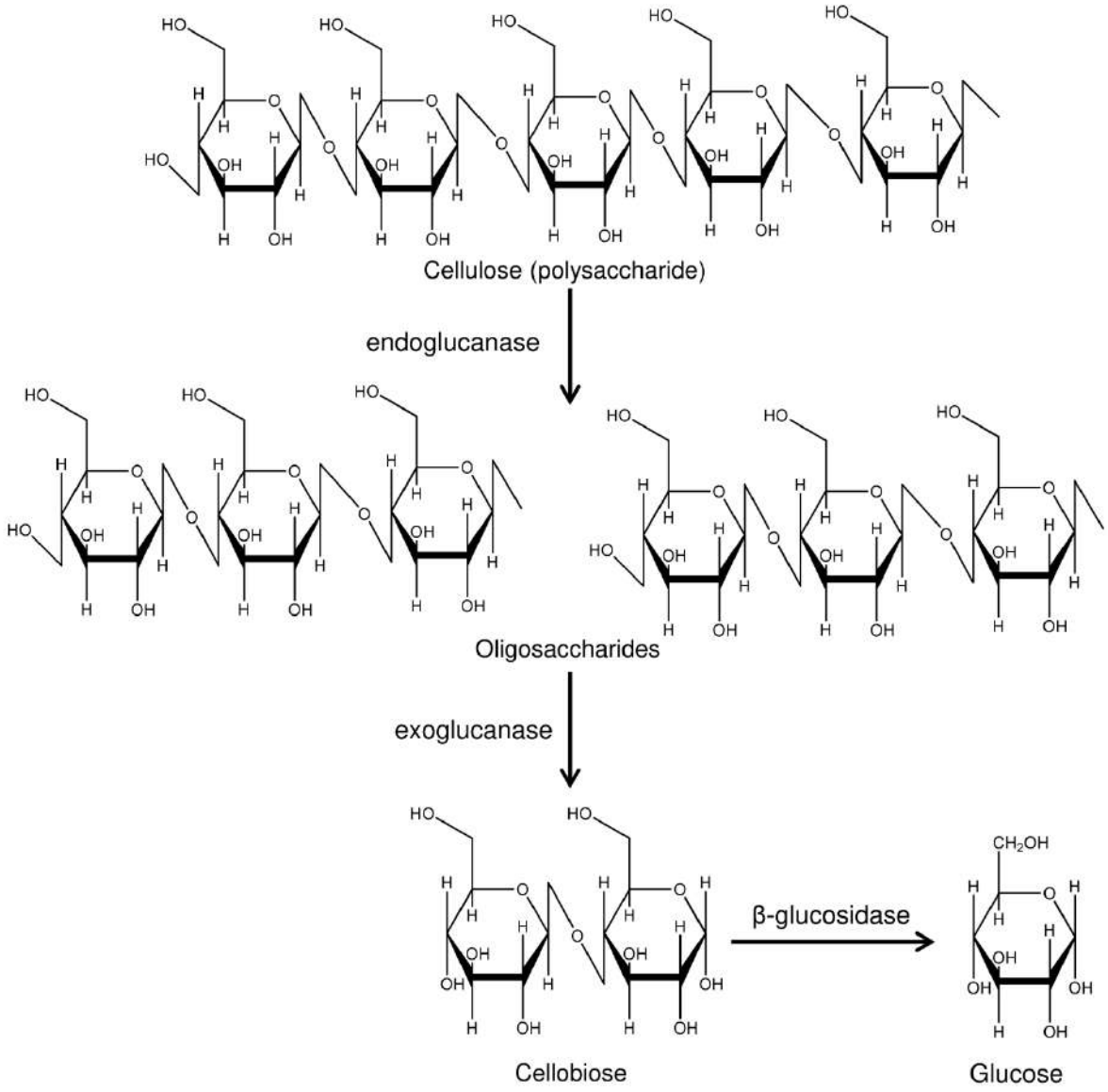

Figure 2.2 Cellulose conversion into glucose via cellulase mediated hydrolysis.

Despite the aforementioned benefits, the catalytic transformation of polysaccharides (cellulose and starch) using enzymes (cellulase and α-amylase) still exists in naive stages and faces key challenges for implementation in the bioprocessing sector. Particularly, the use of free enzymes (i.e., colloidal form) exhibit many limitations, viz., high production cost, low recovery of biocatalyst from the reaction mixture, and extremely low stability of enzymes after every use, eventually making this approach non-sustainable over longer runs. Additionally, large quantities of enzymes are required to produce significant amount of fermentable sugar thus influencing the production cost of bio-chemical product. Considering the usefulness of enzymes to attain the ever-increasing demand of industrial bio-based products, modulation in enzyme properties is an essential step for industrial applications.

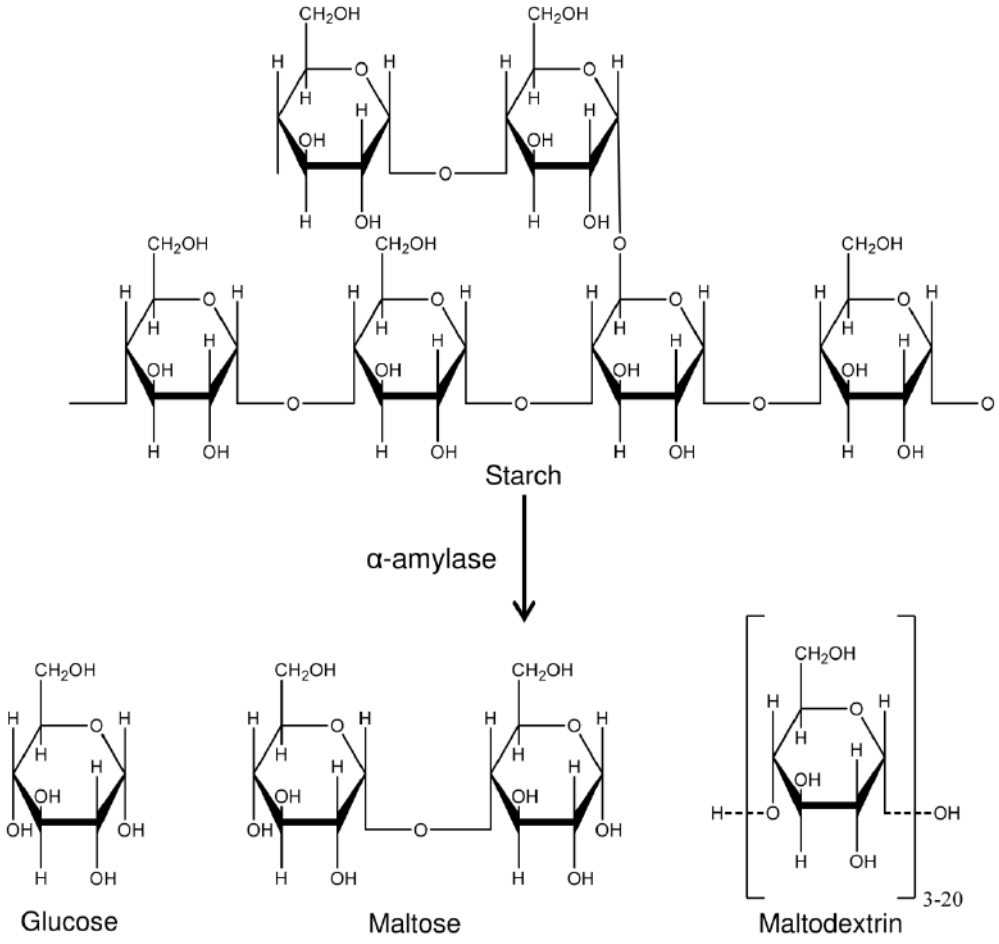

Figure 2.3 Various products formed during α-amylase mediated starch hydrolysis.

Different approaches such as additive approach, chemical modification, protein engineering, and immobilization have been investigated for improvement in enzyme properties (Figure

2.4). Additive approach and chemical modifications are based on alteration of catalytic reaction system and change in enzymatic surface residues or substrate modifications to provide feasible microenvironment for enzyme substrate interaction. The genetic level modifications resulting in overall superior functional properties of enzyme are dealt in protein/enzyme engineering. Enzyme immobilization, deals with attachment of catalyst to a solid support insoluble in the reaction mixture. Additive approach relies on the fact that changing the compositions of reaction mixture has significant impact on the properties of enzymes specifically on catalytic efficiency and selectivity (Liang et al. 2017). Various additives such as organic bases, crown ethers, salts, surfactants, and organic solvents have been reported to improve the overall properties of enzymes, and stabilize the enzyme in a non-aqueous solvent system (Tuñón and Moliner 2016). However, the additives have different impact on different enzymes, and there is no general method to predict the impact as this strategy goes by hit and trial approach (Osbon and Kumar 2019).

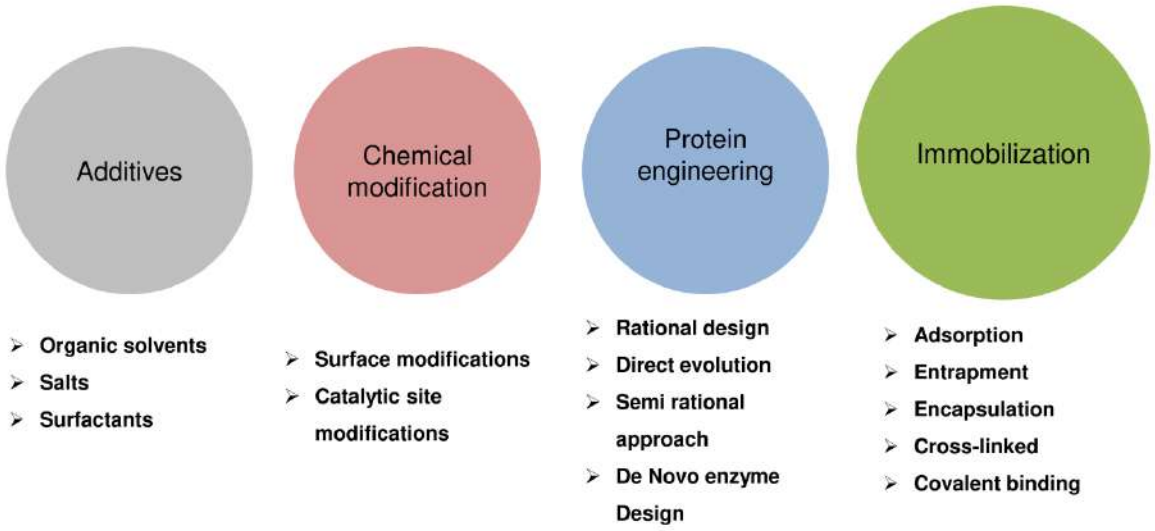

Figure 2.4 Methods commonly used for modification of enzyme properties.

Chemical modification on the other hand, focuses on the impact of different chemicals directly on the enzyme rather than reaction conditions (DeSantis and Jones 1999). Cross-linking with glutaraldehyde, covalent conjugation with polymer polyethylene glycol (PEG), are some of the commonly employed methods, resulting in modification of reactive side chains, introduction of a cofactor, or enhancement of the enzyme stability. Protein engineering basically involve change in genetic structure with help of recombinant DNA technology, computational tools, and modern bioengineering (Woodley 2013). The genetic changes induce variation in primary protein structure, which results in stabilization of

enzyme, broadening of substrate range, and production of high value products. Protein engineering is a laborious procedure and requires deep rooted knowledge of genetic methods and technology.

The enzyme properties modifications using these methods have resulted in superior catalytic efficiency, stability under organic solvents, broad substrate range etc. however the cost and time required for employing these methods, and reusability aspect of produced enzyme limit their application at industrial scale as of now. With technological advances and growing use of prediction models these methods are certainly going to have a long-lasting impact on the bioprocessing sector. The current requirements of industrial sector can be dealt with a method providing more robustness to the naturally peculiar biocatalyst and instil reuse capability. Enzyme immobilization has immerged as a promising approach to deliver industrial biocatalysts with superior properties (Gonçalves et al. 2019).

2.6 Enzyme Immobilization

Enzyme immobilization is defined as a technical process where "enzymes are physically confined or fixed to or within a solid support" creating a heterogeneous immobilized enzyme system. The major components are enzyme, mode of attachment and support matrix, where latter two plays crucial role for the catalytic activity and stability of the enzyme immobilized. The attachment could be weak physical adsorption and ionic linkage to stable covalent linkages, which results in alteration of catalytic activity of enzyme in reaction mixture. While the selection of support dictates the protection from environmental factors and provides stability to the immobilized enzyme.

2.6.1 Immobilization Strategies

The choices of the immobilization strategy significantly affect the catalytic activity and applications of immobilized enzyme. On the other hand, the overall cost of the process is also affected by the immobilization strategy, as the reusability of the immobilized enzyme system strongly depends on the immobilization strategy. Additionally, rigidity/stability of the protein structure and capability to protect enzyme from inhibitor compounds as well as generating microenvironment for enzyme-substrate interaction also depend on the immobilization technique employed. Immobilization strategies can be classified as adsorption, encapsulation/entrapment, cross linked enzyme aggregates and covalent binding.

Adsorption is the simplest technique used for enzyme immobilization, where enzyme molecules solution is incubated with a support matrix for a fixed period of contact time. Enzyme molecules attach to the surface of the support by van der Waals forces, ionic interactions or hydrogen bonding (Jesionowski et al. 2014). The interaction between enzyme and support are rather weak and does not change the native structure of the immobilized enzyme, results in retaining high catalytic activity. Enzyme-carrier affinity is the most critical aspect of adsorption immobilization, which must be there to obtain immobilized enzymes. The weaker bonds present can be easily cleaved due to change in physiological conditions which result in desorption of enzyme from support matrix. Owing to the weak interaction support matrix is not able to protect the enzyme from external factors such as change in pH, temperature or presence of inhibitory moieties. Another critical issue is the non-specific adsorption, which might impact the overall catalytic activity of immobilized enzyme.

Encapsulation process involves the entrapment of enzyme in a polymer matrix, which is permeable for substrate and product. The encapsulation provides protective barrier for enzyme from external environmental parameters. Generally, entrapment matrices are synthesised during the immobilization process, hence the compatibility of the support with enzyme becomes a key aspect while selecting the polymer matrix (Cao 2006). Cross linking is the combination of covalent binding and entrapment, where chemical crosslinker are used to covalently attach enzyme molecules to each other. Crosslinker such as glutaraldehyde and bisisodiacetamide are commonly employed. Degree of crosslinking is key influential factor for the retained enzyme activity in immobilized form.

Covalent binding is the most commonly used immobilization strategy, where enzyme molecules are covalently attached to insoluble support matrix. The strong binding restricts the leaching of immobilized enzyme from the support matrix during catalytic reaction. The close and strong binding between support and enzyme, also govern the thermal stability to the immobilized form of enzyme. The attachment of the enzyme on support surface facilitates the interaction between enzyme and substrate, providing more space for substrate and product movement. However, the strong binding limits the free movement of enzyme molecules thus affecting their catalytic activity. The advantages and limited associated with different immobilization strategy or mode of attachments are listed in Table 2.4. Covalent binding is the preferred immobilization strategy for enzyme immobilization, owing to the advantages offered, and a wide range of support materials have been explored till date for the same.

Table 2.4 Key aspects of immobilization techniques.

Immobilization strategy	Mode of attachment	Advantages	Limitations
Adsorption	Weak bonds (van der Waals forces, ionic interactions, hydrogen bonding)	✓ Simple process ✓ Cheaper ✓ High retained catalytic activity ✓ No conformational change in enzyme	• Desorption (leakage) during reaction • Low stability • Very limited reusability • Non-specific adsorption might occur
Encapsulation and Entrapment	Physical confinement	✓ High retrained activity ✓ Protection from environmental variation ✓ Easy separation from reaction ✓ Allow substrate and product movement	• Limited enzyme loading • Enzyme leakage • Limitations on mass transfer
Cross-linking	Covalent bond between enzyme/cross-linker	✓ Simple process ✓ Strong biocatalyst binding ✓ Leakage prevention ✓ High stability	• Active site alteration • Loss of enzyme activity • Diffusion limitations
Covalent	Covalent binding between enzyme and insoluble support matrix surface	✓ Strong biocatalyst binding ✓ Superior stability ✓ Improved enzyme-substrate contact ✓ Leakage prevention ✓ A range of support can be used	• Limited enzyme mobility • May result in loss of enzyme activity

2.6.2 Support Materials

The catalytic performances of immobilized enzymes are gravely affected by the materials used for enzyme attachment, generally called as carrier or support matrix. The intrinsic characteristics of the support are critically important for this purpose and must be fully explored before immobilization process. The inert nature of support material specifically towards enzyme is a must; it should not interact with enzyme catalytic sites in any way possible. Mechanically and thermally stable supports are preferred, as they can be used under harsh reaction conditions, without being degraded. This feature results in production of highly robust immobilized enzyme, which can be used in a wide range of pH and temperature. Along with these high surface area and specific surface chemistry that allows high enzyme loading while preventing the inhibition caused by produced product are vital for biotechnological applications of immobilized enzymes. Scale-up for industrial level production is obviously targeted hence, cheap and wide availability of the support material must be ensured for superior industrial feasibility. It is apparent that one support material can not possess all the features required; hence selection of appropriate support material must be done with extreme caution. Moreover, the economic cost of modifications steps if required must be considered, as it would affect the cost effectiveness of the final product. The support materials can be classified in two categories according to the chemical compositions, organic and inorganic supports.

Organic Supports

Naturally occurring and synthetic organic materials specifically biopolymers have been widely explored for enzyme immobilization. The unique properties of biopolymers such as biocompatibility, high affinity to proteins, and biodegradability make them an suitable support for enzyme immobilization while retaining high catalytic activities (Krajewska 2004). Moreover, the availability of a wide variety of functional moieties (hydroxyl, amine, carbonyl etc.) allows easy modification/functionalization. Carbohydrates are the most abundant biopolymer available for enzyme immobilization (Elnashar 2011). The renewable nature and abundance of these biopolymers present them as an ideal immobilization support for industrial application (Bilal and Iqbal 2019). Chitosan, chitin, collagen, cellulose, carrageenan, alginate, agarose, gelatin, starch, and pectin have been employed for immobilization of various enzymes. Although the associated advantages make them excellent

support for enzyme immobilization, however the low stability in presence of organic solvents and possibility of microbial attack limit their large-scale industrial applications.

Synthetic polymer has also been used for enzyme immobilization, owing to the distinctive advantage where number of monomer units to form a polymer can be selected as per user's requirement (Maksym et al. 2017). The stability, mechanical strength, and porosity along with the reactive chemical moieties of the formed polymer can be easily manipulated by this feature. The present functional moieties such as carbonyl, carboxyl, hydroxyl, epoxy, and amine groups can be used for functionalization of polymer surface or directly for enzyme binding via adsorption or covalent binding. Moreover, the length of the support–enzyme spacers can also be influenced, where long spacers provide higher conformational flexibility to immobilized enzyme and short spacer help in protecting enzyme from thermal inactivation and leaching during reaction (Cantone et al. 2013). A range of polymers including ion exchange resins/polymers, polyvinyl chloride, polyvinyl alcohol, methacrylated/fumaric acid-modified epoxy, polyaniline, polyamide, polystyrene, polyurethane, and polypropylene have been used for enzyme immobilization. Despite all the advantages, the industrial level applications of synthetic polymers are restricted due to the cost and longer time period required for polymer synthesis and functionalization.

Inorganic Supports

Inorganic materials have been investigated for enzyme immobilization owing to the inherent properties. Inorganic materials have brilliant thermal and mechanical strength, along with excellent microbial resistance. Additionally, the in-built porosity and rigid nature of inorganic materials is added advantage, although organic materials can also be customised to induce porosity, however the sensitivity towards environmental conditions (pH, temperature) limit their usefulness. The porous nature of inorganic materials is hardly influenced by pH or temperature, hence guarantees consistent surface for the immobilized enzymes. Furthermore, the recent advances in material chemistry have opened up new ways for effective functionalization of inorganic materials. A wide range of inorganic materials have been explored for the enzyme immobilization as discussed below.

Silica and silica based materials are the most studied inorganic materials for enzyme immobilization, basically due to the high surface area (300-1500 m^2/g) they possess (Hartmann and Kostrov 2013). The high surface area enables high enzyme loading during

immobilization process and reduced diffusional limitations in subsequent applications. Functionalization of silica materials is also easily attainable due to the presence of reactive functional group on the surface. Pore size, surface chemistry, particles size and morphology are some of the factors affecting the immobilization efficiency on silica materials (Hartmann and Kostrov 2013). Inorganic oxides are another class of inorganic materials which demonstrate inertness, high thermal and mechanical stability, and good sorption capacity. Furthermore, the hydroxyl groups abundance at surface governs them their highly hydrophilic nature, which helps in attaining appropriate functionalization and high enzyme loading. Carbon based materials have also been studied for enzyme immobilization. The porous structure of activated carbons, and charcoals has high available surface area (up to 1000 m^2/g), which along with pore of various sizes assist the immobilization of enzyme molecules. Adsorption of biocatalysts on the surface is the key immobilization strategy used in case of carbon-based material, owing to the presence of functional groups and high adsorption capacity.

Ceramic materials based on nitrides, oxides, alumniosilcates and carbides have also been employed for enzyme immobilization. The formation of these ceramic involve additive components which have significant impact on the features such as rigidity, porosity, and mechanical resistance of final product (Kujawa et al. 2021). The presence of these additives can readily be utilized for enzyme immobilization, without the requirement of any functionalization process. Furthermore, the porous structure availability preserves the catalytic activity of immobilized enzyme and provides an opportunity for continuous operations. Different forms of ceramic materials such as membranes, foams, and beads have been investigated for enzyme immobilization (Kujawa et al. 2021). The changes in reaction conditions such as pH and temperature have no influence on the physical or chemical characteristics of ceramic support, presenting it feasible for industrial applications.

Zeolites are employed as ideal support materials for enzyme immobilization, due to their varying pore structures, thermal stability, low cost, easily modifiable structure and biocompatibility (Zhang et al. 2021). The inherent catalytic activities of zeolites helps in preserving the catalytic activity of enzymes and in some case even enhance it. The improvement in stability of enzyme immobilized on zeolites under varying pH and thermal conditions along with reusability potential has been observed in the past. Only the external

surface of the zeolites can be employed for enzyme immobilization via adsorption, deposition or covalent binding. Entrapment has also been achieved in some cases recently.

According to the requirements of industrial process, researchers have been continuously seeking for support materials with unique physicochemical properties. Attributed to the advances made in area of nanotechnology, the application area of nano-scale materials has expanded in different area such as material science, microelectronics, chemistry environmental science and biotechnology (Liu and Dong 2020). A diverse range of nanoscaffolds such as particles, wires, tubes, rods, sheets and fibers are available nowadays for biotechnology, immunosensing and biomedical areas (Califano et al. 2018; Hasan and Pandey 2021; Chakraborty et al 2022). Nanomaterial as support for biocatalysts provides high surface area, low mass-transfer limitation and easy particle mobility. Owing to their chemical properties, nanomaterials can be furnished with suitable functional groups without disturbing their precise properties. The functionalization enables the ease of immobilization along with improvement in the biocompatibility of support. Considering the relevance to the current work, the enzyme immobilized on nanomaterials is discussed as a separate section below.

2.7 Nanobiocatalysts

The whole enzyme immobilized nanostructure system is termed as a nanobiocatalyst (NBC), where the inherent properties of nanomaterials and enzymes synergistically work under practically relevant conditions. The attachment of biocatalysts i.e., enzymes onto nanomaterials, and subsequent investigation of stability, selectivity, chemical/thermal kinetics are process involved nanobiocatalysis approach. An appropriately functionalized nanomaterial could enhance the enzyme stability and provide a microenvironment for enzyme-substrate interaction, thus resulting in maximum catalytic efficiency. The properties and functions of the nanobiocatalyst can be influenced by, selecting appropriate nanomaterial (size/shape, aspect ratio), introducing specific functionalities on the nanomaterial support, and enhancing the mechanical and thermal stability. Nanomaterials with different shape and size have been investigated in the recent past for formation of nanobiocatalysts.

Owing to the distinctive advantages associated such as large-scale production and presence of functional groups polymeric nanostructures have been widely used for fabrication of nanobiocatalysts. Nanoparticles, nanofibers, nanogels and nanocrystals are some of the

geometric shapes of polymer nanomaterials used for fabrication of nanobiocatalysts. Physical adsorption (nanofibers), encapsulation (nanogels) and covalent binding (nanoparticles) are the commonly employed immobilization strategies for nanobiocatalyst formation. Immobilization of enzymes onto mesoporous silica nanoparticles results in formation of nanobiocatalyst. The easily modifiable surface properties (pore geometry, functional groups, ionic charge) of mesoporous nanoparticles can be used to increase the enzyme loading. Adsorption in the porous structure and covalent binding using the functional groups are the key immobilization methods for attaching enzyme to the silica nanostructures. Carbon nanomaterials nanobiocatalysts have been explored due to the inert and biocompatible nature of carbon nanomaterials. Graphene, single and multiwalled carbon nanotubes (CNTs), and nanodiamond are most commonly used carbon nanomaterials for enzyme immobilization. The naturally adsorptive nature of these nanomaterials can be directly used for enzyme adsorption without chemical modifications. Different functionalization procedures have been developed in the recent past to improve the enzyme loading and subsequent stability. The immobilization of cellulase and α-amylase on different nanomaterials is collated in Table 2.5 and 2.6. Despite the advantages industrial scale utilization of nanobiocatalysts is limited by the cost intensive nanomaterial synthesis and functionalization procedures. The quest for economic support material for immobilization of industrial enzymes is still on-going.

Table 2.5 Various nanomaterials utilized for cellulase immobilization and associated advantage offered.

Support material	Immobilization	Key outcomes	Reference
(Fe_3O_4@SiO_2@p(NIPAM-co-GMA))	Covalent	• Enzyme loading 233 mg/g • Superior thermal and storage stability • Increased substrate affinity • Retained 65.6% catalytic activity after six reuse cycles	Han et al. (2018a)
Fe_3O_4-NH_2@4-arm-PEG-NH_2	Covalent	• Enzyme loading 132 mg/g • Enhanced catalytic activity • Superior operational and storage stability	Han et al. (2018b)
Magnetic Poly (ionic liquid) Support	Covalent	• Enzyme loading 106.1 mg/g • Superior storage stability up to 25 days • Retained 60% activity after six reuse cycles	Hosseini et al. (2018)
Chitosan and alginate beads	Entrapment	• Superior pH and thermal stability • High hydrolysis of pretreated sugarcane bagasse • Retained 50% activity after five reuse cycles	Saha et al. (2019)
PEG hydrogel and sodium polyacrylate on low density polyethylene film	Entrapment and covalent	• 82% and 20% increase in catalytic activity • Retained 93%activity after ten reuse cycles • 89% of filter paper activity after six cycles	Wang et al. (2019c)
Chitosan modified Fe_3O_4/graphene oxide nanocomposite	Covalent	• Retained 78.1% catalytic activity • Increased substrate affinity • Retained 49% activity after eight reuse cycles	Asar et al. (2020)
Wrinkled silica nanoparticles (WSNs)	Adsorption	• Enzyme loading ~70 mg/g • Hydrogen bonding was the key force for adsorption • Retained >70% activity after five reuse cycles	Costantini et al. (2020)
Magnetic Fe_2O_3/Fe_3O_4@SiO_2-CHO nanocomposites	Covalent	• Enhanced thermal stability • Catalytic stability in range of temperature and pH • Retained 71% activity after five reuse cycles	Huang et al. (2020)
Core-Shell Magnetic Gold	Covalent	• Immobilization efficiency 84%	Poorakbar et al. (2020)

Nanoparticles		• Superior pH and thermal stability • Retained 27.61% activity after five reuse cycles	
Iron oxide nanoparticles	Covalent	• Immobilization efficiency 65.55% • Retained 50.34% activity after four reuse cycles	Kaur et al. (2021)
Functionalized magnetic nanoparticles	Covalent	• Enzyme loading 167 mg/g • Superior pH and thermal stability • Retained 73% activity after six reuse cycles	Mariño et al. (2021)
Copper ions loaded Fe_3O_4-iminodiacetic acid nanoparticles	Covalent	• Enzyme loading 33.1 mg/g, activity 154U/g • Retained 75% activity after 28 days storage time • Retained 93% activity after six reuse cycles	Ozyilmaz et al. (2021)
Magnetic graphene oxide	Covalent	• Enzyme loading 140 mg/g, activity 44 FPU/g • Retained >66% activity after ten reuse cycles • Turnover frequency for CMC hydrolysis 0.4020	Paz-Cedeno et al. (2021)
Iron oxide nanoparticles	Covalent	• Immobilization efficiency 86% • Superior storage stability for 1440 h • Retained 60% activity after five reuse cycles	Vijayalakshmi et al. (2021)
Nanoscale Hybrid Polyaniline/Cationic Hydrogel	Adsorption	• Immobilization efficiency 96% • Retained 90% activity after four weeks storage time • Retained 73% activity after nine reuse cycles	Zarei et al. (2021)
Chitosan-coated Fe_3O_4 nanoparticles	Covalent	• Specific activity 25.3 μmol/min/mg • Increased substrate affinity • Retained 51.5% activity after three reuse cycles	Javid et al. (2022)
Wrinkled mesoporous silica nanoparticles	Adsorption	• Enzyme loading 100 mg/g • Retained 83% activity after nine reuse cycles • Retained 89% activity at 70 °C	Pota et al. (2022)
Nickel nanoparticles	Covalent	• Immobilization efficiency 93.4% • Retained 76% activity after ten reuse cycles	Rashid et al. (2022)
Magnetized multiwall carbon nanotubes (m-MWCNTs)	Adsorption	• Immobilization efficiency 95% • Superior pH and thermal stability • Retained >50% activity after five reuse cycles	Yasmin et al. (2022)

Table 2.6 Improvement in intrinsic properties of α-amylase via fabrication of nanobiocatalyst on various nano supports.

Support material	Immobilization	Key outcomes	Reference
Naringin functionalized magnetic nanoparticles	Ionic interactions	• Enzyme loading ~20 µg/mg • Retained 50% activity after ten reaction cycles • Retain 64% activity after six weeks	Defaei et al. (2018)
Chitosan coated Fe_3O_4 MNPs	Covalent	• Enzyme loading ~9 mg/g • Retained 66% activity after 20 days storage time • Retained 79% activity after 20 reuse cycles	Dhavale et al. (2018)
Chitosan-montmorillonite nanocomposite beads	Covalent	• Immobilization efficiency 86% • Retained 95% activity after 40 days storage time • Retained 47% activity after five reuse cycles	Mardani et al. (2018)
Polypyrrole AgNp/Fe_3O_4-nanocomposite	Ionic interactions	• Immobilization efficiency 75% • Retained 80%activity after ten reuse cycles • Increased substrate affinity	Mohamed et al. (2018)
Polyacrylamide-graphene oxide nanocomposites	Entrapment	• Immobilization efficiency 97.5% • Increased substrate affinity • Retained 99.32%activity after five reuse cycles	Mulko et al. (2019)
Chitosan-magnetic nanoparticles	Adsorption and covalent	• Immobilization yield 81.6% • Superior storage (86.4%, 40 days) and thermal stability	Ahmed et al. (2020)
Magnetic chitosan	Adsorption and covalent	• Improved pH stability • Enhanced temperature stability at high temperature • Retained 60% activity after 90 days of storage	Bindu and Mohanan (2020)
Polycaprolactone-grafted magnetic nanoparticles	Covalent	• Immobilization efficiency 61% • Retained 60% activity after five reuse cycles • Retained 57% activity after 120 days storage time	Defaei et al. (2020)
Chitosan-based polymeric micelles	Entrapment	• Enhanced pH resistance capability • High stability and reusability • Reusability up to ten cycles	Kolesnyk et al. (2020)
Modified Na-sepiolite	Adsorption	• Enzyme loading 9.1 mg/g, activity 2.28 U/mg	Mortazavi and Aghaei

		• Resistance for pH and temperature change • Superior thermal stability • Retained 66.7% activity after 30 days storage • Retained 44.2% activity after ten reuse cycles	(2020)
Lysine functionalized magnetic nanoparticles	Cross-linked enzyme aggregates	• Improved pH and thermal stability • Increased substrate affinity	Torabizadeh and Montazeri (2020)
Hydroxyapatite-decorated ZrO_2	Adsorption and ionic interactions	• Immobilization efficiency 84% • Excellent storage stability (69% after 8 week) • Retained 70% activity after ten reuse cycles	Almulaiky et al. (2021)
GO-magnetite nanoparticles	Covalent	• Enzyme loading 77.58 μg/mg • Enhanced half-life at higher temperature • Retained 50% activity after 11 reuse cycles	Desai et al. (2021)
ZnO and Fe_3O_4 nanoparticles	Adsorption	• Enzyme loading 100.8 mg/g for ZnO • Enzyme loading 102.9 mg/g for Fe_3O_4	Długosz et al. (2021)
Magnetic Nanoparticles	Electrostatic interaction and covalent	• Immobilization efficiency 68%, activity 40% • Retained 92% activity after three-month storage time • Retained 82% activity after 15 reuse cycles	Salem et al. (2021)
PAMAM dendrimer-modified magnetic chitosan	Adsorption and covalent	• Immobilization efficiency 93.95% • Retrained 46 and 72%activity for adsorption and covalent methods after ten reuse cycles • Retrained 38 and 56% activity for adsorption and covalent methods after six-month storage time	Unniganapathi and Mohanan Puzhavoorparambil (2021)
Cellulose derivatives	Covalent and hydrophobic interactions	• Covalent immobilization was more effective • Retained 30% activity after seven reuse cycles • Retained 50% activity after 24 days storage time	Verma and Raghav (2021)
Cloisite 30B	Adsorption and covalent	• Immobilization efficiency 93.7%, activity 90.2% • Retained 83.5% activity after 30 days storage time • Retained 79.7% activity after ten reuse cycles	Aghaei et al. (2022)
Zinc sulfide-chitosan hybrid nanoparticles	Covalent	• Enhanced pH and thermal stability • Retained 95% activity after 30 days storage time	Bahri et al. (2022)

2.7.1 Halloysite Nanotubes

Falling in line with greener development strategies, the utilization of naturally occurring nano-scale materials instead of chemically synthesized nano-scale materials have been investigated for various application areas. Halloysite, a dioctahedral 1:1 clay mineral of the kaolin group predominantly occurs in tubular structure, also known as halloysite nanotube. The two mineral layers (tetrahedral silica oxide and octahedral alumina oxide) wrap around each other in 1:1 to form a tubular structure under natural conditions (Singh 1996). Kaolinite and halloysite both are almost similar, only difference is the presence of intercalated monolayer of water molecules between alumina-silica unit layers (Figure 2.5). The general chemical formula of halloysite nanotubes is $Al_2(OH)_4Si_2O_5 \cdot nH_2O$, where n=2, represent the hydrated form of halloysite (halloysite-10 Å), and n=0 represent the dehydrated halloysite (halloysite-7 Å). The dehydrated form of halloysite nanotubes can be obtained by mild heating or vacuum suction of hydrated halloysite (Joussein et al. 2005). Large deposits of halloysite are found in different parts of the word such as USA, Australia, New Zealand, China, Canada and Turkey. Halloysite nanotubes offer several distinctive advantages over synthetic nanotubes (carbon nanotubes) such as low price ($4 per kg as compared to $500 per kg), and abundant global supply (tons per year), which facilitates the scaling up of intended application (Lvov et al. 2008). Due to their natural occurrence, the morphological characteristics of the halloysite nanotubes vary significantly according to their site of origin (Joussein et al. 2005; Cavallaro et al. 2018).

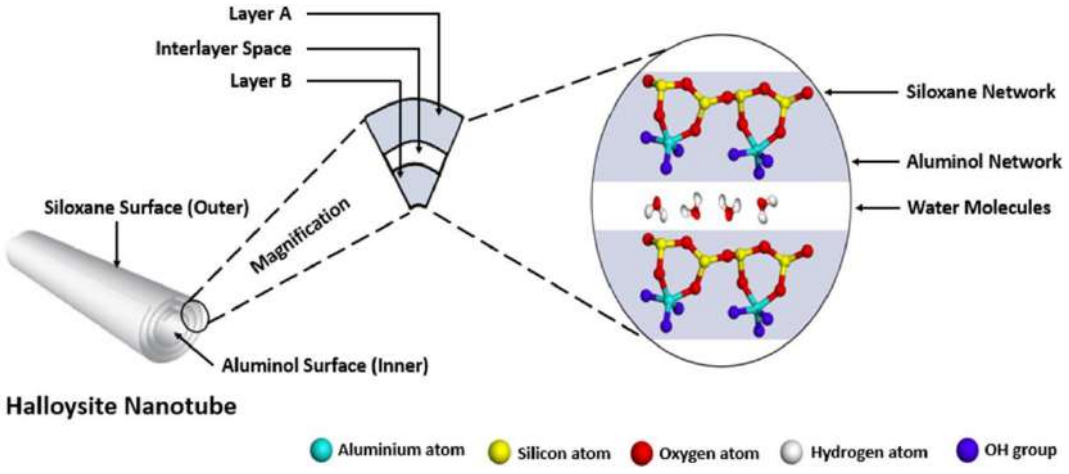

Figure 2.5 Halloysite nanotube structural components (Reprinted with permission from Tharmavaram et al. (2018). Copyright (2018) Elsevier).

The length of halloysite nanotubes commonly fall in range 600-900 nm, with outer diameter 30 to 190 nm, and inner diameter ranges from 10 to 100 nm. The specific surface area of halloysite nanotubes is reported to be 50-60 m^2/g, with pore volume ranging from 0.06-0.25 cm^3/g, much higher than the chemical analogous i.e., kaolinite (Setter and Segal 2020). The high specific surface area and pore volume are attributed to the pores present in halloysite nanotubes, such as hollow mesoscopic lumen, voids formed during agglomerations, and mesopores formed during dehydration process (Joussein et al. 2005; Yuan et al. 2015). The presence of two layer containing different functional moieties governs a dual chemistry characteristic to halloysite nanotubes where outer surface is negatively-charged (silica surface) and inner lumen is positively charged (alumina surface) (Veerabadran et al. 2007). The overall characteristic zeta potential of halloysite nanotubes is around -30 mV in pH range 4-8 (Setter and Segal 2020). Along with impact on overall zeta potential, the change in pH also affects the dispersion behaviour of halloysite nanotubes, where under acidic conditions halloysite dispersion results in agglomeration. On the other hand, halloysite suspension under alkaline pH is stable owing to the van der Waals interaction between the negatively charged halloysite nanotubes (Yuan et al. 2015). Along with aforementioned characteristic the low cytotoxicity and highly biocompatible nature of halloysite nanotubes also encourage their application in biotechnological areas (Setter and Segal 2020). Halloysite nanotubes have excellent mechanical properties, although not comparable with carbon nanotubes (Lvov et al. 2008). The diameter of halloysite nanotubes have been reported as a major factor in the mechanical properties, as larger diameters are associated with lower elastic modulus (Lecouvet et al. 2013). While smaller diameter are linked with higher elastic modulus, which can be attributed to the fact that halloysite nanotubes with smaller diameter has a lower density of structural defects and surface tension effect (Yuan et al. 2015).

Functionalization/Modifications of Halloysite Nanotubes

The unique site-dependent aluminosilicate chemistry where the reactivity of external, internal and interlayer surfaces of halloysite nanotubes are different, offers immense possibilities for surface modifications. Physical modifications and chemical modifications are two commonly employed modification approaches, which induce alteration in physicochemical characteristics of the halloysite nanotubes such as hydrophilicity, solubility, reactivity and biotoxicity (Yuan et al. 2015). The internal and internal surfaces composed of Al-OH groups have high chemical activity and can be easily modified using different methods. However,

the utilization of these surfaces for enzyme immobilization is not beneficial, as internal lumen has permeability and substrate/product flow issue, while the interlayer area limits the extent of enzyme immobilization. The external surface of halloysite is mainly made up of siloxane (Si-O-Si) groups with miniscule aluminol (Al-OH) and silanol (Si-OH) groups present on the edge of external surface. The low chemical reactivity of siloxane groups eliminates the possibility of direct organic compound grafting; however, the negative charge presents the possibility for adsorption of cations. Polymers poly(ethyleneimine), poly(allylamine) hydrochloride, chitosan, pectin, and polydopamine have been used for surface modifications via monolayer formation or layer by layer assembly for various applications. The selection of polymer is based on the specific property such as thermal, mechanical, electrical, or functional moieties, one want to modify (Tharmavaram et al. 2018). Mechanochemical approach has also been investigated where halloysite nanotubes are mixed with the modifying agent to obtain halloysite covered with the modifying agent (Chang et al. 2011). Alkali treatment has also been used for introducing hydroxyl group on the outer surface, and decreasing the halloysite wall thickness thus increasing the lumen size (Zeng et al. 2014). Organic compounds such as surfactants have also been employed for halloysite nanotubes surface modifications. Cationic surfactants can directly be functionalized on negatively charged external halloysite nanotube surface.

Organosilanes have been widely employed for surface modifications of different materials due to the simple reaction procedures and low toxicity. Organosilane functionalization has been explored for halloysite nanotube external surface modification as an excellent coupling agent between halloysite nanotube and guest molecule (Massaro et al. 2017; Tharmavaram et al. 2018). Alkoxy group present in organosilanes, are released due to hydrolysis reaction in presence of water, resulting in generation of free silane groups. Condensation of these silane group results in formation of silanol groups, which via hydrogen bonding gets attached to the surface of halloysite nanotubes. The organosilane grafting is generally carried out in presence of non-polar solvents or solvents with low-vapour pressure. The availability of surface hydroxyl group is a limiting factor for organosilane functionalization of halloysite nanotubes, which can be easily enhanced by removing impurities or via acidic/alkali treatments (Sun et al. 2015). Organosilane such as 3-aminopropyltriethoxysilane, mercaptopropyltriethoxysilane, N-(2-aminoethyl)-3-(trimethoxysilyl) propylamine, and 3-chloropropyltrimethoxysilane have been functionalized on halloysite nanotubes (Massaro et al. 2017).

Attributed to their unique physicochemical attributes, halloysite nanotubes have excellent adsorption capabilities. The negatively charged surface facilitates the adsorption of metal ions which can then be transformed into nanoparticles via already established methods. Second approach is utilizing the organosilane modified halloysite nanotubes for attachment of previously synthesised nanoparticles (Tharmavaram et al. 2018). Numerous metal and metal oxide nanoparticles such as gold, silver, ruthenium, cobalt oxide, iron oxide and titanium oxide nanoparticles have been attached to halloysite nanotubes for imparting antibacterial, conductive, or catalytic activities.

Halloysite Nanotubes based Nanobiocatalyst

The adsorption capability of halloysite nanotube has been exploited for direct enzyme immobilization on halloysite nanotubes. For instance, enzymes like alkaline phosphatase, lipase and β- galactosidase has been immobilized on halloysite nanotubes via adsorption (Pietraszek et al. 2019; Mohammadi et al. 2020; Tizchang et al. 2021). The leaching of enzyme can be controlled by entrapping the enzyme immobilized halloysite nanotubes into polymer matrix such as polyvinyl alcohol/alginate hydrogel and cellulose nanocrystals (Mohammadi et al. 2020; Tizchang et al. 2021). Surface modified halloysite nanotubes such as are widely used support matrix for enzyme immobilization. Chitosan functionalised halloysite nanotubes have been used for immobilization of chloroperoxidase and laccase enzyme via electrostatic interactions or covalent immobilization (Fan et al. 2018; Kadam et al. 2018; Kim et al. 2018; Kadam et al. 2020a; Hürmüzlü et al. 2021; Tharmavaram et al. 2021; Wang et al. 2022b). Superoxide dismutase, β-lactamase, and peroxidase have been immobilized on polymer such as protamine sulfate polyelectrolyte (PSP), poly(ethylene imine), and polydopamine grafted halloysite nanotubes (Katana et al. 2019; Rouster et al. 2019; Ren et al. 2022). Organosilane functionalized halloysite nanotubes have been employed for immobilization of aminoacylase, chloroperoxidase, endoinulinase, and protease enzymes via covalent linkage (Kołodziejczak-Radzimska and Jesionowski 2019; Zhu et al. 2021; Kim et al. 2022b; Singh and Singh 2022a, b, c). Magnetic nanoparticles anchored halloysite nanotubes i.e., magnetic halloysite nanotubes have also been used for enzyme immobilization via functionalization such as chitosan and aminosilane grafting (Kadam et al. 2018; Kim et al. 2018; Kadam et al. 2020c; Zhu et al. 2021; Kim et al. 2022b) (Table 2.7).

Table 2.7 Halloysite nanotube based nanobiocatalysts.

Support	Enzyme	Immobilization	Key outcomes	Reference
Chitosan modified halloysite nanotubes	Chloroperoxidase	Electrostatic interaction	• Enzyme loading 18.3 mg/g, • Retained activity 93.3 % • Enhanced thermal stability • Increased substrate affinity • Retained 62.2% activity after eight reuse cycles	Fan et al. (2018)
Chitosan-functionalized supermagnetic halloysite nanotubes	Laccase	Covalent	• Enzyme loading 92.74 mg/g • Retained activity 92% • Higher pH, temperature, and storage stabilities • Retained 51% activity after 11 reuse cycles	Kadam et al. (2018)
Chitosan functionalized super magnetic halloysite nanotubes	Laccase	Covalent	• Enzyme loading 90 mg/g, • Retained activity 92.41% • Significant anti-proliferation potential against HepG2, H460 Hela, and AGS cells	Kim et al. (2018)
Protamine sulfate polyelectrolyte-Halloysite nanotube	Superoxide dismutase	Adsorption	• Antioxidants in heterogeneous samples	Katana et al. (2019)
Amino-, epoxy- and carbonyl- functionalized halloysite nanotubes	Aminoacylase	Adsorption	• Enzyme loading 176-178 mg/g • Superior chemical and thermal stability • Retained 50% activity after five reuse cycles	Kołodziejczak-Radzimska and Jesionowski (2019)
Halloysite nanotubes	Alkaline phosphatase	Adsorption	• Immobilization efficiency 27% • Enzyme loading 0.135 mg/mg • Enhanced pH and thermal stability	Pietraszek et al. (2019)
Poly (ethylene imine)-Halloysite nanotube assembly	β-lactamase	Encapsulation	• Enzyme loading ~100mg/g support • Superior pH stability • High catalytic activity as compared to enzyme directly adsorbed on films	Rouster et al. (2019)
Tannic acid functionalized	Laccase	Covalent	• Enzyme loading 197.7 mg/g	Zhang et al.

halloysite nanotubes			• Retained activity 55.4% • Superior pH and thermal stability • Retained 70% activity after 30 days storage time • Retained >60% activity after nine reuse cycles	(2019a)
Thiolated chitosan loaded super-magnetic halloysite nanotubes	Laccase	Covalent	• Enzyme loading 144 mg/g, • Retained activity 100% • Improved thermal, storage, and pH stabilities • Retained 61% activity after 15 reuse cycles	Kadam et al. (2020a)
Chitosan-Grafted Halloysite Nanotubes-Fe_3O_4 Composite	Laccase	Covalent	• Enzyme loading 100.12 mg/g • Retained activity 95.13% • Higher pH, temperature, and storage stabilities • Retained 59.88% activity after ten reuse cycles	Kadam et al. (2020c)
Halloysite nanotube in hydrogel	Lipase	Adsorption	• Enzyme loading 0.38 µg/g • Retained activity 121.43% • Superior pH and thermal stability • Retained 67.7% activity after 30 days storage time	Mohammadi et al. (2020)
Chitosan/halloysite beads	Laccase	Covalent	• Immobilization efficiency 94% • Retained 56% activity after 59 days storage time • Retained 49% activity after 15 reuse cycles	Hürmüzlü et al. (2021)
Chitosan functionalized Halloysite Nanotubes	Laccase	Covalent	• Immobilization efficiency 83.4% • Increased substrate affinity • Retained >95% activity after five reuse cycles	Tharmavaram et al. (2021)
Halloysite nanotube-cellulose nanocrystals matrix	β-galactosidase	Adsorption	• Immobilization efficiency 89.5% • Catalytic activity 0.384 U/mg • Superior thermal stability • Retained 75.8% activity after 60 days storage time • Retained ~76% activity after 12 reuse cycles	Tizchang et al. (2021)
Amino modified magnetic halloysite nanotube	Chloroperoxidase	Covalent	• Enzyme loading 90.18 mg/g • Superior thermal stability • Stable in presence of different organic solvents	Zhu et al. (2021)

			• Increased substrate affinity • Retained 92.20% activity after ten reuse cycles	
Magnetic halloysite nanotubes	Lipase	Covalent	• Effective immobilization • Superior reusability potential up to ten cycles • Higher catalytic efficiency	Budhiraja et al. (2022)
Aminosilane functionalized supermagnetic halloysite nanotubes	Protease	Covalent	• Enzyme loading 59.56 mg/g • Retained activity 87% • Excellent anti-biofilm activities	Kim et al. (2022a)
Halloysite nanotubes	Lipase	Ionic adsorption	• Immobilization efficiency 97.1% • Retained activity 83.81 U/g • 8.91-fold increase in half-life at 90 °C	Monteiro et al. (2022)
Dopamine-modified halloysite nanotubes porous microspheres	Peroxidase	Covalent	• Enzyme loading 250.8 mg/g • Superior pH and thermal stability • Retained 57.6% activity after six reuse cycles	Ren et al. (2022)
Aminopropyltriethoxysilane Functionalized Halloysite nanotubes	Endoinulinase	Covalent	• Immobilization efficiency 67.15% • Retained activity 57.20% • Wide range pH and temperature tolerance • 13-fold increase in half-life of enzyme • Retained ~50% activity after three reuse cycles	Singh and Singh (2022a)
Glutaraldehyde modified halloysite nanotubes	Endoinulinase	Covalent	• Immobilization efficiency 82.45% • Retained activity 65.77% • High affinity towards inulin than stachyose • Retained 100% activity after eight reuse cycles	Singh and Singh (2022b)
Hetero-modified halloysite nanotubes	Endoinulinase	Covalent	• Immobilization efficiency 89.61% • Retained activity 70.65% • Wide range pH and temperature tolerance	Singh and Singh (2022c)
Chitosan functionalized halloysite nanotubes	Laccase	Adsorption-covalent binding	• Enzyme loading 60.10 mg/g • Retained 48.56% activity after 28 days storage time • Retained 44.24%activity after eight reuse cycles	Wang et al. (2022b)

Chapter 3

Materials and Methods

3.1 Collection and Processing of Sugarcane Bagasse and Potato Peel Waste

Sugarcane bagasse (SCB) was procured from a local juice vendor in Patiala, Punjab, India (30.3398° N, 76.3869° E). Sugarcane bagasse was initially sun-dried for one-day and washed with hot water to remove dirt and other impurities. The semi-dried SCB was chopped into 40-50 mm pieces and dried in a hot air oven at 60 °C till achieves a constant weight. Dried SCB was milled using a blender and sieved to uniform particle sizes below 4 mm. Powdered SCB was refluxed in a soxhlet apparatus with a mixture of toluene: ethanol (2:1, v/v) for 6 h. The dewaxed SCB was further refluxed using deionized water for 30 min. The dewaxed sample was then oven dried at 60 °C and stored in air tight bags at room temperature (25 °C).

Potato peels were obtained from local restaurant in Patiala, Punjab and were initially washed with deionized water to remove surface dust particles. The peels were dried in an oven below 50 °C and were grinded to <0.5 mm particle size using blender. The powdered potato peel waste (PPW) was then stored in an airtight storage container at room temperature until use.

3.2 Synthesis of Magnetic Halloysite Nanotubes (MHNTs)

0.5 g halloysite nanotubes powder (Sigma Aldrich, USA) was added to a 100 mL deionized water. The suspension was placed in an ultrasonic bath (PCI analytics-9L), operated at 33±3 KHz for 5 min followed by 1 h stirring. A binary mixture of $FeCl_3.6H_2O$ and $FeCl_2.4H_2O$ (Sigma Aldrich, USA) having molar ratios 2:1 was introduced into the halloysite nanotubes (HNTs) suspension under vigorous stirring at 60 °C with nitrogen purging. The final pH of the suspension was kept in range of 9-10 adding ammonia solution (25% v/v) drop-wise. The appearance of black colour indicated the successful synthesis of magnetic nanoparticles. The mixture was further aged at 60 °C for 4 h and washed thrice with deionized water until the final pH of the suspension reached 7. The material was recovered from the reaction mixture using a magnet (Neodymium N42, surface gauss 2980). The extracted material was dried at 60 °C for 24 h, and kept in zip lock air tight bags till further use. The magnetic halloysite nanotubes will be referred as ‘MHNTs’ in subsequent studies. For the preparation of solid acid catalyst, an initial amount of Fe precursor was varied to achieve different loading of magnetic nanoparticles onto MHNTs surface. The initial amounts of the precursors used for MHNTs synthesis are listed in Table 3.1.

Table 3.1 Preparation of magnetic halloysite nanotubes varying the amount of HNTs and Fe precursor.

Sample name	HNTs (mg)	$FeCl_3.6H_2O$ (mg)	$FeCl_2.4H_2O$ (mg)	Total Fe precursor (mg)
1:0.1	500	36.56	13.44	50
1:0.2	500	73.12	26.88	100
1:0.4	500	146.24	53.76	200
1:0.8	500	292.48	107.52	400
1:1	500	365.60	134.40	500
1:2	500	731.19	268.81	1000

3.3 Pretreatment of Sugarcane Bagasse

Solid acid catalyst assisted pretreatment of sugarcane bagasse was performed. The following procedures were used for fabrication of solid acid catalyst and pretreatment of sugarcane bagasse.

3.3.1 Synthesis of Sulfonic Acid-Functionalized MHNTs as Solid Acid Catalyst

A previously reported method (Kumar et al. 2021b) was adopted for modifying MHNTs surface with desired modifications. In brief, MHNTs and 3-mercaptopropyl(trimethoxy)silane (Sigma Aldrich, USA) in 1:1 ratio were suspended in a 50 mL toluene and refluxed for 24 h. The magnetic product at the end of refluxing was washed with toluene to remove any loosely bound molecules. The as obtained mercapto functionalized MHNTs was dried at 60 °C for 24 h and designated as "MHNTs-SH". For the oxidization of mercapto groups, 1 g mercapto functionalized MHNTs was introduced into a solution containing 30% H_2O_2 (50 mL) and conc. H_2SO_4 (0.1 mL). The reaction mixture was stirred for two days. After required duration, the magnetic material was separated using a magnet, washed thrice with deionized water till the suspension attains neutral pH. The sulfonic acid functionalized MHNTs powder was dried at 60 °C for 24 h and termed as 'MHNTs-SO_3H'.

3.3.2 Pretreatment Reactions

1 g of dewaxed SCB was incubated in 100 mL screw cap flask with varying amount (0.1-0.5 g) of sulfonic acid-functionalized MHNTs in 10 mL distilled water. The flasks were then autoclaved (121 °C, 15 psi) for 15 min. The soluble fractions were isolated form the reaction

mixture via centrifugation (3000 rpm, 5 min) and kept for estimating xylose and inhibitory by-products. To the solid fraction left containing insoluble biomass and MHNTs-SO_3H, a 200 mL distilled water was added and the solid acid catalyst (MHNTs-SO_3H) were recovered magnetically. The solid biomass was filtered and dried overnight at 60 °C. The dried biomass (10% w/v solid loading) was further treated with 0.1% NaOH under identical reaction conditions. The treated mixture was filtered to obtain soluble fraction which was used for analysing the inhibitory by-products. The solid insoluble fraction was dried at 60 °C overnight and packed in air tight plastic bags either for compositional analysis or further use.

3.4 Characterisation of Sugarcane Bagasse

The weight of dried biomass before and after pretreatment was used to calculate pretreatment yield using the following equation:

$$\text{Pretreatment yield (\%)} = \frac{\text{Weight after pretreatment (mg)}}{\text{Weight before pretreatment (mg)}} \times 100 \qquad \text{Eq. 3.1}$$

3.4.1 Compositional Analysis

The compositional analysis of raw and pretreated SCB samples was done according to the laboratory analytical procedures (LAPs) developed by National Renewable Energy Laboratory, US, Department of Energy for the standard biomass analyses and also mentioned by Sluiter et al. (2008). In brief, a 300 mg biomass (both raw and pretreated samples) was introduced to a 3 mL sulfuric acid solution (72%) in separate containers and stirred for 1 min. The containers were then incubated for 60 min in a water bath at 30 °C for initiating the hydrolysis. After completion of the hydrolysis period, 84 mL deionized water was added bringing the acid concentration to 4% and the suspension was subsequently autoclaved (121 °C, 15 psi) for 60 min. The mixture obtained was filtered, where the filtrate was used for estimating soluble sugars and acid soluble lignin while the residue material was used to determine acid insoluble lignin.

The liquid hydrolysate samples were filtered through 0.22 μm syringe filters for sugar estimation. Polysaccharide contents (cellulose and hemicellulose) in raw and pretreated SCB samples were calculated from the amount of monosaccharaides present in the hydrolysates. Glucose, mannose, xylose and arabinose were determined by high performance liquid chromatography (Waters 515, Waters, USA) equipped with refractive index detector (Waters, 2414) with an amino column (250x4.6 mm, 5 micron) at 35 °C using water/acetonitrile

(87/13) as mobile phase at a flow rate of 1 mL/min. High purity standards of D (+) glucose, D (+) mannose, D (+) xylose, and L (+) arabinose were used to construct the standard curve. The calculations for cellulose recovery and hemicellulose removal were done using the following formula:

$$\text{Cellulose recovery (\%)} = \frac{\text{Cellulose in pretreated biomass (mg)}}{\text{Cellulose in raw biomass (mg)}} \times 100 \qquad \text{Eq. 3.2}$$

$$\text{Hemicellulose removal (\%)} = \frac{H_1 - H_2}{H_1} \times 100 \qquad \text{Eq. 3.3}$$

Where, H_1 is hemicellulose in raw biomass (mg), and H_2 is hemicellulose in pretreated biomass (mg).

Acid soluble lignin (ASL) was determined by measuring the optical density of filtrates at 240 nm using a UV-Vis spectrophotometer (UV-2600, Shimadzu Corp., Japan). The samples were diluted to the absorbance range of 0.7–1.0 using sulphuric acid (4%, v/v) which also served as the blank. The acid soluble lignin content of the biomass was calculated based on the Beer–Lambert law using formula:

$$\text{ASL (\%)} = \frac{Abs_{240} \times V}{\varepsilon \times W_i \times L} \times 100 \qquad \text{Eq. 3.4}$$

Where Abs_{240} is the absorbance of the solution at 240 nm; V is the total volume of the solution; ε is the absorptivity of biomass at specific wavelength (25 L/g-cm); W_i is the weight of sugarcane bagasse sample; L is the light path length.

For estimation of acid insoluble lignin (AIL), the residual obtained after filtration was transferred to a crucible, and dried at 105 °C until constant weight was achieved. The crucible along with the dried residue were weighed and placed in a furnace at 575 °C for 24 h. Subsequently the weight was determined to calculate the acid insoluble lignin using the following equation:

$$\text{AIL (\%)} = \frac{W_f}{W_i} \times 100 \qquad \text{Eq. 3.5}$$

Where, W_f is the weight of sample after furnace step; W_i is the weight of sugarcane bagasse sample.

Total lignin and lignin removal (%) were calculated using the following equations:

$$\text{Total lignin (\%)} = \text{Acid insoluble lignin (AIL)} + \text{Acid soluble lignin (ASL)} \qquad \text{Eq. 3.6}$$

$$\text{Lignin removal (\%)} = \frac{L_1 - L_2}{L_1} \times 100 \qquad \text{Eq. 3.7}$$

Where, L_1 is total lignin in raw biomass (mg), and L_2 is total lignin in pretreated biomass (mg).

The reuse potential of solid acid catalyst was also determined. The recovered solid acid catalyst (MHNTs-SO_3H) was washed thrice with deionized water and dried at 60 °C for 24 h. The dried solid acid catalyst was used for the pretreatment of fresh sugarcane bagasse over 5 consecutive cycles. The reuse capability was assessed by estimating the xylose produced after each cycle.

3.4.2 Material Characterization

Fourier Transform Infrared (FTIR) Spectroscopy Analysis

The variations in the chemical composition and functional moieties of raw sugarcane bagasse after pretreatment were examined using Fourier transform infrared (FTIR) spectroscopy (Cary 630 FTIR, Agilent Technologies, USA). Raw and pretreated biomass samples were mixed with dried KBr in ratio 1:100 (w/w), and pellets were made using hydraulic press. Spectra were recorded from 4000 cm^{-1} to 400 cm^{-1} at 25 °C with 32 scans at a spectral resolution of 4 cm^{-1}.

X-ray Diffraction (XRD) Analysis

The crystallinity of raw and pretreated SCB samples were determined using X-ray diffractometer, (PANalytical X-pert Pro, The Netherlands). The X-ray diffraction with λ (Cu $K\alpha_1$) = 1.5406 Å and λ (Cu $K\alpha_2$) = 1.5444 Å was operated at 45 kV voltage and 40 mA current. The relative diffracting intensity was recorded in the scanning angle rang of 2θ = 5–45° at the scanning speed of 2° per min. The crystallinity index (CrI) of biomass samples were determined from the XRD data and calculated using the following equation (Segal et al. 1959):

$$\text{CrI (\%)} = \frac{I_{002} - I_{AM}}{I_{002}} \times 100 \qquad \text{Eq. 3.8}$$

Where, I_{002} is max diffraction intensity of the crystalline portion of the biomass (cellulose) around 2θ=21-23°, and I_{AM} is the diffraction intensity of amorphous region (hemicellulose, and lignin) around 2θ=16-18°.

Scanning Electron Microscopy (SEM) Analysis

Any changes in morphological features of sugarcane bagasse samples after pretreatment were observed using SEM (JSM-6510LV, JEOL, Japan) operated at an acceleration voltage of 15 kV. The samples were initially coated through gold sputtering and then placed on an aluminium stub with carbon tape for the scanning.

3.5 The Analysis of Inhibitory by-products

The wash liquid fractions obtained after pretreatment steps were used for the estimation of inhibitory by-products. Total phenolic contents in different wash liquids were determined by Folin-Ciocalteu assay using gallic acid as the standard and were expressed as gallic acid equivalents (g GAE/L) (Kupina et al. 2018). In brief, 1 mL wash liquid was diluted using 15 mL deionised water and 1 mL Folin-Ciocalteu reagent. The solution was mixed properly and 3 mL sodium carbonate solution (20% w/v) was added. The suspension was then incubated at 30 °C for 120 min, and optical density was measured at 765 nm using a UV-Vis spectrophotometer. Total carboxylic acid content (acetic acid, formic acid, levunic acid etc.) of wash liquids was determined using a titration method (Ilanidis et al. 2021b). For this, 3-4 drops of phenolphthalein indicator were added into the liquid samples (5 mL) and the resultant solution was titrated against 200 mM aqueous solution of sodium hydroxide. The wash liquids were filtered using 0.22 μm syringe filters, and analysed using HPLC system equipped with a C18 column and diode-array detector to determine furans derivatives (furfural and hydroxymethylfurfural) concentrations. The mobile phase used was an aqueous solution of methanol and water (4:6) with flow rate of 1 mL/min, and column temperature was set at 35 °C. The standard curves of pure furfural and hydroxymethylfurfural (HMF) were used for quantification.

3.6 Enzymatic Hydrolysis, Glucose Estimation and Saccharification

Enzymatic Hydrolysis of Sugarcane Bagasse

The raw and pretreated sugarcane bagasse samples were subjected to enzymatic hydrolysis using cellulase from *Aspergillus niger* (Sigma Aldrich, USA). The hydrolysis experiments were performed in 250 mL Erlenmeyer flasks containing 100 mL citrate buffer (0.05 M, pH=5) and 1, 2.5, and 5 g dried biomass to achieve 1, 2.5, and 5% w/v substrate loading, respectively. The flasks were agitated at an orbital shaker (150 rpm, 50 °C), and cellulase (20 IU/g substrate) was introduced. Aliquots were withdrawn after 6, 12, 24 and 48 h, and heated

for 5 min at 90 °C for inactivation of cellulase enzyme. The aliquots were then filtered through 0.22 µm syringe filters, and analyzed for the amount of glucose produced.

Glucose Estimation

The glucose produced after hydrolysis was estimated using the dinitrosalicyclic acid (DNSA) method (Miller 1959). Briefly, 3 mL DNSA reagent was added to 1 mL aliquot and placed in a boiling water bath for 15 min. The solution was allowed to cool down to room temperature and the absorbance was recorded at 540 nm. A standard curve of glucose was used for quantification of glucose in the samples.

Cellulose Saccharification

Cellulose saccharification (%) was calculated using the following equation:

$$\text{Saccharification (\%)} = \frac{W_g \times 0.89}{W_c} \times 100 \qquad \text{Eq. 3.9}$$

Where, W_g is weight of glucose produced; the factor 0.89 was used to convert polysaccharide to monosaccharide accounting for water uptake during hydrolysis; W_c is weight of cellulose in the biomass.

3.7 Microbial Fermentation and Ethanol Production

The hydrolysates produced using raw and pretreated sugarcane bagasse samples were tested as substrate for bioethanol production using *Saccharomyces cerevisiae* (MTCC170). For inoculum preparation, lyophilised yeast culture was activated using YPD medium, composed of yeast extract (1%), peptone (2%) and dextrose (2%) and incubated under agitation for 24 h (30 ºC, 200 rpm). The cell count of actively growing *S. cerevisiae* was measured using haemocytometer, corresponding to 300×10^6 cells/mL.

Microbial fermentation (working volume 100 mL) was done in pre-sterilized Erlenmeyer flasks with screw caps. The earlier obtained hydrolysate was transferred to Erlenmeyer flasks, supplemented with yeast extract (0.5%), KH_2PO_4 (0.2%), $MgSO_4$ (0.1%) and pH 5.6. A 5% (v/v) of *S. cerevisiae* as inoculum was added to individual flasks for fermentation. The flasks were incubated in an orbital shaker (30 °C, 150 rpm) for 72 h. During fermentation, aliquots were periodically collected after 24, 48 and 72 h, to quantity the ethanol content.

Ethanol produced during fermentation process was estimated by chromic acid method (Caputi et al. 1968) after distilling the aliquots withdrawn at different time intervals. Distillate (0.5 mL) was mixed with 25 mL potassium dichromate and the solution was incubated in water bath at 80 °C for 15 min. After cooling, the optical density was measured at 600 nm. Ethanol/water (v/v) was used to prepare the standard curve for ethanol estimation.

3.8 Fabrication of Cellulase Nanobiocatalyst (cellulase-MHNTs)

For cellulase immobilization the surface-functionalized MHNTs were generated in two steps. First, amine-modified MHNTs prepared through aminosilane grafting were exposed to glutaraldehyde activation for coupling enzymes (cellulase).

3.8.1 Synthesis of Amino-Functionalized MHNTs

Amino-functionalization of magnetic halloysite nanotubes (MHNTs) was done using an established protocol with slight modifications (Agnihotri et al. 2013). In brief, 2 mL APTES ((3-aminopropyl) triethoxysilane) was added into 98 mL solution of absolute ethanol and acetic acid (5: 3 v/v), stirred vigorously at 60 °C for 15 min. One gram of magnetic halloysite nanotubes were then introduced into the solution under inert atmosphere, followed by sonication for 20 min and stirring at 60 °C for 2 h. The condensation of siloxane bonds was carried out by heating the mixture solution at 120 °C for 60 min. Resultant amine-modified MHNTs were separated using magnet, washed thoroughly with ethanol/acetic acid solution to remove the excess organosilane (APTES) and were finally dried overnight at 60 °C.

3.8.2 Glutaraldehyde Activation on Amine-modified MHNTs

Glutaraldehyde (10 mL, 2.5% v/v) solution was prepared by diluting the commercial glutaraldehyde (25%) in citrate buffer (0.1 M, pH 5). The amino-modified MHNTs were incubated in prepared glutaraldehyde solution, and left for shaking at 120 rpm for 24 h. The resultant glutaraldehyde activated MHNTs were separated from the solution using a magnet and washed several times using citrate buffer to remove the loosely bounded glutaraldehyde molecules.

3.8.3 Optimization of Cellulase Immobilization

Cellulase immobilization optimization was done by screening the critical parameters involved in immobilizations process using single factor study, followed by employing the screened

parameters and their corresponding range in RSM for high loading of cellulase onto magnetic halloysite nanotube-based support matrix. Cellulase immobilization was performed by incubating an appropriate amount of glutaraldehyde-activated amine-modified MHNTs, and cellulase in a buffer solution of appropriate pH (0.1 M, citrate buffer for pH range 4-5, and phosphate buffer for pH 6) under shaking conditions (120 rpm) for 6 h.

Single Factor Study

The three key parameters involved in the immobilization reaction process i.e., amount of support matrix, concentration of cellulase enzyme, and pH of the reaction solution, were investigated by varying one factor while keeping other two factors constant. The amount of glutaraldehyde activated amine modified MHNTs as support matrix was investigated in the range 5-40 mg. The impact of loaded enzyme on corresponding activity was studied separately for better understanding of the complex interaction of densely packed enzyme and activity. The concentration of cellulase enzyme was varied from 0.5 mg/mL to 2.5 mg/mL. The examined range of solution pH was 4-6. Enzyme loading (%) was evaluated for all the reactions and range of individual parameter resulting in high cellulase loading were selected for further optimization.

Response Surface Methodology (RSM)

Design Expert tool (version 6.0.8, Stat-Ease Inc., Minneapolis, USA) was used for experiment designs and statistical analysis. Response Surface Methodology (RSM) is a widely acceptable method for the optimization of system dealing with three or more than three variables (Gunst 1996). The correlation between independent process parameters (support amount, cellulase concentration and pH) and response (cellulase loading%) was determined using a three level, three factor Box-Behnken design (BBD) of response surface methodology (RSM). The optimization for cellulase immobilization were performed by employing varied amount of support (20-30 mg), cellulase concentration (1.25-1.75 mg/mL) prepared in citrate buffer, maintained at varied pH (4.5-5.5). The effective range of parameters obtained from single factor study was coded as -1 (low level), 0 (central point or middle level), and 1 (high level). The factors and their levels studied for cellulase loading onto magnetic matrix are presented in Table 3.2.

Table 3.2 Levels and ranges of independent variables in Box–Behnken experiment design.

Independent variable	Symbol	Coded variable level		
		Low -1	Centre 0	High +1
Support amount (mg)	A	20	25	30
Cellulase conc. (mg/mL)	B	1.25	1.5	1.75
Solution pH	C	4.5	5.0	5.5

The Box-Behnken design (BBD), gave total 13 combinations of independent variables with five replicates at the centre point (total 17 experiments) (Table 3.3). Experiments were performed in triplicates and obtained cellulase loading (%) results for were filled in the experimental table as actual response. Based on the response filled, the quadratic model was suggested for the adequate modelling of the experimental data.

Cellulase loading (%) was represented as a second order polynomial equation to express the effect of different variables:

$$Y = \beta_0 + \sum \beta_i X_i + \sum \beta_{ii} X_i^2 + \sum \beta_{ij} X_i X_j \qquad \text{Eq. 3.10}$$

Where Y= Cellulase loading (%), Xi and Xj = independent variables which affect Y. The regression coefficient was defined as β_0 for the intercept, β_i for linear, β_{ii} for quadratic and β_{ij} for cross product terms.

Table 3.3 RSM based Box-Behnken experimental design for independent variables and their corresponding response (Cellulase Loading (%)) for cellulase immobilization.

RUN	Support amount (mg)	Cellulase conc. (mg/mL)	Solution pH	Loading (%)	
				Actual	Predicted
1	25.00	1.25	5.50	72.82	72.04
2	25.00	1.50	5.00	79.82	78.14
3	20.00	1.50	4.50	77.35	76.38
4	25.00	1.25	4.50	70.31	70.34
5	25.00	1.50	5.00	78.64	78.14
6	20.00	1.50	5.50	72.38	72.19
7	25.00	1.50	5.00	77.97	78.14
8	25.00	1.75	4.50	67.78	68.57
9	20.00	1.25	5.00	74.83	75.81
10	25.00	1.50	5.00	78.02	78.14
11	25.00	1.75	5.50	65.68	65.71
12	25.00	1.50	5.00	76.27	78.14
13	30.00	1.50	5.50	80.48	81.45
14	30.00	1.25	5.00	79.87	79.68
15	20.00	1.75	5.00	69.78	69.97
16	30.00	1.50	4.50	78.24	78.43
17	30.00	1.75	5.00	78.39	77.42

The generated model was evaluated using analysis of variance (ANOVA) for adequacy of model. ANOVA is a statistical diagnostic tool to estimate the performance of tested experiments, by taking into account p-value, lack of fit, multiple correlation coefficients (R^2) and adjusting coefficient of determination (R^2-adj). The designed model was simplified by eliminating parameters or their combinations that were not regarded as statistically significant by the analysis of variance (ANOVA). The model was then validated by performing experiments at the optimum variable conditions for high cellulase loading (%).

Optimal Immobilization Condition

The immobilization reaction was carried out at optimized conditions obtained using BBD of RSM in brief, 20 mg of MHNTs were introduced in 1.44 mg/mL cellulase suspension (citrate buffer, 4.8 pH) and were shaken (120 rpm) continuously at 4 °C for 6 h. The cellulase immobilized MHNTs (cellulase-MHNTs) were separated from the reaction mixture with the help of a magnet followed by washing using the same buffer to remove unbound cellulase enzyme. The cellulase-MHNTs were then stored in citrate buffer (0.1 M, pH 5) at 4 ºC till further use. Residual enzyme concentration in the supernatant was used to determine the extent of enzyme loading.

3.9 Enzyme Loading, Activity and Release Profile

Enzyme Loading

The concentration of enzyme remained in the suspension after immobilization process, was analyzed using Bradford assay (Bradford 1976). Briefly, 5 mL of Bradford reagent was added to 1 mL suspension solution. After 3 minutes, the absorbance of the solution was measured at 595 nm, and protein concentration was determined using a standard curve of bovine serum albumin. Enzyme loading (%) was calculated using the following equation:

$$\text{Enzyme loading (\%)} = \frac{C_0 - C}{C_0} \times 100 \qquad \text{Eq. 3.11}$$

The enzyme loading (mg/g) on support matrix was calculated using the following expression:

$$\text{Enzyme loading (mg/g)} = \frac{(C_0 - C)V}{W} \times 100 \qquad \text{Eq. 3.12}$$

Where C_0 and C are initial and final concentration of enzyme in suspension, V is solution volume in mL, and W is the weight of support used in g.

Cellulase Activity

Endoglucanase activity of cellulase enzyme was determined according to the standard procedure of IUPAC using carboxymethyl cellulose (CMC) as substrate (Hosseini et al. 2018). The cellulase enzyme (0.5 mL) was incubated with 1.5 mL CMC substrate (1 wt%) prepared in citrate buffer (0.1 M, pH=5) at 50 °C for 1 h. The reaction after incubation was stopped by putting the enzyme reaction flask in a boiling water bath for 10 min. The solution was centrifuged (5000 rpm, 5 minutes), and supernatant was used to calculate the amount of reducing sugar liberated by DNSA method as described earlier. One international unit (IU) of enzyme activity is defined as the amount of cellulase that hydrolyses CMC to produce 1 μmol of glucose per minute under standard assay conditions. The catalytic activities of both free and immobilized enzymes carrying equivalent units (2.43 IU) were determined under identical set of experimental conditions.

Release Profile

The effectiveness of immobilization approach was assessed by means of enzyme leached/released from its immobilized state. For release profile, 20 mg cellulase-MHNTs was stirred vigorously (250 rpm) in 10 mL citrate buffer, at 50 °C for 48 h. Aliquots were taken at predefined intervals and the amount of cellulase released was calculated using Bradford assay as explained previously.

3.10 Impact of Process Parameters on Cellulase Activity

The impact of varying process parameters i.e., pH and reaction temperature, storage time on the catalytic activity of free and immobilized cellulase was investigated. The optimum reaction conditions obtained from this study were used for further processing of nanobiocatalyst (cellulase-MHNTs).

Impact of pH

To assess the influence of solution pH on the catalytic potential of free and immobilized cellulase, a wide pH ranges from pH 3 to pH 7 was examined. Equivalent units of both forms of cellulase (6.07 IU) were incubated separately with 50 mL substrate (CMC, 1wt%) in different pH buffers (0.1 M citrate buffer for pH range 3-5, 0.1 M phosphate buffer for pH 6-7), at 50 °C for 30 min. After the incubation period, the catalytic activities of individual samples were determined by reducing sugar estimation using DNSA method described

earlier. The individual highest catalytic activities for both forms were considered 100%, and activities at other pH points were calculated relative to this.

Impact of Temperature

Temperature profile of cellulase (both free and immobilized) was evaluated to determine the temperature well suited for high catalytic activity and deviation in catalytic activity with change in temperature. Free and immobilized forms (6.07 IU of both) were incubated with 50 mL CMC (1wt%, pH 5) in temperature range 30-70 °C for 30 min. The reducing sugar liberated at different temperatures was calculated as per the protocol described earlier. Highest activity obtained was considered 100% and activities at other temperatures were expressed relative to it.

Impact of Storage Time

The extent of time till cellulase enzyme can retain significant amount of its initial catalytic activity was determined by incubating both forms of cellulase in citrate buffer (0.1 M, pH 5) at 4 ºC for 20 days. Aliquots were taken at specific interval of time and the activity assays were carried out as per the protocol described earlier. The initial activity (day one) was considered 100%, and activities on subsequent days were measure relatively.

3.11 Reusability of Cellulase Nanobiocatalyst

The nanobiocatalyst (cellulase-MHNTs) was assessed for its reuse capacity for seven repetitive cycles of CMC hydrolysis. Briefly, immobilized cellulase containing 6.07 IU was introduced in 50 mL CMC solution (1 wt%, pH 5) for 6 h at 50 °C under continuous stirring at 120 rpm. After 6 h, nanobiocatalyst (NBC) was retrieved using a magnet from the solution, and the solution was used for estimation of released glucose using DNSA method. The NBC was washed twice with citrate buffer (0.1 M, pH 5) and then introduced into fresh CMC solution under conditions similar to first cycle. The activity obtained in first cycle was denoted as 100%, and activities during the following cycles were expressed as relative activity. Equivalent units of free enzyme were also incubated under similar conditions for 42 h to assess the impact of immobilization on overall glucose production.

3.12 Kinetics and Thermodynamic Parameters of Free and Immobilized Cellulase

To determine the changes in catalytic activity and stability after immobilization, kinetic and thermodynamic parameters of both free and immobilized cellulase were calculated using the following methods;

Kinetic Parameters

The initial product formation rate for both free and immobilized cellulase were determined by varying the substrate concentrations while keeping the enzyme load constant. The obtained initial product formation rate (V) and substrate concentrations (S) were used to plot Lineweaver–Burk plot (or double reciprocal plot) plots for free and immobilized cellulase. Kinetic parameters i.e., k_M, V_{max} were then obtained from non-linear regression fitting. Catalytic efficiencies (V_{max}/k_M) for both free and immobilized cellulase were also calculated.

Thermodynamic Parameters

Thermodynamic parameters were estimated by thermal irreversible inactivation of free and immobilized cellulase at different temperatures. In brief, both form of cellulase were incubated in citrate buffer (0.1 M pH 5) at various temperatures i.e., 50 °C, 60°C and 70°C for 6 h. Aliquots were taken after 1, 2, 3, 4, 5, and 6 h, cooled on ice for 30 minutes, and mixed with CMC substrate at 50°C for cellulase catalytic activity assay, as described in section 3.10.7. The activity before incubation at higher temperatures was calculated and considered 100%, residual activity was calculated relative compared to this.

Residual activities with time were fitted to first order plot and stability of cellulase under different temperatures was expressed as deactivation constant (k_d), and half-life ($t_{1/2}$), calculated as follows:

$$\ln\left[\frac{A}{A_0}\right] = -k_d t \qquad \text{Eq. 3.13}$$

$$t_{1/2} = \frac{0.693}{k_d} \qquad \text{Eq. 3.14}$$

Where A is residual activity at time t, A_0 is activity at the start, t is the time (h).

Decimal reduction time (D), which is defined as the time at which initial activity is reduced by 90 %:

$$D = \frac{\ln(10)}{k_d} \quad \text{Eq. 3.15}$$

The impact of temperature on cellulase was also correlated through deactivation rate constant using Arrhenius equation:

$$-\ln k_d = \frac{E_d}{R}\left[\frac{1}{T}\right] - \ln A \quad \text{Eq. 3.16}$$

Where E_d is the activation energy for thermal denaturation (KJ/mol), A is residual activity, R is the universal gas constant (8.314 J/mol·K), and T absolute temperature (K).

Based on the transition energy state model, the Eyring equation correlates enzyme catalysis with temperature. The change in Gibbs free energy (ΔG), enthalpy (ΔH), and entropy (ΔS) for thermal denaturation of cellulase were calculated as follows:

$$\Delta G = -RT\ln\left[\frac{hk_d}{k_B T}\right] \quad \text{Eq. 3.17}$$

$$\Delta H = E_d - RT \quad \text{Eq. 3.18}$$

$$\Delta S = \frac{\Delta H - \Delta G}{T} \quad \text{Eq. 3.19}$$

Where E_d is the activation energy for thermal denaturation (KJ/mol), R is the universal gas constant (8.314 J/mol/K), T is the absolute temperature (K), k_d is the deactivation rate constant (h^{-1}), h is the Planck constant (6.626×10^{-34} J·s) and k_B is the Boltzmann's constant, (1.381×10^{-23} J/K).

3.13 Impact of Ionic Liquid on Cellulase Inactivation

Ionic liquids are commonly used for pretreatment and dissolution of cellulose, hence the impact of 1-butyl-3-methylimidazolium chloride ([bmim][Cl] as model ionic liquid, on catalytic activity of free and immobilized cellulase was investigated. Equivalent units (6.07 IU) of both free and immobilized cellulase were incubated for 3 h with different concentrations of [bmim][Cl] (5%, 10%, 20%, 30% v/v) maintained at pH 5 using citrate buffer. After incubation the catalytic activity of both forms were evaluated using two substrates, CMC and pretreated sugarcane bagasse. The activity in absence of ionic liquid was considered 100%, other activities were expressed relatively.

3.14 Cellulose Saccharification Capability

To demonstrate, the practical applicability immobilized cellulase (nanobiocatalyst) was tested for cellulose saccharification. The impact of change in the substrate was also examined, using two different substrates CMC and pretreated sugarcane bagasse. Nanobiocatalyst carrying 12.14 IU of cellulase was incubated in 100 mL substrate (1%, w/v) for 48 h at 50 ºC with continuous shaking (120 rpm). The reaction using free cellulase under identical condition as control was also performed. Aliquots were taken at different intervals and glucose amount produced was assessed using glucose assay kit and the cellulose saccharification (%) was calculated using the following equation:

$$\text{Saccharification (\%)} = \frac{\text{Sugar (g)} \times 0.89}{\text{Cellulose (g)}} \times 100\% \qquad \text{Eq. 3.20}$$

3.15 Continuous Production of High Fructose Syrup

The continuous-flow transformation glucose into fructose was performed in a packed bed reactor (Figure 3.1). The reactor 15 cm x 1 cm (HxD) was used in vertically inverted form where the substrate was pumped upwards using a peristaltic pump. Water from a hot water bath was circulated in outside the reactor walls to control reaction temperature (70 ºC) of whole system.

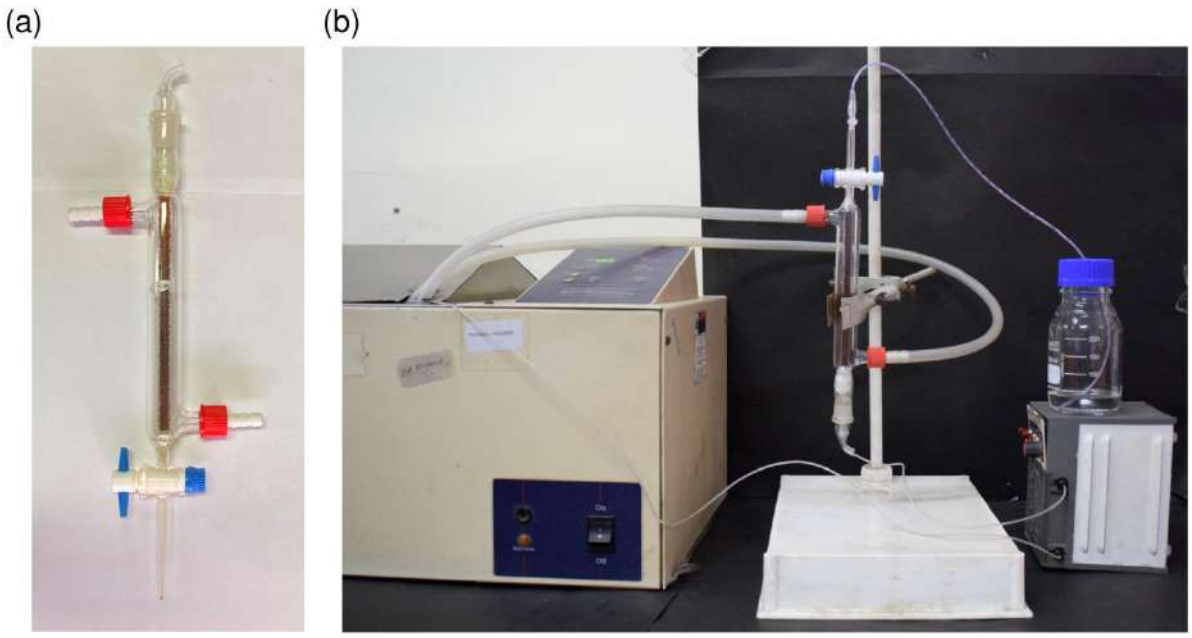

Figure 3.1 Photographic image of (a) Double jacketed reactor packed with immobilized glucose isomerase, and (b) Real-time setup for glucose conversion.

The bed volume of the reactor was 11.78 mL, and a total of 2.1 g immobilized glucose isomerase (Sigma-Aldrich, ≥350 U/g) was packed inside the reactor. Void volume of the packed reactor was found to be 5.23 mL. The substrate solution, augmented with 10 mM Mg^{2+} and 1 mM Co^{2+} was pumped into the packed reactor. Fructose produced was estimated using fructose assay kit. Parameters affecting the conversion (%) were optimised using single factor study and response surface methodology (RSM).

Single Factor Study

The impact of flow rate (0.1-1 mL/min), pH of the reaction (7-9), and temperature of the reaction (50-70 °C) on glucose to fructose conversion (%) were studied using the packed bed reactor. The effective range of individual process parameters resulting in the highest conversion (%) was assessed by varying one factor while keeping the other two factors constant. The range obtained was used for further optimization using RSM.

Experimental Design, Optimization and Statistical Analyses

The combinational impact of independent process parameters on the final outcome can be statistically gauged using RSM. Experiment design and statistical analysis was performed by Design Expert tool (version 6.0.8, Stat-Ease Inc., Minneapolis, USA). Three factors on three levels-based Box-Behnken design (BBD) of response surface methodology (RSM) was employed using independent variable ranges i.e., flow rate (0.1-0.4 mL/min), pH (8-9), and temperature (57.5-62.5 °C). Glucose to fructose conversion (%) was taken as response. The factors and their levels studied for cellulase loading onto magnetic matrix are presented in Table 3.4.

Table 3.4 Levels and ranges of independent variables in Box–Behnken statistical experiment design.

Independent variable	**Symbol**	**Coded variable level**		
		Low -1	Centre 0	High +1
Flow rate (mL/min)	A	0.1	0.25	0.4
pH	B	8	8.5	9
Temperature (°C)	C	57.5	60	62.5

Table 3.5 shows the experimental design and the response data obtained from the 17 trial runs including 12 factorial points and 5 replicates at the center point.

Table 3.5 RSM based Box-Behnken experimental design for independent variables and their corresponding response (conversion (%)) for high fructose syrup production using a packed bed reactor.

RUN	Flow rate (mL/min)	pH	Temperature (°C)	Conversion (%)	
				Actual	Predicted
1	0.25	8	57.5	40.12	40.02
2	0.25	9	57.5	40.64	40.70
3	0.1	8	60	46.55	46.67
4	0.25	8.5	60	46.52	46.46
5	0.4	8	60	41.16	41.20
6	0.25	8.5	60	46.12	46.46
7	0.4	9	60	42.37	42.25
8	0.4	8.5	62.5	42.83	42.85
9	0.1	8.5	62.5	47.24	47.18
10	0.25	8.5	60	46.75	46.46
11	0.1	8.5	57.5	46.81	46.79
12	0.25	8.5	60	46.22	46.46
13	0.4	8.5	57.5	40.42	40.48
14	0.1	9	60	47.49	47.45
15	0.25	9	62.5	42.21	42.31
16	0.25	8.5	60	46.68	46.46
17	0.25	8	62.5	41.23	41.17

Based on the response, the quadratic model was suggested for the adequate modelling of the experimental data. Conversion (%) from glucose to fructose was represented as a second order polynomial equation to express the effect of different variables:

$$Y = \beta_0 + \sum \beta_i X_i + \sum \beta_{ii} X_i^2 + \sum \beta_{ij} X_i X_j \qquad \text{Eq. 3.21}$$

Where Y= Conversion (%) , Xi and Xj = independent variables which affect Y. The regression coefficient was defined as β_0 for the intercept, β_i for linear, β_{ii} for quadratic and β_{ij} for cross product terms.

The statistical significance and other relevant parameters such as lack of fit, multiple correlation coefficients (R^2), and adjusting coefficient of determination (R^2-adj) of tested parameters and their interactions were assessed by analysis of variance (ANOVA). Contour and 3D plots were extracted to understand the relationship and interactions of independent variables with the response (conversion %). The software-proposed values of process parameters for maximum conversion (%) were used to conduct experiments using packed bed reactor. The obtained conversions (%) at different combinations were then compared with predicted values by the model to validate the model ability for this experiment.

Optimal Conversion Condition

The optimum reaction conditions for highest glucose conversion (%) generated by the model was 0.11 mL/min flow rate, 8.43 pH and 60.52 °C temperature. Isomerisation reaction was carried out on the mentioned parameters and the obtained results were compared with the result predicted by the model.

3.16 Fabrication of α-amylase Nanobiocatalyst

For α-amylase immobilization the surface-functionalized MHNTs were generated via dopamine functionalization.

3.16.1 Dopamine Functionalization of Magnetic Halloysite Nanotubes (MHNTs)

Magnetic halloysite nanotubes were functionalized with dopamine as reported earlier (Chao et al. 2013) with slight modifications. In brief, 300 mg MHNTs were dispersed in 50 mL Tris-HCl buffer (0.05 M, pH 8.5) and sonicated for 60 min. Dopamine hydrochloride (0.3 mg) was then introduced into MHNTs solution and the mixture was kept in an orbital shaker for 6 h to obtain polydopamine-coated MHNTs. The solid was separated using a magnet and repeatedly washed with Tris-HCl buffer until the filtrate became colourless and transparent. The obtained powder was dried overnight at 40 °C and denoted as *d*-MHNTs.

3.16.2 Optimization of α-amylase Immobilization

For immobilizing α-amylase, the factors influencing enzyme loading (%) were initially screened using single factor studies to find the effective range. The factors and their range demonstrate critical impact on the extent of α-amylase loading onto *d*-MHNTs. The parameters were then optimised using Box Behnken design of response surface methodology to obtain the most suitable reaction conditions for high α-amylase loading.

Single Factor Studies

Four parameters which might have impact on enzyme loading namely, amount of *d*-MHNTs, amount of α-amylase, pH of immobilization process, and temperature were investigated. Single factor studies were carried out to assess their effective range, by varying a single parameter value while keeping other reaction parameters constant. The ranges of individual parameters were as follows: *d*-MHNTs amount (20-100 mg), α-amylase amount (10-50 mg), pH (5.5-7.5) and temperature (20-50 °C).

Response Surface Methodology (RSM)

Experiment design and statistical analysis were employed to determine reaction parameters imposing direct/indirect impact on the outcome i.e., enzyme loading using "Design Expert" (version 6.0.8, Stat-Ease Inc, Minneapolis, USA). Box-Behnken design (BBD) of response surface methodology (RSM) was employed to design the set of experiments. Based on single factor studies, three parameters, i.e., *d*-MHNTs amount (mg), temperature (°C), and α-amylase load (mg) were used to determine optimum reaction condition. The factor level was coded as -1 (low), 0 (central point), and +1 (high) for all three parameters, as shown in Table 3.6.

Table 3.6 Levels and ranges of independent variables in Box–Behnken statistical experiment design.

Independent variable	**Symbol**	**Coded variable level**		
		Low -1	Centre 0	High +1
d-MHNTs (mg)	A	50	60	70
Temperature (°C)	B	30	35	40
α-amylase (mg)	C	10	15	20

Seventeen sets of experiments were designed using "Design Expert" software. All the experiments were conducted in triplicates and average values were filled in the response column (Table 3.7). The statistical significance and other relevant parameters such as lack of fit, multiple correlation coefficients (R^2), and adjusting coefficient of determination (R^2-adj) of tested parameters and their interactions were assessed by analysis of variance (ANOVA).

The response generated by model i.e., α-amylase loading (%) as a function of studied variables, was represented in the form of a second-order polynomials equations:

$$Y = \beta_0 + \sum \beta_i X_i + \sum \beta_{ii} X_i^2 + \sum \beta_{ij} X_i X_j \qquad \text{Eq. 3.22}$$

Where Y= α-amylase loading (%), X_i and X_j = independent variables which affect Y. The regression coefficient was defined as β_0 for the intercept, β_i for linear, β_{ii} for quadratic and β_{ij} for cross product terms.

Table 3.7 Box-Behnken experimental design for variables and their corresponding response (% loading) for α-amylase immobilization onto *d*-MHNTs.

RUN	*d*-MHNTs (mg)	Temperature (°C)	α-amylase (mg)	Loading (%)	
				Actual	Predicted
1	60.00	35.00	15.00	66.27	66.32
2	70.00	40.00	15.00	67.19	66.56
3	60.00	40.00	10.00	70.72	70.47
4	70.00	30.00	15.00	62.88	62.98
5	60.00	30.00	10.00	67.04	66.07
6	50.00	40.00	15.00	63.29	63.19
7	60.00	40.00	20.00	61.07	62.04
8	60.00	35.00	15.00	65.92	66.32
9	50.00	30.00	15.00	56.18	56.80
10	60.00	35.00	15.00	67.11	66.32
11	60.00	30.00	20.00	56.24	56.49
12	70.00	35.00	20.00	59.19	58.84
13	50.00	35.00	10.00	62.72	63.07
14	60.00	35.00	15.00	66.83	66.32
15	60.00	35.00	15.00	65.49	66.32
16	50.00	35.00	20.00	55.02	54.15
17	70.00	35.00	10.00	67.06	67.93

The model was used to obtain theoretical reaction conditions, optimum for high α-amylase loading (%) and experiments were performed on suggested reaction conditions to gauge the efficiency of the model.

Optimal Immobilization Condition

Based on BBD-lead experiments design, the optimized reaction conditions for immobilizing α-amylase were as follows; 62.48 mg *d*-MHNTs were homogeneously dispersed in 20 mL phosphate buffer (0.05 M, pH 6.5), and 17.91 mg α-amylase (165 IU/mg) was introduced into the solution. The solution was left in a shaker (40 °C) for immobilization reaction to proceed. The enzyme-loaded *d*-MHNTs were magnetically recovered and washed with buffer solution to remove loosely bound enzymes. The obtained α-amylase immobilized *d*-MHNTs were stored at 4 °C till further use.

3.17 Enzyme loading, Activity and Leaching

Enzyme Loading

The extent of α-amylase loading onto *d*-MHNTs was calculated by measuring the concentration of α-amylase that remained in the suspension after removing immobilized α-amylase using the Bradford assay as described earlier.

α-amylase Activity

The amylolytic activity of α-amylase was determined through the production of reducing sugars using starch (1% w/v) as the substrate. Fresh stocks of starch and α-amylase were prepared in phosphate buffer (0.05 M, pH 6.5) and incubated at 40 ºC for reaction initiation. Aliquots were withdrawn after required intervals, and the amount of reducing sugars was quantified using the dinitrosalicylic acid (DNSA) method. One unit (IU) of enzyme activity is defined as the amount of enzyme required to liberate one µmol of reducing sugar per minute under standard conditions. Free and immobilized α-amylase possessing equivalent units of α-amylase were exposed to identical reaction conditions to determine the retained catalytic activity. The activity of the free enzyme was considered 100%.

Leaching

The 'efficiency' of immobilization in terms of enzyme leachability was evaluated by suspending 100 mg nanobiocatalyst (*d*-MHNTs/α-amylase) in a 10 mL phosphate buffer (0.05 M, pH 6.5) supplemented either with 1.0 M NaCl or 1.0% (v/v) Triton X-100 as separate studies. The incubation period was 12 h at room temperature (25° C) under orbital shaking (250 rpm). Afterward, the nanobiocatalyst was carefully removed using a magnet (Neodymium N42, surface gauss 2980) and protein concentration in the supernatant was determined using Bradford's method. The protein present as supernatant would be the leached enzyme desorbed from the surface, whose proportion (%) relative to the total immobilized enzyme was estimated.

3.18 Impact of Process Parameters on α-amylase Activity

The optimum reaction condition for catalytic activity of immobilized α-amylase was determined by conducting experiment on varying process parameters (pH, temperature and storage time). The attained results were compared with free α-amylase to collect information regarding any variation in catalytic activity at different reaction conditions.

Impact of pH

To determine the optimum operational pH of free enzyme and the nanobiocatalyst (*d*-MHNTs/α-amylase), similar units (300 IU) were introduced to different buffers (pH 4.5-8.0) under identical conditions (6 h, 40 °C). The catalytic activities of individual samples were determined as described earlier. The optimum (highest) activity obtained was considered 100%, and activities at other points were calculative relative to it.

Impact of Temperature

The optimal operational temperature was determined by incubating both forms of enzyme (300 IU, each) at different temperatures (30-60 ºC); pH 6.5. The catalytic activities were determined for each sample, considering the highest activity as 100%. The relative activities at other temperatures were calculated for individual samples (free and immobilized α-amylase).

Impact of Storage Time

The storage potential of NBC and free α-amylase (300 IU, each) was evaluated by storing them over 30 days in phosphate buffer (0.05 M, pH 6.5) at 4 °C. Aliquots were withdrawn periodically to determine the relative catalytic activity, considering the enzyme activity on first day as 100%.

3.19 Reusability of α-amylase Nanobiocatalyst

To determine the reuse potential of nanobiocatalyst, 10 mg nanobiocatalyst was incubated with 100 mL starch (1% w/v) solution for 3 h at 50 ºC. After every cycle, the nanobiocatalyst was separated, washed with buffer solution, and reintroduced into fresh starch solution. After separation of nanobiocatalyst the activity was determined by measuring the reducing sugars liberated. The activity of first cycle was considered 100%, and activities of other cycles were calculated relative to it. Equivalent units of free enzyme were also incubated under similar conditions for 30 h to assess the difference in reducing sugar production under similar reaction conditions.

3.20 Kinetics and Thermodynamic Parameters of Free and Immobilized α-amylase

The respective variation in kinetic parameters associated with catalytic activity and thermodynamic parameters representing the thermal stability were estimated using the following methods.

Kinetic Parameters

The rate of product formation was determined by varying substrate concentrations (1-10 mg/mL) with free and immobilized α-amylase. The kinetic parameters were calculated using the Lineweaver-Burk plot. The kinetic reaction parameters (k_M, V_{max}) of α-amylase before and after immobilization were compared.

Thermodynamic Parameters

Thermodynamic parameters of free and immobilized α-amylase were assessed by determining their catalytic activity at different temperatures. In brief, both forms (300 IU each) were incubated at temperatures (40, 50 and 60 °C), and aliquots were withdrawn after specific time intervals for analyzing the catalytic activity. The aliquots were mixed with starch (1% w/v) at 40°C for α-amylase catalytic activity assay. The thermodynamic parameters were determined as described earlier.

3.21 Influence of Metal Ions and Cellulose as Contaminants on α-amylase Activity

The catalytic activity of free and immobilized α-amylase in the presence of cellulose was assessed under identical conditions. In brief, equivalent units (300 IU) were incubated to starch (10 mL, 1% w/v) solutions comprising a serial concentration of cellulose (0-1% w/v). For evaluating the impact of metal ions, equivalent units of both forms were incubated separately with 5 mM metal ions (Ca^{+2}, Fe^{+2}, K^{+}, Zn^{+2}, Mg^{+2}, Cu^{+2}, Na^{+}) for 30 minutes. Subsequently, starch (1% w/v) was introduced into the enzyme-metal ion solution, and catalytic activities were determined. In the absence of contaminants (cellulose/metal-ions), the catalytic activity was considered as 100% and other activities were expressed relatively. Protein structure of α-amylase from SWISS-MODEL repository was accessed for illustrating the interaction between different metal ions and protein structure of α-amylase.

3.22 Potential Application of α-amylase Nanobiocatalyst for Potato Peel Waste Valorization

The developed nanobiocatalyst was tested for different application related to industrial sector including continuous production of reducing sugar stream, development of a hydrolysate medium for growth of various microorganisms, subsequent utilisation for production of single cell protein and in biocementation application.

3.22.1 Continuous Hydrolysis of Starch extracted from Potato Peel Waste

Starch extraction from Potato Peel Waste

Powdered PPW (20 g) was introduced in 100 mL distilled water and kept for 24 h with mild stirring (200 rpm). The formed slurry was allowed to stand for 1 h and the supernatant was decanted leaving all water insoluble particles as sediments. The sediment was resuspended in distilled water while the suspension was allowed to settle for next 1 h. The wet cake obtained

after decanting supernatant was dried overnight at 50 °C, subsequently crushed to fine powder, weighed and denoted as the extracted starch. Aliquots were drawn from PPW solution at different time intervals to determine starch yield as dry weight.

$$\text{Extraction yield (mg/g)} = \frac{\text{Dry weight of white powder (mg)}}{\text{Dry weight of PPW (g)}} \quad \text{Eq. 3.23}$$

The starch recovery (%) was determined by comparing the starch composition of white powder extracted with the original PPW.

$$\text{Starch recovery (\%)} = \frac{\text{Starch present in white powder (g)}}{\text{Starch present in PPW (g)}} \quad \text{Eq. 3.24}$$

Compositional Analysis

The moisture content of potato peel waste was determined by gravimetric method based on oven drying. In brief, 5 g powdered potato peel waste was dried at 105 ºC to a constant weight, the weight before and after were recorded and moisture (%) was calculated as follows:

$$\text{Moisture (\%)} = \left[\frac{W_2 - W_f}{W_f - W_1}\right] \times 100 \quad \text{Eq. 3.25}$$

Where W_1 is the weight of empty crucible, W_2 is the weight of the crucible and sample, and W_f is the constant weight of crucible and sample after drying at 105 °C.

The ash content was determined by ignition of powdered potato peel waste at 550 °C as per AOAC method (Horwitz 2010). In brief, the sample obtained after moisture content analysis (dried to constant weight at 105 °C) were placed in muffle furnace at 550 °C overnight. The weight was recorded after cooling the crucible containing sample in a desiccator. The following equation was used for the estimation of ash (%):

$$\text{Ash (\%)} = \frac{W_r}{W_f} \times 100 \quad \text{Eq. 3.26}$$

Where W_r is the weight of residue and crucible after incineration at 550 °C, and W_f is the constant weight of crucible and sample after drying at 105 °C.

The fiber in potato peel waste sample was determined using AOAC standard method (Horwitz 2010). Briefly, 1 g moisture free powdered potato peel waste was mixed in 200 mL sulphuric acid (1.25%), and incubated in boiling water bath for 30 min. The digested sample was filtered, and residue was washed to remove remaining acids. Washed residue was then

dried in an oven at 105 °C until constant weight. The dried residue was then shifted to a muffle furnace at 550 °C for 6 h. The crucible containing incinerated residue was cooled in a desiccator and weighed. The fiber in the potato peel waste was calculated using the equation:

$$\text{Fiber (\%)} = \frac{W_2}{W_1} \times 100 \qquad \text{Eq. 3.27}$$

Where W_2 is the weight after incineration at 550 °C, and W_1 is the initial moisture free weight.

Total carbohydrates were estimated using standard colorimetric method (Dubois et al. 1956). Briefly, 2 mL of clear aqueous solution of the carbohydrates extracted from PPW was mixed with 0.05 mL phenol (80%). Afterwards, 5 mL concentrated sulfuric acid was introduced into the solution, and then incubated at 30 °C for 15 min. The optical densities of the yellow-orange-coloured samples were measured at 490 nm. Total reducing sugars were estimated using dinitrosalicylic acid (DNSA) method discussed earlier (Miller 1959). The protein amount was determined using Lowry's method (Lowry 1951). In brief, 0.2 mL of protein sample extracted from potato peel waste was mixed with 4.8 mL analytical reagent and incubated at room temperature (25 °C) for 10 min. Afterwards, 0.2 mL of Folin-Ciocalteau reagent was added and the solution was incubated at room temperature (25 °C) for 30 min, followed by absorbance measurement at 750 nm. Bovine serum albumin was used to plot standard curve.

Continuous Hydrolysis Assessment

Nanobiocatalyst was evaluated for the continuous hydrolysis of the starch extracted from potato peel waste. In brief, the substrate solution was prepared by adding 1 g of extracted starch into 90 mL phosphate buffer (0.05 M, pH 6.5) and was kept at 70 ºC for 15 min. The starch suspension and the nanobiocatalyst (10 mg in 10 mL phosphate buffer) were incubated separately at operating temperature (50 °C). After achieving the temperature, both suspensions were mixed and kept under continuous stirring for 72 h (120 rpm, 50 °C). Aliquots were drawn at a defined interval and analyzed to reduce sugar production.

3.22.2 Development of Hydrolysate Broth Medium from Potato Peel Waste

An attempt was made for nanobiocatalyst-assisted conversion of potato peel waste (PPW) into a microbial growth medium. To prepare a liquid broth, potato peel waste (5 g) was mixed in phosphate buffer under stirring for 24 h (120 rpm, 50 ºC). The suspension was then

filtered, and the clear filtrate was used directly as a growth medium, as PPW medium. Similarly, another growth medium was prepared from the nanobiocatalyst-treated potato peel waste. For this, 5 g potato peel waste was suspended in 100 mL phosphate buffer onto which 100 mg nanobiocatalyst was introduced and kept at stirring for 24 h (120 rpm, 50 ºC). Afterward, the nanobiocatalyst was recovered using a magnet, and the final suspension was designated as PPW_{NBC} medium.

Protein content in the formulated media (PPW and PPW_{NBC}) was estimated through Lowry's method (Lowry 1951). Total carbohydrates were determined using colorimetric method of Dubois (Dubois et al. 1956). Reducing sugars in broth media (PPW and PPW_{NBC}) were quantified using a spectrophotometric method, proposed by Miller (Miller 1959).

Bacterial Growth Analysis

For bacterial growth the pH of the PPW and PPW_{NBC} media were adjusted to 7, and were autoclaved (121 ºC, 15 min). Agar (2% w/v) was used as a solidifying agent for bacterial culture plating. Commercially available nutrient broth/nutrient agar (NM) was employed as a reference for bacterial culture. *Escherichia coli* were employed as the representative bacterial species for evaluating the potential of nanobiocatalyst to transform PPW into a growth medium for bacterial growth. Non-pathogenic strain of *E. coli* MTCC 739 (ATCC 10536) was procured from Microbial Type Culture Collection and Gene Bank, CSIR-IMTECH, Chandigarh (India) and was used after repeated sub culturing, as per specifications.

E. coli culture was maintained on agar plate that was kept at 4 °C. A 1 mL inoculum of overnight grown culture was inoculated into sterilised 50 mL of broth (PPW medium, PPW_{NBC} medium and nutrient broth) in a 250 mL Erlenmeyer flask and incubated at 37 °C with shaking at 150 rpm. The growths of bacterial culture in broths were gauged by measuring the optical density at 600 nm, at different time intervals. Specific growth rate (μ_{max}) was determined in the exponential phase, as follows:

$$\mu_{max} = \frac{\Delta \log A_{600nm}}{\Delta t} \qquad \text{Eq. 3.28}$$

Where A_{600nm} is the absorbance of bacterial samples at 600 nm, and Δt represents the time span.

The bacterial growth on the solidified medium was assessed, by spreading appropriate dilution (100 µL). For serial dilutions sterile saline was used.

Single Cell Protein Production

For fungal growth the pH of PPW and PPW_{NBC} media was adjusted to 5 and autoclaved (121 ºC, 15 min). Commercially available potato dextrose broth (PDB) was employed as a reference medium for fungal culture. *Aspergillus niger* was employed as the representative fungal species for evaluating fungal growth and the production of single cell protein. Non-pathogenic strain of *A. niger* MTCC 282 (ATCC 6275) was procured from Microbial Type Culture Collection and Gene Bank, CSIR-IMTECH, Chandigarh (India) and was used after repeated sub culturing, as per specifications. For *A. niger*, inoculum was prepared by inoculating discrete colonies into 50 mL broth from a well grown culture on potato dextrose agar plates and incubated for 5 days. The broth medium (PPW, PPW_{NBC} and PDB) in each flask was inoculated with 1 mL of *A. niger* inoculum (10^6 spores/mL). The media were kept on orbital shaker (150 rpm, 28±2 °C) for 8 days. After required period of incubation, dry weight (DW) was determined by filtering cultures followed by drying at 90 °C until constant weight was achieved. Protein content of dried fungal biomass was estimated through Lowry's method (Lowry 1951). Total carbohydrates were determined using colorimetric method (Dubois et al. 1956). For nucleic acid quantification, spectroscopic method was followed.

Biocementation Application

The industrial potential of PPW_{NBC} media was evaluated and compared with the commercially available nutrient broth (NB) for growing calcifying bacteria *Bacillus* sp. CT5 in biocementation applications. The bacterial culture was grown in autoclaved PPW_{NBC} broth and a blend formulation of PPW_{NBC}:NB, i.e., 75:25, 50:50, 25:75, 0:100% v/v. For precipitation of calcium carbonate (bio cement), the growth media were augmented with filter-sterilized urea (2% w/v) and $CaCl_2$ (25 mM) and were incubated at 37 °C under shaking conditions (120 rpm). Calcium carbonate ($CaCO_3$) precipitation under different growth media was also evaluated by growing bacteria for 96 h. The $CaCO_3$ content was determined by the EDTA titration method (APHA 1989).

3.23 Statistical analysis

All the experiments were performed in triplicates and the data is represented as mean ± standard deviation. The results were analyzed using ANOVA followed by Tukey's post hoc test ($p<0.05$). Statistical analysis was performed using Graph Pad Prism 7 software and $p< 0.05$ was considered significant.

Chapter 4

Results and Discussion

4.1 Magnetic Halloysite Nanotubes (MHNTs)

A schematic representation for *in-situ* synthesis of iron oxide nanoparticles (IONPs) onto halloysite nanotubes (HNTs) surface via a simple chemical co-precipitation method is shown in Figure 4.1. A homogenous suspension of HNTs was prepared by ultrasonic treatment and stirring under inert atmosphere. The change in colour of HNTs suspension from whitish to light yellow following addition of iron precursors indicated successful dissolution of iron precursors into their ionic forms (Fe^{2+}/Fe^{3+}). A unique surface chemistry of halloysite nanotubes with negatively charged surface facilitated the adsorption of iron ions (Fe^{2+}/Fe^{3+}) onto the outer surface. The drop-wise addition of ammonia solution turned the colour of suspension from light to dark brown, and finally to black. The appearance of black colour indicated successful synthesis of magnetic nanoparticles. The high available surface area of halloysite nanotubes was anticipated to assist the uniform loading of IONPs. However, the extent of uniformity could not be predicted by mere theoretical characteristics. To assess uniform and efficient loading of iron oxide nanoparticles, various initial amount of iron precursors were scrutinized.

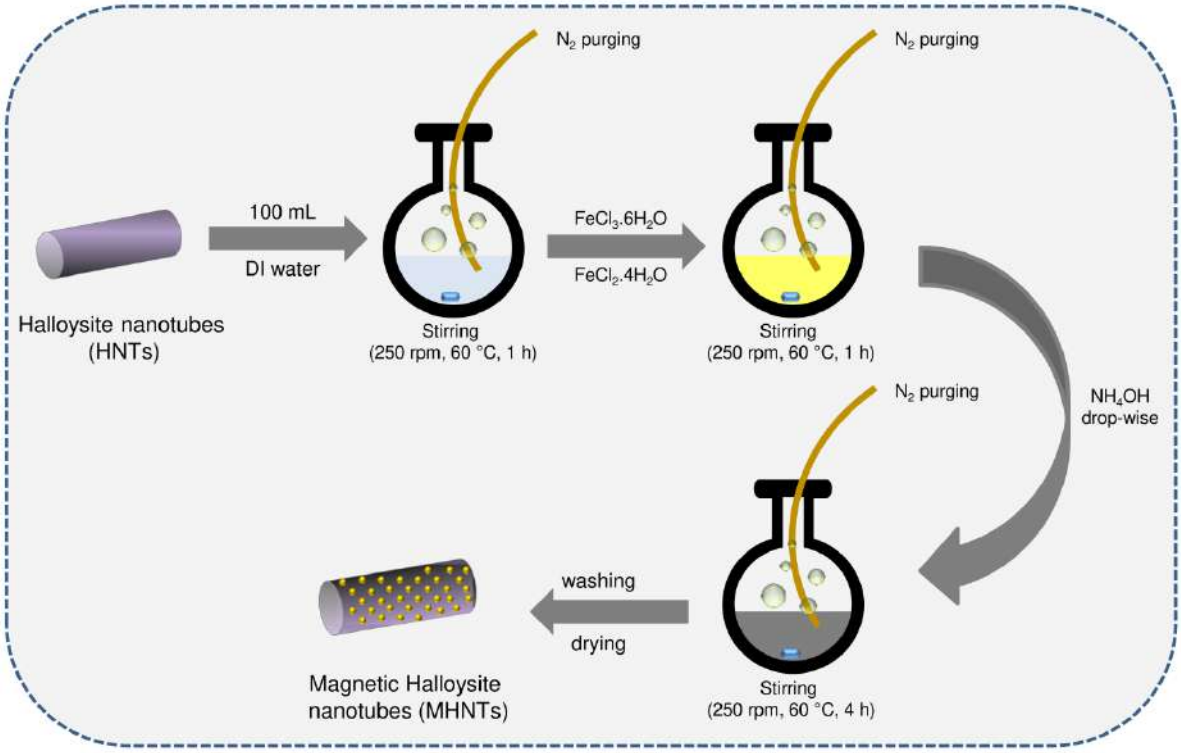

Figure 4.1 Schematic representation of *in-situ* synthesis of iron oxide nanoparticles onto the halloysite nanotube surface.

4.1.1 Characterisation of Magnetic Halloysite Nanotubes (MHNTs)

The chemical and structural properties of bare HNTs and synthesised MHNTs were evaluated by FTIR analysis over the range of 4000−400 cm^{-1} as shown in Figure 4.2(a). The double absorption bands at 3701 and 3623 cm^{-1} in pristine HNTs were related to stretching vibrations of hydroxyl groups at the surface of HNTs, whereas peak at 911 $cm^{-1}$was due to the O–H deformation of inner hydroxyl groups (Luo et al. 2010). The appearance of a band around 1637 cm^{-1} was attributed to bending vibrations of adsorbed water (Zhong et al. 2014). A peak at 1032 cm^{-1} was assigned to in-plane stretching vibration of Si–O, while band at 752 cm^{-1} correspond to Si–O perpendicular stretching in HNTs (Kang et al. 2017). The Si–O and Al–O stretching bands were presented at 535 and 467 cm^{-1}, respectively (Tierrablanca et al. 2010). The characteristic peaks of iron oxide nanoparticles in MHNTs were analysed. Fe–O stretching vibrations around 580 cm^{-1} were apparently overlapped by bending vibrations of Si–O. No significant changes were induced in the backbone structure of HNTs after immobilizing IONPs onto their surface. This validates a successful integration of magnetic character onto a non-magnetic material, i.e., HNTs and has been quantified in later section.

The variations in iron precursor on backbone crystallinity of HNTs were examined through XRD analyses (Figure 4.2b). The diffraction peaks in MHNTs sample with 2θ value of 12.06, 20.25 and 24.9 are attributed to 001, 020 and 002 planes of halloysite (JCPDS Card No. 29-1487), respectively (Lun et al. 2014). The dehydrated state and nanotubular structure of halloysite were evident from the presence of 001 plane at 12.06° with basal spacing of 0.724 nm. The absence of a sharp peak at ~8.7° can be ascribed to hydrated status of halloysite (10 Å form) (Levis and Deasy 2002; Zhang et al. 2013; Kumar-Krishnan et al. 2016). The dehydrated state was also evident from the presence of 002 basal plane at 24.9° (Barman et al. 2020). The data aligned well to the fact that halloysite were procured in dried powder form. The emergence of new diffraction peaks (2θ) in MHNTs at 30.43°, 35.64°, 43.28°, 57.33°, and 62.97° fully complied with the characteristic data of magnetite phase (JCPDS Card No. 01-075-0449). The peaks were attributed to 220, 311, 400, 511 and 440 basal planes of Fe_3O_4 nanoparticles, indicating the successful anchoring of magnetite nanoparticles on the surface of HNTs (Xie et al. 2011; Kadam et al. 2017).With increase in the amount of initial Fe precursor, peak intensities concomitantly increased. This confirms the gradual increase in loaded magnetite nanoparticles. The characteristic peaks of halloysite were retained in all MHNTs samples even after loading IONPs. This is consistent with FTIR results. A subtle

change in HNTs from white to brown and eventually black was evident from the photographic images in Figure 4.2 (c).

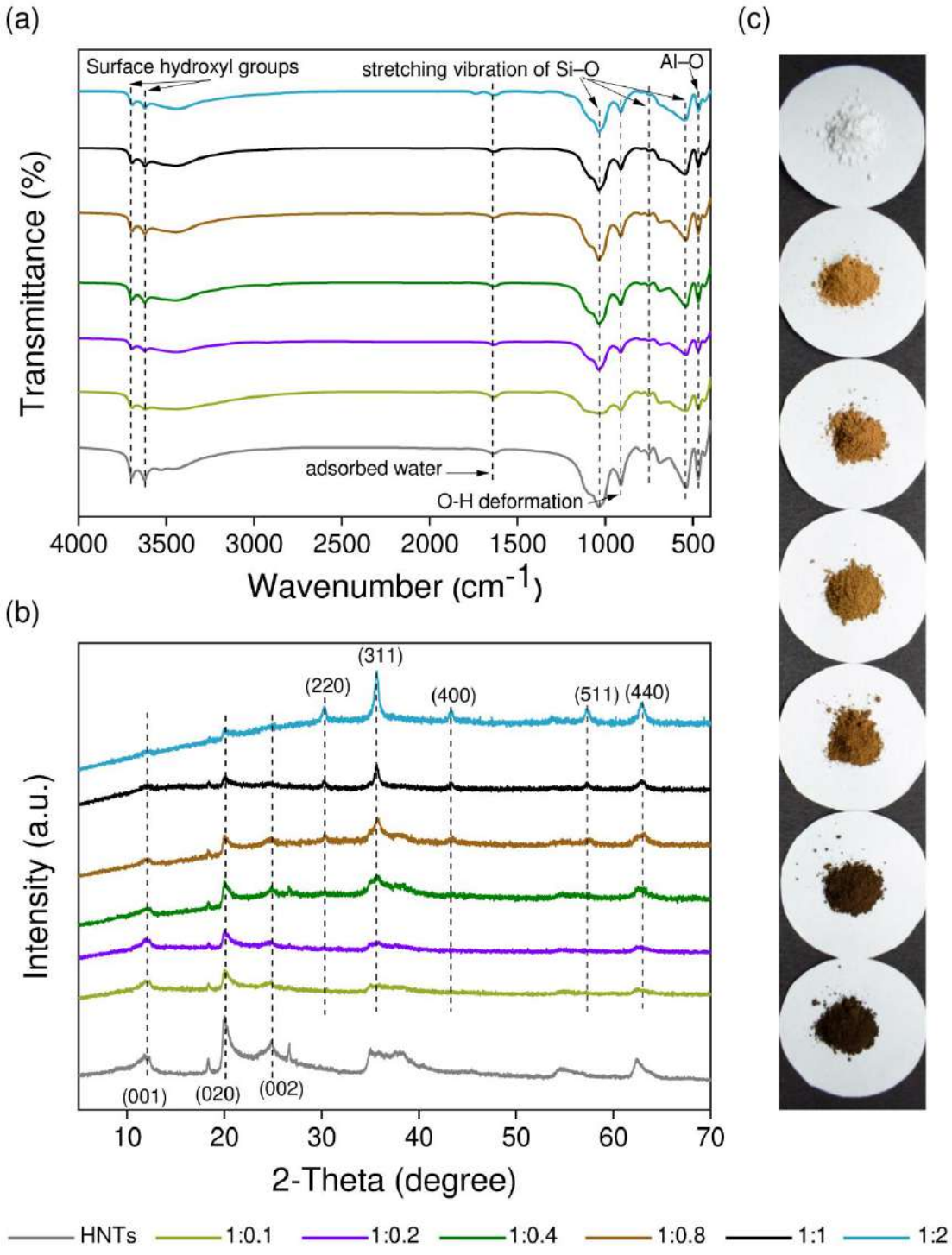

Figure 4.2 (a) FTIR, (b) XRD analyses, and (c) photographic image of bare HNTs and synthesised MHNTs sample after varying the amount of iron precursor.

Bare HNTs and MHNTs samples were analysed using field emission-scanning electron microscopy to compare their topographical characteristics (Figure 4.3). The micrograph of HNTs demonstrated cylindrical shaped tubes along with open end lumens and smooth outer surface (Figure 4.3a). An increase in roughness of surface and appearance of patches in MHNTs samples indicated successful attachment of iron oxide nanoparticles in clustered forms. In MHNTs having HNTs:Fe precursor (1:0.1), iron oxide (Fe_3O_4) nanoparticles exhibited random and uncontrolled distribution due to high surface area available for iron ions to adhere (Figure 4.3b). MHNTs synthesised using HNTs:Fe precursor (1:1) showed the best uniformity (Figure 4.3c-f). Increasing the amount beyond this resulted in agglomeration of IONPs onto the surface of HNTs as clearly visible in Figure 4.3(g). Elemental mapping of bare halloysite nanotube indicated the presence of Al and Si element, whereas no Fe element was detected. A consistent increase in Fe element explained a higher loading of IONPs on HNTs surface. The appearance of Al and Si in all samples validated the intact nature of HNTs which corroborates well with FTIR and XRD analyses.

Considering these observations and based on our earlier findings, it is recommended to choose a uniform surface of MHNTs for utilizing their high surface area. Also, an appropriate loading of IONPs is essential to ensure recovery of MHNTs from the reaction mixture. Hence, MHNTs synthesized using HNTs:Fe precursor (1:1) was selected as the best suited immobilization template for enzymes, as shown in further studies.

4.2 Sulfonic acid-Functionalized MHNTs as Solid Acid Catalyst

Acid functionalized materials are well suited for catalytic applications including the pre-treatment strategies of biomass (Qi et al. 2018; Qi et al. 2019; Xu et al. 2019; Testa and La Parola 2021). The benefits offered by these solid acid catalysts viz. better control on reaction, easy recovery and reusability have gained tremendous attention in recent times. Further, nanomaterials-derived solid acid catalysts offer superior surface area for anchoring acids moieties, which results in improved catalytic activity (Testa and La Parola 2021). Halloysite nanotubes have exposed silanol groups on outer surface which present them as silica-analogs (Yuan et al. 2015). The outer surface of halloysite can be covalently modified using a wide range of organic compounds, specifically organosilanes due to their superior affinity (Yuan et al. 2008; Massaro et al. 2017; El-Soad et al. 2020). Various functionalities can be incorporated using appropriate modification of organosilane terminal groups (Tharmavaram et al. 2018).

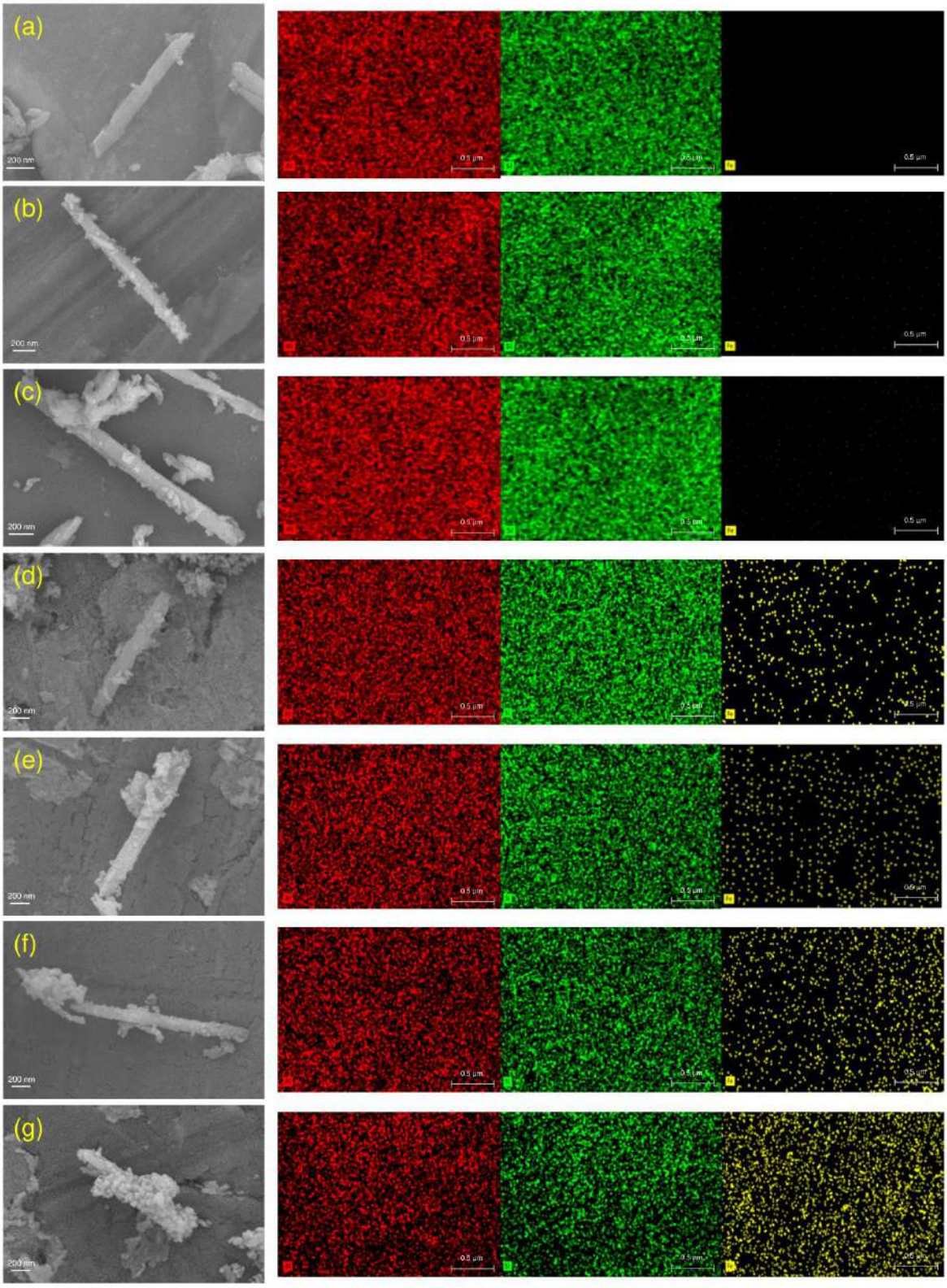

Figure 4.3 FE-SEM micrographs and elemental mapping of (a) bare HNTs and (b-g) MHNTs synthesised using various ratios of HNTs:Fe precursor (b) 1:0.1 (c) 1:0.2 (d) 1:0.4 (e) 1:0.8 (f) 1:1 and (g) 1:2 . Red, green and yellow signifies the intensity distribution of aluminium (Al), silicon (Si) and iron (Fe) elements over the scanned area.

For this purpose, the sulfonic acid functionalization of MHNTs was carried out via thiol group grafting and subsequent oxidation as shown in the Figure 4.4. Here, grafting of mercaptosilane groups onto MHNTs was carried out by refluxing them with 3-mercaptopropyl(trimethoxy)silane (MPTMS) in presence of toluene. The mecapto/thiol groups were then oxidized into sulfonic acid groups at room temperature in the presence of hydrogen peroxide. The as obtained sulfonic acid functionalised MHNTs (MHNTs-SO_3H) were easily separated from the reaction mixture using a magnet. The MHNTs-SO_3H will be used as solid acid catalyst for the pretreatment of sugarcane bagasse.

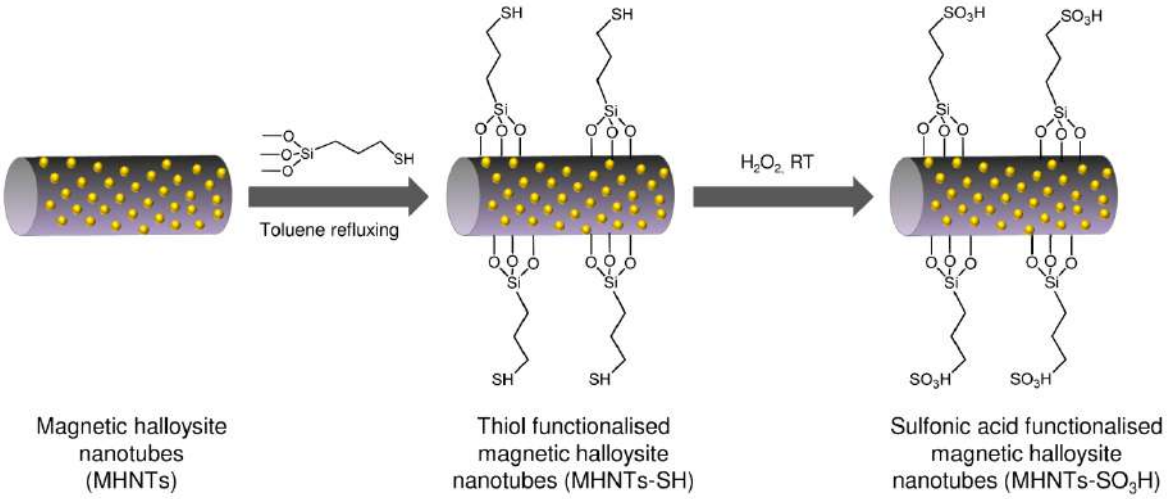

Figure 4.4 Surface functionalization steps for grafting sulfonic acid moieties on magnetic halloysite nanotubes to form a solid-acid catalyst.

4.2.1 Material Characterization of Solid Acid Catalyst

Synthesized solid acid catalyst was systematically investigated for physiochemical characteristics i.e., surface chemistry, microstructure and magnetization capability. FTIR spectrum of both MHNTs and MHNT-SO_3H demonstrated hydroxyl group peaks (3696, 3626, 1634, and 913 cm^{-1}) and Si-O stretching vibrations (1040, 752 and 535 cm^{-1}) which are the characteristic of halloysite nanotubes (Figure 4.5a). Peaks of –SO_3H group were reported in the range 1000-1200 cm^{-1}, specifically O=S=O asymmetric and symmetric stretching modes, which coincided with the vibration bands due to the existence of Si-O-Si groups in HNTs (Wang et al. 2019a).

Further, bending vibrations of SO-H bond of sulfonic acid groups overlapped with O-H deformation peak of HNTs. However, the sulfonic-acid functionalization was also evident

through the presence of peaks ~1400 cm^{-1} region, ascribed to stretching vibration of S=O groups (Zhou et al. 2014). The emergence of peaks associated with methylene stretching at 2922 and 2857 cm^{-1} confirmed the attachment of propyl group with HNTs (Kumar et al. 2021b). In another study, variation in crystal structures of MHNTs before and after sulfonic-acid functionalization were analysed using XRD (Figure 4.5b). The characteristic peaks of halloysite nanotube and Fe_3O_4 nanoparticles were present in both the forms. This indicates that no change occurred in MHNTs crystallinity after acid functionalization.

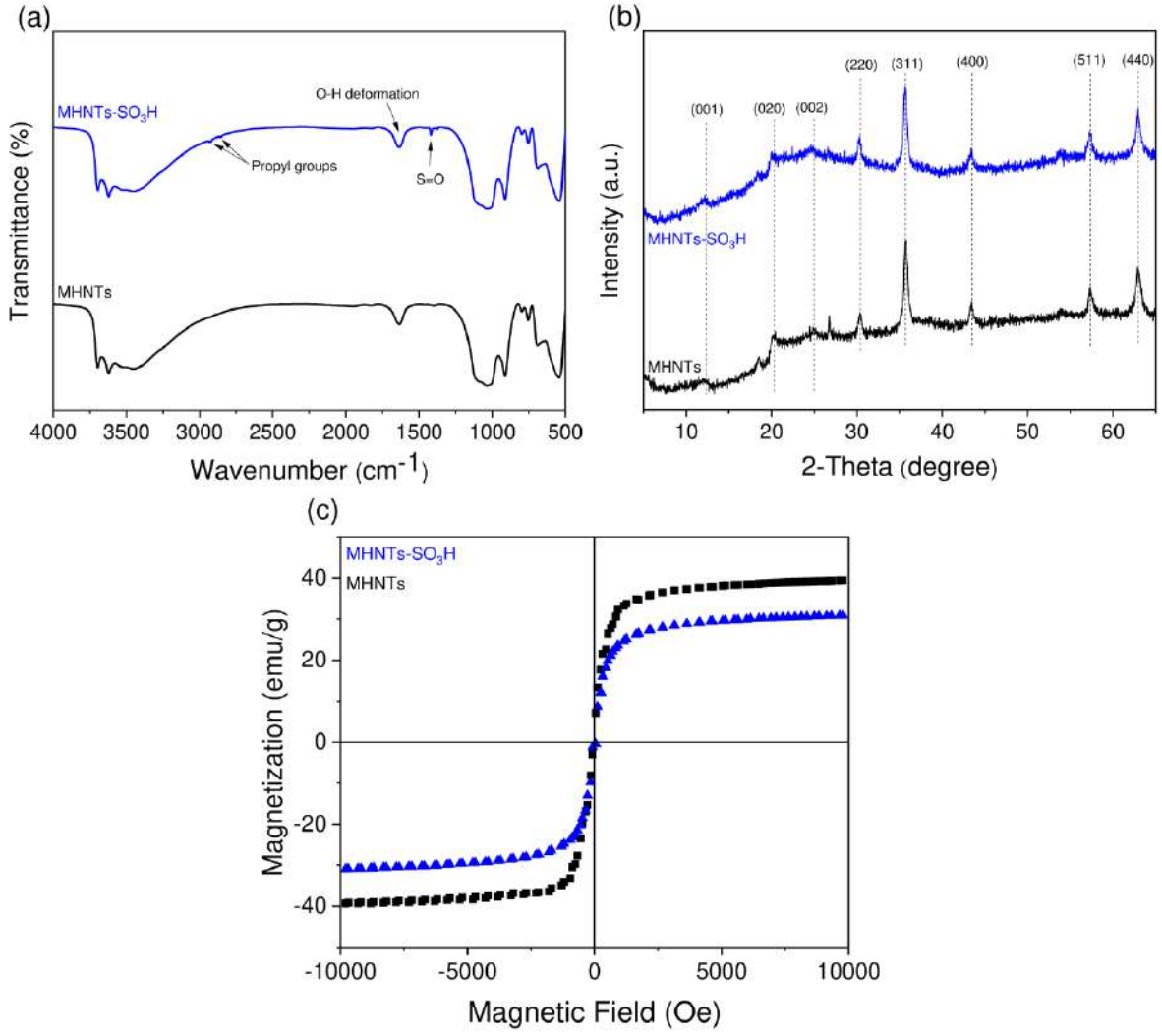

Figure 4.5 (a) FTIR, (b) XRD, and (c) Magnetic hysteresis loops analysis of MHNTs and sulfonic acid functionalized magnetic halloysite nanotubes (MHNTs-SO_3H).

The magnetic behaviour of the MHNTs and synthesised solid acid catalyst was also investigated by vibrating sample magnetometer. The magnetization saturation values calculated from magnetic hysteresis loop were 39.42 and 30.86 emu/g for MHNTs and MHNTs-SO_3H, respectively (Figure 4.5c). A decrease in magnetic saturation value after

acidic functionalization was attributed to the attachment of non-magnetic silane layers during surface modification. Nonetheless, a high magnetic saturation value with negligible coercivity and remanence was an indicative of super-paramagnetic behaviour of MHNTs-SO_3H. This would render easy separation and fast recovery from working vessels after the reaction.

Solid acid catalyst was analyzed for any morphological or topographical changes on HNTs using field emission-scanning electron microscopy (Figure 4.6a). The presence of intact HNTs and IONPs was clearly visible from the micrograph signifying no impact on the morphological attributes of halloysite nanotubes and nanoparticles. The observations of FE-SEM were in good corroboration with FTIR, XRD and VSM analyses. Overall, the functionalization of sulfonic acid groups on the magnetic halloysite nanotube and its capability to be separated from any reaction solution could be manifested by the characterisation studies of solid acid catalyst. The Energy dispersive X-Ray (EDX) spectra of MHNTs-SO_3H demonstrated the presence of S element, validating the sulfonic acid functionalization of MHNTs (Figure 4.6b). The compositional analysis revealed the 0.62 wt% loading of element S. The acidity of synthesised solid acid catalyst was found to be 0.38 mmol H^+/g.

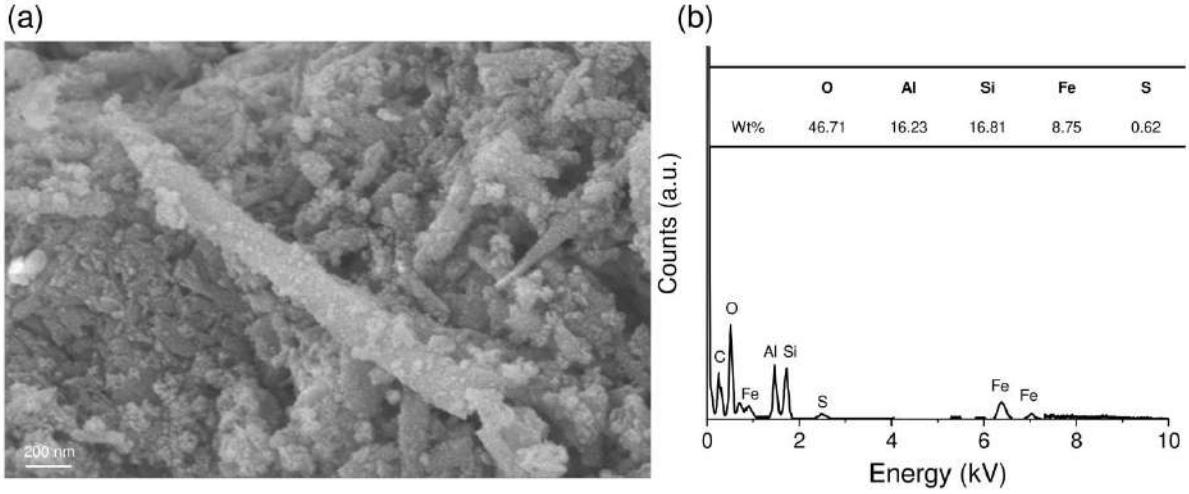

Figure 4.6 (a) FE-SEM micrograph of solid acid catalyst (MHNTs-SO_3H) displaying intact structure of magnetic halloysite nanotube, and (b) EDX analysis of MHNTs-SO_3H.

4.3 Pretreatment of Sugarcane Bagasse using Solid Acid Catalyst

Sugarcane bagasse pretreatment was performed using a two-step procedure. First step involves primary treatment of sugarcane bagasse with solid acid catalyst followed by a

secondary treatment using diluted alkaline solution. The capability of solid acid catalyst was evaluated by engaging different amount of MHNTs-SO_3H (0.1 to 0.5 g) for treatment of 1 g sugarcane bagasse, while keeping the same alkaline treatment conditions for all the samples.

4.3.1 Biophysical Characterisation of Biomass

The raw and pretreated sugarcane bagasse samples were subjected to FTIR spectroscopic analysis (Figure 4.7a). A broad appeared at 3414 cm^{-1} in both untreated and pre-treated sugarcane bagasse samples belongs to O-H stretching of intermolecular hydrogen bonds of cellulose-I. The adsorption peak at 2903 cm^{-1} corresponds to asymmetric and symmetric vibrations (C-H stretching) due to cellulose. The peak at 1734 cm^{-1} was attributed to C=O bonds of acetyl and ester linkages existing in hemicellulose content (Laluce et al. 2019). The presence of absorption bands at 1632, 1604 and 1512 cm^{-1} were associated with C=C stretching of aromatic rings found in lignin (Singh 2020). Additionally, the peak at 1248 cm^{-1} indicated the presence of C–O out of plane stretching due to aryl groups in lignin. A multiple adsorption peaks at 1426, 1374 and 1326 cm^{-1} were the result of CH_2 bending, C-H deformation and O-H bending in cellulose, respectively. A vivid absorption bands at 1054 cm^{-1} occurred due to C-OH stretch of carboxylic acid group present in cellulose (Singh 2020). The existence of cellulose was further confirmed due to absorption at 899 cm^{-1}, which is a characteristic peak of β-glycosidic linkages between glucose units (Laluce et al. 2019).

In case of pre-treated biomass samples, reduction in peak intensity of hemicellulose and lignin were observed. A reduced peak of C=O bonds in pre-treated samples indicated an effective hydrolysis of the hemicellulose component of sugarcane bagasse by the solid acid catalyst. Peak intensity, ascribed to lignin component was also drastically reduced validating the successful delignification through sequential dilute alkaline pretreatment process. In biomass samples treated with ≤0.3 g solid acid catalyst, peak reduction was comparatively lower as compared to the samples pre-treated with higher amount of solid acid catalyst (0.4 & 0.5 g). The reason could be limited hydrolysis of the hemicellulose component, leaving behind strong hemicellulose-lignin interactions which were relatively hard to break with dilute alkaline pre-treatment. Overall, the observation validated the reduction in recalcitrance of biomass after pretreatment owing to the removal of hemicellulose and lignin content.

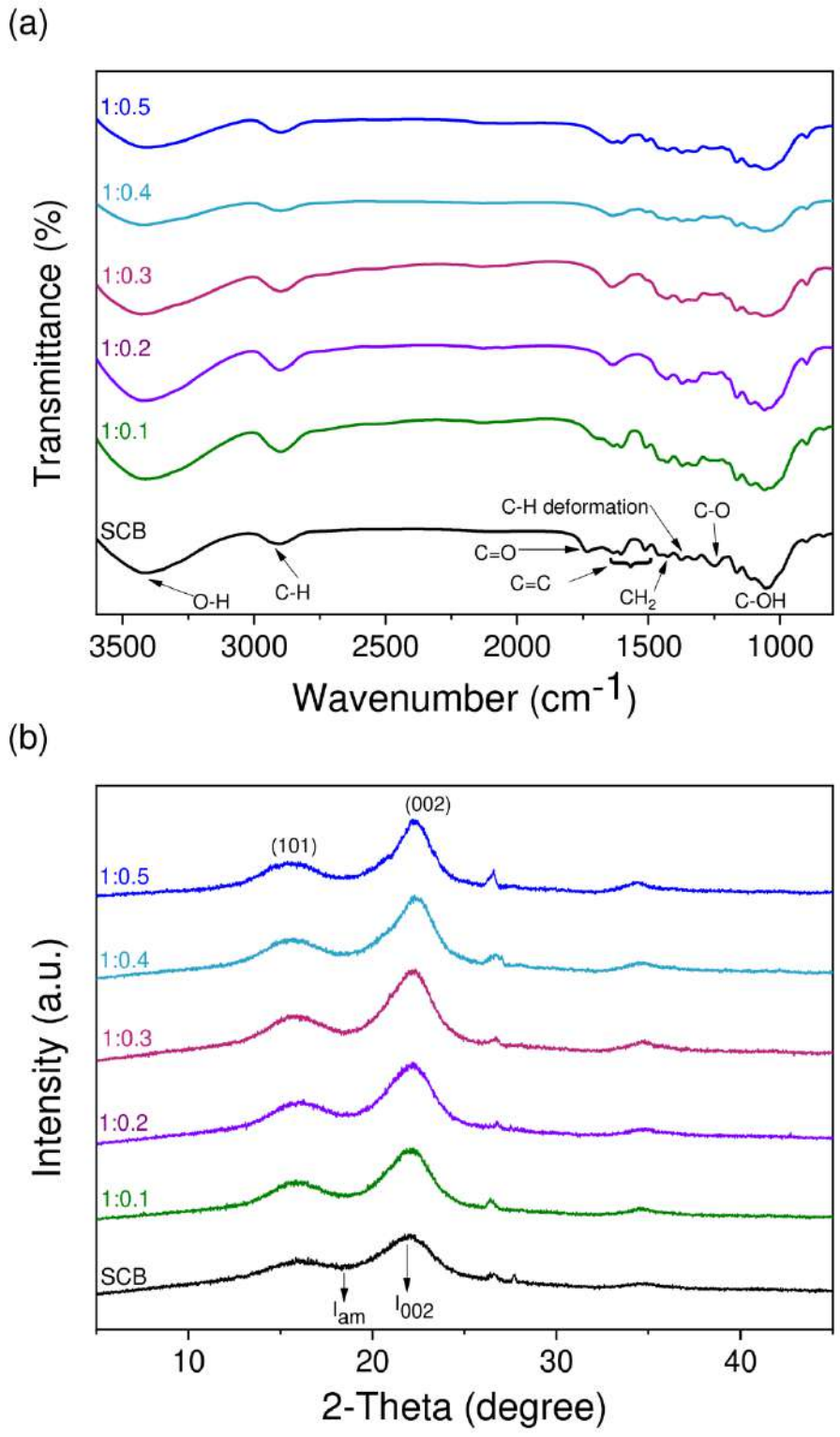

Figure 4.7 (a) FTIR and, (b) XRD analyses of raw and pretreated samples.

In order to determine enzyme accessibility to cellulose content, the crystallinity of lignocellulosic biomass has to be assessed. The presence of amorphous hemicellulose and lignin component hinders the enzymatic hydrolysis of cellulose by restricting the contact

between cellulase enzyme and cellulose. XRD patterns were employed to calculate crystallinity index (CrI), which revealed the impact of pretreatment on the overall crystallinity of lignocellulosic biomass. A consistent increase in diffraction intensity of (0 0 2) crystalline plane was observed in samples pretreated with increasing solid acid catalyst amount from 0.1 to 0.5 g (Figure 4.7b). Crystallinity index of raw sugarcane bagasse was recorded at 46.79 which increased to 57.05 when treated with 0.1 g solid acid catalyst. Hydrolysis of hemicellulose and solubilisation of lignin components are the prime causes behind the increase in crystallinity index after pre-treatment (Fan et al. 2021).

The pretreatment condition could also triggered partial removal of amorphous cellulose, which might also resulted in increased CrI value (Chourasia et al. 2021). With increase in solid acid amount, a continuous rise in CrI values was observed attaining 59.81, 61.16, 62.38 and 65.98 after pre-treatment with 0.2, 0.3, 0.4, and 0.5 g solid acid catalyst, respectively. A nominal increase in CrI values at higher solid acid catalyst amount was manifested due to superior harsh pre-treatment conditions that facilitated cellulose disaggregation/solubilisation and limiting the overall crystallinity of the biomass (Sharma et al. 2019b). Collectively, all the results favoured towards establishing a more effective pre-treatment strategy of biomass using solid-acid catalyst.

Raw and pre-treated sugarcane bagasse samples were also analysed using Scanning Electron Microscopy (SEM) to perceive any morphological changes in biomass structure. Raw sugarcane bagasse sample appeared as a complete lignocellulosic structure, where all the components were present in form of a compact bundle (Figure 4.8a). The patchy/rough surface was also evident which might occur due to grinding and removal of extractives. It was also noted that the ends of lignocellulosic biomass were not scattered, indicating cellulose components were still covered by hemicellulose and lignin (Pereira et al. 2011). Sugarcane bagasse pre-treated with solid acid catalyst revealed noticeable alterations in biomass structure with fibres' detachment and forming a loose matrix with enhanced porosity (Figure 4.8b-f). A superior visible porosity validates the removal of amorphous components i.e., hemicellulose and lignin from biomass (Chen et al. 2012). An increase in solid acid amount resulted in superior exfoliation of sugarcane bagasse cell wall, attributed to higher removal of hemicellulose component. This was followed by dilute alkaline pre-treatment step which facilitated the removal of lignin component, initiating physical breakdown and abrupt rupture to the compact structure. The detachment of hemicellulose and lignin component was

clearly evidenced in pre-treated samples, specifically with 0.3-0.5 g solid acid catalyst, where a large proportionate of disrupted fibres was observed (Figure 4.8d-f). Similar findings were reported previously when using acidic alkaline sequential pre-treatment (Chen et al. 2012; Giese et al. 2013; Chandel et al. 2014; Philippini et al. 2019; Ascencio et al. 2020).

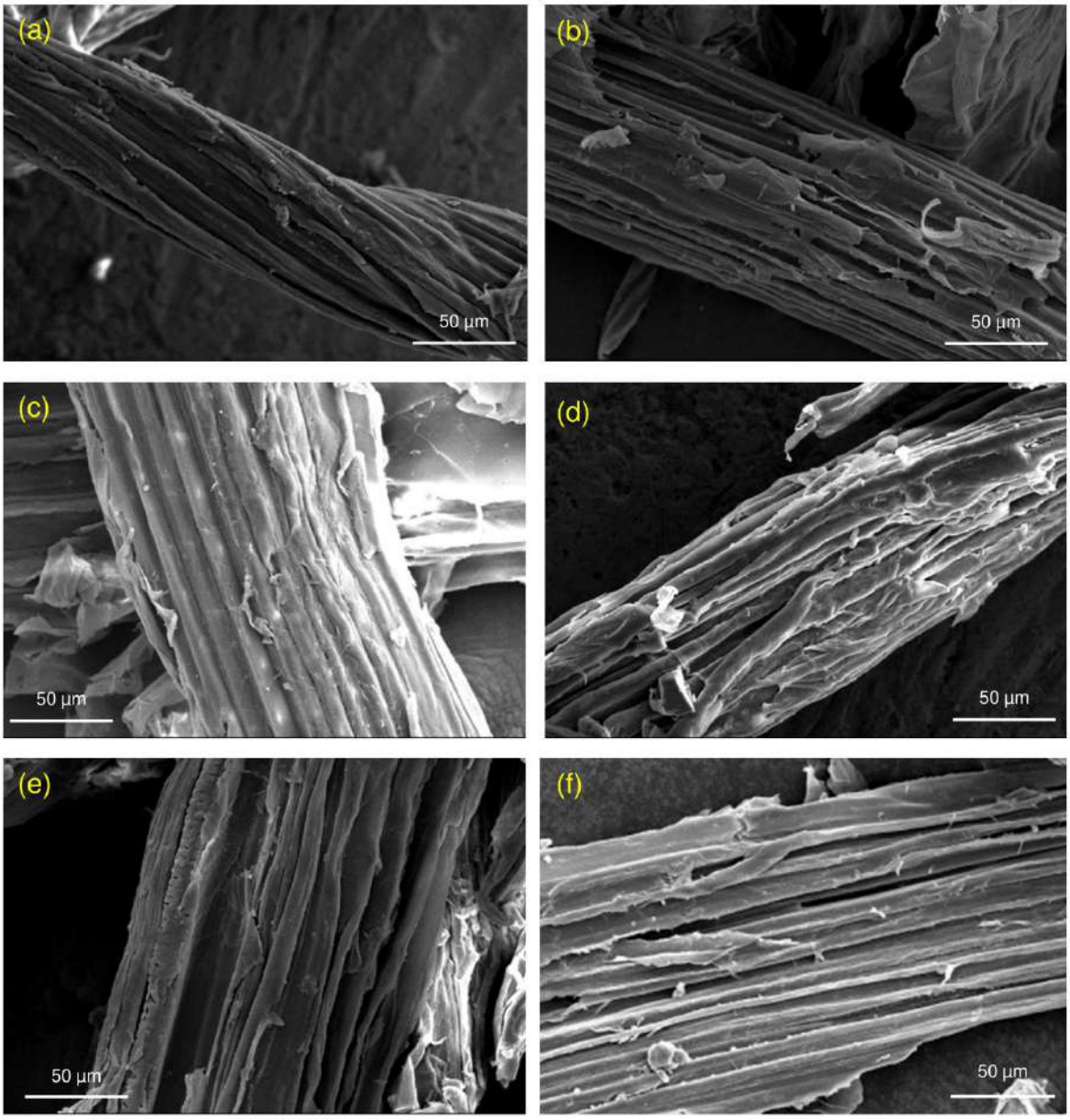

Figure 4.8 SEM micrographs of (a) untreated sugarcane bagasse, and sugarcane bagasse pre-treated with (b) 1:0.1, (c) 1:0.2, (d) 1:0.3, (e) 1:0.4 and (f) 1:0.5 (Sugarcane bagasse: Solid acid catalyst).

4.3.2 Compositional Analysis of Biomass

The compositional analysis of raw sugarcane bagasse revealed 42.36% cellulose, 26.65% hemicellulose and 21.72% lignin content (Table 4.1). The pre-treated sugarcane bagasse samples however demonstrated a significant variation in its composition from raw sample. The SCB sample treated with minimum amount (0.1 g) of solid acid catalyst exhibited 49.97% cellulose, 22.38% hemicellulose and 15.41% lignin content. A rise in cellulose content became more prominent (52.80-58.13%) when higher amount of solid acid catalyst (0.2-0.5 g/g SCB) was used for pretreatment. On contrary, hemicellulose and lignin content consistently decreased in SCB samples while treating with higher amount of solid acid catalyst. The SCB sample pretreated using 0.5g/g SCB had 58.13% cellulose, 9.49% hemicellulose and 12.51% lignin content. The increase in cellulose content could be attributed to the efficient removal of hemicellulose and lignin content by solid acid catalyst-assisted pre-treatment approach. As alkaline pre-treatment was kept same for all samples, an increase in overall cellulose content verified the significance of solid acid catalyst based pre-treatment for biomass transformations.

Table 4.1 Compositional analysis of raw and pre-treated sugarcane bagasse samples.

Sample	Cellulose (wt %)	Hemicellulose (wt %)	Lignin (wt %)
SCB	42.36 ± 1.24^{d}	26.65 ± 0.87^{a}	21.72 ± 0.63^{a}
SCB:SAC (1:0.1)	49.97 ± 0.59^{c}	22.38 ± 0.44^{b}	15.41 ± 0.34^{b}
SCB:SAC (1:0.2)	52.80 ± 1.04^{bc}	21.08 ± 0.47^{b}	15.05 ± 0.33^{bc}
SCB:SAC(1:0.3)	54.96 ± 1.30^{ab}	15.60 ± 0.34^{c}	14.45 ± 0.42^{bc}
SCB:SAC (1:0.4)	57.81 ± 1.22^{a}	13.87 ± 0.39^{d}	13.91 ± 0.27^{c}
SCB:SAC (1:0.5)	58.13 ± 0.57^{a}	9.49 ± 0.14^{e}	12.51 ± 0.20^{d}

*SCB=Sugarcane bagasse; SAC=Solid acid catalyst i.e., MHNTs-SO_3H). ¶Data is presented as mean ± standard deviation of three replicates. Means with different superscript letters are different by Tukey's post-hoc test ($p<0.05$).

The recovery and removal of individual components was also assessed to understand the mechanism and to determine the impact of solid acid catalyst amount on pre-treatment. The biomass recovery decreased with increase in solid catalyst amount during pre-treatment of sugarcane bagasse. The biomass recovery of 84.23%, 79.36%, 76.05%, 71.63%, and 69.41% was obtained with 0.1, 0.2, 0.3, 0.4 and 0.5g solid acid catalyst/g SCB, respectively (Figure 4.9a). The trend observed was endorsed by superior hemicellulose and lignin removal from

biomass samples in presence of high solid catalyst amount. Similarly, a declining pattern was also recorded in case of cellulose recovery while increasing the amount of solid acid catalyst during pre-treatments (Figure 4.9b). Sugarcane bagasse sample pretreated with 0.1 g solid acid catalyst recorded the highest cellulose recovery of 99.37%, whereas biomass sample treated with 0.5 g solid acid catalyst resulted in only 95.25% cellulose recovery. The samples pretreated using 0.2, 0.3 and 0.4 g solid acid catalyst revealed cellulose recovery of 98.93%, 98.67%, and 97.74% respectively. It is hypothesized that an increased protonation in presence of high solid acid catalyst amount is the key cause for partial solubilisation of cellulose component, resulting in reduced recovery of cellulose component after pretreatment.

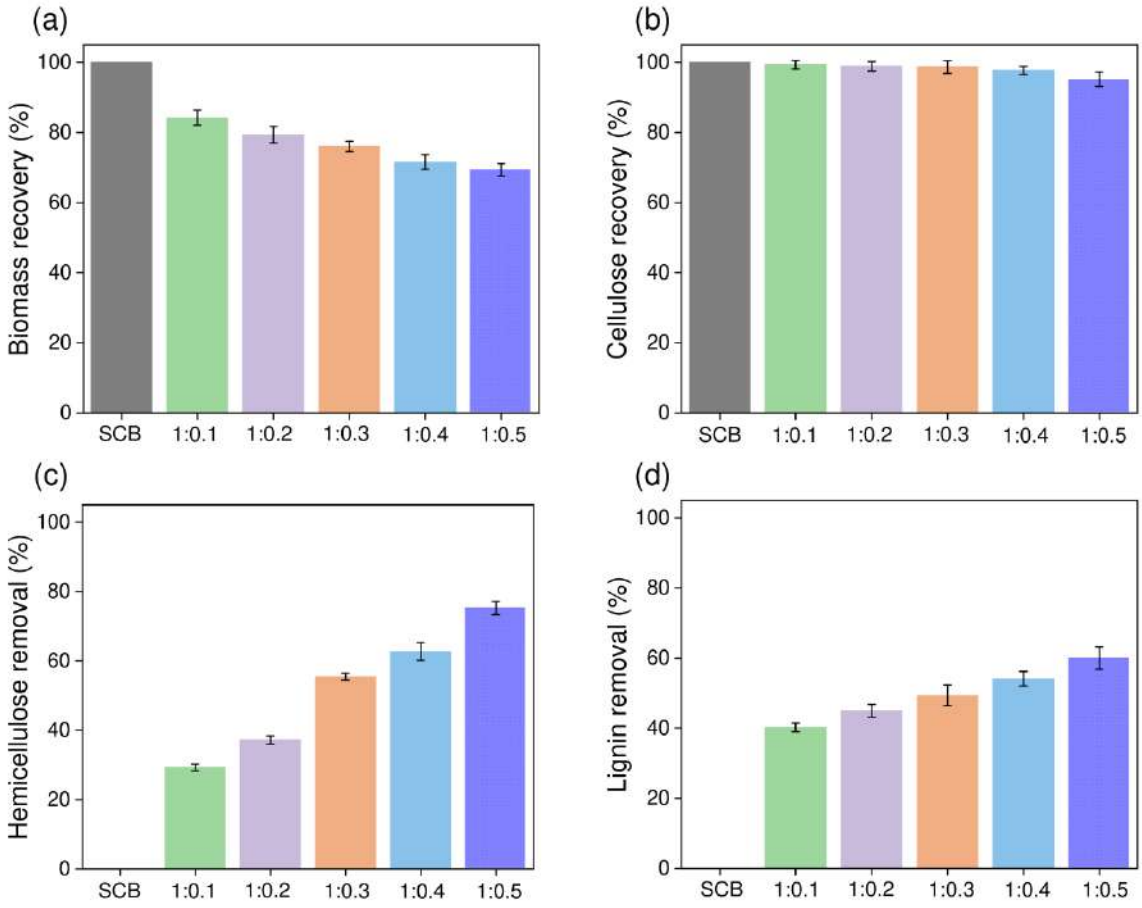

Figure 4.9 (a) Biomass recovery, (b) Cellulose recovery, (c) Hemicellulose removal, and (d) Lignin removal after pretreatments using different amount of solid acid catalyst.

On the other hand, with increase in solid acid catalyst from 0.1 g to 0.5 g per g of sugarcane bagasse, hemicellulose removal significantly increased from 29.25% to 75.27% (Figure 4.9c). The samples pretreated using 0.2, 0.3 and 0.4 g solid acid catalyst resulted in hemicellulose removal of 37.22%, 55.47%, and 62.73%, respectively. A higher hemicellulose removal

could be attributed to significant acidic capability of the solid acid catalyst which depolymerizes the hemicellulose component of biomass dissociating β-(1–4) glycosidic bonds (Li et al. 2018; Qi et al. 2018; Lu et al. 2021). Further investigation revealed a direct connection between solid acid catalyst amount and delignification of the biomass. The dilute alkaline treatment conditions were kept constant for all the samples, interestingly biomass sample treated with higher amount of solid acid catalyst resulted in higher delignification (Figure 4.9d). The lignin removal of 40.24%, 47.16%, 49.40%, 51.37% and 60.02% was recorded for sample treated with 0.1, 0.2, 0.3, 0.4 and 0.5 g solid acid catalyst, respectively. The removal of hemicellulose component in first step provided easy access to the alkaline liquid catalyst, facilitating the rupturing of ester bonds between lignin-hemicelluloses, resulting in superior delignification. From the observations, conclusion can be drawn that pretreatment approach developed here was efficient for removal of hemicellulose and lignin component. Thus obtained pretreated sugarcane bagasse had exposed and easily accessible cellulose content for further processing.

4.3.3 Xylose Release

The liquid fraction recovered after solid acid catalyst pretreatment was used for xylose estimation. As discussed in the compositional analysis of pretreated sugarcane bagasse samples, the hemicellulose removal is caused by depolymerisation of the polysaccharide component via cleavage of β-(1–4) glycosidic bonds. The depolymerisation results in release of soluble monosaccharide xylose into the liquid fraction. Xylose is considered to be a promising renewable resource for production of various biochemicals. Furthermore, xylose is used in a wide range of industrial sectors including, food, beverage, pharmaceutical, personal care products, agriculture, and animal/poultry feed. The most prominent use of xylose is in food and beverage industry as a flavouring agent and diabetic sweetener. Hence, for effective valorization of the sugarcane bagasse, the quantification of xylose released is critical.

It was observed that release of xylose was proportional to the amount of solid acid catalyst used, where increase in solid acid concentration resulted in higher release of xylose in the liquid fraction (Table 4.2). The SCB sample pretreated with 0.1 g solid acid catalyst resulted in liberation of 6.21g/L xylose. A gradual increase in xylose present in the filtrateto 8.31, 13.67, and 15.26 g/L was observed in case of pretreatment carried out using 0.2, 0.3, and 0.4 g solid acid catalyst, respectively. Highest xylose (18.76 g/L) was liberated in case of liquid

obtained after pretreatment of sugarcane bagasse using 0.5 g solid acid catalyst. From the observed data it can be concluded that solid acid catalyst effectively hydrolysed the hemicellulose content in the sugarcane bagasse. The hydrolysis of hemicellulose into xylose using different solid acid catalysts has also been reported earlier (Li et al. 2018; Qi et al. 2018; Ingle et al. 2020a).

4.3.4 Inhibitors Analysis

The estimation of inhibitory compounds produced during pretreatment process is an important aspect for subsequent enzyme saccharification and fermentation, as these inhibitors along with residual lignin might impede the activity of enzymes and microorganisms (Ladeira-Ázar et al. 2019; Panakkal et al. 2022). Inhibitors produced during pretreatment process are majorly classified into three categories, weak carboxylic acids (such as levulinic, acetic, and formic acids),furan derivatives (furfural, and hydroxymethylfurfural (HMF)), and phenolic compounds (Mood et al. 2013). The concentrations of inhibitors also varied on varying the solid acid catalyst amount (Table 4.2).

Table 4.2 Xylose released and inhibitors produced during pretreatment.

Sample	Xylose (g/L)	TCAC (g/L)	Furfural (g/L)	HMF (g/L)	Total phenolics (g/L)
SCB:SAC (1:0.1)	6.21 ± 0.13^{d}	0.017 ± 0.00^{d}	0.001 ± 0.00^{c}	ND	1.42 ± 0.05^{d}
SCB:SAC (1:0.2)	8.31 ± 0.16^{c}	0.05 ± 0.002^{d}	0.006 ± 0.00^{c}	0.001^{cd}	1.62 ± 0.03^{c}
SCB:SAC(1:0.3)	13.67 ± 0.36^{b}	0.21 ± 0.006^{c}	0.014 ± 0.00^{bc}	0.004^{c}	1.94 ± 0.05^{b}
SCB:SAC (1:0.4)	15.26 ± 0.47^{b}	0.48 ± 0.013^{b}	0.050 ± 0.002^{b}	0.008^{b}	2.10 ± 0.05^{b}
SCB:SAC (1:0.5)	18.76 ± 0.68^{a}	0.96 ± 0.024^{a}	0.104 ± 0.005^{a}	0.014^{a}	2.62 ± 0.06^{a}

*SCB=Sugarcane bagasse; SAC=Solid acid catalyst (MHNTs-SO_3H); TCAC=total carboxylic acid content. ¶Data is presented as mean ± standard deviation of three replicates. Means with different superscript letters are different by Tukey's post-hoc test ($p<0.05$).

Carboxylic acids are formed during pretreatment of lignocellulosic biomass, due to hydrolysis of acetyl group of hemicellulose, and thermochemical degradation of polysaccharides in presence of acids (Jönsson et al. 2013). The total carboxylic acid content was determined to estimate the extent of these acids produced during the solid acid catalyst assisted pretreatment of sugarcane bagasse. It was noted that increase in the solid acid catalyst amount prompted an incline in the concentration of total carboxylic acids. The carboxylic acid content was estimated to be 0.017, 0.050, 0.212, and 0.484 g/L in case of

liquid obtained after pretreatment with 0.1, 0.2, 0.3 and 0.4 g solid acid catalyst, respectively. The highest carboxylic acid content (0.967 g/L) was observed when 0.5 g solid acid catalyst was used for pretreatment. However, the highest carboxylic content of 0.967 g/L is significantly lower than the total carboxylic acid content produced during conventional liquid acid pretreatment process reported in literature (Ingle et al. 2020b; Ilanidis et al. 2021a).

The biomass samples treated with 0.1 g solid acid catalyst resulted in formation of 0.001 g/L furfural, which further increased on increasing the solid acid catalyst amount. For sugarcane bagasse samples treated with 0.2, 0.3, and 0.4 g solid acid catalyst, the furfural concentration was estimated to be 0.006, 0.014, 0.050 g/L, respectively. Highest furfural (0.104 g/L) was present in the liquid fraction obtained after biomass treatment with 0.5 g solid acid catalyst. The high formation of furfural in presence of high solid acid catalyst amount could be attributed to the increased dehydration of pentose sugars liberated during pre-treatment, under acidic environment. The dehydration of hexoses sugars on the other hand results in formation of HMF, which was significantly lower as compared to furfural, with values recorded at ND, 0.001, 0.004, 0.008, 0.014 g/L for biomass treated with 0.1, 0.2, 0.3, 0.4 and 0.5 g solid acid catalyst, respectively. The impact of furan derivatives concentrations on catalytic activity of enzyme is unknown; however they have significant impact on the fermentation process as they induce reduction in membrane permeability which results in longer log phase during microbial growth (Larsson et al. 1999; Mhlongo et al. 2015). The concentrations of carboxylic acids and furans depend on the severity of the pretreatment conditions used; the low concentrations obtained during the employed pretreatment strategy demonstrate its immense potential for industrial scale applications.

During mild alkaline treatment step, a range of phenolic compounds are formed due to the fragmentation and oxidation of lignin content. Both lignin and phenolics hamper the hydrolysis and reduce sugar yields during enzymatic saccharification (Ximenes et al. 2011; Guo et al. 2014; Ko et al. 2015). The total phenolic content increased with increase in amount of solid acid catalyst used for biomass pre-treatment from 1.425 g/L to 2.621 g/L for sugarcane bagasse treated with 0.1 and 0.5 g solid acid catalyst, respectively. The higher concentration of phenolics could be ascribed to the easy access of dilute alkaline catalyst to lignin components due to higher removal of hemicellulose. The filtration step after the alkaline treatment results in elimination of the maximum phenolic compound produced due to their high solubility.

The results obtained demonstrated less production of inhibitory compounds and the preferred activity of solid acid catalyst towards hemicellulose component. For the betterment of the subsequent enzymatic hydrolysis of cellulose component, removal of lignin is easily achievable using dilute alkaline treatment. Overall, the employed strategy of subsequent solid acid catalyst and dilute alkaline pretreatment is established as a better approach than conventionally used liquid chemical pretreatment methods.

4.3.5 Reusable Potential of Solid Acid Catalyst

The solid acid catalyst was examined for five consecutive sugarcane bagasse pretreatment cycles. Considering the observations in previous sections, solid acid catalyst was clearly responsible for hemicellulose hydrolysis. Hence, xylose released in the liquid after solid acid catalyst pretreatment was used to gauge the reusability potential of solid acid catalyst. A gradual decline in xylose release was observed after every reuse (Figure 4.10). The process conditions, where 0.1 g solid acid catalyst was used for the pre-treatment of one gram of sugarcane bagasse, xylose released in 1st cycle was estimated to be 6.21 g/L, which reduced to 2.97 g/L after 5th cycle. In case of 0.2 g solid acid catalyst, the xylose release reduced to 4.48 g/L in 5th cycle from 8.3 g/L in 1st cycle. Similar results were obtained in case of 0.3, 0.4 and 0.5 g solid acid catalysts where xylose was recorded at 13.61, 15.18, and 18.49 g/L in 1st cycle, which reduced to 8.16, 9.56, and 12.33 g/L in 5th cycle, respectively.

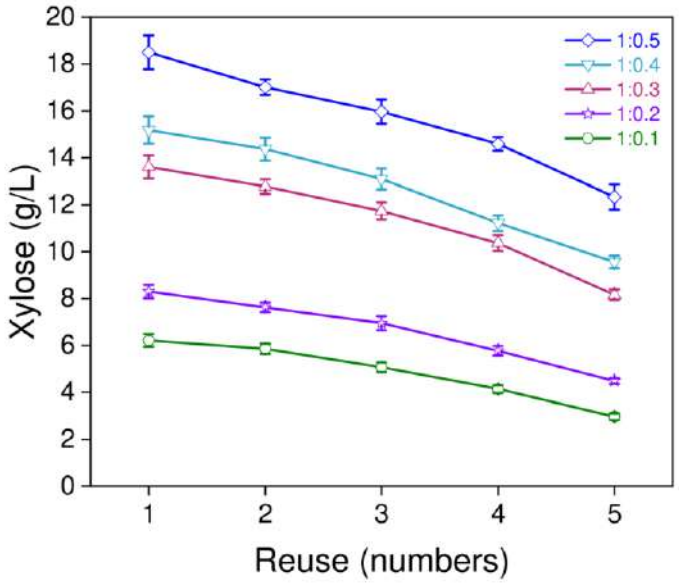

Figure 4.10 The extent of xylose release during pre-treatment steps after repeated use of solid-acid catalyst.

It was worth noting that the reusability capability obtained in this study is much higher than any solid acid catalyst used for sugarcane bagasse treatment, which can be credited to efficient attachment of sulfonic acid groups to MHNTs surface. Although, a slightly lowering in pre-treatment capacity of MHNTs-SO_3H after five cycles was attributed to the loss of few sulfonic acid groups present on the surface of solid acid catalyst (Wang et al. 2012; Ingle et al. 2020a; Ingle et al. 2020b). Conclusively, the solid acid catalyst (MHNTs-SO_3H) developed in this study demonstrated excellent hemicellulose removal capability and reusability for pretreatment of lignocellulosic biomass. The developed solid acid catalyst has scope to improve the overall activity and selectivity for futuristic applications.

4.4 Enzymatic Saccharification and Fermentation

To further validate the capability of employed pre-treatment approach, enzymatic hydrolysis of pre-treated SCB samples and its subsequent fermentation for ethanol production was performed. An efficient pre-treatment of biomass would result in higher enzymatic saccharification of cellulose component and thus, higher ethanol yield.

4.4.1 Enzymatic Saccharification

The impact of varying substrate loadings of biomass (1, 2.5 and 5 wt%) on cellulose saccharification using cellulase enzyme was investigated for 48 h (Figure 4.11a). Untreated sugarcane bagasse exhibited low enzyme conversion efficiency, attaining maximum saccharification of 22.04 with glucose yield of 104.90 mg/g SCB for 2.5 wt% biomass loading. Lowest saccharification (20.02%) was recorded for 1 wt% loading with glucose yield 95.38 mg/g SCB. On the other hand, a biomass loading of 5 wt% resulted in 20.41% cellulose saccharification with glucose yield of 97.16 mg/g of SCB. The recalcitrant nature of raw sugarcane bagasse limits enzyme-substrate interactions preserving the structure from hydrolysis. The enzymatic hydrolysis of SCB samples pretreated using different amount of solid acid catalysts showed remarkable results. The enzymatic hydrolysis of biomass treated with 0.1 g solid acid catalyst resulted in cellulose saccharification of 40.06, 45.69, and 42.88% for biomass loading of 1. 2.5, and 5 wt% respectively. The glucose yields for increased loading were recorded at 224.95, 256.55, and 240.73 mg/g biomass. A rise in saccharification and glucose yield as compared to untreated SCB validated the efficiency of adopted pre-treatment procedures. The superior hydrolysis efficiency could be attributed to the removal of hemicellulose and lignin contents from biomass, resulting in higher exposure

of cellulose component for enzymatic hydrolysis. Furthermore, cellulose saccharification of 43.56, 50.80, and 46.54%was observed for 1, 2.5, and 5 wt% SCB samples treated with 0.2 g solid acid catalyst. The respective glucose yields were 258.41, 301.35, and 276.11 mg/g biomass.

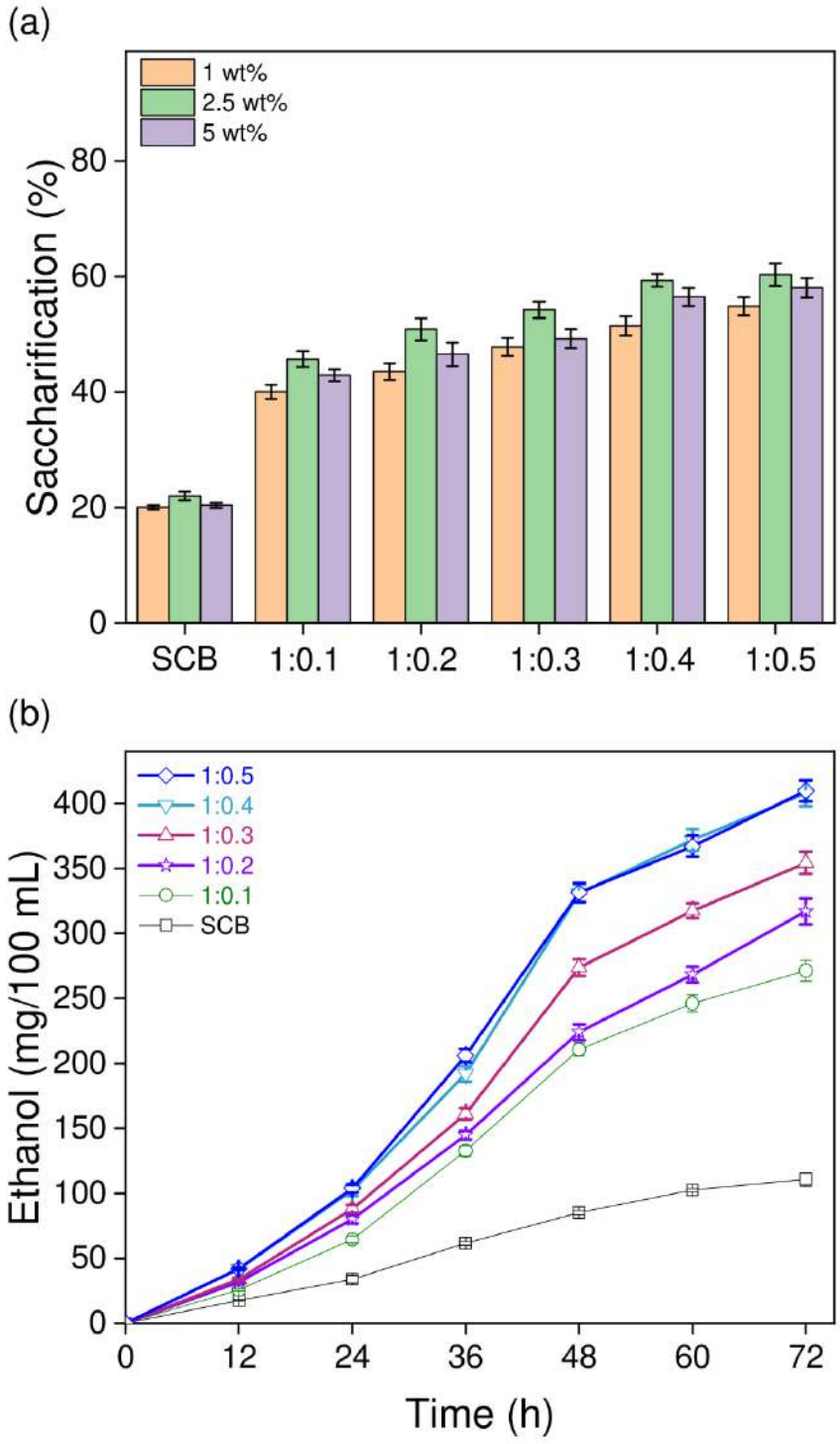

Figure 4.11 (a) Enzymatic saccharification at different substrate loadings, and (b) Ethanol yield from hydrolysates of sugarcane bagasse.

In case of SCB pre-treated using 0.3 g solid acid catalyst, maximum hydrolysis (54.27% with 353.13 mg glucose per g biomass) was witnessed for 2.5 wt% substrate loading. The biomass loading of 1 and 5 wt% resulted in comparatively lower saccharification value of 47.79 and 49.23%, respectively. Similar results were also obtained for samples treated with 0.4 and 0.5 g solid acid catalysts where 59.34% (385.44 mg glucose per g biomass) and 60.32% (393.99 mg glucose per g biomass) cellulose saccharification was noted for 2.5 wt% substrate loading.

A slight increase in saccharification could be attributed to higher inhibitory by-products produced during pretreatment with 0.5 g solid acid catalyst, which limited cellulase activity. The recorded data indicated that increase in biomass loading from 1 to 2.5 wt% prompted increase in cellulose saccharification, in all the studied samples. The trend was because of the presence of sufficient substrate for enzyme interaction. However, increase in biomass loading from 2.5 to 5 wt% inhibited the cellulose saccharification. The decline could be due to the changes in the rheological properties of the fibrous suspension at higher biomass concentrations. The inadequate mixing and limited heat transfer were the key elements in destabilizing the enzyme-substrate complex formation in the dense fibrous suspension. Additionally, inhibition effects from the high substrate amount and inhibitory products concentration were also the factors affecting the cellulose saccharification at higher substrate loading.

4.4.2 Fermentation of Solid Acid Catalyst-Derived Hydrolysate

Considering a higher saccharification and glucose yields, hydrolysates produced using 2.5 wt% biomass loading of all samples were further used for fermentation. *S. cerevisiae* MTCC170 strain was used as inoculum to utilise hydrolysate as substrate. The fermentation process was performed for 72 h, and ethanol produced was measured at different intervals. Results demonstrate that the ethanol production increased with time and increased rapidly between 24-48 h (Figure 4.11b). After 48 h, the rate of ethanol production started to decline due to the depletion of glucose (substrate) concentration. From hydrolysate of untreated sugarcane bagasse sample 110.77 mg/100 mL ethanol yield was observed after 72 h fermentation time. From hydrolysate of pretreated samples ethanol yield of 271.35, 317.16, 354.36, and 408.02 mg/100 mL was recorded for bagasse pretreated using 0.1, 0.2, 0.3, and 0.4 g solid acid catalyst, respectively. A consistent increase in ethanol yield validated the

absence of major inhibitory compounds produced during pre-treatment process till the solid acid catalyst load of 0.4 g/g SCB. The ethanol production from hydrolysates of bagasse treated using 0.4 g and 0.5 g solid acid catalyst (409.70 mg/100 mL) were comparable. It indicates that at high solid acid catalyst load, fermentation inhibiting compounds may be produced which aligned well with results observed during inhibitor analyses.

4.4.3 Mass Balance of Ethanol Production from SCB

To conclude, all the data recorded was used to perform a mass balance to determine the effectiveness of pretreatment of sugarcane bagasse using different solid acid catalyst amount (0.1-0.5 g) for bioethanol production. Taking 1 g dried sugarcane bagasse, the reduction in hemicellulose and lignin content was evident, along with enrichment of cellulose content in recovered biomass (Figure 4.12). Furthermore a superior impact of different pretreatments on cellulase saccharification was also manifested. The cellulase-mediated hydrolysis of untreated sugarcane bagasse demonstrated 22.04% cellulose saccharification which increased to 60.32% for sugarcane bagasse pretreated using 0.5 g solid acid catalyst. The highest glucose release (272.71 mg) was obtained from SCB sample pre-treated with 0.4 g solid acid catalyst, owing to higher cellulose content (414 mg) than the biomass sample pre-treated using 0.5 g solid acid catalyst (403.5 mg). Overall a 263.15% increase in glucose release was observed as compared to untreated sugarcane bagasse (103.63 mg). Furthermore, all pre-treated samples displayed significantly higher bioethanol yield compared to the untreated sugarcane bagasse. The ethanol yield was directly related to the amount of glucose released during cellulase mediated cellulose saccharification. The samples pretreated using 0.1, 0.2, 0.3, 0.4 and 0.5 g solid acid catalyst revealed 2.06, 2.27, 2.43, 2.64 and 2.57 fold increase in ethanol yield compared to untreated sugarcane bagasse (43.78 mg). Maximum bioethanol conversion efficiency (83.23%) was obtained using SCB pre-treated using 0.4 g solid acid catalyst indicating this pre-treatment condition as the best for efficient valorization of SCB. Ethanol yield attained in this work is comparable to other recent reports (Dionísio et al. 2021; Valladares-Diestra et al. 2021; de Oliveira Rodrigues et al. 2022) validating the effectiveness of solid acid catalyst-mediated pre-treatment approach, developed in this research which has immense potential to be examined further.

The key points taken for future work includes selection of nanomaterial with higher specific surface area for acidic modifications, an appropriate ratio of solid acid catalyst to biomass for

during the pre-treatment, and an optimized loading of substrate for enzymatic saccharification. The glucose release and subsequent fermentation are two crucial phases for biomass valorisation. Hence, due importance should also be given while selecting appropriate enzyme consortium and microorganism strain with high bioconversion efficiency. Finally, simultaneous saccharification and fermentation (SSF) is another interesting process which can bring down the overall duration and processing cost and must be exploited to the current work in future.

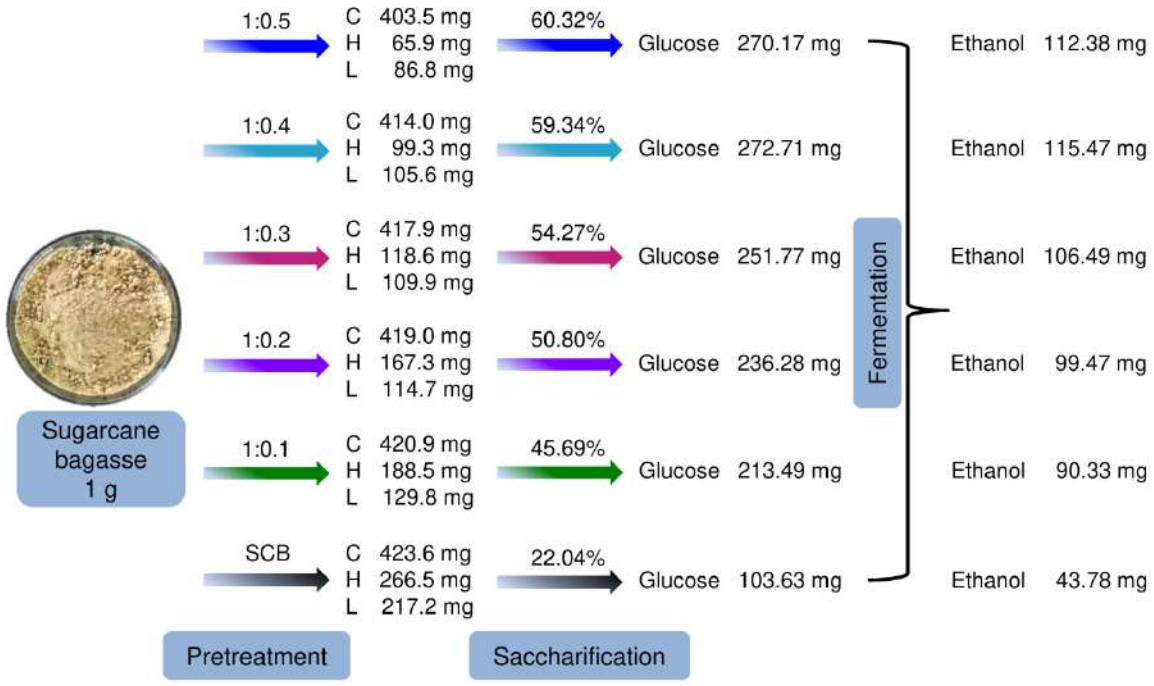

Figure 4.12 Mass balances for ethanol production from 1 g dried sugarcane bagasse via solid acid catalyst mediated pretreatments.

4.5 Development of Cellulase based Nanobiocatalyst

A schematic representation for developing a novel nanobiocatalyst via surface functionalization employing magnetic halloysite nanotubes (MHNTs) is shown in Figure 4.13. Interestingly, the choice of selecting HNTs as an immobilizing template warrants two important considerations. First, the exterior surface of HNTs offers a large surface area which can be modified undergoing specific surface chemistry (Yuan et al. 2015). We have evidenced that uniform silanol (Si-OH) sites over silica-based materials can be transformed into a much stronger siloxane (Si-O-Si) bonds through aminosilanization causing orientation of amine groups away from the surface(Agnihotri et al. 2013). In addition to this, a strong hydrogen bonding might also occur between amino groups of the organosilanes and silanol groups. Secondly, the enzyme immobilized on external surface of HNTs also ensures maximum interaction between the substrate (CMC) and immobilized enzyme overcoming external mass transfer limitations in a manner its catalytic behaviour would not be compromised.

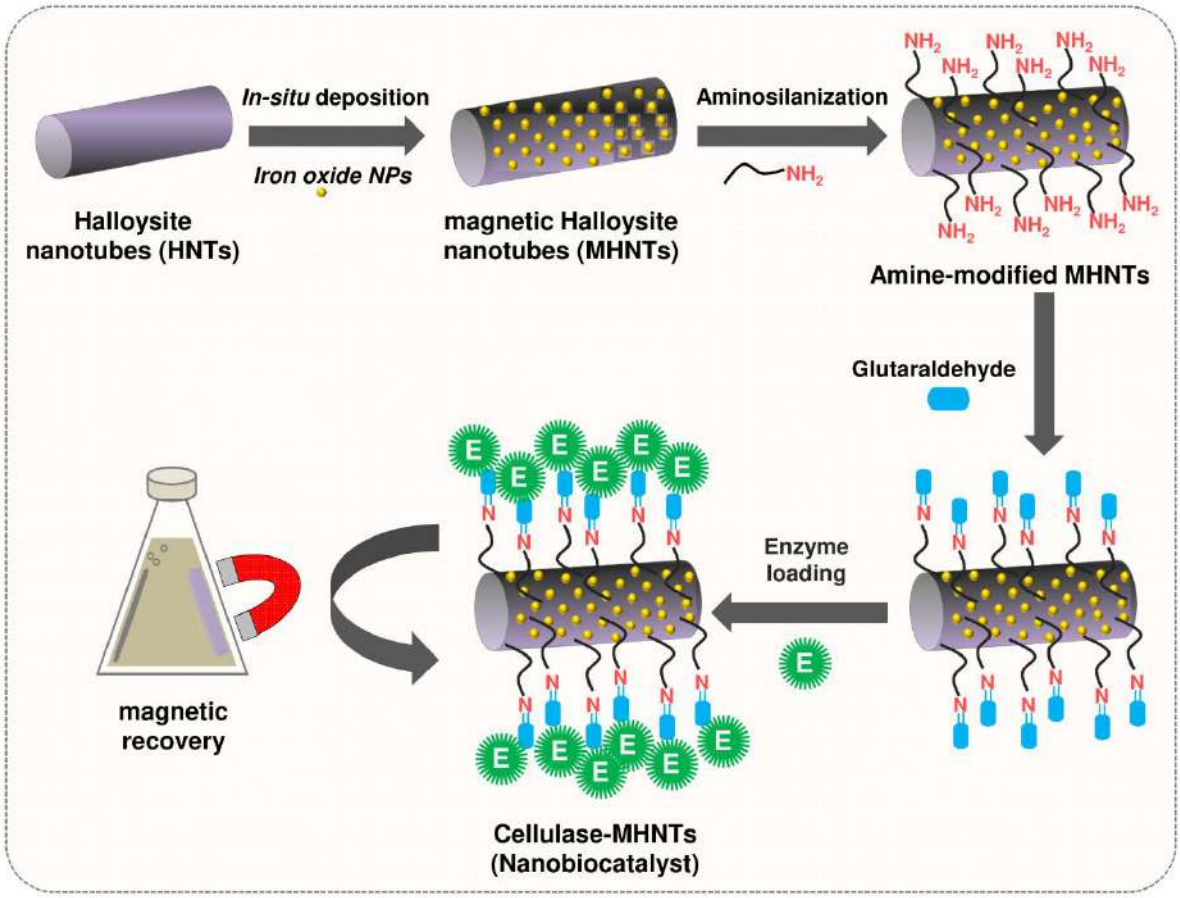

Figure 4.13 Schematic representation of cellulase immobilization on magnetic halloysite nanotubes via aminosilane functionalization and gluteraldehyde activation.

The use of enzyme immobilized on halloysite nanotubes requires additional filtration and centrifugation step for separation of the immobilized enzyme out of reaction mixture, leading to increase in overall cost of the process (Zhai et al. 2010; Chao et al. 2013; Tully et al. 2016; Katana et al. 2019). Employing magnetic halloysite nanotubes would resolve the issue; hence the same were used for faster and efficient recovery of the nanobiocatalyst from the reaction mixture (Kadam et al. 2018; Kim et al. 2018; Kadam et al. 2020a; Zhu et al. 2021). We also employed pretreated sugarcane bagasse as substrate, though at a very low concentration of 1% w/v. It is evidenced through this study that such a diluted substrate suspension behaved similar to CMC in terms of its aqueous solubility. As a combined effect, the aminosilanization of magnetic HNTs facilitated a dense, multipoint anchoring of enzyme on outer surface of HNTs. The multipoint anchoring of enzyme indicates a strong interaction between enzyme and support matrix via crosslinking than its restriction, where the use of crosslinker can offer two basic advantages for immobilization. First, it may improve the stable anchoring of enzymes over a solid support while the arm space of crosslinker would govern the mobility of enzyme with required flexibility to interact with the substrate molecules. The as developed nanobiocatalyst, i.e. cellulase immobilized MHNTs was analyzed further through several characterization studies before employing it for biocatalytic experiments.

4.5.1 Characterisation of Cellulase Immobilized Magnetic Halloysite Nanotubes (cellulase-MHNTs)

The variation in surface characteristics of MHNTs after APTES functionalization, and cellulase immobilization were initially assessed using FTIR spectroscopy over the range of 4000−400 cm^{-1} (Figure 4.14a). After aminosilane grafting, emergence of new peaks at 3369, 2925, 2854, and 1245 cm^{-1}, was observed which were assigned to symmetric and asymmetric vibrations of N−H_2, C−H_2, C−H_2, and C−N bonds, respectively. The presence of these peaks confirmed the successful aminosilane grafting and presence of amine functional moieties at the outer surface of magnetic halloysite nanotubes (Yuan et al. 2008). In case of cellulase immobilized amino-modified MHNTs, two peaks, were detected at 1600 and 3430 cm^{-1}which were credited to the stretching vibrations of amide-I bands and amine groups, respectively (Khoshnevisan et al. 2011). The peaks matches well with the FTIR spectra of free cellulase indicating the effective immobilization of cellulase onto the magnetic halloysite nanotubes. Furthermore, the presence of characteristic peaks of MHNTs in both amine

modified MHNTs and cellulase-MHNTs validated the intact nature of backbone structural components i.e., halloysite nanotubes and iron oxide nanoparticles. Overall, the inherent backbone structural integrity after aminosilane functionalization and subsequent enzyme immobilizations well as the stable binding of cellulase over the functionalized MHNTs matrix were concluded from the observed FTIR results.

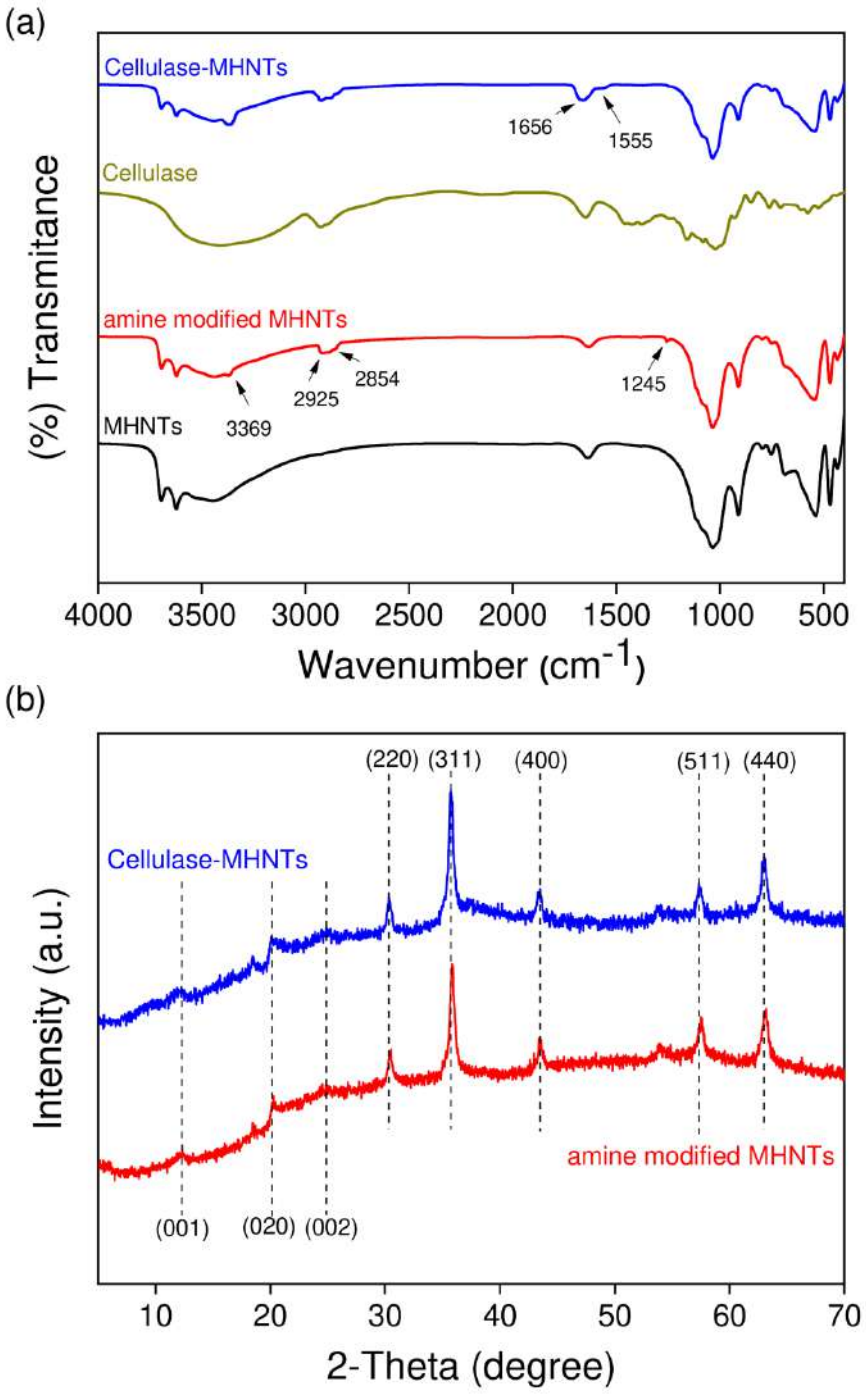

Figure 4.14 Characterization of MHNTs, amine modified MHNTs and Cellulase-MHNTs through (a) FTIR spectroscopy, and (b) XRD analyses.

To determine any changes either in the backbone structure or crystalline nature, XRD analyses were performed on amine modified MHNTs and cellulase-MHNTs samples. As shown in Figure 4.14(b), the characteristic peak of halloysite nanotubes at 2θ=12.21° was observed in both samples, which confirmed the existence of nanotubular structure of the HNTs matrix. This peak was attributed to (001) plane of the HNTs with basal spacing 0.724 nm (JCPDS Card No. 29-1487) as discussed earlier (Zhang et al. 2013; Kumar-Krishnan et al. 2016). The iron oxide nanoparticles anchoring was evident from the intrinsic peaks at 2θ = 30.43°,35.78°,43.47°, 57.46° and 63.09° which is attributed to (220), (311), (400), (511), (440) planes of the magnetite Fe_3O_4 (JCPDS Card No. 01-075-0449). The recorded peaks confirmed the presence of magnetic nanoparticles over HNTs surface even after aminosilane functionalization and subsequent cellulase immobilization (Kadam et al. 2017). Furthermore, the absence of any new peak in the spectra concludes that the functionalization or loading of cellulase on to MHNTs did not alter the physicochemical characteristics of the backbone HNTs support matrix.

The magnetic behaviours of MHNTs, amine modified MHNTs and cellulase-MHNTs were investigated using vibrating sample magnetometer where magnetization curves indicate sample magnetization in response to the applied magnetic field (Figure 4.15a). Highest saturation magnetization was observed in case of MHNTs with value 40.68 emu/g along with zero coercivity and remanence. The observed features were characteristic of superparamagnetic materials, indicating that the anchoring of iron oxide nanoparticles onto halloysite nanotubes transformed them into magnetically recoverable material while not influencing the inherent crystalline characteristic. On the other hand, amine-modified MHNTs, before and after enzyme immobilization demonstrated the saturated values of magnetization as 32.54 and 28.68 emu/g, respectively. The overall decreases in saturation magnetization value were attributed to the loading of non-magnetic materials in form of aminosilane, glutaraldehyde and cellulase enzyme. Nonetheless, the magnetic property of the formed nanobiocatalyst (NBC) was satisfactory for the intended application, as the magnetic recovery was not at all compromised. The easy separation capability of NBC was clearly evident from the photographic image (inset).

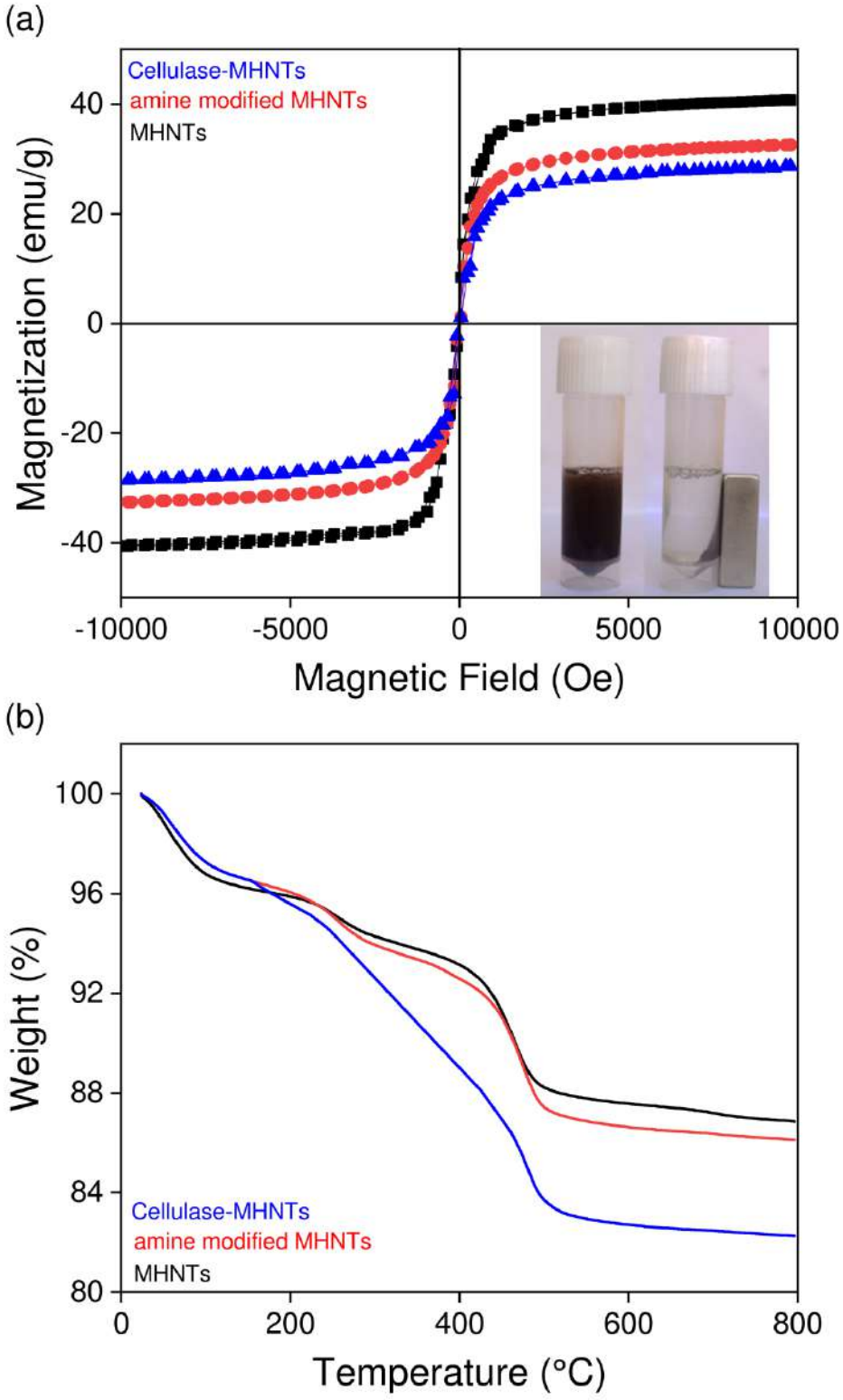

Figure 4.15 Characterization of MHNTs, amine modified MHNTs and Cellulase-MHNTs through (a) Magnetic hysteresis loops, Inset photographic image shows ease in separating the nanobiocatalyst from a colloidal suspension, and (b) thermogravimetric analysis (TGA).

Thermogravimetric analyses (TGA) of all samples were performed to confirm the amine functionalization of MHNTs and immobilization of cellulase over amine-modified MHNTs via glutaraldehyde crosslinking (Figure 4.15b). Pristine MHNTs sample (without amine-functionalization) was taken as a negative control. For all samples, the dehydration occurred between 30 and 200 °C, which is typical characteristic of halloysite nanotubes (Fakhrullina et al. 2019); however there was a slight difference in the thermogram of MHNTs as compared to amine modified MHNTs and cellulase-MHNTs. The slight difference is attributed to the decreased amount of adsorbed H_2O at the surface of Hal nanotubes due to the presence of organosilanes (Pandey et al. 2017). From 200 to 400 °C the partial degradation of organic compounds took place, was clearly evident from the thermogram of amine modified MHNTs and cellulase-MHNTs. The higher weight loss in case of cellulase-MHNTs in this range was attributed to the presence of glutaraldehyde and protein cellulase, as this is also a typical degradation temperature range for proteins. Furthermore, organic content decomposition continued till 800 °C along with dehydroxylation of the HNTs (Zhang et al. 2019b). Considering the differences in thermogram profiles it was clear that there was no change in structural integrity of MHNTs after functionalization and immobilization of cellulase, validating the outcome of FTIR and XRD analyses. Amine modified MHNTs demonstrated a 0.73% higher weight loss as compared to its pristine counterpart (MHNTs), which was attributed to the additional thermal loss of organosilane functionalized onto MHNTs. On contrary, the cellulase immobilized MHNTs depicted ~12.82% weight loss within 150-500°C temperature, which confirms the presence of cellulase binding over MHNTs. A simple mass balance was applied for determining the immobilization efficiency of cellulase through UV-Vis spectroscopy (Bradford assay), which matched well with that of TGA data.

Furthermore, the detailed surface elemental composition investigations of cellulase-MHNTs to confirm successful functionalisation and cellulase immobilization, was done by XPS analysis. X-ray photoelectron spectroscopy (XPS) is considered as one of the most sensitive techniques for evaluating the surface chemistry of nanomaterials. Figure 4.16(a) depicts a wide scan spectrum of the nanobiocatalyst (cellulose-MHNTs), where the existence of binding energy peaks of Al 2p, Si 2p, C 1s, N 1s, O 1s,and Fe 2p, respectively was recorded. These peaks were indicative of the successful anchoring of iron oxide nanoparticles over HNTs, amine functionalization, and subsequent loading of cellulase enzyme. A high resolution spectrum of Fe 2p revealed two spin−orbit doublets at 712.18 eV (Fe $2p_{3/2}$) and 725.51 eV (Fe $2p_{1/2}$) (Figure 4.16b). The energy separation of 13.4 eV is a characteristics

marker for a chemical shift difference between the Fe^{2+} and Fe^{3+} states present in Fe_3O_4nanoparticles (Wilson and Langell 2014). A further deconvolution of the Fe spectra gave rise to two peaks in the Fe $2p_{3/2}$ spin orbit peak which were attributed to the existence of Fe^{2+} and Fe^{3+}. On the other side, the existence of a satellite peak between the Fe $2p_{3/2}$ and Fe $2p_{1/2}$ peaks was credited to the presence of a small amount of Fe_2O_3 (Wilson and Langell 2014). The obtained results were in good accordwith the previous reports, confirming the presence of Fe_3O_4 in the nanobiocatalyst.

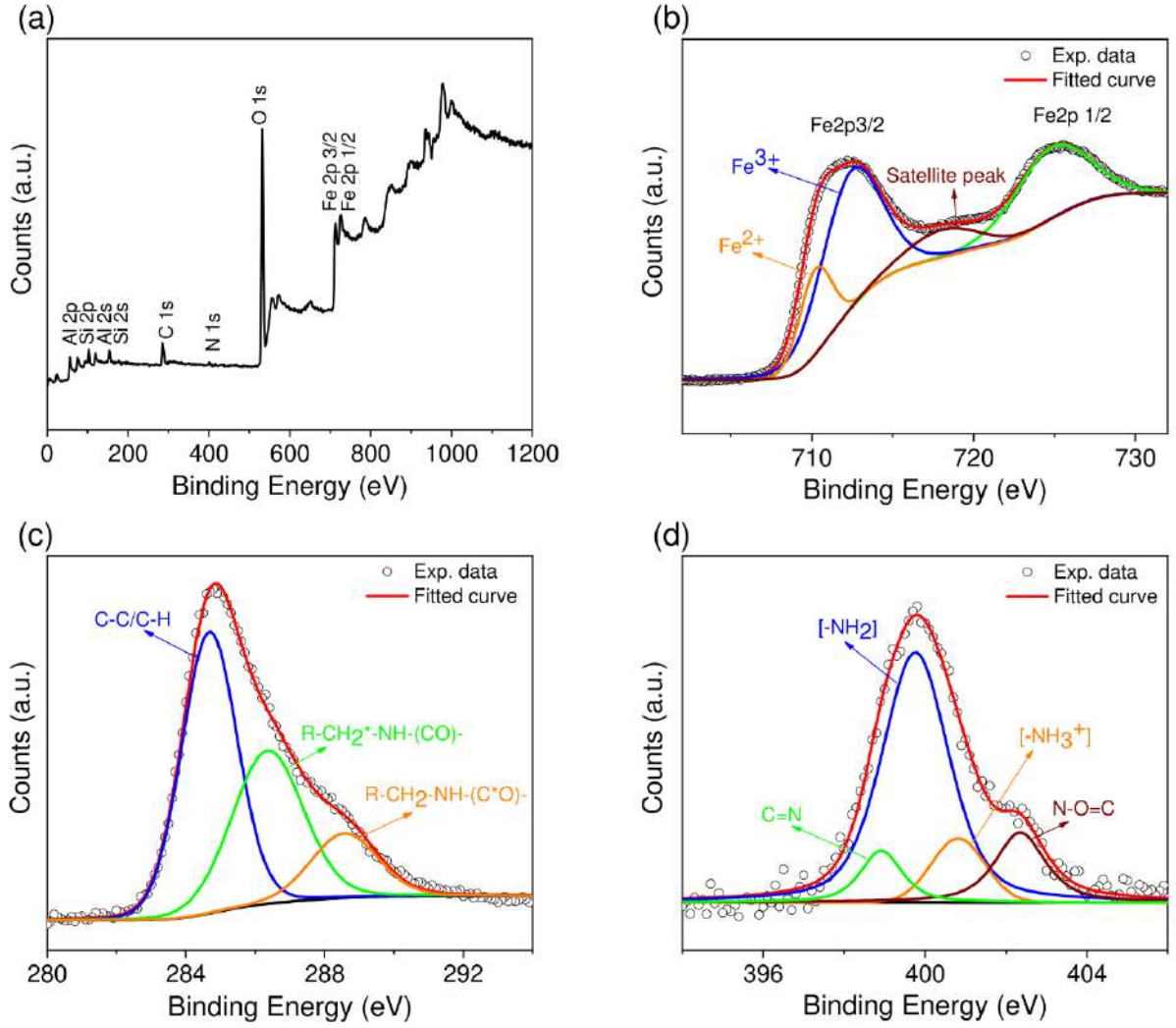

Figure 4.16 XPS spectral analysis of nanobiocatalyst (cellulase-MHNTs) (a) scan survey, (b) high resolution spectra of Fe 2p peak, (c) high resolution spectra of C 1s peak, and (d) high resolution spectra of N 1s peak.

In C 1s high resolution spectra, a peak centered at 284.6 eV was assigned to sp^2 hybridized carbon (C−C and C−H bonds) (Wang et al. 2014). This was further deconvoluted into two

peaks at 286.3 and 288.5 eV, which were ascribed to $R-CH_2*-NH-(CO)-/R-CH_2-NH-(C*O)-$ and the amide bonding (R−CONH−) group, respectively (Libertino et al. 2008) (Figure 4.16c). Since these functional moieties are the characteristic features of a protein's structures, the loading of cellulase enzyme onto MHNTs matrices was established. In addition to this, a high resolution N 1s spectrum was deconvoluted into four distinct peaks that correspond to the C=N bond (398.9 eV) (Park et al. 2011), amine group from APTES and cellulase (399.7 eV), hydrogen-bonded amine ($H-NH_2$) orprotonated amine (400.8 eV), and N−O=C (402.3 eV) (Acres et al. 2012; Mazzotta et al. 2015) (Figure 4.16d). The lower intensity of the protonatedamine and high intensity of the NH_2 group peak endorsesed the high loading of cellulase, as the amine groups were pointing away from the substrate. The obtained data confirmed thecovalent immobilization of cellulase onto APTES functionalgroups via cross-linking with glutaraldehyde.

The structural morphology of MHNTs was investigated by transmission electron microscopy. The HR-TEM image confirms the successful loading of iron oxide nanoparticles on the surface of HNTs, where a distinct interface between two nanoscale structures was observed (Figure 4.17a). This validates the fact that an in situ synthesis of magnetic nanoparticles and theirsubsequent immobilization was facilitated through a one-stepprotocol rendering the inherent morphology of HNTs intacteven after loading iron oxide nanoparticles (Figure 4.17b). The size of iron oxide nanoparticles were found to be 3-6 nm range with circular and quasi-polyhedral shape. Energy-dispersive X-ray spectra confirmed the presence of iron along with the characteristic elements of HNTs (Figure 4.17c). The nanobiocatalyst (cellulase-MHNTs) were investigated through FE-SEM where the cellulase enzyme was found to be densely anchored over amine-modified MHNTs with a high payload (Figure 4.17d). The intact morphology of HNTs was corroborated with the results obtained through XRD analyses. The corresponding elemental mapping further confirms the effective distribution of iron oxide nanoparticles throughout the sample (Figure 4.17e).

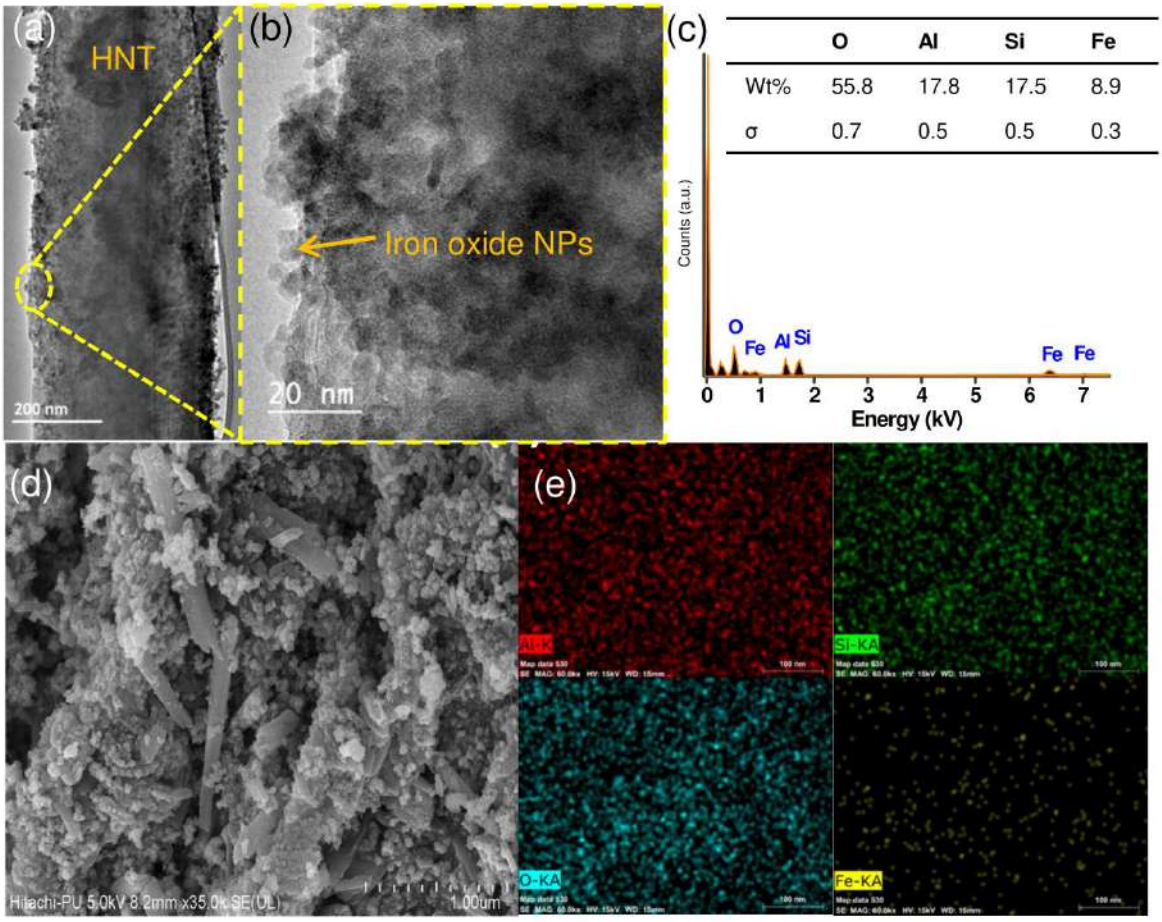

Figure 4.17 (a) TEM micrograph, (b) Corresponding HR-TEM image, (c) EDS spectra and weight basis composition of MHNTs, (d) FE-SEM micrograph of cellulase-MHNTs, and (e) Elemental mapping of aluminum, silicon, and oxygenand iron element.

4.6 Cellulase Immobilization

For immobilization of cellulase enzyme on magnetic halloysite nanotubes, parameters affecting the immobilization process were investigated using one factor at a time approach. The parameters and their range having most significant impact on the loading of cellulase were further used for optimization using response surface methodology (RSM).

4.6.1 Single Factor Study

The three independent factors, i.e., amount of support matrix (amine modified glutaraldehyde activated MHNTs) (mg), cellulase concentration (mg/mL), and pH of the solution, which might affect the enzyme loading were investigated. A wide range for each parameter was investigated to constraint the range to be used for RSM design. For single factor study with

varying support amount (5-40 mg), cellulase concentration (1.5 mg/mL) and pH (5) were kept constant (Figure 4.18a). Increasing the amount of support from 5 mg to 40 mg resulted in a gradual increase in cellulase loading from 27.38% to 84.10%. The high enzyme loading was attributed to the availability of multiple anchoring sites over MHNTs. To evaluate the impact of high enzyme loading on the final catalytic activity of cellulase, the activity of immobilized enzyme using different support amount were assessed for their corresponding catalytic activity (Figure 4.18b). The recorded data revealed that a significant reduction in catalytic activity of the immobilized cellulase was manifested when the amount of support was increased beyond 20 mg despite the high enzyme loading. This reduction in catalytic activity was attributed to steric hindrance posed by the immobilized enzymes due to high payload. Though, such decline in catalytic activity of cellulase (enzyme units/g of support) beyond 20 mg support was marginal, which could be compensated by prolonging the duration of biocatalytic reaction, which would result in better substrate conversion. Since it was desirable to choose a minimum amount of nano-biocatalytic system which could perform better for cellulose hydrolysis than its corresponding higher enzyme loading, 20-30 mg range of support matrix amount was chosen for further optimization experiments.

On the other hand, single factor study on cellulase concentration (0.5-2.5 mg/mL) was performed with 20 mg support amount and pH 5 (Figure 4.18c). A consistent decrease in the enzyme loading was evident from the recorded data. The limited number of anchoring sites was the reason behind the observed trend. Considering the results, the range 1.25-1.75 mg/ mL of enzyme concentration was selected for RSM. The studies using pH range 4-6 were conducted while keeping support amount (20 mg), and cellulase concentration (1.5 mg/mL) (Figure 4.18d). Solution pH displayed the least impact with enzyme loading varying within a short range from 72.97 to 76.71%. However, the combinational influence of pH with other factors could not be predicted solely using single factor studies. Therefore, pH range from 4.50 to 5.50 was chosen to study the overall impact of pH along with other parameters on enzyme loading (%).

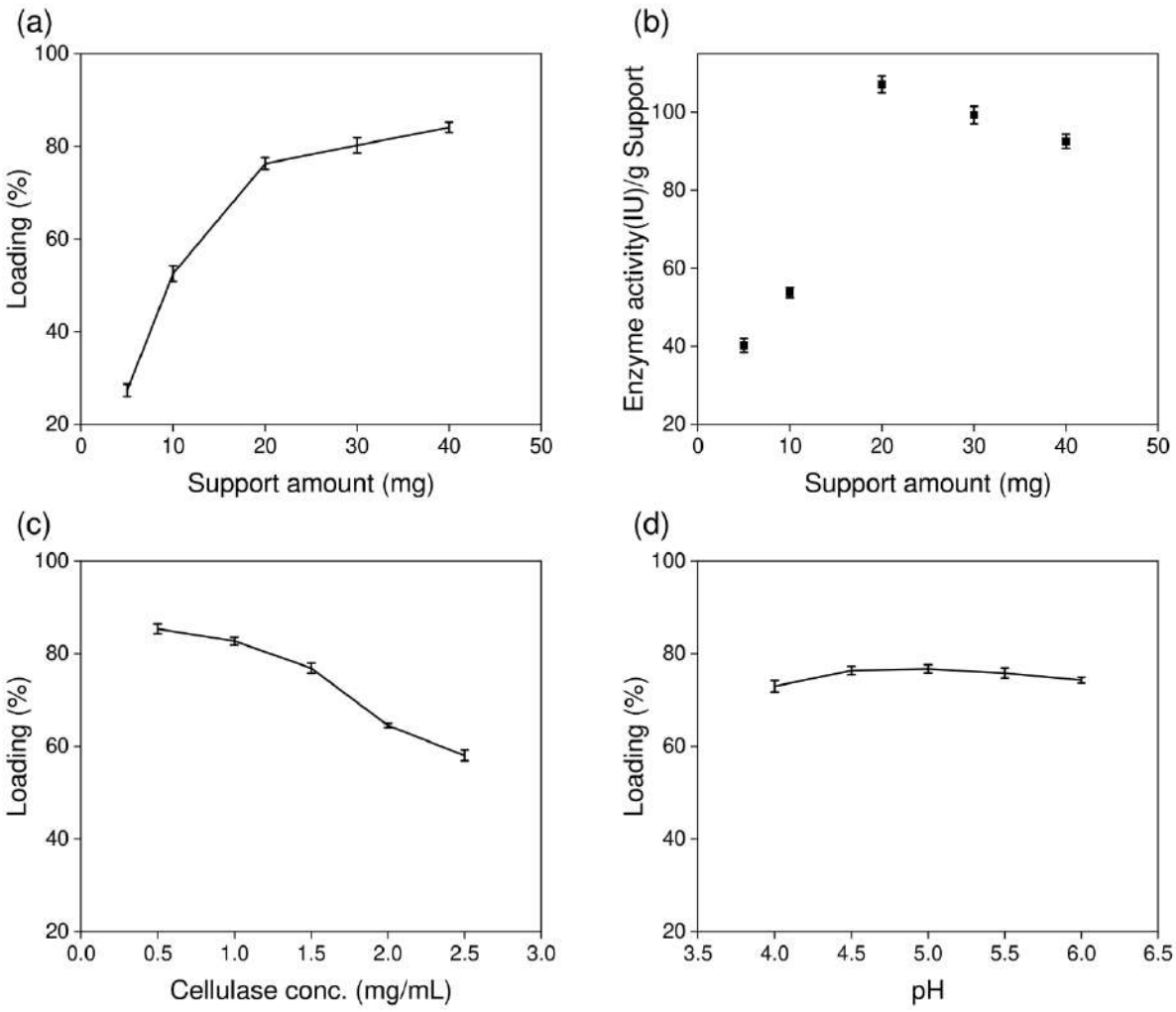

Figure 4.18 (a) Impact of support amount (mg) on cellulase loading (%), (b) Enzyme catalytic activity with varying support amount (mg), (c) Impact of cellulase concentration (mg/mL) and (d) Impact of pH on cellulase loading (%).

4.6.2 Box Behnken Design (BBD)

The operational ranges of independent parameters having a positive effect on the response, as obtained by single-factor studies, were statistically optimized employing response surface methodology, using Box-Behnken design. Multiple regression analysis was done to resolve the polynomial coefficients for each term of the equation. The actual factors controlling the immobilization efficiency of cellulase over MHNTs and their combinational impact is represented in form of a regression equation as the following:

$$Y = -371.09675-9.64850A+269.54600B+147.25500C+0.11077A^2-83.13200B^2 -15.20300C^2+0.71400AB+0.72100AC-9.22000BC$$

Where, Y is enzyme loading (%), A is amount of support (mg), B is concentration of cellulase enzyme (mg/mL), and C is solution pH.

The significance of predicted model was evaluated using Analysis of variance (ANOVA), which indicated this model to be highly significant (Table 4.3). Model F-value (21.41) observed in Fisher's F-test confirmed the adequacy of model for the selected parameters. A p-value of 0.0003 also signifies that the model accurately summarizes the relationship between selected factors and the response. The probability of error because of the noise was only 0.03%. The lack of fit F-value of 1.04 indicates this value to be insignificant relative to pure error.

Table 4.3 ANOVA for response surface quadratic model.

Source	**Sum of Square**	**DF**	**Mean Square**	**F Value**	**Prob>F**	**Remarks**
Model	324.61	9	36.07	21.41	0.0003	significant
A	64.07	1	64.07	38.03	0.0005	
B	32.81	1	32.81	19.47	0.0031	
C	0.67	1	0.67	0.40	0.5475	
A^2	32.29	1	32.29	19.17	0.0032	
B^2	113.67	1	113.67	67.48	< 0.0001	
C^2	60.82	1	60.82	36.11	0.0005	
AB	3.19	1	3.19	1.89	0.2114	
AC	13.00	1	13.00	7.71	0.0274	
BC	5.31	1	5.31	3.15	0.1190	
Residual	11.79	7	1.68			
Lack of Fit	5.18	3	1.73	1.04	0.4640	not significant
Pure Error	6.61	4	1.65			
Cor Total	336.40	16				

*A: Support amount (mg); B: cellulase conc. (mg/mL); C: solution pH

The multiple correlation coefficients (R^2), which measures the extent of variance from the model's mean value, indicated a close proximity among independent variables viz. amount of MHNTs, conc. of enzyme and solution pH (Table 4.4). R^2 value obtained from ANOVA was

in accordance with the defined limit for the model to be effective. The predicted R^2 (0.7229) and adjusting coefficient of determination (R^2-adj=0.9199) for calculated optimal conditions were in good harmony with the value of multiple correlation coefficients (R^2=0.9649), indicating that the model can predict 96.49% of the values.

Table 4.4 Coefficients of determination for response surface quadratic model.

Std. Dev.	1.30	R^2	0.9649
Mean	75.21	Adjusted R^2	0.9199
C.V.	1.73	Predicted R^2	0.7229
PRESS	93.20	Adeq. Precision	15.847

Figure 4.19 demonstrates contour plots and 3-D surface graphical representations for the response generated, i.e., enzyme loading (%). The response is represented as height in each of the 3D surface plots. The optimum conditions contributing towards maximum loading of enzyme on to support matrix were as follows: 20 mg support amount, 1.44 mg/mL cellulase concentration, and 4.8 solution pH. The model was further validated by carrying out immobilization procedure under optimized conditions, where a maximum immobilization of 77.5%, was obtained which was in good agreement with model's predicted value (78.7%). The averages of three replicates were tested and mean values are reported.

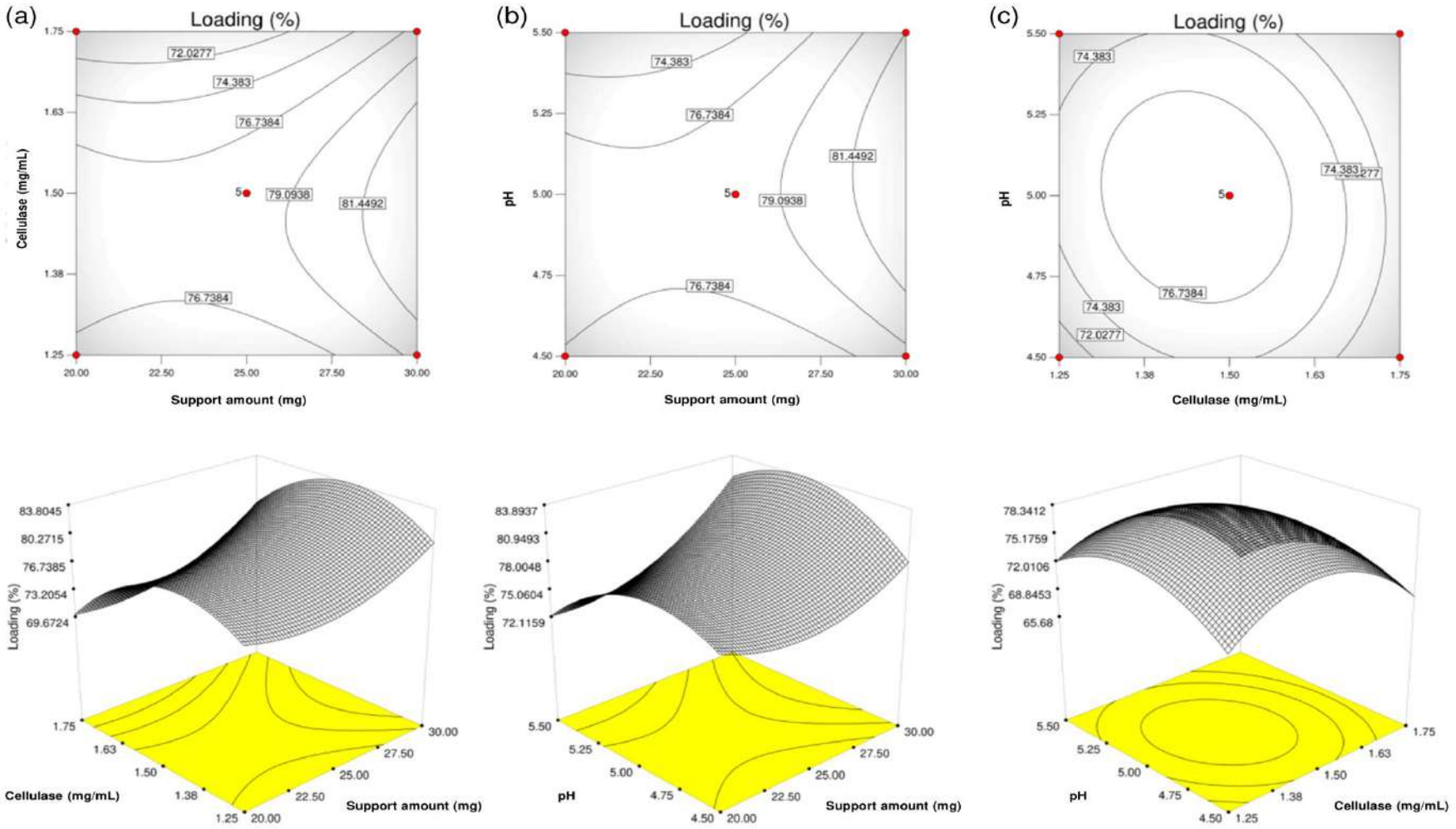

Figure 4.19 2D contour and 3D response surface plots for analyzing the interaction effects between (a) Cellulase concentration and support amount, (b) pH and support amount, and (c) pH and cellulase concentration.

4.7 Evaluation of Biocatalytic Characteristics

The loading of cellulase enzyme was investigated for 48 h at the optimized values predicted by the model. It was evident from the observed data that enzyme loading significantly increased with time until 6 h (77.5 ± 1.1%),increased slowly after this point and attained a maximum value of 83.2 ± 2.3% in 48 h (Figure 4.20a). Taking into consideration the peculiar nature of enzyme, 6 h reaction time was selected as the optimum immobilization time. Interestingly, the biocatalytic activity of cellulase-MHNTs was marginally decreased to only 93.4% as compared to free cellulase. The impact of the amine functionalization of MHNTs over cellulase immobilization and its biocatalytic activity was correlated using release profile study. The corresponding release kinetics further revealed that ~21.9% of total immobilized cellulase was released in the reaction system over a period of 48 h. Both results clearly demonstrated the effectiveness of the immobilization strategy without compromising its catalytic activity much. In fact, after immobilizing cellulase onto MHNTs, the nanobiocatalyst demonstrated heterogeneous catalysis, where the CMC substrate was easily accessible to the enzyme catalytic sites with insignificant external mass transfer limitations. After the enzymatic reaction, the resultant molecules i.e., glucose, rediffuse out of the catalytic templates as reaction products.

4.7.1 Impact of Process Parameters

The influence of various process parameters on the catalytic performance of cellulase-MHNTs was determined and compared with free cellulase. The investigation over a pH range (3-7) revealed that the optimum pH for both free and immobilized cellulase was at pH 5 (Figure 4.20b). Immobilized cellulase showed distinct residual activities over a broad pH range (3−7); though varying pH from optimum value adversely affected the catalytic activity. However the reduction in activity was minor as compared to free cellulase which was found to be more sensitive towards pH change. For instant, at pH=6 free cellulase could only retain 35% of its optimum activity, whereas nanobiocatalyst was able to retain 60% of its catalytic activity under similar test conditions. The obtained results demonstrated that immobilization reduced the sensitivity of cellulase, which was attributed to the protection of conformational structure of cellulase due to the multipoint attachment with support matrix. In a few recent reports, cellulase immobilization over styrene/maleic anhydride nanoparticles (Wang et al. 2018) and magnetic nanocomposites (Jordan et al. 2011; Abraham et al. 2014; Hosseini et al.

2018) has also witnessed a significant improvement in their pH dependent stability, similar to our work.

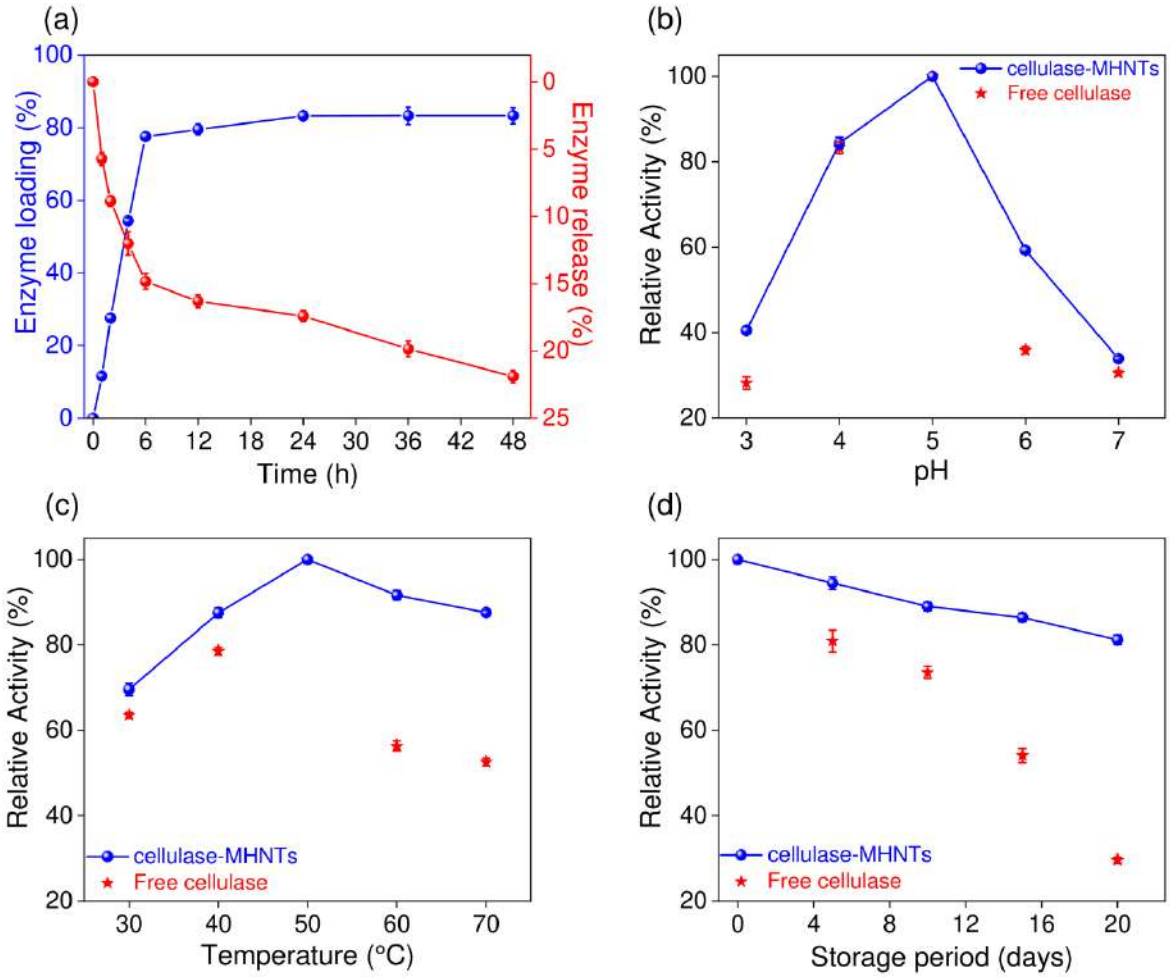

Figure 4.20 (a) Enzyme loading and its subsequent release kinetics, the impact of (b) solution pH, (c) working temperature, (d) storage duration on catalytic activity of free cellulase and nanobiocatalyst (cellulase-MHNTs).

Similarly, the activity assays at varying temperatures (30−70 °C) revealed 50 °C as an optimal temperature for both forms of cellulase (Figure 4.20c). Increasing temperature to 60 °C lead to only 56.33% activity of free enzyme, whereas, the activity of immobilized cellulase was marginally reduced to 91.67%. The cellulase-MHNTs could retain a minimum of ~70% residual activity regardless of temperature variations (30−70 °C) which was likely due to the immobilization induced heat resistance of enzymes. This was further verified by exposing both free cellulase and cellulase-MHNTs to 70 °C at pH 5 for 6 h. As expected, the residual activity of free cellulase was severely affected and reached to ~12.63 ± 0.7% after 6

h. Whereas, immobilized cellulase could manage to retain ~76.6 ± 0.5% activity within the similar time period. An improved thermal resistance of immobilized cellulase confirmed their stability under high temperature, which can be exploited for utilization under harsh processing conditions.

Considering the fact that the majority of free enzymes fail to retain their catalytic activity after being stored for long durations, the residual activities of cellulase existing in different states was evaluated by storing them at 4 °C for 20 days. As depicted in Figure 4.20(d), while free cellulase could retain only 29.6% of its initial activity, the NBC retained 81.2% activity even after 20 days of storage. Interestingly, the activity of free cellulase decreased sharply after 10 days and became even lower in the following days while cellulase-MHNTs displayed a linear trend in % activity loss, much lower than the former one. These observations again supported our hypothesis that a multipoint anchoring of enzymes with amine-modified MHNTs surface not only allowed an easy access of substrate to the active sites of immobilized enzyme but also offered them even more flexibility and robustness to withstand harsh processing conditions. Even if the covalent binding of cellulase causes lowering in their kinetic values (k_M and V_{max}), immobilized cellulase would still be advantageous in terms of its affordability, reusability, and potential efficiency.

4.7.2 Reusability Potential of the Nanobiocatalyst

Reusability performance of the NBC was tested over seven repeated cycles under the optimized conditions. A total of 216.34 mg glucose/g CMC was produced using the nanobiocatalyst over seven batches which was ~5.8 fold higher as obtained through free cellulase. Although results suggested a loss in catalytic performance of the NBC after every usage, still ~68.2% of the initial activity could be retained after the seventh cycle (Figure 4.21a). Corresponding glucose production also depicted a marginal reduction from 37.2 to 25.4 mg glucose/g CMC after the first to seventh uses (Figure 4.21b). Although, the loss of material could have been a major cause for lowering in the biocatalytic activity of the enzyme over repeated usage, we were able to recover the nanobiocatalyst over 99% on a mass balance basis. Further, no significant release of cellulase enzyme was detected into the solution within 6 h after repeated use. Hence, a reduction in the catalytic activity of immobilized cellulase was more likely due to the enzyme inactivation mechanisms over repeated cycles, as demonstrated elsewhere (Lupoi and Smith 2011).

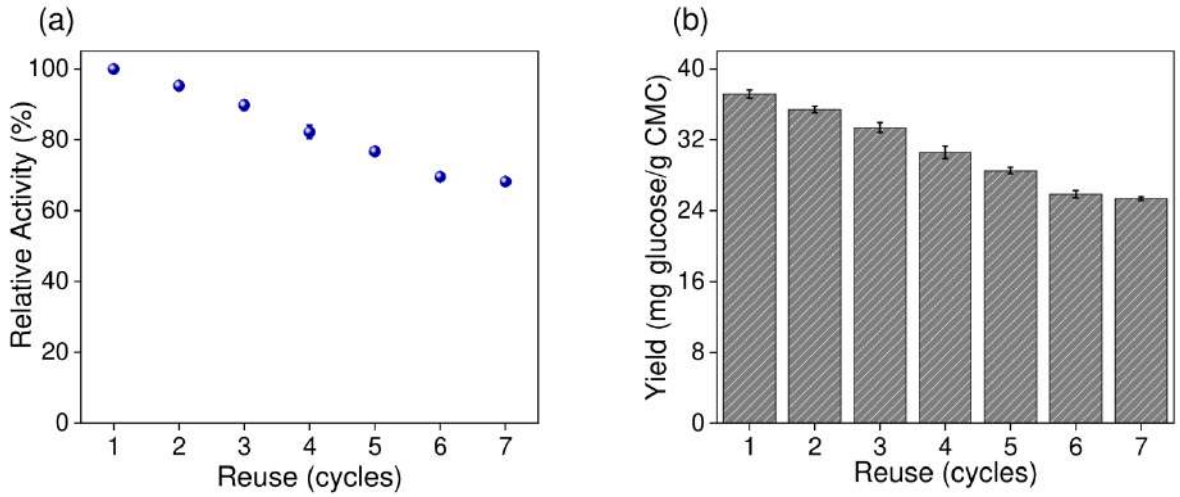

Figure 4.21 (a) The variation in catalytic activity of nanobiocatalyst after every reuse cycle, and (b) Corresponding yield of glucose (mg glucose/g CMC) in each cycle.

4.8 Kinetic and Thermodynamics Parameters

The kinetic parameters (k_M, V_{max}, and catalytic efficiency) of free cellulase and cellulase-MHNTs were tested separately treating a wide range of substrate concentrations (CMC, 100−5000 μM). Free and immobilized enzymes both obeyed the Henri−Michaelis−Menten kinetics model (Figure 4.22a). The apparent k_M of cellulase-MHNTs was slightly higher (1423 μM) than that of free cellulase (1288 μM) which is likely due to the lower affinity of enzymes toward the substrate after immobilization (Figure 4.22b). It is evidenced that the diffusion limitations of the substrate near close vicinity of the immobilized enzyme and/or localized conformational changes at the active sites of enzyme would be the responsible causes for the increase in the k_M value (Das et al. 2018; Kadam et al. 2018). However, a proportionate increase in k_M values of the enzyme after immobilization onto nanomaterials was found to be much lower as reported in other studies (Wu et al. 2005; Khoshnevisan et al. 2011; Abraham et al. 2014; Kadam et al. 2018). This can be ascribed to the efficient loading of enzyme and high specific surface area of MHNTs which minimized any changes in structural conformations and/or mass transfer constraints. Similarly, no significant variation in V_{max} values was observed before (10.1 μM/min) and after immobilizing cellulase (11.7 μM/min). It was established that the microenvironment near immobilized enzymes would have an unnoticeable impact on overall catalytic activity of the NBC. Further, the catalytic efficiency (V_{max}/ k_M) of the nanobiocatalyst was increased by 5% more than that of the free cellulase at 50 °C.

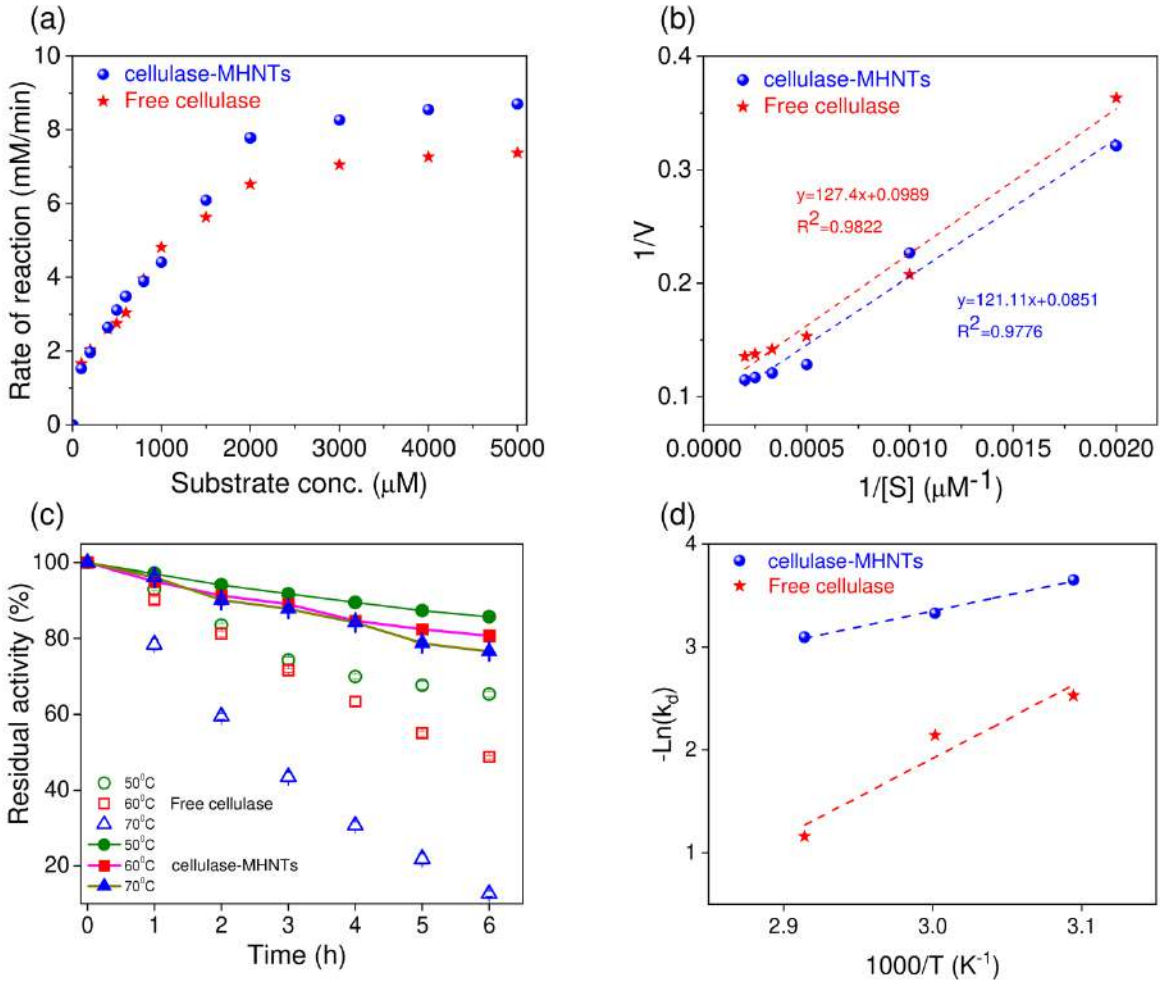

Figure 4.22 (a) Michaelis-Menten plot of free and immobilized α-amylase, (b) Line weaver-Burk plot, (c) Impact of elevated temperatures on both free and immobilized cellulase, and (d) Arrhenius plot.

The thermodynamic parameters of irreversible thermal inactivation of both forms of cellulase were monitored at optimum and higher temperature range (50−70°C) (Figure 4.22c). At optimal temperature (50 °C), the thermal deactivation rate constant (k_d) of nanobiocatalyst was found to be 3.12-fold lower than that of free cellulase (Table 4.5). The half-life of the immobilized form was 3.08-fold higher than the free cellulase, indicating the slower denaturation and superior thermal stability of immobilized cellulase.

Table 4.5 A comparative summary of thermodynamic parameters before and after immobilization of cellulase.

Parameters	Temperature (°C)	Free Enzyme (cellulase)	Nanobiocatalyst (cellulase-MHNTs)
k_d (h^{-1})	50	0.080	0.025
	60	0.12	0.036
	70	0.31	0.045
Half-life, $t_{1/2}$ (h)	50	8.67	26.75
	60	5.91	19.30
	70	2.20	15.29
D-value	50	28.81	88.90
	60	19.64	64.13
	70	7.34	50.82
E_d (kJ/mol)		28.11	28.14
ΔH (kJ/mol)	50	25.42	25.45
	60	25.34	25.37
	70	25.26	25.29
ΔG (kJ/mol)	50	108.14	111.17
	60	110.51	113.79
	70	111.11	116.63
ΔS (J/mol·K)	50	255.98	265.25
	60	263.57	273.61
	70	265.67	282.65

Furthermore, the values of activation energy for thermal denaturation (E_d), enthalpy change (ΔH), Gibbs free energy change (ΔG), and entropy change (ΔS) were obtained as 28.11 kJ/mol, 25.42 kJ/mol, 108.14 kJ/mol, and 255.98 J/mol·K, respectively for free cellulase, whereas, the corresponding values for immobilized cellulase-MHNTs were found to be 28.14 kJ/mol, 25.45 kJ/mol, 111.17 kJ/mol, and 265.25 J/mol·K. Higher E_d value indicated superior energy requirement to thermally inactivate the immobilized enzyme, suggesting higher thermal stability as compared to free cellulase. The increase in enthalpy change (ΔH), and Gibbs free energy change (ΔG) after immobilization are associated with superior thermal and conformational stability of immobilized cellulase. An increase in the ΔS value after

immobilization could be indicative of the increasing order of randomness at the nanobio interface of the nanobiocatalyst. Similar results were obtained at higher temperatures (60 and 70 °C) demonstrating the potential of immobilization support matrix for industrial engagement.

4.9 Influence of Ionic liquid presence on Catalytic Activity

Ionic liquid (IL) based pretreatments have been established as an integrated technology in contemporary methods for recovering cellulosic components and their possible conversion into other value-added products (Datta et al. 2010). Although such strategies seem effective in solubilizing cellulose to a large extent, the presence of even a trace amount of ILs creates unfavourable conditions for enzymatic hydrolysis, rendering those pretreatment strategies incompatible for further downstream processing (Zhou et al. 2019). Considering this as a challenge, we also tried to elucidate the commercial viability of cellulase-MHNTs in industrial bioprocesses hypothesizing its IL-tolerant ability as compared to free cellulase suspensions. Regardless of the substrate employed, i.e., CMC and pretreated sugarcane bagasse (SCB), the cellulase-MHNTs demonstrated an improved ionic liquid tolerant ability over free cellulase under all the tested conditions. In the case of CMC as a substrate (Figure 4.23a), free cellulase rapidly lost its residual activity from 75.2% to 14.3%, i.e., ~5.2-fold while increasing the concentration of [bmim][Cl] from 5 to 30% (v/v), whereas, cellulase-MHNTs depicted much higher stability and their residual activity was reduced from 91.6% to 61.2% under similar conditions. A similar trend was observed when CMC substrate was replaced with the pretreated sugarcane bagasse, where the immobilized enzyme retained half of its activity while the activity of free enzyme was adversely affected and came down to only 5.8% (Figure 4.23b).

It was clearly observed that the cellulase-MHNTs manifested a much superior catalytic activity at higher concentrations of ionic liquid ([bmim][Cl], ≥10% v/v) than free cellulase for hydrolyzing either CMC or the pretreated sugarcane bagasse. The presence of two different sources of cellulose did not affect the hydrolytic potential of cellulase-MHNTs at the corresponding [bmim][Cl] concentrations, which confirms that the catalytic activity of immobilized cellulase was not significantly compromised. Rather, immobilized cellulase appeared to be more shielded than its free form, where the presence of the support matrix, i.e., HNTs, could have contributed to improve its tolerant ability against harsh processing of

IL treatments. Based on this study, [bmim][Cl] ionic liquid could be a promising pretreatment solvent for rapid cellulose hydrolysis, which marked less influence on enzyme inactivation, particularly using the cellulase-MHNTs system.

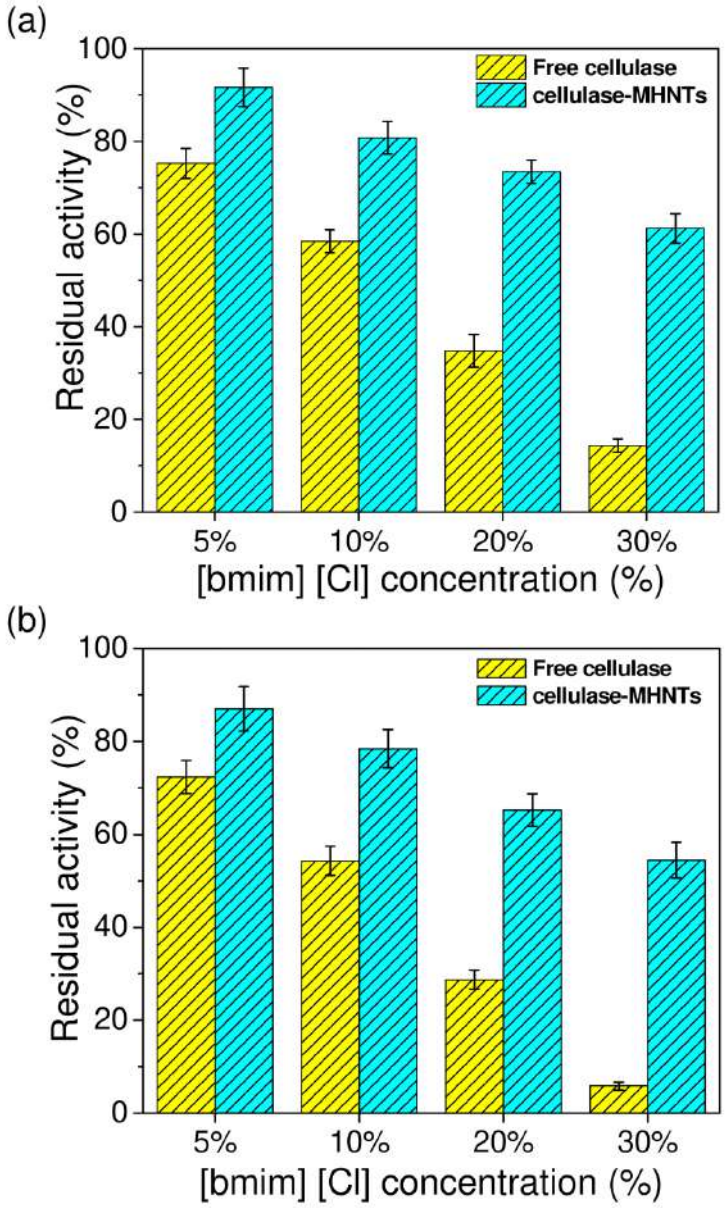

Figure 4.23 Impact of ionic liquid on activity of free and immobilized cellulase when substrate was (a) CMC, (b) pretreated SCB.

4.10 Cellulose Saccharification using Nanobiocatalyst

To determine the practical affordability utilizing this nanobiocatalyst, an operational study was attempted to evaluate the continuous hydrolysis of CMC, as a model substrate over a long duration. Although an increase in reducing sugars (i.e., product) in the hydrolysate is

known to elicit inhibitory effects on cellulase activity (Xiao et al. 2004), we still could be able to run this saccharification process over 48 h without any adverse response.

As shown in Figure 4.24(a), the extent of CMC hydrolysis (% saccharification) could be achieved to nearly 50.2% in 48 h with a glucose yield of 0.56 g glucose/g CMC. The production of glucose was calculated to be 5.64 g/L with 1% CMC as substrate. We obtained better results in comparison to an earlier report where cellulase immobilized onto colloidal magnetic nanoparticles catalyzed the hydrolysis of cellulose with 5.5 g/L production of glucose with 10% substrate in 24 h (Xu et al. 2011). Those authors claimed no further increase in either cellulose hydrolysis or glucose productivity beyond 24 h, thus limiting their long-term applicability. Another study also evidenced that only up to a maximum of 45.3% saccharification could be achieved with ~2.3 g/L glucose production in 24 h, while no change was observed even after introducing another batch of immobilized enzymes in the reaction mixture (Wang et al. 2011).

We further evaluated the efficacy of cellulase-MHNTs, the nanobiocatalytic system in converting a non-feed, lignocellulosic biomass into an edible biochemical product, i.e., glucose. Pretreated sugarcane bagasse, was chosen as the substrate, which was hydrolyzed using NBC under identical conditions as mentioned in case with CMC. Figure 4.24(b) shows that changing the source of the substrate from CMC to pretreated biomass did not affect the biocatalytic potential of cellulase-MHNTs where a maximum of 46.5% saccharification with 521.9 mg glucose/g pretreated SCB (glucose yield) could be achieved over 48 h of continuous run. As evident from Figure 4.24(b), the glucose yield decreased from 144.24 mg/g to 76.21 mg/g during the first and the last quarter of reaction time, respectively. A decrease in glucose yield can be attributed to enzyme inactivation due to the prolonged exposure to reaction mixture constituents. Moreover, the impact of other factors such as substrate depletion, product inhibition (Rodrigues et al. 2013), and recalcitrant nature of the extracted cellulose (Tian et al. 2017) cannot be ignored, which could have also contributed toward decline in glucose yield. Since a longer run of the process beyond 48 h might have resulted in even further reduction in glucose yield per unit time, the nanobiocatalyst was recovered after 48 h of continuous run. Together, these findings provide compelling evidence that an improved glucose yield using nanobiocatalyst was an outcome of the enhanced saccharification of insoluble cellulose into soluble glucose, where the impact of enzyme inactivation due to reaction conditions was minimized. This appeared to be a feasible strategy

achieving high-cellulose hydrolysis concurrent with yielding high production of glucose, particularly using lignocellulosic biomass.

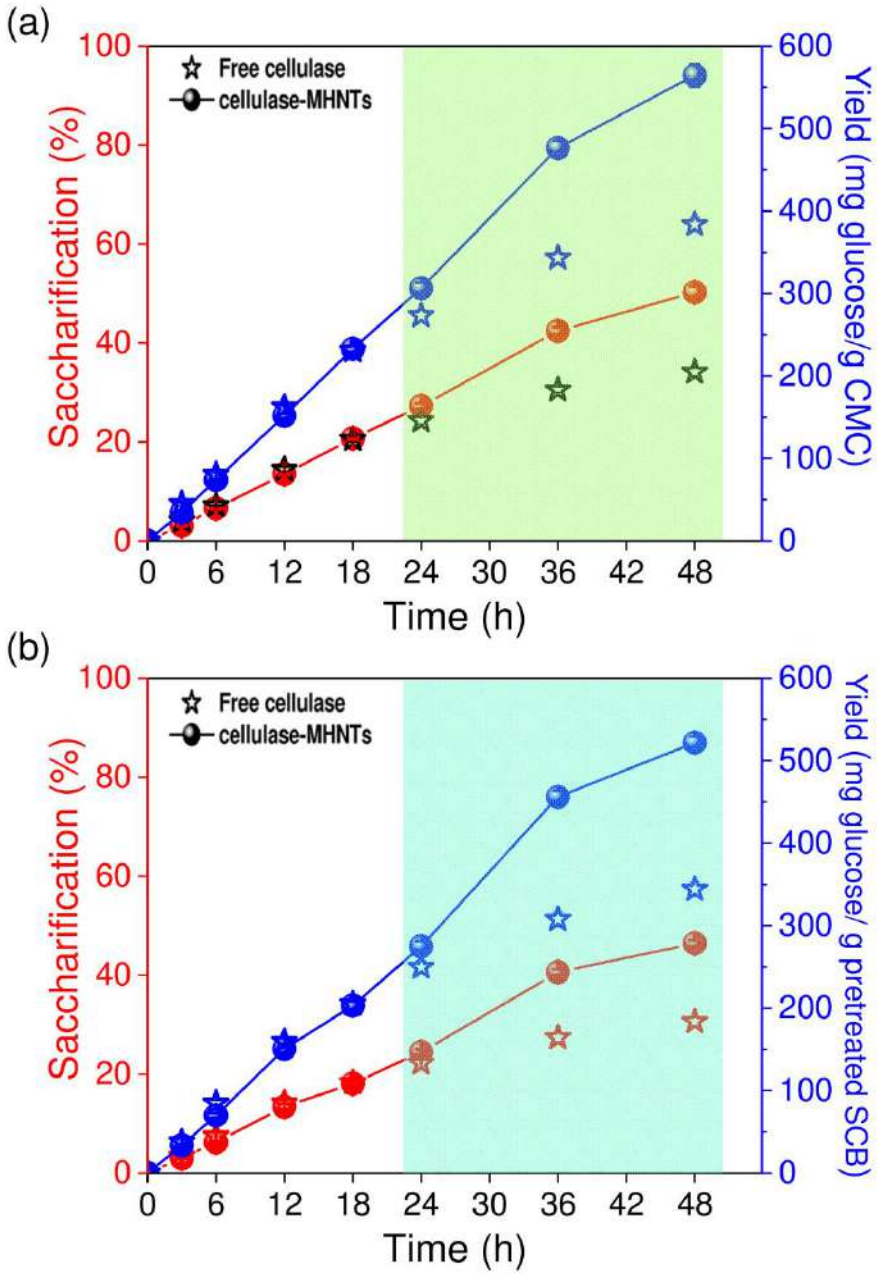

Figure 4.24 Impact of change in substrate on cellulase saccharification capability of free and immobilized cellulase when substrate was (c) CMC, and (d) pretreated SCB.

Glucose determination using HPLC and standard assay kits also confirmed the absence of other soluble cellooligomers (i.e., cellobiose/cellotrioses) in hydrolysate. Summarizing this, we validate our hypothesis where a dense immobilization of cellulase on to MHNTs was

anticipated to facilitate maximum cellulose−cellulase interactions without mass transfer limitations concurrent with its high conversion into glucose hydrolysate.

4.11 Production of Fructose Syrup Using Packed Bed Reactor

Immobilized enzyme filled packed bed reactors in batch and continuous operating modes have been explored for heterogeneous biocatalytic reactions in laboratory, pilot, and industry scales (Bajić et al. 2017). Packed bed reactors as continuous operation bioreactor provide inherent advantages such as limited enzyme leaching, easily scalable systems and most importantly eliminate the probable inhibition due to high concentration of substrate or product. The production of various industrially important biochemicals has been achieved with high efficiency using packed bed reactors (Sánchez et al. 2000; Xue et al. 2013).

The glucose stream produced using pretreated sugarcane bagasse and cellulase nanobiocatalyst was utilised for fructose syrup production. A packed bed reactor packed with commercially available immobilized glucose isomerase was used for the fructose syrup production. The process parameters involved were first investigated using single factor study to determine the effective range of variable having most significant impact on the conversion of glucose to fructose. The variable and their effective range were then optimised using Box Behnken design of response surface methodology.

4.11.1 Single Factor Studies

The key factors for packed bed reactor based continuous processing include substrate concentration, substrate flow rate, pH, and temperature of the system. As substrate concentration is constant in this case, other factors i.e., substrate flow rate, pH, and temperature were investigated using single factor study. The close inspection of flow rate provides critical information for efficient conversion of substrate and to reduce overall cost in industrial process as its affects the reaction time of substrate and biocatalyst. Substrate flow rate was investigated in the range 0.1-1 mL/min, while pH and temperature of the packed bed reactor were kept at 8 and 60 °C, respectively. From the observed data it was inferred that with increase in flow rate, glucose conversion into fructose decreased (Figure 4.25a). The results are attributed to the effect of residence time or reaction time of substrate and biocatalyst, at higher flow rate (low residence time) the biocatalyst had very limited time to

interact with substrate hence the conversion was low. Considering the efficient conversion the flow rate range of 0.1 to 0.4 mL/min was selected for further optimization.

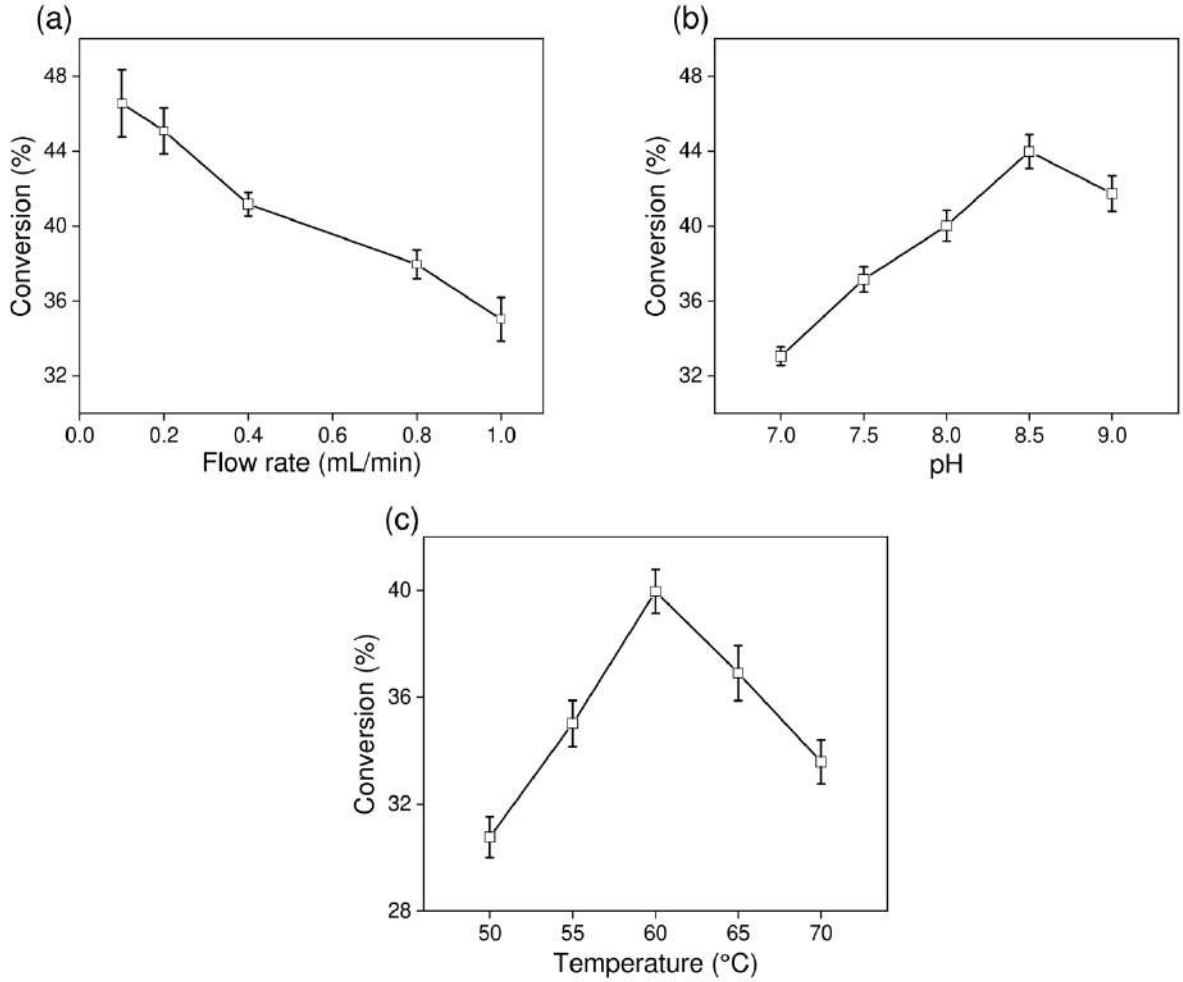

Figure 4.25 The impact of individual process parameters (a) flow rate (mL/min), (b) pH, and (c) Temperature (°C) while transforming glucose into fructose in a packed bed rector using immobilized glucose isomerase.

The range of pH (7.0-9.0) was examined by keeping flow rate at 0.5 mL/min and temperature at 60 °C. Maintaining pH below 8 resulted a sharp decline in glucose conversion (%), which might be attributed to deviation from the optimum pH of immobilized glucose isomerase (Figure 4.25b). Highest conversion was observed at pH 8.5, which decreased again by increasing pH to 9. To achieve high conversion, a pH range of 8.0-9.0 was used in response surface methodology. Similar results were obtained in temperature studies, where an increase in conversion from 30.76 to 39.96% was witnessed while raising temperature from 50 to 60 °C, respectively (Figure 4.25c). The substrate flow rate and pH were kept at 0.5 mL/min and 8.0. Further increase in temperature resulted in decrease in conversion (%). Considering the

experiential results temperature range 57.50 to 62.50 C was selected for optimization using response surface methodology.

4.11.2 Box Behnken Design

The effective ranges of factors obtain from single factor study were used for optimizing the Box-Behnken design of response surface methodology. The experiments were conducted at 17 sets of factor range combinations, and BBD model was used to perform multiple regression analysis. The influence of individual factors and their combinations on the conversion (%) of glucose into fructose was represented in form of an equation:

$$Y = -2252.61833-118.02500A+176.81250B+51.74800C+26.83333A^2-10.68500B^2 -0.43820C^2+0.90000AB+1.32000AC-0.092000BC$$

Where, Y is conversion (%), A is flow rate (mL/min), B is pH of the system, and C is temperature (°C) of the system.

Table 4.6 ANOVA for response surface quadratic model.

Source	**Sum of Square**	**DF**	**Mean Square**	**F Value**	**Prob>F**	**Remarks**
Model	128.73	9	14.30	262.29	< 0.0001	significant
A	56.76	1	56.76	1040.94	< 0.0001	
B	1.67	1	1.67	30.54	0.0009	
C	3.81	1	3.81	69.85	< 0.0001	
A^2	1.53	1	1.53	28.14	0.0011	
B^2	30.04	1	30.04	550.95	< 0.0001	
C^2	31.58	1	31.58	579.15	< 0.0001	
AB	0.018	1	0.018	0.33	0.5813	
AC	0.98	1	0.98	17.97	0.0038	
BC	0.053	1	0.053	0.97	0.3575	
Residual	0.38	7	0.055			
Lack of Fit	0.067	3	0.022	0.28	0.8371	not significant
Pure Error	0.32	4	0.079			
Cor Total	129.11	16				

*A: flow rate (mL/min); B: pH; C: temperature (°C)

Analysis of variance (ANOVA) was used to determine significance of the predicted model (Table 4.6). Fisher's F-test revealed Model F-value of 262.29 with p value <0.0001, indicating the adequacy of model for the selected parameters. Based on the parameter F-value and p value A, B, C, A^2, B^2, C^2, and AC were found to be significant factors. Furthermore F-value of 0.28 indicated non-significant lack of fit, which also validated the compatibility of the generated model for the parameters studied.

The multiple correlation coefficients (R^2), which measures the extent of variance from the model's mean value, indicated a close proximity among independent variables viz. amount of MHNTs, conc. of enzyme and solution pH (Table 4.7). R^2 value obtained from ANOVA was in accordance with the defined limit for the model to be effective. The predicted R^2 (0.9879) and adjusting coefficient of determination (R^2-adj=0.9932) for calculated optimal conditions were in good harmony with the value of multiple correlation coefficients (R^2=0.9970).

Table 4.7 Coefficients of determination for response surface quadratic model.

Std. Dev.	0.23	R^2	0.9970
Mean	44.20	Adjusted R^2	0.9932
C.V.	0.53	Predicted R^2	0.9879
PRESS	1.56	Adeq. Precision	41.464

The 2-D contour plots and 3-D surface plots were used to navigate through impacton response (conversion (%)) induced by variation in the independent factors (Figure 4.26). Furthermore, numerical optimization of the selected parameter was carried out for high conversion (%), while keeping all the factors in range. The optimum reaction conditions for highest conversion (%) generated by the model was 0.11 mL/min flow rate, 8.43 pH and 60.52 °C temperature. The accuracy of model was tested by conducting experiment on the reaction conditions, and conversion of 48.85% was archived in 1 h reaction time. The close proximity of experimental value (48.85%) and predicted value (49.39%) confirmed the competence of the generated model for prediction of conversion (%).The averages of three replicates were tested and mean values are reported. Transformation of this system to an industrial scale might pave path for even greater value addition.

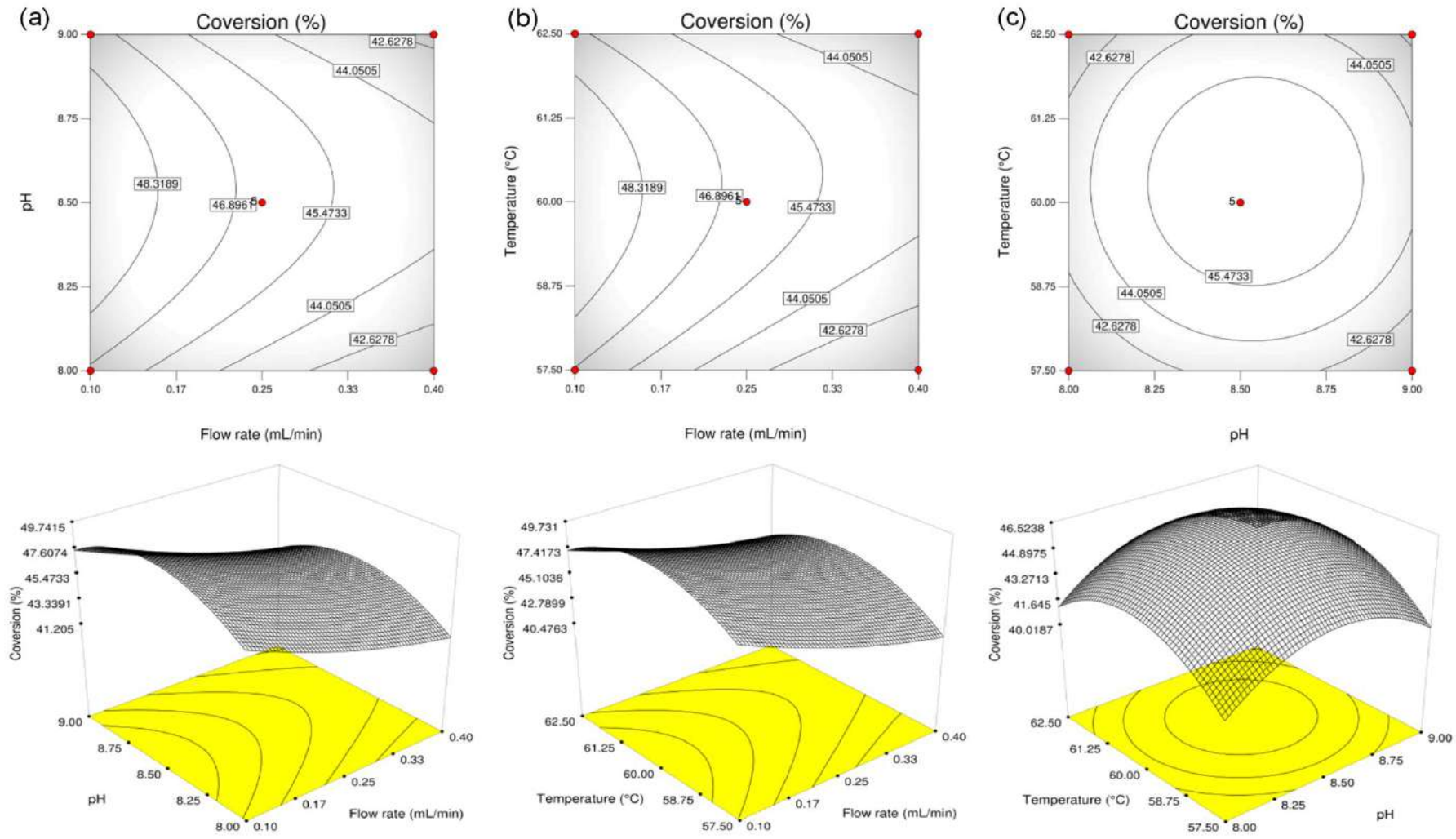

Figure 4.26 2D contour and 3D response surface plots for analyzing the interaction effects between (a) pH and flow rate, (b) Temperature and flow rate, and (c) Temperature and pH.

4.12 Development of α-amylase Nanobiocatalyst

When enzymes with bulky substrates, viz. α-amylase, are immobilized onto the bulk support materials, their limited surface area creates steric hindrances in binding with the active site of enzymes, leading to a complete loss of catalytic activity (Gupta et al. 2022a). In contrast, nanomaterials with a high surface area/volume ratio (halloysite nanotubes, here) facilitate a better conformational motility of enzymes even after immobilization, there by inducing a flexible enzyme structure with enhanced protein unfolding (Liu and Dong 2020). This provides a more favorable reaction condition for maximizing substrate−enzyme interactions at active sites, circumventing steric hindrances and improving catalytic activity. Further, in comparison to the traditional immobilization methods such as entrapment/encapsulation, the surface bound enzymes offer insignificant mass transfer limitations, resulting in enhanced catalytic activity at a comparatively lower payload level (Seenuvasan et al. 2020). The biocompatible nanomaterial emerges as an excellent support to improve the catalytic potential of immobilized enzymes and further prevent undesirable changes in the enzyme structure.

Halloysite nanotubes provide a large specific surface area for high and efficient biomolecule immobilization and other unique physicochemical properties (Tully et al. 2016).As reported recently, iron oxide nanoparticles were anchored on the surface of halloysite nanotubes through an in situ approach, which served as a primary template for surface modification (Sillu and Agnihotri 2020). Figure 4.27 illustrates polydopamine functionalization of magnetic halloysite nanotubes (*d*-MHNTs) and subsequent immobilization of α-amylase. Immersing MHNTs into an alkaline dopamine solution spontaneously generated a thin, surface-adherent polydopamine coating onto MHNTs due to the oxidative self-polymerization of dopamine (Ariaeenejad et al. 2021). The resulting *d*-MHNTs were used for immobilization of α-amylase. Polydopamine acted as a non-specific biomimetic cross-linker to bind enzymes due to quinones, which are reactive toward the nucleophilic groups on enzymes. The covalent coupling between amino groups of enzyme and quinones of polydopamine may occur via Michael addition and/or Schiff base formation (Chao et al. 2013; Chao et al. 2014). The as-synthesized *d*-MHNTs after immobilization of α-amylase, now termed *d*-MHNTs/α-amylase, were evaluated through materialistic characterization and compared to their pristine counterparts before determining their biocatalytic potential.

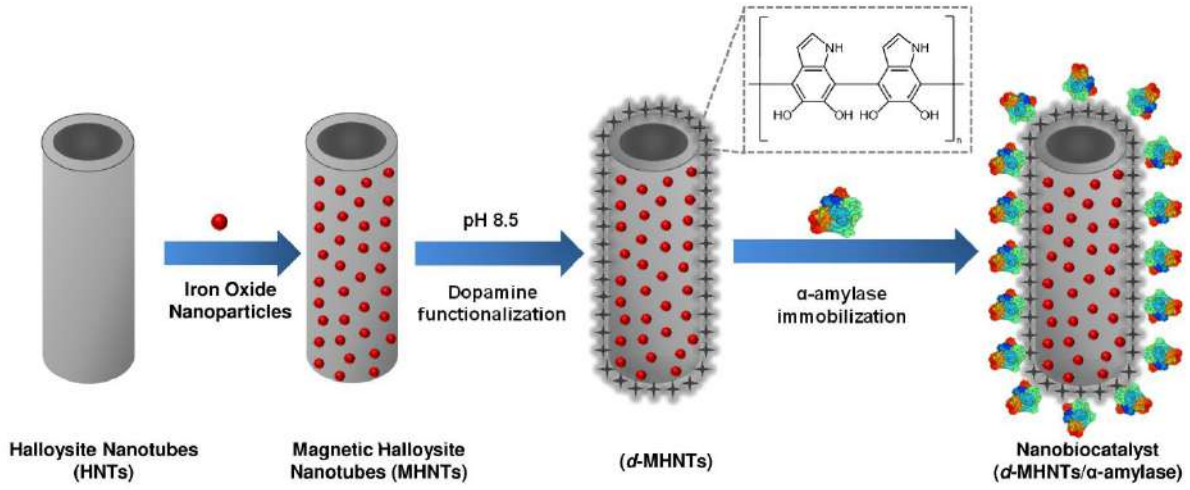

Figure 4.27 Schematic representation of α-amylase immobilization on dopamine functionalized magnetic halloysite nanotubes.

4.12.1 Material Characterization

The variation in functional moieties of MHNTs after dopamine functionalization and subsequent immobilization of α-amylase on *d*-MHNTs were determined through FTIR spectroscopy (Figure 4.28a). The obtained results indicated that that *d*-MHNTs could preserve the inherent absorption peaks at 3694, 3621, 1033, and 910 cm^{-1} ascribed to hydroxyl (−OH) groups, Si−O stretching, and the bending vibrations of Al−OH, respectively, even after dopamine functionalization and α-amylase immobilization. Both samples (*d*-MHNTs and *d*-MHNTs/α-amylase) showed a characteristic vibrational band in the near-infrared region (<800 cm^{-1}, Fe−O), which established the magnetic nature of MHNTs (Sillu and Agnihotri 2020). The absorption peaks at 3444 and 1640 cm^{-1} were ascribed to the stretching vibrations of amino ($-NH_2$) and carbonyl (−C=O) groups of polydopamine, respectively (Chao et al. 2013). The overlapped characteristic peaks of α-amylase with *d*-MHNTs at 1536 and 1426 cm^{-1} further confirmed the successful loading of α-amylase and irreversible bonding between enzyme and polydopamine.

XRD analyses were done to evaluate the structural integrity of *d*-MHNTs before and after immobilizing α-amylase (Figure 4.28b). The presence of characteristic diffraction peaks (JCPDSCard No. 29-1487) in both samples indicated that the crystallinity of HNTs remained intact after polydopamine functionalization, since the attachment of IONPs occurred only on the surface, not in the interlayer. The distinctive peaks of magnetite Fe_3O_4 (JCPDS Card No.

01-075-0449) at 2θ =30.34, 35.65, 43.33, 57.29, and 62.93° were attributed to the (220), (311), (400), (511), and (440) planes of Fe−O crystals, respectively. It was established through the observed results that the adopted surface functionalization protocol was efficient in immobilizing α-amylase without adversely affecting the crystallinity of either HNTs or IONPs (Kadam et al. 2017; Sillu and Agnihotri 2020).

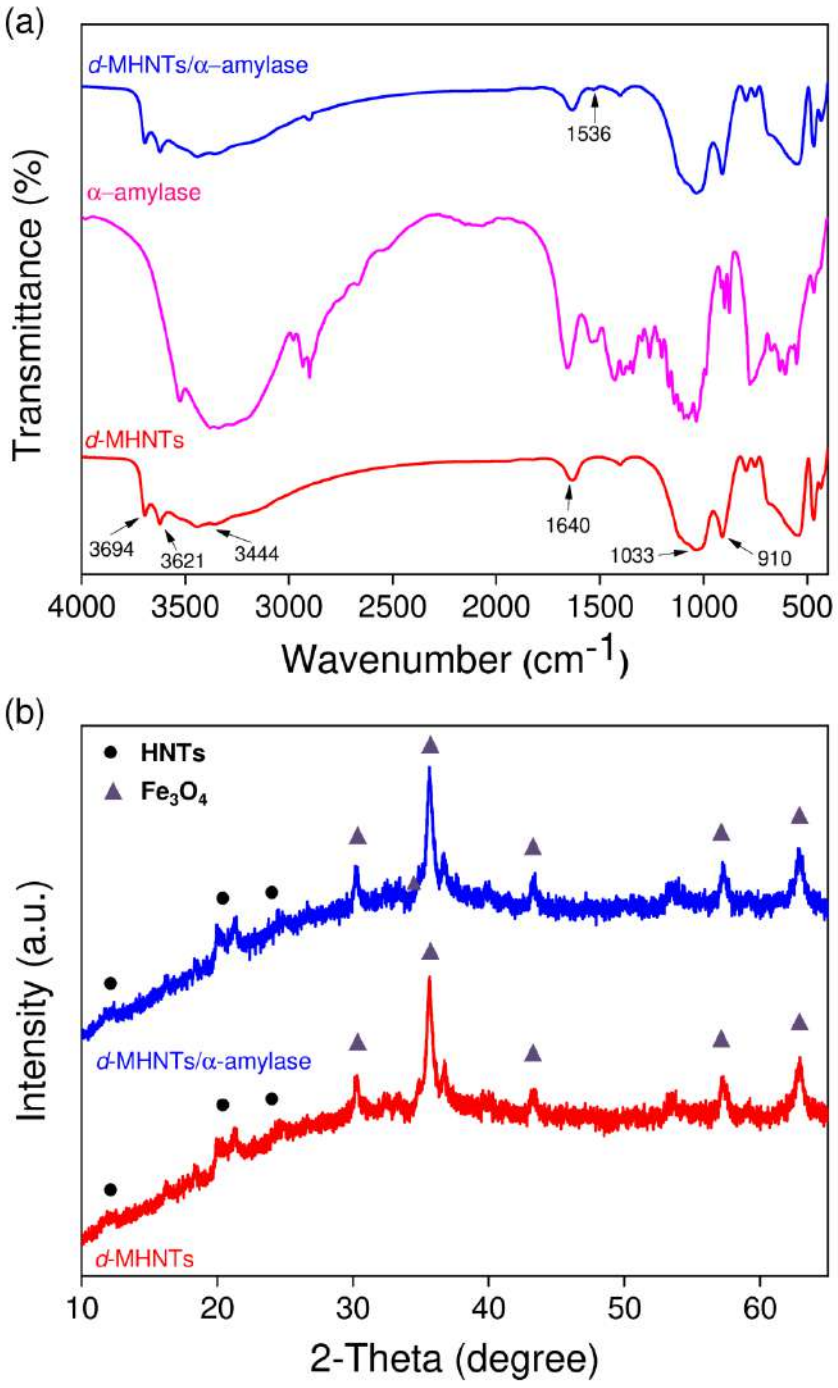

Figure 4.28 Characterization of *d*-MHNTs, and *d*-MHNTs/α-amylase through (a) FTIR spectroscopy, (b) XRD analyses.

Immobilizing enzymes onto a magnetic support is one way to improve their recovery from the reaction mixture, thus promoting its reuse. A vibrating sample magnetometer was employed to assess the impact of enzyme immobilization on *d*-MHNTs (Figure 4.29a). The magnetization curve revealed that *d*-MHNTs and *d*-MHNTs/α-amylase had a marginal reduction in magnetization saturation values, i.e., 32.5 and 28.7 emu/g respectively, which occurred solely due to the presence of an additional nonmagnetic content (α-amylase) in the latter. However, such variation did not significantly affect the separation efficiency of the immobilized enzyme (inset image). Since both samples demonstrated superparamagnetism with zero coercivity and remanence, *d*-MHNTs/α-amylase was established as a promising magnetic template, which was easily removable from the reaction vessel through a simple magnet.

To further support our hypothesis of achieving stable functionalization followed by enzyme immobilization, thermogravimetric analyses (TGA) of samples were carried out (Figure 4.29b). While the TGA curve of *d*-MHNTs demonstrated a 16.22 wt% weight loss in the 0−800 °C temperature range, which was evidently higher than weight loss exhibited by MHNTs in the similar range. The higher weight loss was ascribed to the presence of polydopamine on its surface confirming the successful functionalization (Chao et al. 2013). On a similar note, the TGA curve of *d*-MHNTs/α- amylase depicted even a greater weight loss of 18.59 wt%, which was attributed to the immobilized α-amylase.

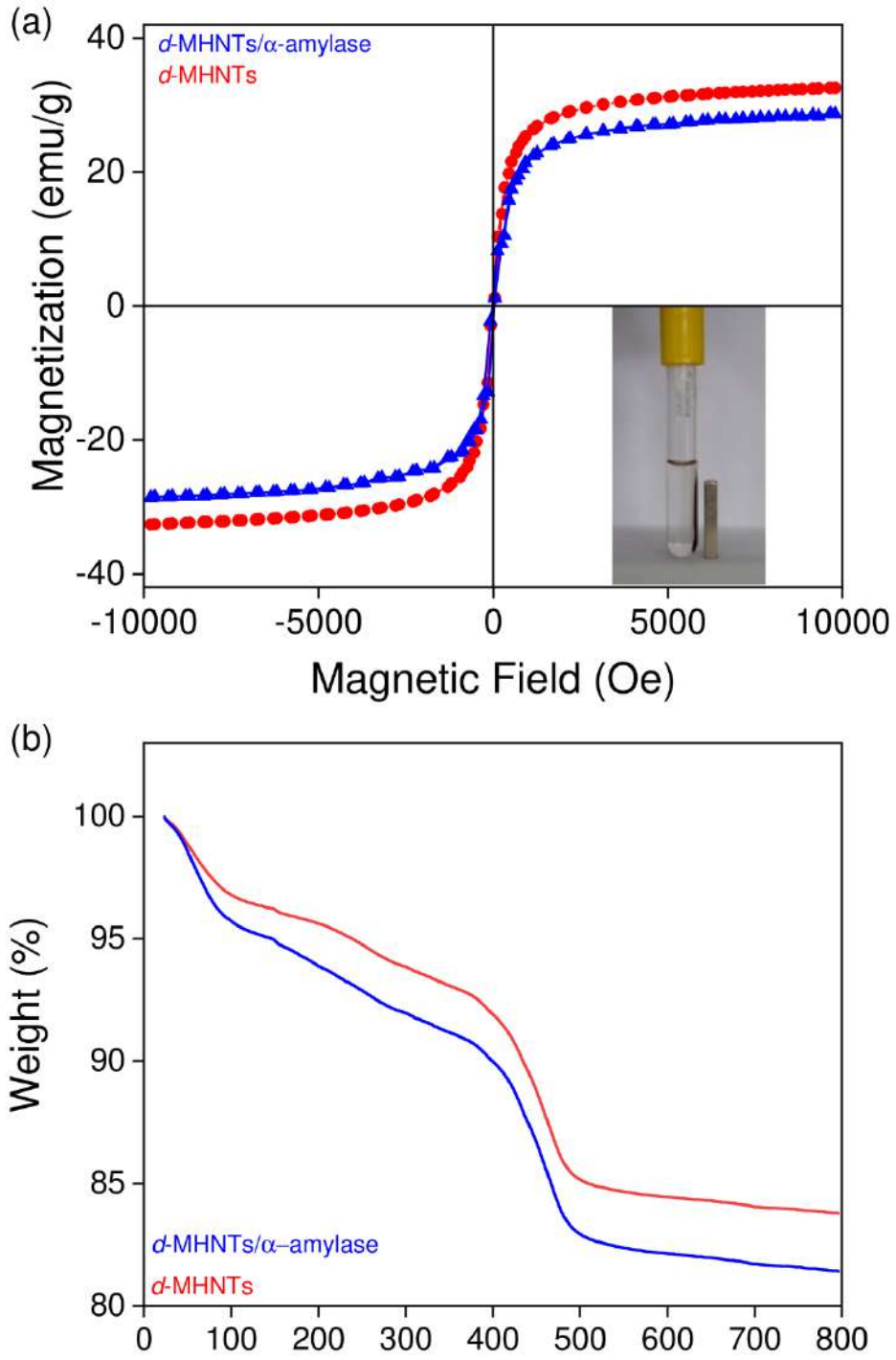

Figure 4.29 Characterization of *d*-MHNTs, and *d*-MHNTs/α-amylase through (a) Magnetic hysteresis loops, Inset photographic image shows ease in separating the nanobiocatalyst from a colloidal suspension, and (b) thermogravimetric analysis (TGA).

Finally, *d*-MHNTs/α-amylase was also examined through FE-SEM to evaluate the morphology of its backbone structure after enzyme loading. It was evident that the surface

topography of HNTs (Figure 4.30a) was significantly changed after incorporating IONPs and enzyme immobilization with the desired surface modifications. The in-site synthesis of iron oxide nanoparticles, dopamine coating and α-amylase immobilization resulted in appearance of patches and comparatively rough surface as can be seen in the micrograph (Figure 4.30b). The elemental mapping further confirmed a homogeneous distribution of all components of HNTs and IONPs, which validates the conclusions derived through XRD, VSM, and TGA analyses (Figure 4.30c).

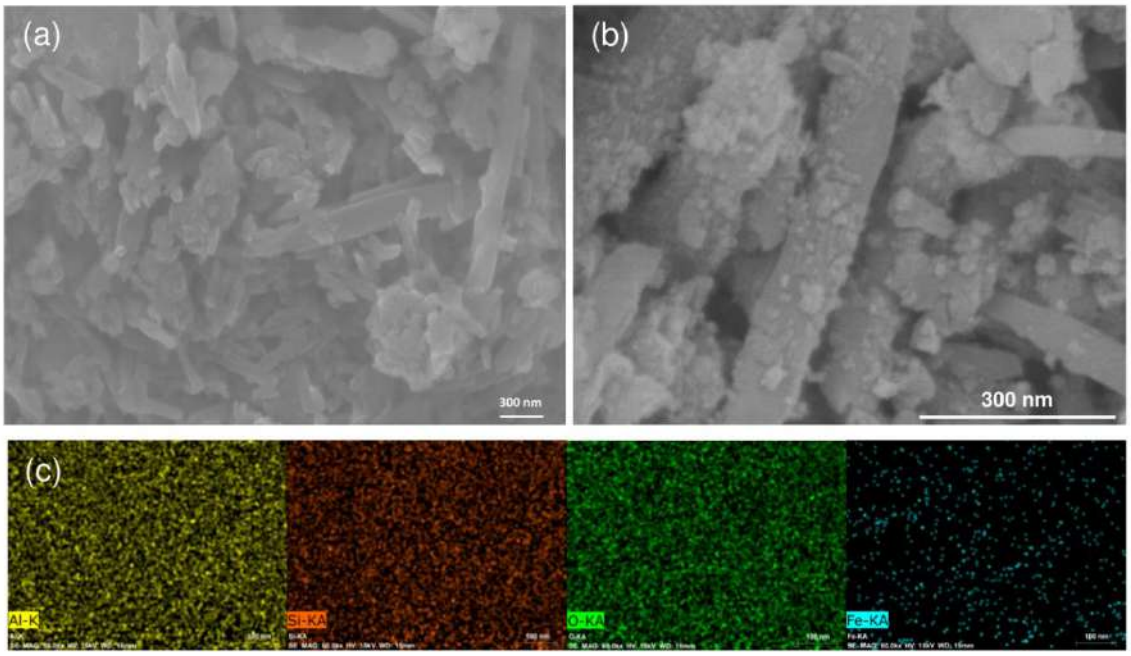

Figure 4.30 (a) SEM micrograph of halloysite nanotubes, (b) FE-SEM micrograph of *d*-MHNTs/α-amylase, and (c) Elemental mapping of aluminium (Al), silicon (Si), oxygen (O) and iron (Fe) element.

4.13 α-amylase Immobilization

The factors involved in immobilization reaction has significant impact on the overall enzyme loading as well as the corresponding catalytic activity, hence the parameters were initially examined using single factor study. The effective ranges obtained were then used for high enzyme loading optimization using response surface methodology (RSM).

4.13.1 Single Factor Study

Four major parameters in the immobilization process, i.e., amount of support matrix (*d*-MHNTs), amount of enzyme, pH and temperature of the reaction, were selected and

evaluated individually to determine the range in terms of their impact on enzyme loading and corresponding α-amylase activity. As shown in Figure 4.31(a), the loading of α-amylase gradually increased from 13.43 to 74.15% with an increase in *d*-MHNTs amount from 20 to 100 mg. The consistent increase in enzyme loading demonstrated the increase in available binding sites with increasing amount of support. However, the corresponding enzyme activity demonstrated increase till 60 mg *d*-MHNTs attaining the highest value (89.72%) and decreased after that. The decrease in catalytic activity was attributed to steric hindrance posed by the immobilized enzymes due to high payload. In case of varying the enzyme amount, the α-amylase loading steadily decreased (81.05 to 55.29%) while increasing the amount of enzyme from 5 to 25 mg, keeping all other parameters constant (Figure 4.31b).As the support amount was kept constant, the limited binding sites available to anchor enzyme molecules resulted in decrease of enzyme loading. In this case, the corresponding enzyme activity constantly increased throughout the range, which was attributed to the limited amount of *d*-MHNTs which if present in higher amount also cause inhibition of enzyme activity. Interestingly, with 15 mg enzyme amount 88.85% catalytic activity of immobilized α-amylase (64.20% enzyme loading) was recorded. Further increase in enzyme amount to 20 mg resulted in retained catalytic activity of 90.80% with 61.46% enzyme loading. The reaction in presence of 25 mg enzyme amount demonstrated 92.16% catalytic activity while enzyme loading was 55.29%.

The impact of different solution pH was assessed to determine the best range for efficient α-amylase immobilization (Figure 4.31c). The change in solution pH (5.5-7.5) had no significant effect on α-amylase loading or the retained activity, where enzyme loading remained in range 62.43 to 65.42%. The retained activity was also recorded in a very narrow range 87.61-89.18%. Furthermore, a noteworthy change in enzyme loading was observed when temperature of the immobilization reaction was changed from 20 to 50 °C (Figure 4.31d). The loading (%) increased from 54.95 to 65.67% when temperature was raised from 20 to 40 °C, however further increasing the temperature to 50 °C resulted in sudden decrease of enzyme loading to 57.69%. Similar pattern was observed for the retained catalytic activity where 64.79, 70.29, 77.81 and 67.89% catalytic activity was recorded at 20, 30, 40 and 50 °C, respectively. The enzyme denaturation at high temperature was key factor behind the reduced enzyme loading and retained activity. Based on the single-factor studies, the amount of support matrix (50-70 mg), enzyme load (10-20 mg), and reaction temperature (30-40 ºC) were selected as three independent variables.

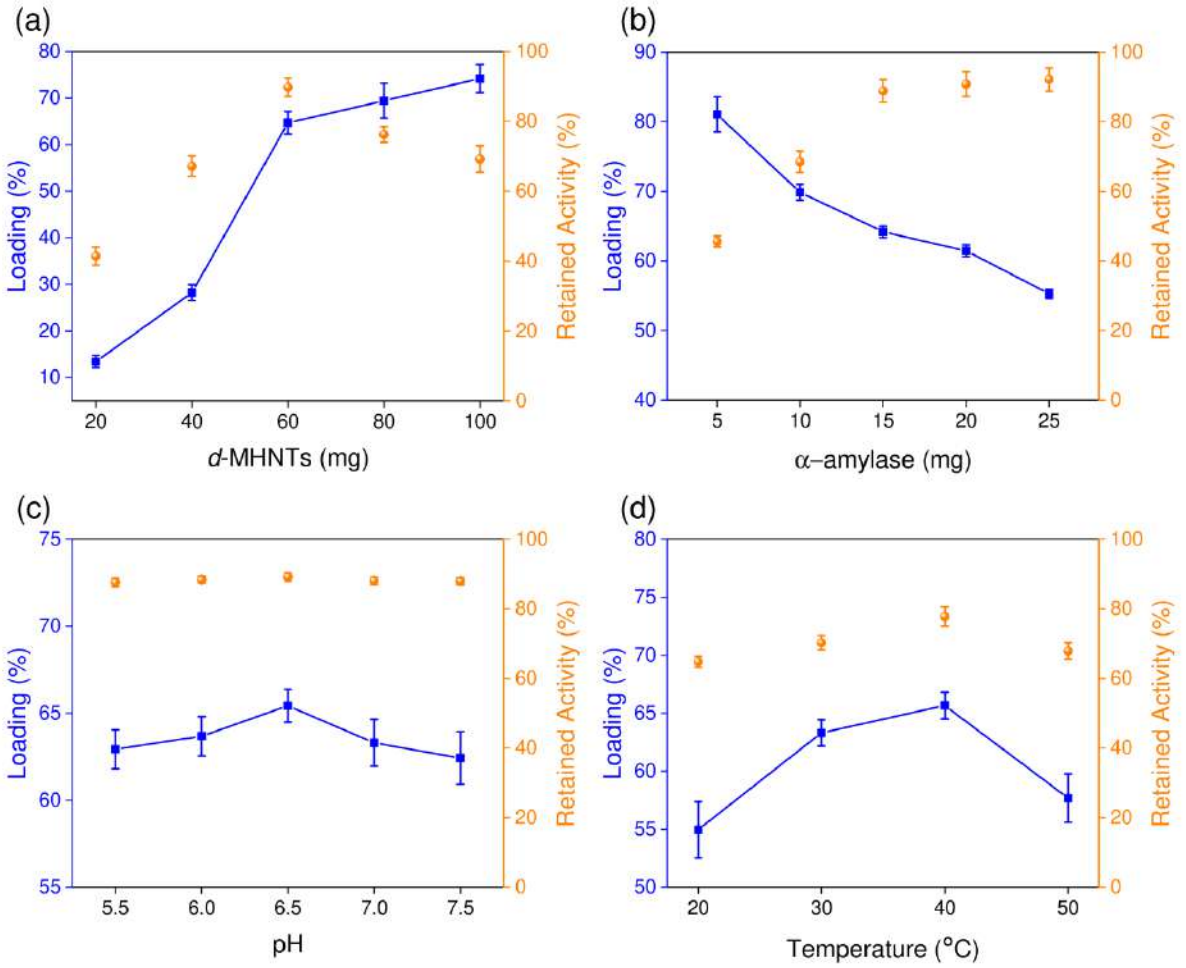

Figure 4.31 (a) Impact of support amount (mg), (b) Impact of α-amylase amount (mg), (c) Impact of reaction pH, and (d) Impact of reaction temperature (°C) on α-amylase loading (%) and retained activity (%).

4.13.2 Box Behnken Design (BBD)

Box-Behnken design (BBD) of response surface methodology was adopted for optimizing the immobilization process using selected parameters and their effective range.

In Table 4.8, the model competency was evaluated using analysis of variance (ANOVA). The obtained F-value of 40.62 (p-value <0.0001) and a lack of fit F-value of 3.52, both at 95% confidence level suggested the generated model to be significant. The harmony of generated model with the experimental data can be interpreted by a low p-value and insignificant lack of fit F-value. It also endorses that any variation in the observations occurred solely due to a real cause, i.e., change in the independent variables, not by any kind of error or noise.

Table 4.8 ANOVA for response surface quadratic model.

Source	Sum of Square	DF	Mean Square	F Value	Prob>F	Remarks
Model	329.93	9	36.66	40.62	< 0.0001	significant
A	45.65	1	45.65	50.59	0.0002	
B	49.65	1	49.65	55.02	0.0001	
C	162.18	1	162.18	179.72	< 0.0001	
A^2	47.38	1	47.38	52.50	0.0002	
B^2	1.44	1	1.44	1.59	0.2472	
C^2	16.37	1	16.37	18.14	0.0037	
AB	1.96	1	1.96	2.17	0.1840	
AC	7.225E-003	1	7.225E-003	8.006E-003	0.9312	
BC	0.33	1	0.33	0.37	0.5641	
Residual	6.32	7	0.90			
Lack of Fit	4.58	3	1.53	3.52	0.1278	not significant
Pure Error	1.74	4	0.43			
Cor Total	336.25	16				

*A: *d*-MHNTs amount (mg); B: Temperature (°C); C: α-amylase amount (mg)

The BBD produced a regression equation for estimation of immobilization efficiency in the form of enzyme loading (%) as the final result as follows:

$$\text{Loading (\%)} = -143.21775+4.76702A+2.80235B+1.11440C-0.033545A^2-0.023380B^2 -0.078880C^2+0.014000AB-8.50000E-004AC+0.011500BC$$

Where A, B, and C are the amount of *d*-MHNTs (mg), Temperature (°C), and amount of α-amylase (mg), respectively.

The obtained R^2 value of 0.9812 indicated a great correlation between predicted and experimental values (Table 4.9). The values of adj-R^2=0.9571 and pre-R^2=0.7739 were also in reasonable agreement, indicating the suitability of generated model. The signal to noise ratio was found to be 22.407, which further confirms the good efficiency of created model.

Table 4.9 Coefficients of determination for response surface quadratic model.

Std. Dev.	0.95	R^2	0.9812
Mean	63.54	Adjusted R^2	0.9571
C.V.	1.49	Predicted R^2	0.7739
PRESS	76.01	Adeq. Precision	22.407

The generated response for the independent variables was plotted as contour plots and 3-D surface graphical representations (Figure 4.32). The optimized conditions generated by BBD model were: 62.48 mg *d*-MHNTs, 40ºC temperature, and 17.91 mg α-amylase, which theoretically expected to yield 65.32% enzyme loading. The predicted model was validated by conducting experiments at model conditions where, loading of 64.7±0.5% could be achieved, which matches well with the theoretical value. Averages of three replicates were tested, and mean values were reported.

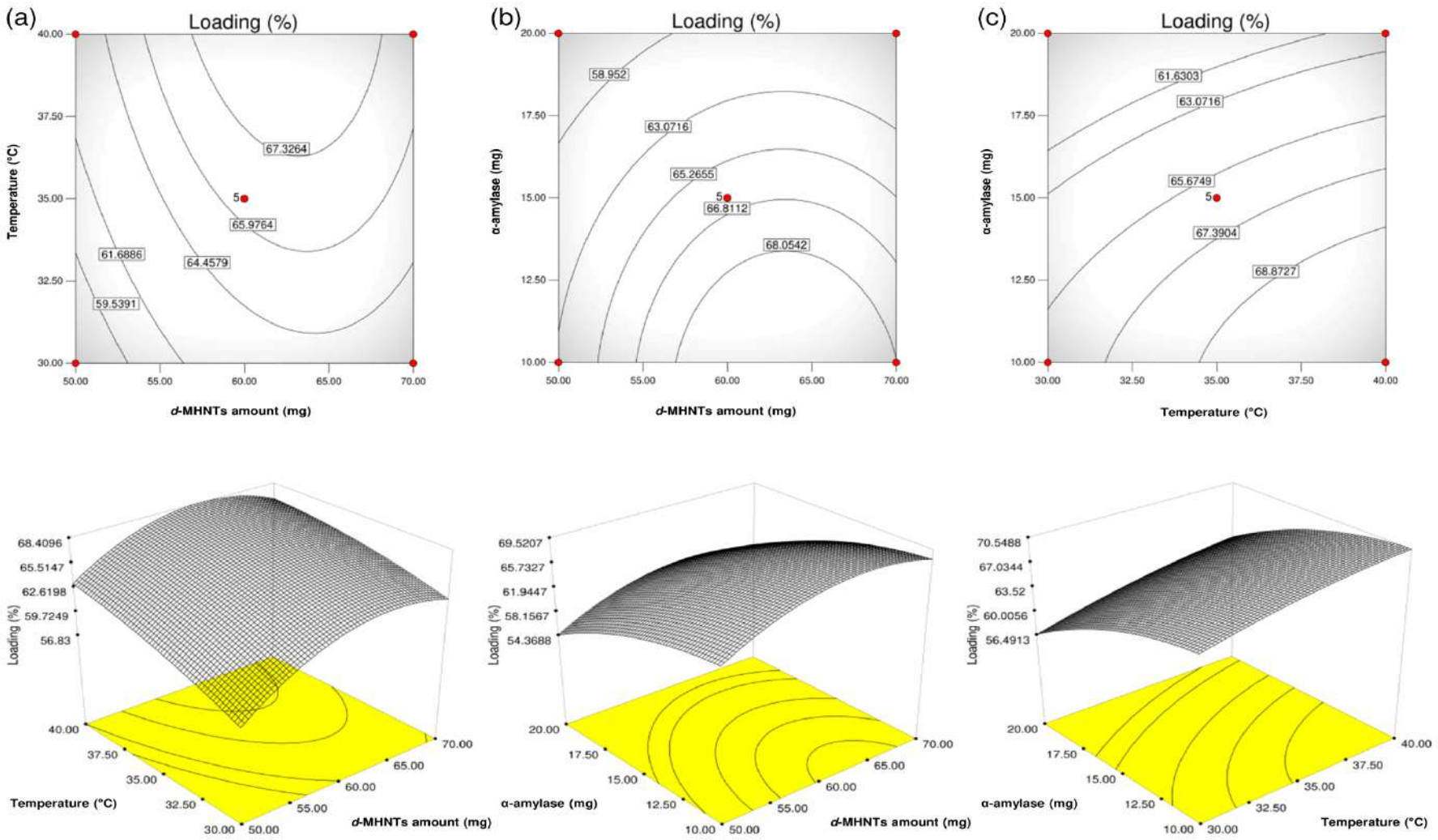

Figure 4.32 2D contour and 3D response surface plots for analyzing the interaction effects between (a) *d*-MHNTs amount and temperature, (b) *d*-MHNTs amount and α-amylase amount, and (c) temperature and α-amylase amount, on α-amylase loading (%).

4.14 Evaluation of Biocatalytic Characteristics

The extent of immobilization was investigated on the optimised conditions obtained using response surface methodology to evaluate its effect on enzyme loading and corresponding retained biocatalytic activity (Figure 4.33a). The results indicate that the enzyme loading increased and reached a plateau after 8 h of incubation. This duration facilitated the required microenvironment over polydopamine-modified MHNTs to immobilize α-amylase, resulting in a very high enzyme loading: i.e., 185.5 mg/g of *d*-MHNTs. The retained activity of α-amylase in an immobilized state demonstrated a similar trend. The surface anchoring of enzymes onto nonporous halloysite nanotubes reduced the harmful effects of substrate diffusion resistance (An et al. 2020). However, the retained activity of immobilized α-amylase was drastically reduced by extending the duration beyond 8 h, which was attributed to the dense packing of enzymes (Klapiszewski et al. 2018). Hence, an optimal reaction time of 8 h was considered for further studies, which possesses the virtue of high enzyme loading (64.7 ± 0.5%) with high retained activity (89.3 ±1.8%). Further, the leaching of immobilized enzymes in the presence of different desorbant solutions provided critical information regarding the category of immobilization (adsorption, affinity, or covalent attachment). We observed marginal leaching of enzymes in the presence of ionic (2.62%) and detergent (3.87%) solvents. The results indicated hardly any ionic or hydrophobic interactions between the enzyme and support (Rodrigues de Melo et al. 2017; Coutinho et al. 2018). Rather, covalent bonding existed between α- amylase and the dopamine-functionalized MHNTs.

4.14.1 Impact of Process Parameters

The effect of reaction pH on the biocatalytic activity of α-amylase in a free versus immobilized state was assessed. The initial activities of both free (300 IU, pH 6) and immobilized (268.3 IU, pH 6.5) α-amylase at the corresponding optimal pH values was considered to be 100% while their relative activities were calculated under various conditions of process parameters. The pH of the reaction medium had a more profound effect on the catalytic activity of α-amylase in the free form than in the immobilized form (Figure 4.33b). At extreme pH values, free α-amylase could retain only 20% (pH 4.5) and 30% (at pH 8.0) of its original activity in comparison to its optimal pH of 6.0. Immobilizing α- amylase, however, significantly broadened its operational pH range from 5 to 7.5, retaining >60% catalytic activity in comparison to its optimum activity (pH 6.5).

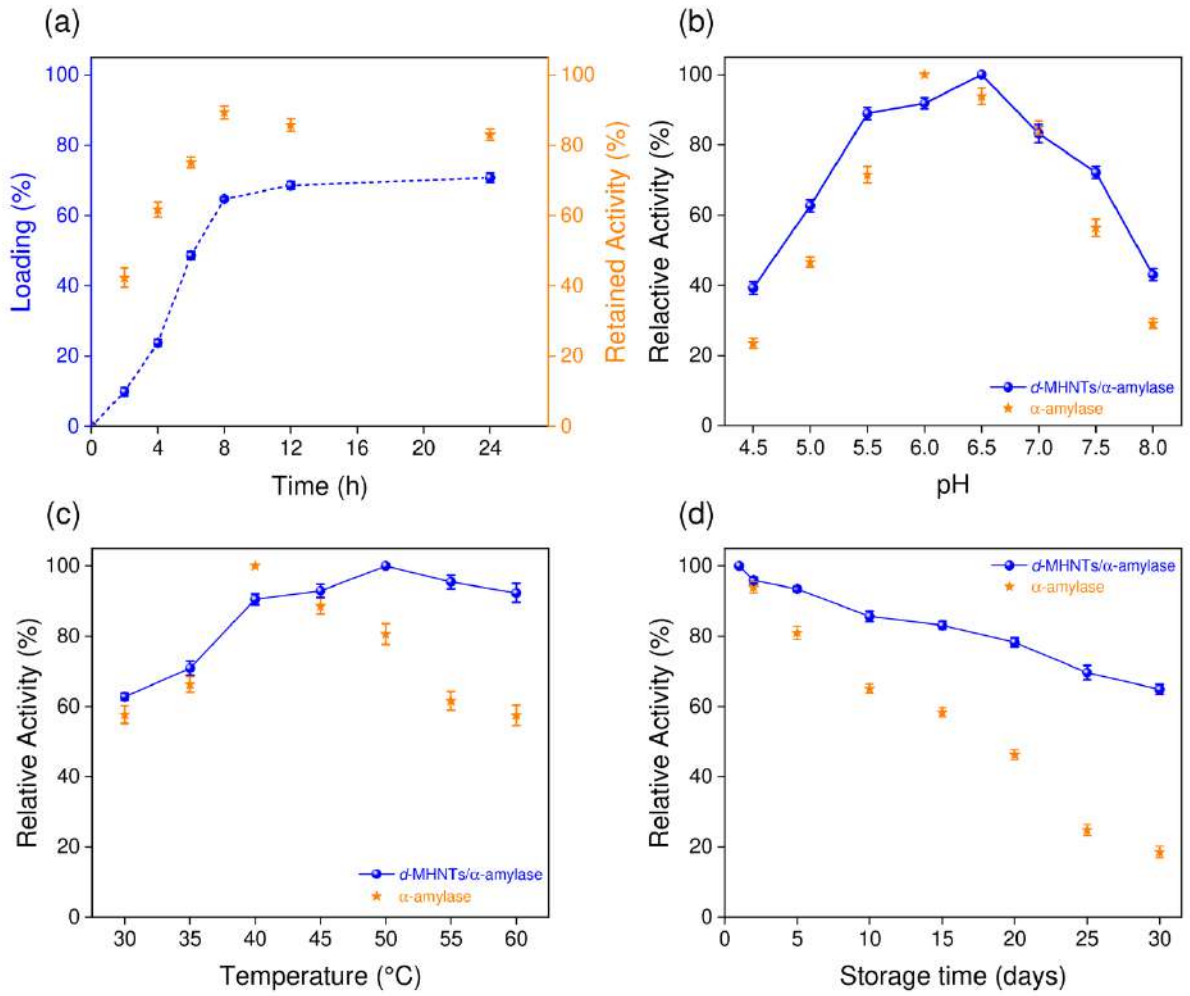

Figure 4.33 (a) α-amylase loading and corresponding retained activity, the impact of (b) solution pH, (c) working temperature, (d) storage duration on catalytic activity of free α-amylase and nanobiocatalyst (*d*-MHNTs/α-amylase).

For evaluating the effect of reaction temperature, the activities of free α-amylase (300 IU, 40 °C) and immobilized α-amylase (272.3 IU, 50 °C) at their respective optimal temperatures were considered as 100% (Figure 4.33c). Similar catalytic activity of both forms of α-amylase at a lower temperature range (30−45 °C) was observed. Beyond 45 °C, free α-amylase gradually lost its catalytic activity due to thermal degradation of its enzymatic structure and could retain only 42.5% of its original activity at 60 °C in compared to its optimum temperature (40 °C). In contrast, *d*-MHNTs/α-amylase exhibited a superior catalytic potential where 92.3% catalytic activity of α-amylase was retained in comparison to the corresponding optimal activity (50 °C). The reduced temperature sensitivity was attributed to an increase in the rigidity of the peptide structure of the enzyme after immobilization, which contributed to improved thermal resistance(Antony et al. 2016). Overall, the immobilization

matrix preserved the structure of α-amylase against any conformational changes prompted by varying reaction conditions and demonstrated a greater utility of dopamine-functionalized MHNTs for enzyme immobilization.

The storage stability of free α-amylase and the nanobiocatalyst was inspected at 4 °C for 30 days (Figure 4.33d). The activity on day 1, of both free (300 IU) and immobilized (269.7 IU) enzymes was considered to be 100%. Free α- amylase, due to the long-term exposure (30 days), could retain only 18.5 ± 1.7% of its initial catalytic activity, due to either the instability of the subunits or inactivation at low temperatures, whereas *d*-MHNTs/α-amylase could preserve over 64% of its biocatalytic activity and mitigated the possibilities of activity reduction under the relevant conditions. The improved storage stability was credited to the stiffness brought upon by multipoint attachment between α-amylase and *d*-MHNT, preserving the inherent structure of α-amylase. In addition, curved surface geometries of support matrices have also been reported to suppress lateral interactions between adjacent enzymes, thus improving the enzyme activity by suppressing the steric hindrance(Chao et al. 2013).

4.14.2 Reusability Potential of the Nanobiocatalyst

The reusability potential of the nanobiocatalyst was evaluated by measuring its catalytic activity during starch hydrolysis for 10 consecutive cycles under the optimized process conditions (Figure 4.34a). The results indicated that the nanobiocatalyst could retain more than 56% of its initial activity even after 10 cycles. As reported before, a drop in the catalytic activity of the immobilized enzyme was inevitable and majorly occurred either due to leaching of weakly anchored enzyme molecules or the conformational changes at the active sites of enzymes when binding to the support materials. Enzyme leaching was ruled out, since the amount of immobilized enzyme recovered after every cycle was always higher than 99%. Since enzyme reutilization is critical for many bioprocesses, the utility of immobilized α-amylase was evaluated in terms of its capacity to produce reducing sugars per cycle (Figure 4.34b). The production of reducing sugars gradually declined with every reuse, going from 15.9 to 9.03 mg/g starch after the 1^{st} and 10^{th} cycles, respectively. However, it was noteworthy that the total production of reducing sugar for the entire 10 cycles of nanobiocatalyst was much higher (121.25 mg/g starch) than that in the continuous reaction of free α-amylase (48.84 mg/g starch) over a similar duration.

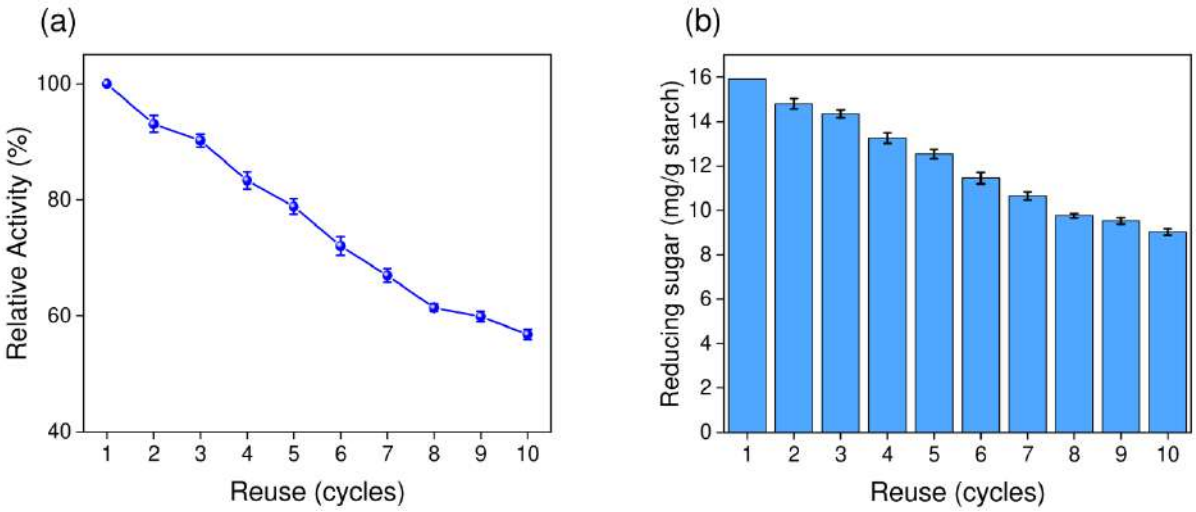

Figure 4.34 (a) The impact on catalytic activity of nanobiocatalyst after every reuse cycle, and (b) Corresponding yield of reducing sugar (mg/g starch) in each cycle.

4.15 Thermodynamics and Kinetic Parameters

Thermodynamic and kinetic parameters provide vital information regarding the thermal behavior of enzymes, rates of reaction, and the reaction mechanism, which are critical for designing a biocatalytic process. Various thermal characteristics of α- amylase in free and immobilized states were monitored over the desired working temperature range (40−60 °C) (Figure 4.35a). We found the thermal deactivation rate constant (k_d) of nanobiocatalyst to be ~4.2−4.7-folds lower than that of free α-amylase at 50 and 60 °C. This confirms the much-improved stability and slower denaturation of α-amylase when it is immobilized onto magnetic halloysite nanotubes (Table 4.10). The half-life of α-amylase in its two states gradually decreased on an increase in the temperature, *d*-MHNTs/α-amylase demonstrated 2.5, 4.3, and 4.7-fold higher half-lives in comparison to that of free α-amylase at temperatures of 40, 50, and 60 °C, respectively. The superior half-life and operational stability of enzyme at elevated temperatures indicate that immobilized α-amylase was "more shielded" toward any unforeseen reasons for inactivation (Rodrigues et al. 2021). This was well supported by the decimal reduction time (D value), which indicated that immobilized α-amylase would take more time to denature than free enzyme. Further, a higher thermal inactivation energy or energy of denaturation (E_d) for the nanobiocatalyst (165.59 kJ/mol) in comparison to that for the free enzyme (156.14 kJ/mol) revealed that more energy would be required to denature the immobilized enzyme.

Similarly, immobilized α-amylase exhibited higher values of enthalpy change, ΔH (162.99 kJ/mol), and Gibbs free energy change, ΔG (80.85 kJ/mol), in comparison to its free form (Figure 4.35b). The higher total energy required for enzyme denaturation indicates the superior thermal stability of immobilized enzymes in comparison to free enzymes. Moreover, a higher value of the entropy change (ΔS) in the nanobiocatalyst in comparison to that of its free form is a sign of more disorder at the nanobio interface, which is beneficial for the operational flexibility of enzymes in industrial bioprocessing. The obtained results validate multipoint attachments of α-amylase molecules with dopamine-functionalized MHNTs toward establishing a stable enzyme−support system that enhances the conformational flexibility of immobilized enzymes. The conclusion drawn here is well corroborated by a few recent reports (Ahmed et al. 2017; Morellon-Sterling et al. 2021; Rodrigues et al. 2021).

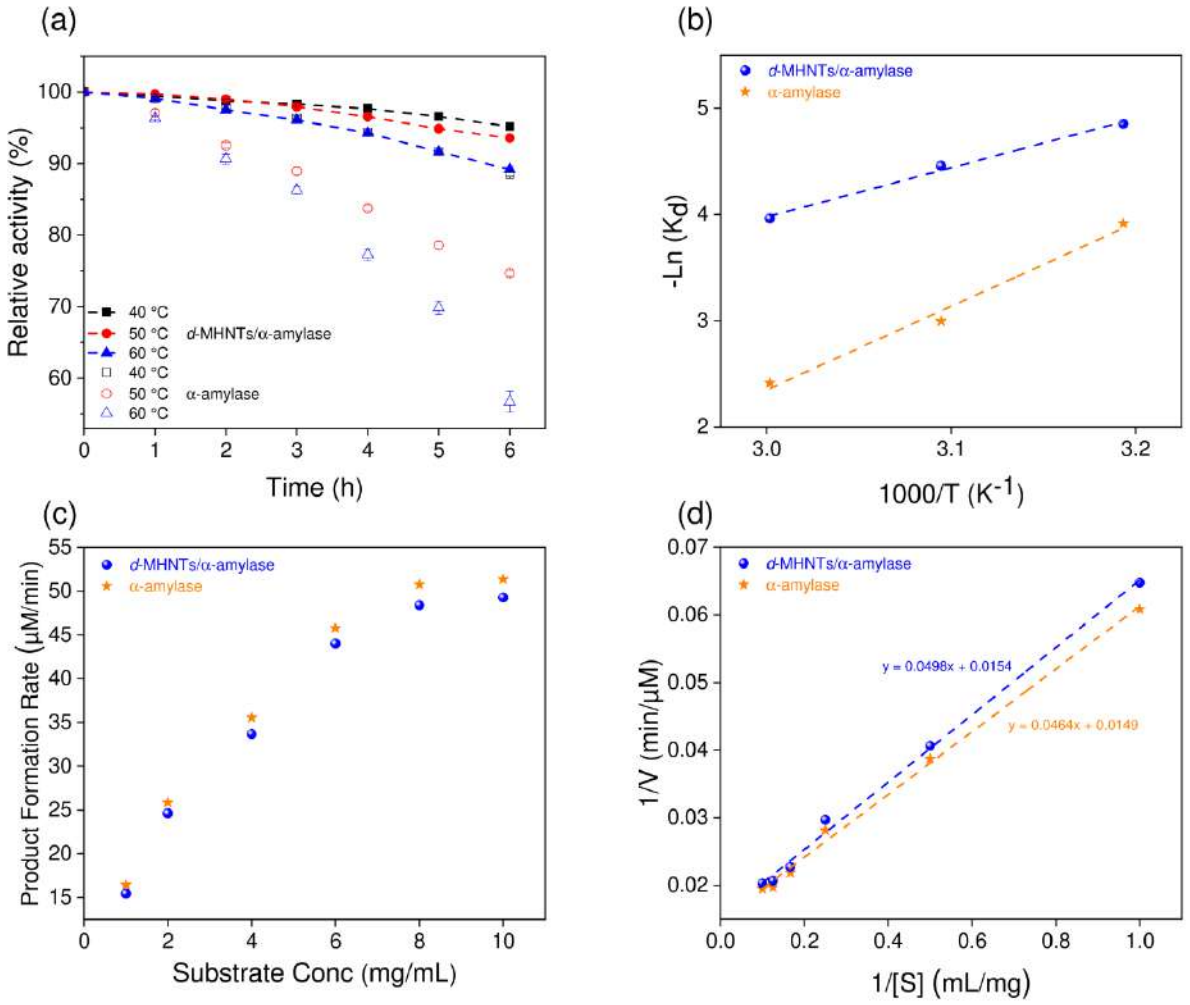

Figure 4.35 (a) Impact of elevated temperatures on both free and immobilized α-amylase, (b) Arrhenius plot, (c) Michaelis-Menten plot of free and immobilized α-amylase, and (d) Lineweaver-Burk plot.

Kinetic parameters for free α-amylase and the nanobiocatalyst were investigated using a Michaelis−Menten plot and a Lineweaver−Burk plot by varying substrate concentrations (Figure 4.35 c-d). After immobilization, a slight increase in k_M value was observed while the maximum reaction velocities (V_{max}) were estimated to be 67.11 and 64.93 μM/min for *d*-MHNTs/α-amylase and free α-amylase, respectively. Diffusional limitations is the rationale behind such a minor variation in kinetic parameters, as immobilization inevitably restricts enzyme movement in comparison to its colloidal state, we still could manage to improve other aspects of enzymes that have been limiting their commercial use by promoting reuse, and operational stability, without altering the kinetics.

Table 4.10 A comparative summary of thermodynamic parameters before and after immobilization of α-amylase.

Parameters	**Temperature (°C)**	**Free Enzyme (α-amylase)**	**Nanobiocatalyst (*d*-MHNTs/ α-amylase)**
k_d (h^{-1})	40	0.019	0.007
	50	0.049	0.011
	60	0.089	0.019
Half-life, $t_{1/2}$ (h)	40	34.77	89.10
	50	13.86	59.69
	60	7.74	36.39
D-value	40	115.54	296.07
	50	46.05	198.34
	60	25.74	120.92
E_d (kJ/mol)		156.14	165.59
ΔH (kJ/mol)	40	153.54	162.99
	50	153.45	162.91
	60	153.37	162.82
ΔG (kJ/mol)	40	78.41	80.85
	50	78.36	82.29
	60	79.09	83.38
ΔS (J/mol·K)	40	239.91	262.30
	50	232.39	249.49
	60	222.98	238.48

4.16 Effect of the presence of Cellulose and Metal Ions on Catalytic Activity

The presence of soluble and insoluble dietary fibers, specifically cellulose in the starch, extracted from potato peel waste could unexpectedly influence the α-amylase activity (Table 4.11). Hence, the retained catalytic activity of both free and immobilized enzymes was evaluated in the presence of different cellulose concentrations. As expected, a significant deterioration in the activity of α-amylase in both forms was observed for all cellulose concentrations (Figure 4.36a). Free α-amylase appeared to be extremely sensitive even on introduction of 0.25% (w/v) cellulose, where only 87% activity could be retained with respect to the control. Further, the incremental addition of cellulose (0.5−1% w/v) caused a greater decrease in its catalytic activity from 75.8% to 47.6%, respectively. In contrast, *d*-MHNTs/α-amylase exhibited better biocatalytic power at the similar cellulose concentrations investigated, and it could retain a remarkable 83% activity even at 1% (w/v) concentration. Although the mechanism of inhibitory effects of cellulose on the amylolytic process is still unclear, a decrease in the catalytic activity occurred because of the "adherent" nature of α-amylase toward non-starch polysaccharides, i.e., cellulose, making them inaccessible to starch due to steric hindrances (Patel et al. 2017). The result corroborates a similar fact where cellulose adversely affected amylolysis by impairing the catalytic efficiency of free α-amylase. However, the superior activity of *d*-MHNTs/α-amylase is governed by a more favorable interaction between cellulose−polydopamine (present in the support matrix) and cellulose−amylase so that most of the active sites could remain available for starch molecules (Han et al. 2016).

The presence of metal traces in extracted polysaccharides is a common hurdle for their subsequent hydrolysis, as metal ions might also interfere with the active sites of enzymes. We observed that both Ca^{2+} and Mg^{2+} boosted the relative activities of free α-amylase to 125.4% and 106.6%, respectively (Figure 4.36b), since these metal ions act as allosteric activators and help in the stabilization of the three-dimensional structure of α-amylase (Okwuenu et al. 2017). However, Fe^{2+} and Cu^{2+} ions inhibited the enzyme activity to the greatest extent with catalytic losses of 37% and 43%, respectively, in comparison to the control. This indicates the importance of cysteine residues for the activity of α-amylase, since the sulfhydryl groups of cysteine occasionally act as a ligand of metal ions (Figure 4.36c). It is also likely that calcium ions between the substrate-binding domains of α-amylase would be replaced by divalent metal ions, leading to structure destabilization. In contrast, immobilized enzymes

exhibited a more profound and beneficial effect on their activity in comparison to free enzymes in the presence of metal ions. The most significant effect appeared in Ca^{2+}, where immobilized enzymes could attain 51% more activity in comparison to the control. The superior activity is attributed to the "shielding" and robustness of the enzyme-immobilization matrix, which attenuated the likely replacements of Ca^{2+} ions at the active sites and protected the intrinsic structure of α-amylase (Pascoal et al. 2011). The presence of a biomimetic coating on MHNTs proves to be advantageous in both aspects, and the results validate its superiority for immobilizing α-amylase.

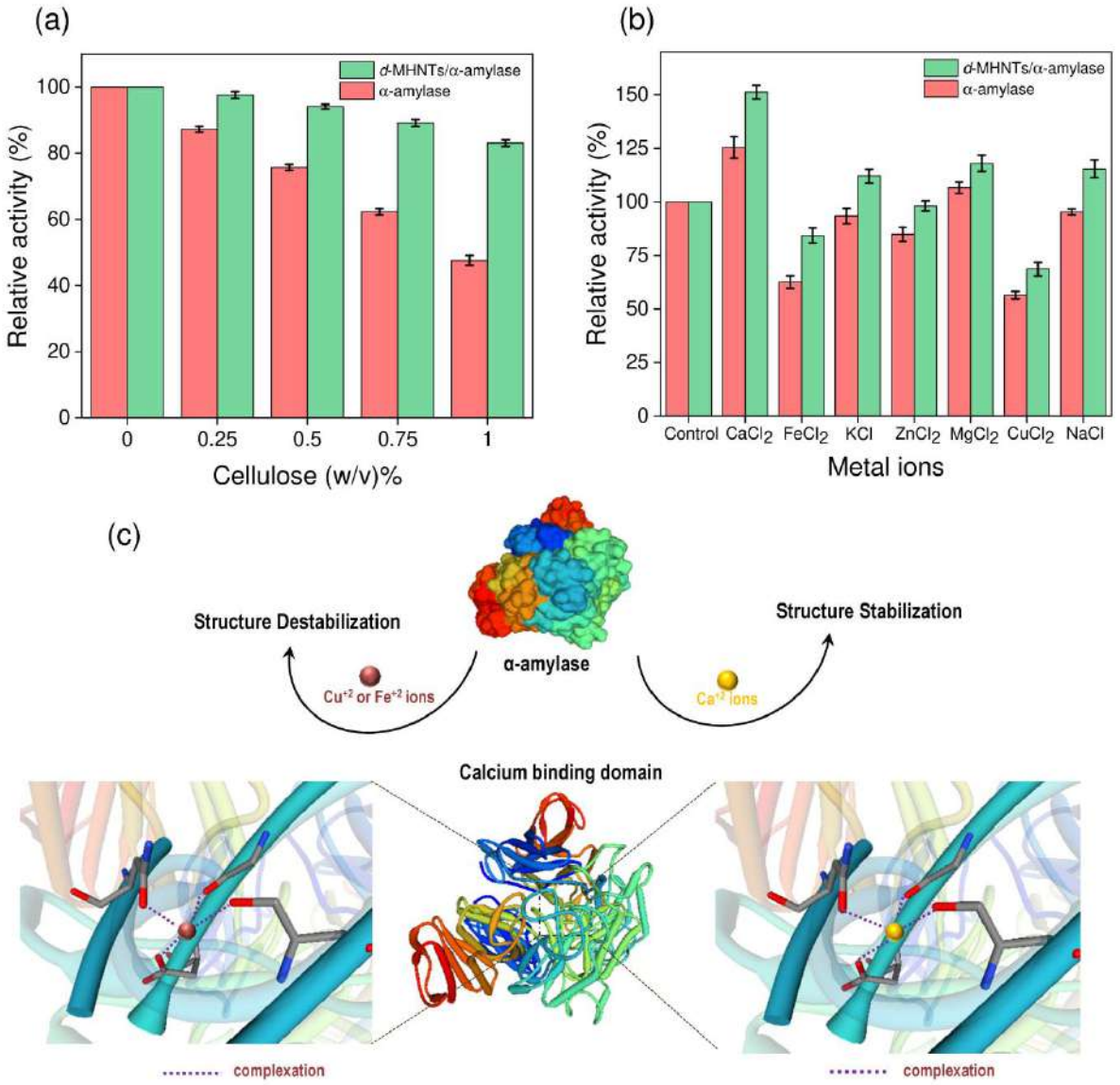

Figure 4.36 (a) Impact of cellulose concentration, (b) Impact of metal ions on catalytic activity of free and immobilized α-amylase, and (c) Proposed mechanism for enzyme structure stabilization or destabilization.

4.17 Starch Extraction and Characterization

The efficiency of starch extraction method was evaluated in terms of the extraction yield and starch recovery (%) (Figure 4.37a).The yield of extracted starch enhanced with increasing stirring time, which is due to the dissolution of water-soluble components. After 24 h of stirring, the starch yield was found to be 413 mg/g PPW, while starch recovery was estimated to be above 73%. The high yield and recovery of starch obtained with this method established the potency of this method for starch extraction. The extracted starch was then characterized using FTIR, which demonstrated the absorbance bands at 1010, 1160, and 1710 cm^{-1} referring to vibrational stretching of C-O-H, C-O/C-C, and C=O, respectively present in starch structure (Figure 4.37b) (Van Soest et al. 1995). The peaks at 1640 and 3310 cm^{-1}were attributed to the adsorbed water and -OH group, respectively (Fang et al. 2002; Kizil et al. 2002; Cisek et al. 2018).

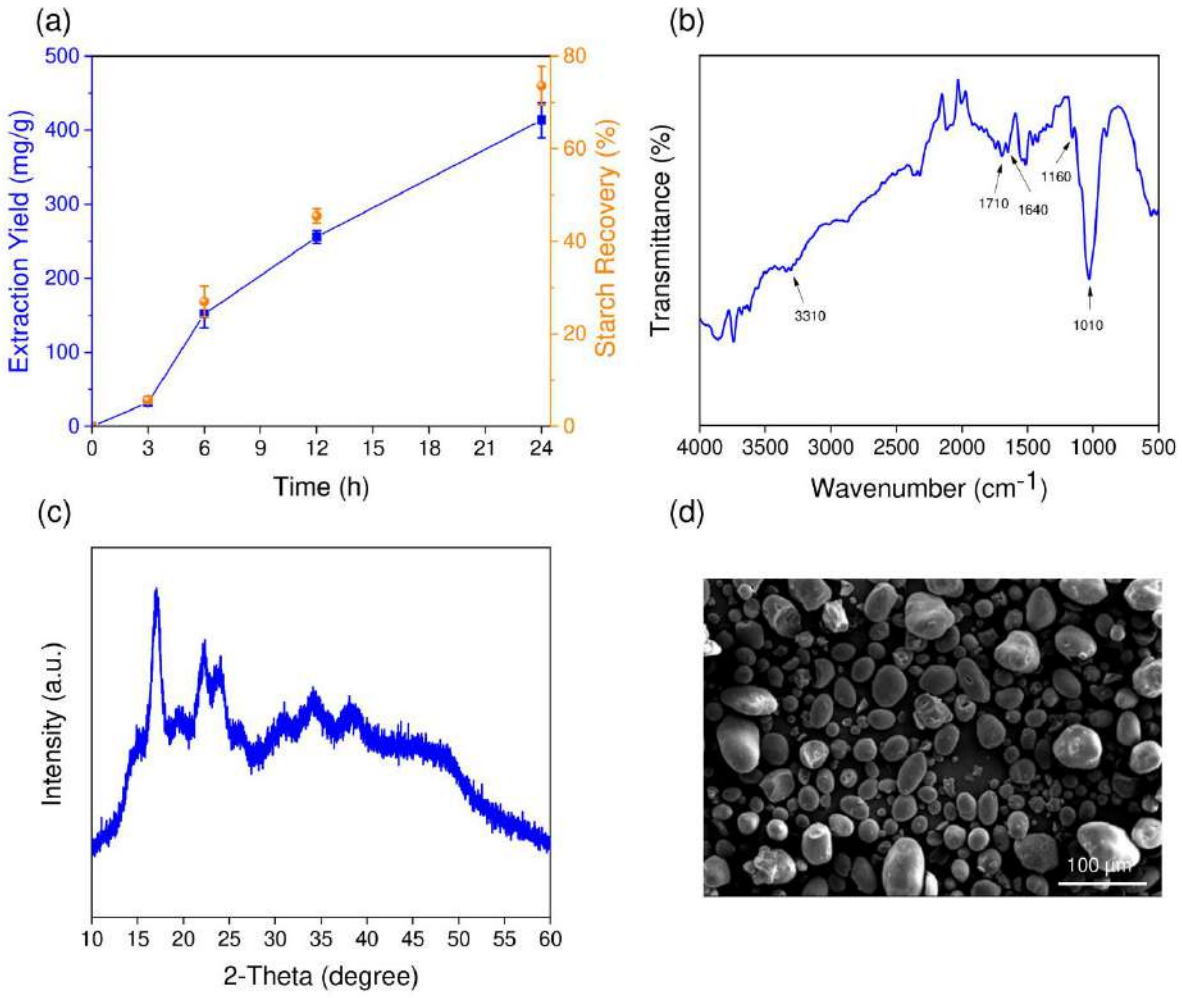

Figure 4.37 (a) Extraction yield and starch recovery from potato peel waste (b) FTIR spectra, (c) XRD spectra, and (d) SEM micrograph of extracted starch.

The X-ray diffractogram of extracted starch demonstrated a typical 'B' type X-ray pattern with characteristics diffraction peaks at 2θ=16.9°, 19.6°, 22.2° and 24.0° (Figure 4.37c) (Yu et al. 2013; CASTAñO et al. 2014; Pozo et al. 2018). Overall, the existence of characteristic peaks in FTIR and XRD confirmed the existence of starch as a major fraction in the suspension, while the emergence of other peaks corresponded to other component present in the material like cellulose, protein and lipids. SEM micrograph further confirms the granular morphology of starch, having oval and ellipsoid shapes of varying sizes (Figure 4.37d).

Further, potato peel waste and extracted starch were biochemically characterized for their compositional analyses (Table 4.11). The starch component increased from 56.21 wt% in PPW to 75.23 wt% in extracted starch, validating the efficiency of extraction process. The notable difference revealed by the analysis was that after extraction the amount of reducing sugars and protein are comparatively lower based on dry weight/weight. The soluble nature of protein and reducing sugars might be attributed for these observations. Furthermore, a decrease in relative fiber component after extraction was also recorded. Overall from the physical and biochemical analyses observations the enrichment of starch component in extracted starch was established. The extracted starch was further employed for continuous hydrolysis using the fabricated α-amylase nanobiocatalyst (*d*-MHNTs/α-amylase).

Table 4.11 A comparative compositional analysis of the pineapple peel waste (PPW) and the extracted starch

Parameters	**PPW (dry wt. %)**	**Extracted Starch (dry wt. %)**
Moisture	5.89 ± 0.48^{a}	5.28 ± 0.62^{a}
Total carbohydrates	65.22 ± 2.97^{b}	83.22 ± 3.4^{a}
Starch	56.21 ± 2.77^{b}	75.23 ± 2.11^{a}
Reducing sugars	0.42 ± 0.17^{a}	0.08 ± 0.02^{b}
Ash	6.42 ± 0.61^{a}	5.23 ± 1.08^{b}
Protein	14.64 ± 1.72^{a}	6.01 ± 1.31^{b}
Fiber	24.31 ± 2.45^{a}	18.72 ± 1.66^{b}

¶Data is presented as mean ± standard deviation of three replicates. Means with different superscript letters are different by Tukey's post

4.18 Nanobiocatalytic Conversion of Extracted Starch into Biochemical Products

The fabricated nanobiocatalyst i.e., *d*-MHNTs/α-amylase was evaluated for a real-time application, i.e., for the continuous production of high maltose-containing syrupthat fermentation industries could use (Figure 4.38a). The nanobiocatalyst was able to produce 276.8 mg reducing sugar/g extracted starch in 72 h of continuous operation without significantly compromising its biocatalytic activity. The continuous increase in the reducing sugar (dextrin, maltose, or maltotriose) signified the superior stability over a long run and immense potential for employment in industrial sector. Further, it is a well-documented fact that the organic waste generated in kitchens, food processing plants, and restaurants is enriched with complex nutrients and the hydrolysis of such waste is critical in transforming agro/food waste into a growth medium for microorganisms. Hence, the dual functionality of the nanobiocatalyst to hydrolyze the biopolymeric content in potato peel waste to generate fermentable sugars and liberate soluble proteins/other micronutrients was also investigated to formulate a medium directly from PPW.

4.18.1 Analysis of Hydrolysate Broth Medium

Liquid broth suspensions prepared, i.e., PPW and PPW_{NBC} media, were evaluated for compositional analyses (Table 4.12). As expected, the amount of reducing/non-reducing sugars obtained after nanobiocatalytic treatment was 3-fold higher (1.328 g/100 mL) in comparison to the PPW medium. The protein content was also enhanced from 21 to 123 mg/100 mL in the hydrolysate, indicating that the biocatalytic treatment using immobilized α-amylase induced "starch depolymerization", which diminished the recalcitrant nature of potato peel waste, resulting in a greater release of soluble proteins.

Table 4.12 A comparative compositional analysis of PPW and nanobiocatalyst treated PPW media formulations.

Parameters	**PPW (g/100 mL)**	**PPW_{NBC} (g/100 mL)**
Total carbohydrates	0.487 ± 0.01^{b}	1.328 ± 0.02^{a}
Reducing sugars	0.008 ± 0.00^{b}	1.123 ± 0.01^{a}
Protein	0.021 ± 0.00^{b}	0.123 ± 0.00^{a}

¶Data is presented as mean ± standard deviation of three replicates. Means with different superscript letters are different by Tukey's post-hoc test ($p<0.05$).

This hydrolysate suspension was envisaged as a consortium of energy sources along with the presence of other nutrients that can mimic the nutritive complex medium required for microbial/fermentation growth.

4.18.2 Bacterial Growth

To confirm the accessibility of leached nutrients in hydrolysate to microorganisms, the growth characteristics of *E. coli* in PPW and PPW_{NBC}-based media suspensions were compared to nutrient medium (NM, positive control) broth. The growth curves of the untreated PPW suspension manifested a prolonged lag phase in comparison to PPW_{NBC} and NM (Figure 4.38b), whereas *E. coli* grown on PPW_{NBC} and NM media showed similar growth pattern up to the lag phase, which indicated that microbes find little differences while they perform their structural reorganization during adaptation.

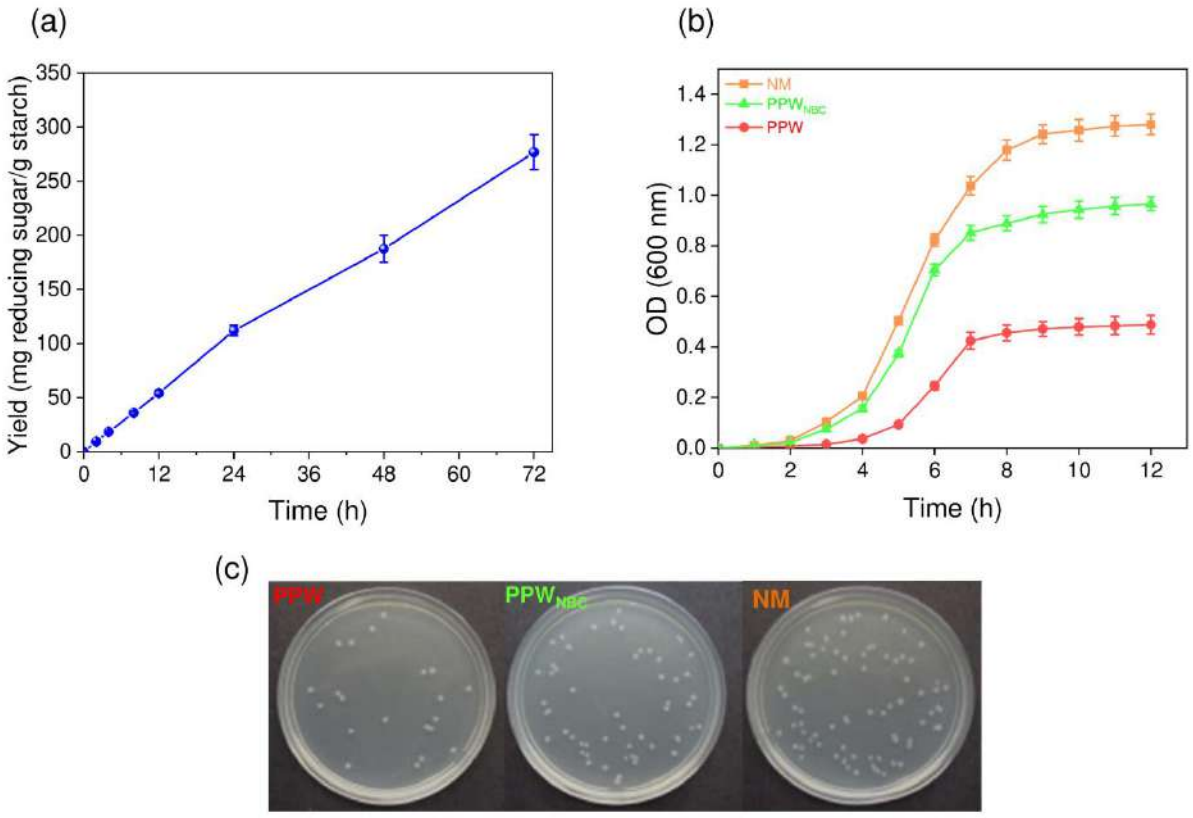

Figure 4.38 (a) Continuous starch hydrolysis of extracted starch, (b) Bacterial growth curve, and (c) Photographic image of bacterial colony on different media formulations.

A noticeable difference was observed in the lag phase, where the specific growth rate (μ) was reduced in the case of untreated PPW ($0.13 \pm 0.018\ h^{-1}$) and PPW_{NBC} ($0.24 \pm 0.009\ h^{-1}$) in comparison to the NM broth ($0.32 \pm 0.016\ h^{-1}$). The overall growth followed the order NM >

PPW_{NBC}> PPW. The nutrient broth, being a defined medium, was best suited for microbial growth in comparison to other complex media sources. However, the inherent richness of PPW_{NBC} (carbon source-reducing sugars, nitrogen source-proteins, and micronutrients) made it equally capable of supporting bacterial growth in comparison to the untreated PPW. Thus, PPW_{NBC} can be a feasible alternative to the existing complex media formulations without supplementing any external nutrients. In a solid culture, the growth of *E. coli* exhibited a similar pattern, where both NM and PPW_{NBC} were utilized well with no variation in the colony morphology. At the same time, PPW medium appeared to be least suited to the microorganisms (Figure 4.38c).

4.18.3 Single Cell Protein Production

The formulated medium was also evaluated for the production of *A. niger* biomass (Figure 4.39a). In comparison to potato dextrose broth (PDB, 100%), PPW and PPW_{NBC} media showed 37% and 80% biomass productions, respectively (Figure 4.39b).

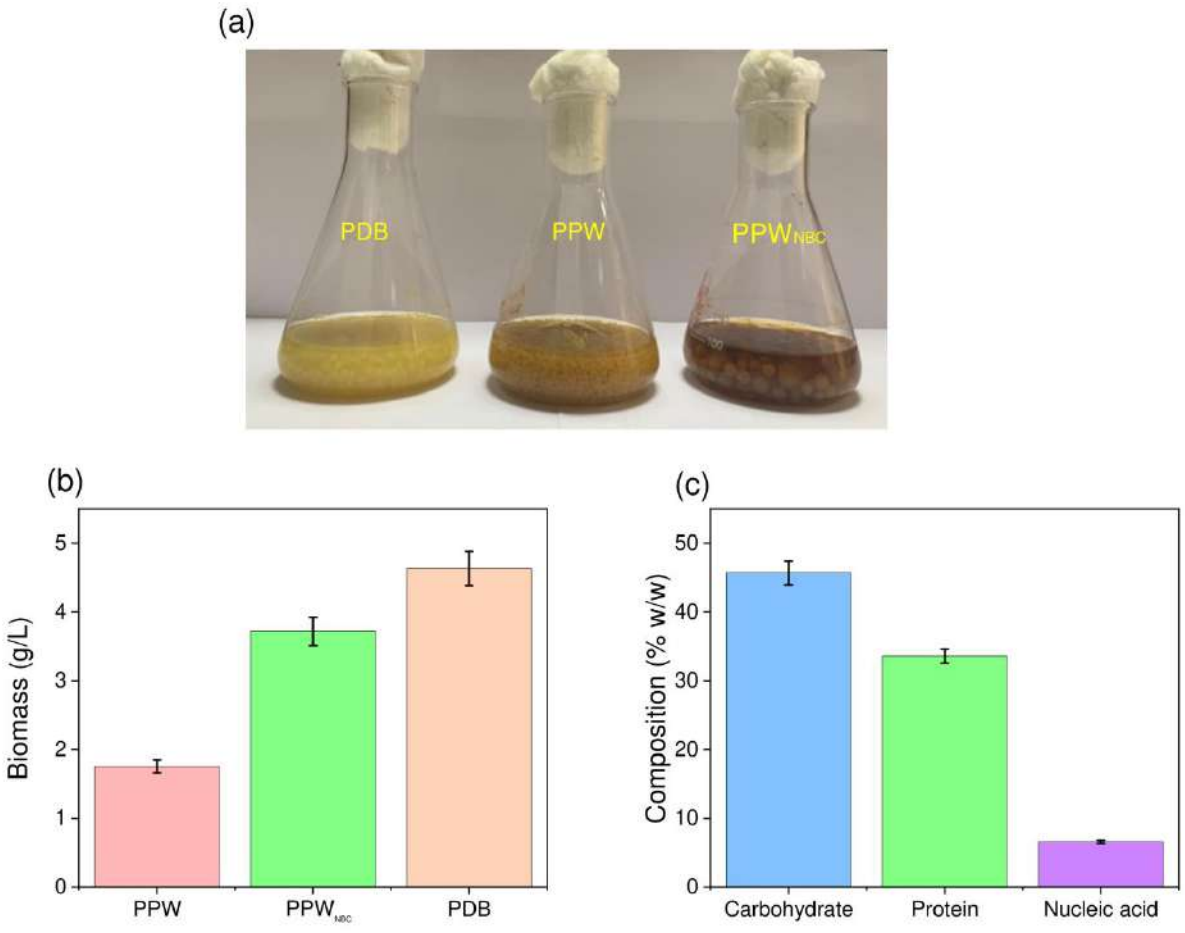

Figure 4.39 (a) Fungal biomass growth on different media, (b) Dry fungal biomass (g/L) on different media, and (f) Compositional analysis of produced biomass as single-cell protein.

A higher amount of nutrient availability in the treated hydrolysate (PPW_{NBC}) was attributed for the better growth. The quantitative estimation of the single-cell protein (SCP/dried biomass PPW_{NBC} medium) revealed carbohydrates to be the primary components (45.7% w/w), followed by proteins (34.0% w/w) and nucleic acids (6.6% w/w) (Figure 4.39c). The biomass with higher nucleic acid content could be used after treatment for nucleic acid reduction as a protein additive in animal feeding (Ravindra 2000). The overall characterization of the produced biomass confirms the acceptable performance of the formulated medium for SCP production.

4.18.4 Biocementation Application

Finally, we tested the potential industrial relevance of the nanobiocatalyst to enhance the strength and durability of construction materials through biocementation (Microbially induced calcium precipitation). The waste hydrolysate (PPW_{NBC}) favored an excellent calcium carbonate precipitation capability of calcifying bacteria, *B. subtilis* CT-5, thus acting as a promising medium alternative. The results indicated that, while the maximum growth was observed in nutrient broth, PPW_{NBC} also supported microbial growth (Figure 4.40a). On a similar note, calcium carbonate precipitation was highest in NB medium (189.4 ± 2.0 mg/100 mL) in comparison to blend formulations (Figure 4.40b).

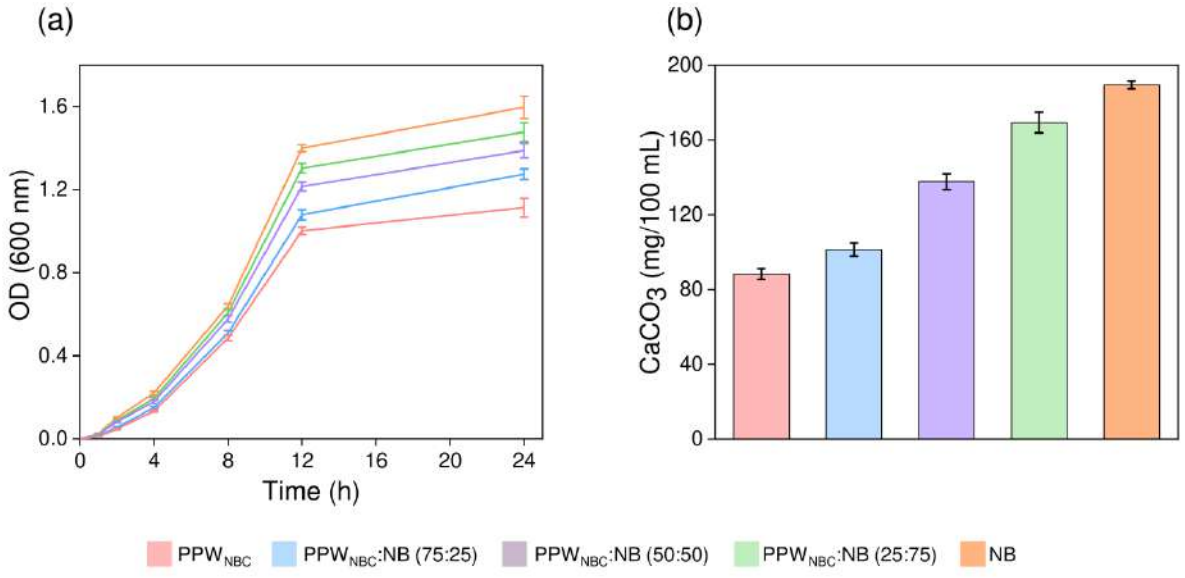

Figure 4.40 (a) Growth of calcifying bacteria *Bacillus* sp. CT5 on different media formulations, and (b) Effect of different media compositions on calcium carbonate precipitation.

The $CaCO_3$ precipitations recorded in other media formulations such as PPW_{NBC}:NB(25:75), PPW_{NBC}:NB (50:50), and PPW_{NBC}:NB (75:25) were 169.3 ± 5.5, 137.7 ± 4.2, and 101.3 ± 3.5 mg, respectively. PPW_{NBC} alone had the lowest calcium carbonate precipitation, 88.2 ± 2.9 mg. The accessibility to preferred nitrogen sources has been linked to superior bacterial enzymatic activity (Hammami et al. 2018). The limited availability of nitrogen sources in PPW_{NBC} might have affected the ureolytic activity and lowered the amount of $CaCO_3$ precipitation. However, the addition of a nitrogen source might further improve the growth and $CaCO_3$precipitation abilities of PPW_{NBC}. This indicates that the nanobiocatalyst-derived hydrolysate suspension can be used as a substitute for existing media formulations, which may decrease the operational cost of biocementation on a commercial scale (Achal et al. 2011).

Chapter 5

Conclusions

Abundant agri-food waste, as low-cost raw material has the potential to substitute the conventionally used edible feedstock for the producing biochemical products. The effective utilization of agri-food waste could provide a viable route to meet current and future demands of biochemical products while minimizing the negative impact of direct waste disposal. The value generation might pave the path for a feasible circular bio-economy where components having no practical applications or economic value are only disposed off. This study is an attempt to formulate a feasible strategy to biotransform non-edible feedstock into value-added products using nanomaterial-enzyme system, termed nanobiocatalyst. The effective valorization of sugarcane bagasse, an agricultural waste from sugar industry and potato peel waste produced by food processing industry was investigated in the research work. The following conclusions are drawn based on the research work carried out:

5.1 Pretreatments of Lignocellulosic Biomass

- Sulfonic acid functionalized magnetic halloysite nanotubes were investigated for pre-treatment of sugarcane bagasse. Solid acid catalyst treatment and subsequent dilute alkaline treatment were employed as a two-step pretreatment approach under autoclave conditions.

- Mercaptosilane grafting followed by condensation and oxidation resulted in high loading of acidic group (-SO_3H). The magnetic characteristic provided easy recovery of the solid acid catalyst (MHNTs- SO_3H) from reaction mixture with high retained activity.

- The selectivity of solid acid catalyst for hemicellulose component hydrolysis was evident from physicochemical analyses of pretreated biomass and wash liquids. On the other hand, dilute alkaline pretreatment was held responsible for SCB delignification. Optimizing the pretreatment process revealed that only a higher amount of solid acid catalyst is effective in stimulating a superior hemicellulose and lignin removal.

- The pretreatment capacity of fabricated solid acid catalyst was evident from high xylose production, minimal inhibitory compound formation and highly accessible cellulose content, which can be easily extended to other lignocellulosic biomass samples.

- Enhanced glucose (2.63 folds) and bioethanol (2.64 folds) production was achived in pre-treated biomass than raw sugarcane bagasse.

- The industrial scale transformation of this approach is feasible considering the low cost involved while synthesizing solid acid catalyst and its subsequent pretreatment procedure. The immobilization of cellulase could provide even higher feasibility for effective transformation of sugarcane bagasse into value-added products.

5.2 Cellulase-based Nanobiocatalyst

- An attempt was made to develop a novel tool for biocatalytically converting cellulose into glucose with high yield and saccharification via magnetically separable halloysite nanotubes (MHNTs) as an immobilization matrix.
- The nanobiocatalyst was fabricated by immobilizing cellulase on to magnetic halloysite nanotubes (HNTs) through amine surface functionalization. Statistical optimization of the immobilization process enabled lower enzyme dosage for achieving higher catalytic yield, thereby avoiding the loss of an extra load of enzyme and making the process cost-effective.
- Structural characterization confirmed the successful loading of cellulase onto MHNTs without losing their biocatalytic activity. A high payload of cellulase did not compromise their inherent biocatalytic characteristics and remained unaffected by any exterior mass transfer limitations.
- Immobilized cellulase displayed enhanced activity under harsh process conditions (pH), superior stability at elevated temperatures, ionic liquid-tolerant characteristics and storage capability than free cellulase. The magnetic nature of NBC enabled separating it from the reaction mixture after completion of the reaction. The NBC retained ~67.8% of its original activity after 7 reuse, produced nearly 5.8 fold higher glucose productivity as compared to its free form and was 100% recoverable using a magnet.
- Regardless of the substrate, NBC was found equally efficacious in hydrolyzing the insoluble, agro-residue biomass into soluble glucose residues, which can be used in fermentation and bioprocessing further.
- The optimization of continuous biocatalytic transformation of glucose stream into fructose using packed immobilized glucose isomerase reactor revealed a high glucose conversion into fructose, revealing the significance of this approach for direct production of an industrially relevant product.

- The sustainability and eco-friendly endeavors of this approach would pave the way toward valorization and consolidated bioprocessing of cellulose materials.

5.3 α-amylase based Nanobiocatalyst

- The nanobiocatalyst developed in this work consists of magnetic halloysite nanotubes (MHNTs), which acted as an immobilization matrix for α-amylase via biomimetic functionalization. The nanobiocatalyst exhibited good biocompatibility with abundant anchoring sites to govern a high loading of α-amylase and preserved its residual biocatalytic activity.
- The immobilization imparted greater stability to enzyme to sustain harsh process conditions, greater thermal stability, improved reaction kinetics, improved tolerance to contaminants e.g., cellulose/metal ions and insured excellent reusability over 10 cycles. The obtained results established the "conformational resistance" and "shielding" effect of the enzyme−halloysite nanotube system after immobilization.
- The immobilized α-amylase demonstrated an excellent catalytic efficiency for the continuous production of reducing sugars in 72 hours from the extracted starch.
- As a green and sustainable strategy, utilizing all soluble/ partially soluble components of potato peel waste in bioprocess applications was also attempted. The nanobiocatalyst-treated potato peel waste was used as a fermentation media for microbial growth of *E. coli*. The hydrolysate also enabled batch production of single-cell protein, *A. niger* as a dietary supplement.
- A blend formulation (50%:50% v/v) consisting of a hydrolysate and a commercial growth medium resulted in ~73% microbial-induced calcium carbonate precipitation, reducing the overall cost.
- The successful implantation of this strategy at a larger scale in future will open new dimensions in transforming other food waste materials into biochemical products of commercial relevance.

Overall, the low cost of backbone structure (halloysite nanotubes) and simple functionalization procedures reported here provide an opportunity for a viable translation of our technology to a commercial scale to valorize zero-value food waste. Indeed, the results reported herein deliver crucial expansions in means of greener pretreatment strategies, effective and efficient nanobiocatalysts development for continuous valorization of agri-food waste. Yet the unpredictable and unforeseen future urges even superior efforts and advanced strategies from us.

Future Scope of the Work

A few critical suggestions for future researchers working in the area are outlined below based on the knowledge gained during this research work:

- Beyond imposing stringent guidelines and policy frameworks on food business operators for reducing agri-food waste, nation seeks more scientific efforts to innovate as to how such a wonderful source of nutrients can be repurposed for human consumption or at least could be transformed into industrial products with higher economic value.
- An efficient categorization mechanism is required to sort agri-food waste either based on their inherently critical component (cellulose, starch, bioactive compounds etc.), facilitating their easy processing.
- The solid acid catalysts has proved to be efficient for removing hemicellulose form the lignocellulosic biomass. Yet, there is much scope to develop a reproducible approach to remove lignin as well and produce minimum inhibitory byproducts. The use of solid base catalysts instead of liquid alkaline catalyst could be a potent strategy for effective delignification of lignocellulosic biomass.
- The investigation of other naturally occurring nanoscale materials with high surface and mechanical properties could pave path for greener nanobiocatalysts.
- A strong recommendation is given to adopting surface-functionalization protocols employing more eco-friendly/natural crosslinkers than chemical compounds. This would certainly enhance biocompatibility and facilitate a more appropriate microenvironment for maximizing enzyme-substrate interaction.
- This work summarizes the pretreatment, hydrolysis, and fermentation steps for agri-food valorizations as three major processes done individually. Designing an integrated, continuous reactor would minimize the overall time/cost involved and greatly boost its acceptance in the industry.

Bibliography

1. Abraham RE, Verma ML, Barrow CJ, Puri M (2014): Suitability of magnetic nanoparticle immobilised cellulases in enhancing enzymatic saccharification of pretreated hemp biomass. Biotechnology for Biofuels. 7(1): 1-12.

2. Achal V, Mukherjee A, Sudhakara Reddy M (2011): Microbial Concrete way to enhance the durability of building structures. Cell. 2: 1-6.

3. Acheampong NA, Akanwariwiak WG, Mensah M, Fei-Baffoe B, Offei F, Bentil JA, Imoro AZ, Borquaye LS (2022): Conversion of cassava peels into bioethanol using the OSTEP approach. Biomass Conversion and Biorefinery. 1: 1-14.

4. Acres RG, Ellis AV, Alvino J, Lenahan CE, Khodakov DA, Metha GF, Andersson GG (2012): Molecular structure of 3-aminopropyltriethoxysilane layers formed on silanol-terminated silicon surfaces. The Journal of Physical Chemistry C. 116(10): 6289-6297.

5. Aditya A, Chattopadhyay S, Jha D, Gautam HK, Maiti S, Ganguli M (2018): Zinc oxide nanoparticles dispersed in ionic liquids show high antimicrobial efficacy to skin-specific bacteria. ACS Applied Materials & Interfaces. 10(18): 15401-15411.

6. Agarwal NK, Kumar M, Kumar SS, Singh L, Vijay VK, Kumar V (2022): Anaerobic digestion of sugarcane bagasse for biogas production and digestate valorization. Chemosphere. 295. doi:https://doi.org/10.1016/j.chemosphere.2022.133893

7. Agbor VB, Cicek N, Sparling R, Berlin A, Levin DB (2011): Biomass pretreatment: fundamentals toward application. Biotechnology Advances. 29(6): 675-685.

8. Aghaei H, Mohammadbagheri Z, Hemasi A, Taghizadeh A (2022): Efficient hydrolysis of starch by α-amylase immobilized on cloisite 30B and modified forms of cloisite 30B by adsorption and covalent methods. Food Chemistry. 373: 1-9.

9. Agnihotri S, Mukherji S, Mukherji S (2013): Immobilized silver nanoparticles enhance contact killing and show highest efficacy: elucidation of the mechanism of bactericidal action of silver. Nanoscale. 5(16): 7328-7340.

10. Ahamed MI, Prasad R (2021): Microbial biosurfactants: preparation, properties and applications. Springer Nature, Springer Nature

11. Ahmed IN, Chang R, Tsai W-B (2017): Poly (acrylic acid) nanogel as a substrate for cellulase immobilization for hydrolysis of cellulose. Colloids and Surfaces B: Biointerfaces. 152: 339-343.

12. Ahmed SA, Abdella MA, El-Sherbiny GM, Ibrahim AM, El-Shamy AR, Atalla SM, Hassan ME (2020): Catalytic, kinetic and thermal properties of free andimmobilized Bacillus subtilis-MK1 α-amylase on Chitosan-magnetic nanoparticles. Biotechnology Reports. 26: 1-12.

13. Almeida FL, Prata AS, Forte MB (2022): Enzyme immobilization: what have we learned in the past five years? Biofuels, Bioproducts and Biorefining. 16(2): 587-608.

14. Almulaiky YQ, Khalil N, El-Shishtawy RM, Altalhi T, Algamal Y, Aldhahri M, Al-Harbi SA, Allehyani ES, Bilal M, Mohammed MM (2021): Hydroxyapatite-decorated

ZrO2 for α-amylase immobilization: Toward the enhancement of enzyme stability and reusability. International Journal of Biological Macromolecules. 167: 299-308.

15. Ambatkar N, Jadhav DD, Deshmukh A, Sattikar P, Wakade G, Nandi S, Kumbhar P, Kommoju P-R (2021): Functional screening and adaptation of fungal cultures to industrial media for improved delignification of rice straw. Biomass and Bioenergy. 155: 1-10.

16. Amicarelli V, Bux C (2020): Food waste measurement toward a fair, healthy and environmental-friendly food system: A critical review. British Food Journal. 123(8): 2907-2935.

17. Amicarelli V, Lagioia G, Bux C (2021): Global warming potential of food waste through the life cycle assessment: An analytical review. Environmental Impact Assessment Review. 91: 1-11.

18. An J, Li G, Zhang Y, Zhang T, Liu X, Gao F, Peng M, He Y, Fan H (2020): Recent advances in enzyme-nanostructure biocatalysts with enhanced activity. Catalysts. 10(3): 1-15.

19. Antony N, Balachandran S, Mohanan P (2016): Immobilization of diastase α-amylase on nano zinc oxide. Food chemistry. 211: 624-630.

20. APHA (1989): American Public Health Association (APHA) Standard methods for the examination of water and wastewater (17th ed.) vol 6. American Public Health Association, Washington, DC,

21. Ariaeenejad S, Motamedi E, Salekdeh GH (2021): Immobilization of enzyme cocktails on dopamine functionalized magnetic cellulose nanocrystals to enhance sugar bioconversion: A biomass reusing loop. Carbohydrate Polymers. 256: 1-12.

22. Arshadi M, Attard TM, Lukasik RM, Brncic M, da Costa Lopes AM, Finell M, Geladi P, Gerschenson LN, Gogus F, Herrero M (2016): Pre-treatment and extraction techniques for recovery of added value compounds from wastes throughout the agri-food chain. Green Chemistry. 18(23): 6160-6204.

23. Arya PS, Yagnik SM, Rajput KN, Panchal RR, Raval VH (2022): Valorization of agro-food wastes: ease of concomitant-enzymes production with application in food and biofuel industries. Bioresource Technology. 361: 1-12.

24. Asar MF, Ahmad N, Husain Q (2020): Chitosan modified Fe3O4/graphene oxide nanocomposite as a support for high yield and stable immobilization of cellulase: its application in the saccharification of microcrystalline cellulose. Preparative Biochemistry & Biotechnology. 50(5): 460-467.

25. Ascencio JJ, Chandel AK, Philippini RR, da Silva SS (2020): Comparative study of cellulosic sugars production from sugarcane bagasse after dilute nitric acid, dilute sodium hydroxide and sequential nitric acid-sodium hydroxide pretreatment. Biomass Conversion and Biorefinery. 10(4): 813-822.

26. Ávila PF, Forte MB, Goldbeck R (2018): Evaluation of the chemical composition of a mixture of sugarcane bagasse and straw after different pretreatments and their effects on

commercial enzyme combinations for the production of fermentable sugars. Biomass and Bioenergy. 116: 180-188.

27. Ayodele BV, Alsaffar MA, Mustapa SI (2020): An overview of integration opportunities for sustainable bioethanol production from first-and second-generation sugar-based feedstocks. Journal of Cleaner Production. 245: 118857. doi:https://doi.org/10.1016/j.jclepro.2019.118857

28. Bahri S, Homaei A, Mosaddegh E (2022): Zinc sulfide-chitosan hybrid nanoparticles as a robust surface for immobilization of Sillago sihama α-amylase. Colloids and Surfaces B: Biointerfaces. 218: 1-10.

29. Bajić M, Plazl I, Stloukal R, Žnidaršič-Plazl P (2017): Development of a miniaturized packed bed reactor with ω-transaminase immobilized in LentiKats®. Process Biochemistry. 52: 63-72.

30. Barman M, Mahmood S, Augustine R, Hasan A, Thomas S, Ghosal K (2020): Natural halloysite nanotubes/chitosan based bio-nanocomposite for delivering norfloxacin, an anti-microbial agent in sustained release manner. International Journal of Biological Macromolecules. 162: 1849-1861.

31. Ben-Othman S, Jõudu I, Bhat R (2020): Bioactives from agri-food wastes: Present insights and future challenges. Molecules. 25(3): 1-34.

32. Berbel J, Posadillo A (2018): Review and analysis of alternatives for the valorisation of agro-industrial olive oil by-products. Sustainability. 10(1): 1-9.

33. Berlin A, Balakshin M, Gilkes N, Kadla J, Maximenko V, Kubo S, Saddler J (2006): Inhibition of cellulase, xylanase and β-glucosidase activities by softwood lignin preparations. Journal of Biotechnology. 125(2): 198-209.

34. Bhagwat S, Ratnaparkhe S, Kumar A (2015): Biomass pre-treatment methods and their economic viability for efficient production of biofuel. British Biotechnology Journal. 8(2): 1-17.

35. Bhat R (2017): Sustainability challenges in the agrofood sector. John Wiley & Sons,

36. Bhatia SK, Joo H-S, Yang Y-H (2018): Biowaste-to-bioenergy using biological methods–a mini-review. Energy Conversion and Management. 177: 640-660.

37. Bhavya M, Hebbar HU (2019): Sono-photodynamic inactivation of Escherichia coli and Staphylococcus aureus in orange juice. Ultrasonics Sonochemistry. 57: 108-115.

38. Bilal M, Asgher M, Cheng H, Yan Y, Iqbal HM (2019): Multi-point enzyme immobilization, surface chemistry, and novel platforms: a paradigm shift in biocatalyst design. Critical Reviews in Biotechnology. 39(2): 202-219.

39. Bilal M, Ashraf SS, Ferreira LFR, Cui J, Lou W-Y, Franco M, Iqbal HM (2020): Nanostructured materials as a host matrix to develop robust peroxidases-based nanobiocatalytic systems. International Journal of Biological Macromolecules. 162: 1906-1923.

40. Bilal M, Iqbal HM (2019): Naturally-derived biopolymers: Potential platforms for enzyme immobilization. International Journal of Biological Macromolecules. 130: 462-482.

41. Bindu V, Mohanan P (2020): Thermal deactivation of α-amylase immobilized magnetic chitosan and its modified forms: A kinetic and thermodynamic study. Carbohydrate Research. 498: 1-9.

42. Bittencourt GA, de Souza Vandenberghe LP, Valladares-Diestra K, Herrmann LW, de Mello AFM, Vásquez ZS, Karp SG, Soccol CR (2021): Soybean hulls as carbohydrate feedstock for medium to high-value biomolecule production in biorefineries: A review. Bioresource Technology. 339: 1-12.

43. Bolaji I, Nejad B, Billham M, Mehta N, Smyth B, Cunningham E (2021): Multi-criteria decision analysis of agri-food waste as a feedstock for biopolymer production. Resources, Conservation and Recycling. 172: 1-11.

44. Bradford MM (1976): A rapid and sensitive method for the quantitation of microgram quantities of protein utilizing the principle of protein-dye binding. Analytical Biochemistry. 72(1-2): 248-254.

45. Budhiraja M, Ali A, Tyagi V (2022): First biocatalytic synthesis of piperidine derivatives via an immobilized lipase-catalyzed multicomponent reaction. New Journal of Chemistry. 46(10): 4837-4849.

46. Califano V, Sannino F, Costantini A, Avossa J, Cimino S, Aronne A (2018): Wrinkled silica nanoparticles: Efficient matrix for β-glucosidase immobilization. The Journal of Physical Chemistry C. 122(15): 8373-8379.

47. Campo ID, Alegría I, Zazpe M, Echeverria M, Echeverría I (2006): Diluted acid hydrolysis pretreatment of agri-food wastes for bioethanol production. Industrial Crops and Products. 24(3): 214-221.

48. Cantone S, Ferrario V, Corici L, Ebert C, Fattor D, Spizzo P, Gardossi L (2013): Efficient immobilisation of industrial biocatalysts: criteria and constraints for the selection of organic polymeric carriers and immobilisation methods. Chemical Society Reviews. 42(15): 6262-6276.

49. Cao L (2006): Carrier-bound immobilized enzymes: principles, application and design. John Wiley & Sons,

50. Caputi A, Ueda M, Brown T (1968): Spectrophotometric determination of ethanol in wine. American Journal of Enology and Viticulture. 19(3): 160-165.

51. Carlier S, Hermans S (2020): Highly efficient and recyclable catalysts for cellobiose hydrolysis: Systematic comparison of carbon nanomaterials functionalized with benzyl sulfonic acids. Frontiers in Chemistry. 8: 1-9.

52. Carmona-Cabello M, Garcia IL, Leiva-Candia D, Dorado MP (2018): Valorization of food waste based on its composition through the concept of biorefinery. Current Opinion in Green and Sustainable Chemistry. 14: 67-79.

53. CASTAñO J, Rodríguez-Llamazares S, Contreras K, Carrasco C, Pozo C, Bouza R, Franco C, Giraldo D (2014): Horse chestnut (Aesculus hippocastanum L.) starch: basic physico-chemical characteristics and use as thermoplastic material. Carbohydrate Polymers. 112: 677-685.

54. Cavallaro G, Chiappisi L, Pasbakhsh P, Gradzielski M, Lazzara G (2018): A structural comparison of halloysite nanotubes of different origin by Small-Angle Neutron Scattering (SANS) and Electric Birefringence. Applied Clay Science. 160: 71-80.

55. Chakraborty N, Narayanan V, Gautam HK (2022): Nano-Therapeutics to Treat Acne Vulgaris. Indian Journal of Microbiology. 62: 1-8.

56. Chandel AK, Antunes FA, Anjos V, Bell MJ, Rodrigues LN, Polikarpov I, de Azevedo ER, Bernardinelli OD, Rosa CA, Pagnocca FC (2014): Multi-scale structural and chemical analysis of sugarcane bagasse in the process of sequential acid–base pretreatment and ethanol production by Scheffersomyces shehatae and Saccharomyces cerevisiae. Biotechnology for Biofuels. 7(1): 1-17.

57. Chandel AK, Garlapati VK, Singh AK, Antunes FAF, da Silva SS (2018): The path forward for lignocellulose biorefineries: bottlenecks, solutions, and perspective on commercialization. Bioresource Technology. 264: 370-381.

58. Chang PR, Xie Y, Wu D, Ma X (2011): Amylose wrapped halloysite nanotubes. Carbohydrate Polymers. 84(4): 1426-1429.

59. Chang VS, Holtzapple MT (2000): Fundamental factors affecting biomass enzymatic reactivity. In: Twenty-first symposium on biotechnology for fuels and chemicals. Springer, pp 5-37

60. Chao C, Liu J, Wang J, Zhang Y, Zhang B, Zhang Y, Xiang X, Chen R (2013): Surface modification of halloysite nanotubes with dopamine for enzyme immobilization. ACS Applied Materials & Interfaces. 5(21): 10559-10564.

61. Chao C, Zhang B, Zhai R, Xiang X, Liu J, Chen R (2014): Natural nanotube-based biomimetic porous microspheres for significantly enhanced biomolecule immobilization. ACS Sustainable Chemistry & Engineering. 2(3): 396-403.

62. Chen M-N, Mo L-P, Cui Z-S, Zhang Z-H (2019): Magnetic nanocatalysts: synthesis and application in multicomponent reactions. Current Opinion in Green and Sustainable Chemistry. 15: 27-37.

63. Chen W-H, Ye S-C, Sheen H-K (2012): Hydrolysis characteristics of sugarcane bagasse pretreated by dilute acid solution in a microwave irradiation environment. Applied Energy. 93: 237-244.

64. Chouhan AS, Sarma A (2011): Modern heterogeneous catalysts for biodiesel production: A comprehensive review. Renewable and Sustainable Energy Reviews. 15(9): 4378-4399.

65. Chourasia VR, Pandey A, Pant KK, Henry RJ (2021): Improving enzymatic digestibility of sugarcane bagasse from different varieties of sugarcane using deep eutectic solvent pretreatment. Bioresource Technology. 337: 1-8.

66. Cisek R, Tokarz D, Kontenis L, Barzda V, Steup M (2018): Polarimetric second harmonic generation microscopy: An analytical tool for starch bioengineering. Starch-Stärke. 70(1-2): 1-46.

67. Collazo-Bigliardi S, Ortega-Toro R, Boix AC (2018): Isolation and characterisation of microcrystalline cellulose and cellulose nanocrystals from coffee husk and comparative study with rice husk. Carbohydrate Polymers. 191: 205-215.

68. The Compulsory Food Waste Reduction Bill. (2018). http://164.100.47.4/billstexts/RSBillTexts/AsIntroduced/comlsry%20food-E-21619.pdf.

69. Costa S, Summa D, Semeraro B, Zappaterra F, Rugiero I, Tamburini E (2020): Fermentation as a strategy for bio-transforming waste into resources: lactic acid production from agri-food residues. Fermentation. 7(1): 1-12.

70. Costantini A, Venezia V, Pota G, Bifulco A, Califano V, Sannino F (2020): Adsorption of cellulase on wrinkled silica nanoparticles with enhanced inter-wrinkle distance. Nanomaterials. 10(9): 1-14.

71. Coutinho TC, Rojas MJ, Tardioli PW, Paris EC, Farinas CS (2018): Nanoimmobilization of β-glucosidase onto hydroxyapatite. International Journal of Biological Macromolecules. 119: 1042-1051.

72. Dahunsi SO, Ogunwole JO, Owoseni AA, Olutona GO, Nejo YT, Atobatele OE (2022): Valorization of pineapple peel and poultry manure for clean energy generation. Food and Energy Security. 11(1): 1-18.

73. Das R, Talat M, Srivastava O, Kayastha AM (2018): Covalent immobilization of peanut β-amylase for producing industrial nano-biocatalysts: a comparative study of kinetics, stability and reusability of the immobilized enzyme. Food Chemistry. 245: 488-499.

74. Datta S, Holmes B, Park JI, Chen Z, Dibble DC, Hadi M, Blanch HW, Simmons BA, Sapra R (2010): Ionic liquid tolerant hyperthermophilic cellulases for biomass pretreatment and hydrolysis. Green Chemistry. 12(2): 338-345.

75. de Oliveira Rodrigues P, da Silva Barreto E, Brandão RL, Gurgel LVA, Pasquini D, Baffi MA (2022): On-site produced enzyme cocktails for saccharification and ethanol production from sugarcane bagasse fractionated by hydrothermal and alkaline pretreatments. Waste and Biomass Valorization. 13(1): 95-106.

76. de Oliveira Santos VT, Siqueira G, Milagres AMF, Ferraz A (2018): Role of hemicellulose removal during dilute acid pretreatment on the cellulose accessibility and enzymatic hydrolysis of compositionally diverse sugarcane hybrids. Industrial Crops and Products. 111: 722-730.

77. de Souza JB, Michelin M, Amâncio FL, Brazil OAV, Maria de Lourdes T, Ruzene DS, Silva DP, Mendonça MdC, López JA (2020): Sunflower stalk as a carbon source inductive for fungal xylanase production. Industrial Crops and Products. 153: 1-7.

78. Dedenaro G, Costa S, Rugiero I, Pedrini P, Tamburini E (2016): Valorization of agri-food waste via fermentation: production of L-lactic acid as a building block for the synthesis of biopolymers. Applied Sciences. 6(12): 1-12.

79. Defaei M, Taheri-Kafrani A, Miroliaei M, Yaghmaei P (2018): Improvement of stability and reusability of α-amylase immobilized on naringin functionalized magnetic nanoparticles: A robust nanobiocatalyst. International Journal of Biological Macromolecules. 113: 354-360.

80. Defaei M, Taheri-Kafrani A, Miroliaei M, Yaghmaei P (2020): Alpha-amylase immobilized on polycaprolactone-grafted magnetic nanoparticles: improving stability and reusability. Journal of Chemical Technology & Biotechnology. 95(8): 2243-2250.

81. Desai RP, Dave D, Suthar SA, Shah S, Ruparelia N, Kikani BA (2021): Immobilization of α-amylase on GO-magnetite nanoparticles for the production of high maltose containing syrup. International Journal of Biological Macromolecules. 169: 228-238.

82. DeSantis G, Jones JB (1999): Chemical modification of enzymes for enhanced functionality. Current Opinion in Biotechnology. 10(4): 324-330.

83. Dey T, Bhattacharjee T, Nag P, Ghati A, Kuila A (2021): Valorization of agro-waste into value added products for sustainable development. Bioresource Technology Reports. 16: 1-15.

84. Dhavale R, Parit S, Sahoo SC, Kollu P, Patil P, Patil P, Chougale A (2018): α-amylase immobilized on magnetic nanoparticles: reusable robust nano-biocatalyst for starch hydrolysis. Materials Research Express. 5(7):

85. Dhepe PL, Sahu R (2010): A solid-acid-based process for the conversion of hemicellulose. Green Chemistry. 12(12): 2153-2156.

86. DiCosimo R, McAuliffe J, Poulose AJ, Bohlmann G (2013): Industrial use of immobilized enzymes. Chemical Society Reviews. 42(15): 6437-6474.

87. Dionísio S, Santoro D, Bonan C, Soares L, Biazi L, Rabelo S, Ienczak J (2021): Second-generation ethanol process for integral use of hemicellulosic and cellulosic hydrolysates from diluted sulfuric acid pretreatment of sugarcane bagasse. Fuel. 304: 1-9.

88. Długosz O, Matysik J, Matyjasik W, Banach M (2021): Catalytic and antimicrobial properties of α-amylase immobilised on the surface of metal oxide nanoparticles. Journal of Cluster Science. 32(6): 1609-1622.

89. Dos Santos AC, Ximenes E, Kim Y, Ladisch MR (2019): Lignin–enzyme interactions in the hydrolysis of lignocellulosic biomass. Trends in Biotechnology. 37(5): 518-531.

90. Dtie U (2009): Converting waste agricultural biomass into a resource. Compendium of technologies Osaka, United Nations Environment Programme:

91. Dubois M, Gilles KA, Hamilton JK, Rebers Pt, Smith F (1956): Colorimetric method for determination of sugars and related substances. Analytical Chemistry. 28(3): 350-356.

92. Dutta S, Iris K, Fan J, Clark JH, Tsang DC (2022): Critical factors for levulinic acid production from starch-rich food waste: solvent effects, reaction pressure, and phase separation. Green Chemistry. 24(1): 163-175.

93. El-Soad AA, Pestov A, Tambasova D, Osipova V, Martemyanov N, Cavallaro G, Kovaleva E, Lazzara G (2020): Insights into grafting of (3-Mercaptopropyl) trimethoxy silane on halloysite nanotubes surface. Journal of Organometallic Chemistry. 915: 1-6.

94. Elnashar M (2011): Biotechnology of biopolymers. BoD–Books on Demand,

95. Esteban J, Ladero M (2018): Food waste as a source of value-added chemicals and materials: a biorefinery perspective. International Journal of Food Science & Technology. 53(5): 1095-1108.

96. Fakhrullina Gl, Khakimova E, Akhatova F, Lazzara G, Parisi F, Fakhrullin R (2019): Selective antimicrobial effects of curcumin@ halloysite nanoformulation: a Caenorhabditis elegans study. ACS Applied Materials & Interfaces. 11(26): 23050-23064.

97. Fan M, Zhao C, Huang X, Zhang H, Xie J (2021): Enhanced digestibility and fermentability of sugarcane bagasse in biofuel production by surfactant-assisted dilute acid pretreatment. Industrial Crops and Products. 172: 1-9.

98. Fan X, Hu M, Li S, Zhai Q, Wang F, Jiang Y (2018): Charge controlled immobilization of chloroperoxidase on both inner/outer wall of NHT: improved stability and catalytic performance in the degradation of pesticide. Applied Clay Science. 163: 92-99.

99. Fang J, Fowler P, Tomkinson J, Hill C (2002): The preparation and characterisation of a series of chemically modified potato starches. Carbohydrate Polymers. 47(3): 245-252.

100. FAO (2009): How to Feed the World in 2050. Insights from an Expert Meet. FAO:

101. FAO (2011): Global food losses and food waste – Extent, causes and prevention. Rome:

102. Feng G, Fang Z (2013): Solid-and nano-catalysts pretreatment and hydrolysis techniques. In: Pretreatment Techniques for Biofuels and Biorefineries. Springer, pp 339-366

103. Feng L, Perschke YML, Fontaine D, Ward AJ, Eriksen J, Sørensen P, Møller HB (2019): Co-ensiling of cover crops and barley straw for biogas production. Renewable Energy. 142: 677-683.

104. Fitzgerald ND (2017): Chemistry challenges to enable a sustainable bioeconomy. Nature Reviews Chemistry. 1(10): 1-3.

105. Froese AG, Sparling R (2021): Cross-feeding and wheat straw extractives enhance growth of Clostridium thermocellum-containing co-cultures for consolidated bioprocessing. Bioprocess and Biosystems Engineering. 44(4): 819-830.

106. Gardy J, Osatiashtiani A, Céspedes O, Hassanpour A, Lai X, Lee AF, Wilson K, Rehan M (2018): A magnetically separable SO4/Fe-Al-TiO2 solid acid catalyst for biodiesel production from waste cooking oil. Applied Catalysis B: Environmental. 234: 268-278.

107. Gautam K, Vishvakarma R, Sharma P, Singh A, Gaur VK, Varjani S, Srivastava JK (2022): Production of biopolymers from food waste: constrains and perspectives. Bioresource Technology. 361: 1-12.

108. Gawande MB, Hosseinpour R, Luque R (2014): Silica sulfuric acid and related solid-supported catalysts as versatile materials for greener organic synthesis. Current Organic Synthesis. 11(4): 526-544.

109. Giese EC, Pierozzi M, Dussán KJ, Chandel AK, da Silva SS (2013): Enzymatic saccharification of acid–alkali pretreated sugarcane bagasse using commercial enzyme preparations. Journal of Chemical Technology & Biotechnology. 88(7): 1266-1272.

110. Giummarella N, Pu Y, Ragauskas AJ, Lawoko M (2019): A critical review on the analysis of lignin carbohydrate bonds. Green Chemistry. 21(7): 1573-1595.

111. Gkantzou E, Chatzikonstantinou AV, Fotiadou R, Giannakopoulou A, Patila M, Stamatis H (2021): Trends in the development of innovative nanobiocatalysts and their application in biocatalytic transformations. Biotechnology Advances. 51: 1-26.

112. Gonçalves MCP, Kieckbusch TG, Perna RF, Fujimoto JT, Morales SAV, Romanelli JP (2019): Trends on enzyme immobilization researches based on bibliometric analysis. Process Biochemistry. 76: 95-110.

113. Gong C, Singh A, Singh P, Singh A (2021): Anaerobic digestion of agri-food wastes for generating biofuels. Indian Journal of Microbiology. 61(4): 427-440.

114. González-García S, Gullón P, Gullón B (2019): Bio-compounds production from agri-food wastes under a biorefinery approach: exploring environmental and social sustainability. In: Quantification of Sustainability Indicators in the Food Sector. Springer, pp 25-53

115. Guisan JM, Gloria F-L, Javier R-M, Daniel M-G (2022): Enzyme Immobilization Strategies for the design of robust and efficient biocatalysts. Current Opinion in Green and Sustainable Chemistry. 35: 1-10.

116. Gunst RF (1996): Response surface methodology: process and product optimization using designed experiments. Technometrics. 38(3): 284-286

117. Guo F, Fang Z, Xu CC, Smith Jr RL (2012): Solid acid mediated hydrolysis of biomass for producing biofuels. Progress in Energy and Combustion Science. 38(5): 672-690.

118. Guo F, Shi W, Sun W, Li X, Wang F, Zhao J, Qu Y (2014): Differences in the adsorption of enzymes onto lignins from diverse types of lignocellulosic biomass and the underlying mechanism. Biotechnology for Biofuels. 7(1): 1-10.

119. Gupta A, Thengane SK, Mahajani S (2020): Kinetics of pyrolysis and gasification of cotton stalk in the central parts of India. Fuel. 263: 1-13.

120. Gupta N, Beliya E, Paul JS, Jadhav S (2022a): Nanoarmoured α-amylase: A route leading to exceptional stability, catalysis and reusability for industrial applications. Coordination Chemistry Reviews. 464: 1-20.

121. Gupta P, Paul S (2014): Solid acids: Green alternatives for acid catalysis. Catalysis Today. 236: 153-170.

122. Gupta P, Prakash N, Ramawat Y, Rajput P, Fayaz A, Roy TK (2022b): Halloysite Nanotubes Functionalized Sulfonic Acid: Synthesis, Spectroscopic Characterization,

Computational Studies and Application for the Synthesis of 1, 4-Dihydropyridines. Letters in Organic Chemistry. 19(1): 19-27.

123. Gutierrez-Macias P, Montanez-Barragan B, Barragan-Huerta BE (2015): A review of agro-food waste transformation into feedstock for use in fermentation. Fresenius Environmental Bulletin. 24(11): 3703-3717.

124. Habashy MM, Ong ES, Abdeldayem OM, Al-Sakkari EG, Rene ER (2021): Food waste: a promising source of sustainable biohydrogen fuel. Trends in Biotechnology. 39(12): 1274-1288.

125. Hall M, Bansal P, Lee JH, Realff MJ, Bommarius AS (2010): Cellulose crystallinity–a key predictor of the enzymatic hydrolysis rate. The FEBS journal. 277(6): 1571-1582.

126. Hammami A, Bayoudh A, Abdelhedi O, Nasri M (2018): Low-cost culture medium for the production of proteases by Bacillus mojavensis SA and their potential use for the preparation of antioxidant protein hydrolysate from meat sausage by-products. Annals of Microbiology. 68(8): 473-484.

127. Han J, Rong J, Wang Y, Liu Q, Tang X, Li C, Ni L (2018a): Immobilization of cellulase on thermo-sensitive magnetic microspheres: improved stability and reproducibility. Bioprocess and Biosystems Engineering. 41(7): 1051-1060.

128. Han J, Wang L, Wang Y, Dong J, Tang X, Ni L, Wang L (2018b): Preparation and characterization of Fe3O4-NH2@ 4-arm-PEG-NH2, a novel magnetic four-arm polymer-nanoparticle composite for cellulase immobilization. Biochemical Engineering Journal. 130: 90-98.

129. Han Y, Wu X, Zhang X, Zhou Z, Lu C (2016): Dual functional biocomposites based on polydopamine modified cellulose nanocrystal for Fe3+-pollutant detecting and autoblocking. ACS Sustainable Chemistry & Engineering. 4(10): 5667-5673.

130. Hartmann M, Kostrov X (2013): Immobilization of enzymes on porous silicas–benefits and challenges. Chemical Society Reviews. 42(15): 6277-6289.

131. Hasan A, Pandey LM (2021): Implications of the Nanoscopic Surface Modification on the Protein Adsorption and Cell Adhesion. In: Biobased Nanotechnology for Green Applications. Springer, pp 423-460

132. Herbaut M, Zoghlami A, Habrant A, Falourd X, Foucat L, Chabbert B, Paës G (2018): Multimodal analysis of pretreated biomass species highlights generic markers of lignocellulose recalcitrance. Biotechnology for Biofuels. 11(1): 1-17.

133. Horwitz W (2010): Official methods of analysis of AOAC International. Volume I, agricultural chemicals, contaminants, drugs/edited by William Horwitz. Gaithersburg (Maryland): AOAC International, 1997.,

134. Hosseini SH, Hosseini SA, Zohreh N, Yaghoubi M, Pourjavadi A (2018): Covalent immobilization of cellulase using magnetic poly (ionic liquid) support: improvement of the enzyme activity and stability. Journal of Agricultural and Food Chemistry. 66(4): 789-798.

135. Huang W, Pan S, Li Y, Yu L, Liu R (2020): Immobilization and characterization of cellulase on hydroxy and aldehyde functionalized magnetic Fe2O3/Fe3O4 nanocomposites prepared via a novel rapid combustion process. International Journal of Biological Macromolecules. 162: 845-852.

136. Huang Y-B, Fu Y (2013): Hydrolysis of cellulose to glucose by solid acid catalysts. Green Chemistry. 15(5): 1095-1111.

137. Hürmüzlü R, Okur M, Saraçoğlu N (2021): Immobilization of Trametes versicolor laccase on chitosan/halloysite as a biocatalyst in the Remazol Red RR dye. International Journal of Biological Macromolecules. 192: 331-341.

138. Hýsek Š, Podlena M, Bartsch H, Wenderdel C, Böhm M (2018): Effect of wheat husk surface pre-treatment on the properties of husk-based composite materials. Industrial Crops and Products. 125: 105-113.

139. Ilanidis D, Stagge S, Jönsson LJ, Martín C (2021a): Effects of operational conditions on auto-catalyzed and sulfuric-acid-catalyzed hydrothermal pretreatment of sugarcane bagasse at different severity factor. Industrial Crops and Products. 159: 1-14.

140. Ilanidis D, Wu G, Stagge S, Martín C, Jönsson LJ (2021b): Effects of redox environment on hydrothermal pretreatment of lignocellulosic biomass under acidic conditions. Bioresource Technology. 319: 1-11.

141. Ingle AP, Chandel AK, Antunes FA, Rai M, da Silva SS (2019): New trends in application of nanotechnology for the pretreatment of lignocellulosic biomass. Biofuels, Bioproducts and Biorefining. 13(3): 776-788.

142. Ingle AP, Philippini RR, da Silva SS (2020a): Pretreatment of sugarcane bagasse using two different acid-functionalized magnetic nanoparticles: a novel approach for high sugar recovery. Renewable Energy. 150: 957-964.

143. Ingle AP, Philippini RR, de Souza Melo YC, da Silva SS (2020b): Acid-functionalized magnetic nanocatalysts mediated pretreatment of sugarcane straw: an eco-friendly and cost-effective approach. Cellulose. 27(12): 7067-7078.

144. Ingle AP, Philippini RR, Rai M, da Silva SS (2020c): Catalytic hydrolysis of cellobiose using different acid-functionalised Fe3O4 magnetic nanoparticles. IET Nanobiotechnology. 14(1): 40-46.

145. Intasian P, Prakinee K, Phintha A, Trisrivirat D, Weeranoppanant N, Wongnate T, Chaiyen P (2021): Enzymes, in vivo biocatalysis, and metabolic engineering for enabling a circular economy and sustainability. Chemical Reviews. 121(17): 10367-10451.

146. Isikgor FH, Becer CR (2015): Lignocellulosic biomass: a sustainable platform for the production of bio-based chemicals and polymers. Polymer Chemistry. 6(25): 4497-4559.

147. Javid A, Amiri H, Kafrani AT, Rismani-Yazdi H (2022): Post-hydrolysis of cellulose oligomers by cellulase immobilized on chitosan-grafted magnetic nanoparticles: A key stage of butanol production from waste textile. International Journal of Biological Macromolecules. 207: 324-332.

148. Jeoh T, Ishizawa CI, Davis MF, Himmel ME, Adney WS, Johnson DK (2007): Cellulase digestibility of pretreated biomass is limited by cellulose accessibility. Biotechnology and Bioengineering. 98(1): 112-122.

149. Jesionowski T, Zdarta J, Krajewska B (2014): Enzyme immobilization by adsorption: A review. Adsorption. 20(5): 801-821.

150. Jethani H, Hebbar UH (2021): Plant-based biopolymers: emerging bio-flocculants for microalgal biomass recovery. Reviews in Environmental Science and Bio/Technology. 20(1): 143-165.

151. Jönsson LJ, Alriksson B, Nilvebrant N-O (2013): Bioconversion of lignocellulose: inhibitors and detoxification. Biotechnology for Biofuels. 6(1): 1-10.

152. Jordan J, Kumar CS, Theegala C (2011): Preparation and characterization of cellulase-bound magnetite nanoparticles. Journal of Molecular Catalysis B: Enzymatic. 68(2): 139-146.

153. Joussein E, Petit S, Churchman J, Theng B, Righi D, Delvaux B (2005): Halloysite clay minerals—a review. Clay Minerals. 40(4): 383-426.

154. Ju X, Engelhard M, Zhang X (2013): An advanced understanding of the specific effects of xylan and surface lignin contents on enzymatic hydrolysis of lignocellulosic biomass. Bioresource Technology. 132: 137-145.

155. Kadam AA, Jang J, Jee SC, Sung J-S, Lee DS (2018): Chitosan-functionalized supermagnetic halloysite nanotubes for covalent laccase immobilization. Carbohydrate Polymers. 194: 208-216.

156. Kadam AA, Jang J, Lee DS (2017): Supermagnetically tuned halloysite nanotubes functionalized with aminosilane for covalent laccase immobilization. ACS Applied Materials & Interfaces. 9(18): 15492-15501.

157. Kadam AA, Sharma B, Shinde SK, Ghodake GS, Saratale GD, Saratale RG, Kim D-Y, Sung J-S (2020a): Thiolation of chitosan loaded over super-magnetic halloysite nanotubes for enhanced laccase immobilization. Nanomaterials. 10(12): 1-20.

158. Kadam AA, Shinde SK, Ghodake GS, Saratale GD, Saratale RG, Sharma B, Hyun S, Sung J-S (2020b): Chitosan-grafted halloysite nanotubes-Fe3O4 composite for laccase-immobilization and sulfamethoxazole-degradation. Polymers. 12(10): 1-17.

159. Kang H, Liu X, Zhang S, Li J (2017): Functionalization of halloysite nanotubes (HNTs) via mussel-inspired surface modification and silane grafting for HNTs/soy protein isolate nanocomposite film preparation. RSC Advances. 7(39): 24140-24148.

160. Karthikeyan A, Sivakumar N (2010): Citric acid production by Koji fermentation using banana peel as a novel substrate. Bioresource Technology. 101(14): 5552-5556.

161. Kassim FO, Thomas CP, Afolabi OO (2022): Integrated conversion technologies for sustainable agri-food waste valorization: A critical review. Biomass and Bioenergy. 156: 1-14.

162. Katana B, Rouster P, Varga Gb, Muráth S, Glinel K, Jonas AM, Szilagyi I (2019): Self-assembly of protamine biomacromolecule on halloysite nanotubes for immobilization of superoxide dismutase enzyme. ACS Applied Bio Materials. 3(1): 522-530.

163. Kaur M, Verma YP, Chauhan S (2020): Effect of chemical pretreatment of sugarcane bagasse on biogas production. Materials Today: Proceedings. 21: 1937-1942.

164. Kaur P, Taggar MS, Kalia A (2021): Characterization of magnetic nanoparticle–immobilized cellulases for enzymatic saccharification of rice straw. Biomass Conversion and Biorefinery. 11(3): 955-969.

165. Kawaguchi H, Hasunuma T, Ogino C, Kondo A (2016): Bioprocessing of bio-based chemicals produced from lignocellulosic feedstocks. Current Opinion in Biotechnology. 42: 30-39.

166. Khoshnevisan K, Bordbar A-K, Zare D, Davoodi D, Noruzi M, Barkhi M, Tabatabaei M (2011): Immobilization of cellulase enzyme on superparamagnetic nanoparticles and determination of its activity and stability. Chemical Engineering Journal. 171(2): 669-673.

167. Kim M, Jee SC, Sung J-S, Kadam AA (2018): Anti-proliferative applications of laccase immobilized on super-magnetic chitosan-functionalized halloysite nanotubes. International Journal of Biological Macromolecules. 118: 228-237.

168. Kim M, Shin MK, Sung J-S, Kadam AA (2022): Supermagnetic halloysite nanotubes surface-tuned with aminosilane for protease immobilization and applied for eradication of bacterial biofilm. Applied Surface Science. 593: 1-14.

169. Kizil R, Irudayaraj J, Seetharaman K (2002): Characterization of irradiated starches by using FT-Raman and FTIR spectroscopy. Journal of Agricultural and Food Chemistry. 50(14): 3912-3918.

170. Klapiszewski Ł, Zdarta J, Jesionowski T (2018): Titania/lignin hybrid materials as a novel support for α-amylase immobilization: A comprehensive study. Colloids and Surfaces B: Biointerfaces. 162: 90-97.

171. Klein O, Nier S, Tamásy C (2022): Towards a Circular Bioeconomy? Pathways and Spatialities of Agri-Food Waste Valorisation. Journal of Economic and Human Geography. 113(2): 194-210.

172. Ko JK, Ximenes E, Kim Y, Ladisch MR (2015): Adsorption of enzyme onto lignins of liquid hot water pretreated hardwoods. Biotechnology and Bioengineering. 112(3): 447-456.

173. Kolesnyk I, Konovalova V, Kharchenko K, Burban A, Kujawa J, Kujawski W (2020): Enhanced transport and antifouling properties of polyethersulfone membranes modified with α-amylase incorporated in chitosan-based polymeric micelles. Journal of Membrane Science. 595: 1-11.

174. Kołodziejczak-Radzimska A, Jesionowski T (2019): Characterization of amino-, epoxy- and carbonyl-functionalized halloysite and its application in the immobilization of

aminoacylase from Aspergillus melleus. Physicochemical Problems of Mineral Processing. 55: 128-139.

175. Konde KS, Nagarajan S, Kumar V, Patil SV, Ranade VV (2021): Sugarcane bagasse based biorefineries in India: potential and challenges. Sustainable Energy & Fuels. 5(1): 52-78.

176. Konwar LJ, Mäki-Arvela Pi, Mikkola J-P (2019): SO3H-containing functional carbon materials: synthesis, structure, and acid catalysis. Chemical Reviews. 119(22): 11576-11630.

177. Körner P, Jung D, Kruse A (2018): The effect of different Brønsted acids on the hydrothermal conversion of fructose to HMF. Green Chemistry. 20(10): 2231-2241.

178. Kover A, Kraljić D, Marinaro R, Rene ER (2021): Processes for the valorization of food and agricultural wastes to value-added products: recent practices and perspectives. Systems Microbiology and Biomanufacturing. 2: 1-17.

179. Krajewska B (2004): Application of chitin-and chitosan-based materials for enzyme immobilizations: a review. Enzyme and Microbial Technology. 35(2-3): 126-139.

180. Kruyeniski J, Ferreira PJ, Carvalho MdGVS, Vallejos ME, Felissia FE, Area MC (2019): Physical and chemical characteristics of pretreated slash pine sawdust influence its enzymatic hydrolysis. Industrial Crops and Products. 130: 528-536.

181. Kujawa J, Głodek M, Li G, Al-Gharabli S, Knozowska K, Kujawski W (2021): Highly effective enzymes immobilization on ceramics: Requirements for supports and enzymes. Science of The Total Environment. 801: 1-24.

182. Kumar-Krishnan S, Hernandez-Rangel A, Pal U, Ceballos-Sanchez O, Flores-Ruiz F, Prokhorov E, De Fuentes OA, Esparza R, Meyyappan M (2016): Surface functionalized halloysite nanotubes decorated with silver nanoparticles for enzyme immobilization and biosensing. Journal of Materials Chemistry B. 4(15): 2553-2560.

183. Kumar A, Kumar V, Singh B (2021a): Cellulosic and hemicellulosic fractions of sugarcane bagasse: Potential, challenges and future perspective. International Journal of Biological Macromolecules. 169: 564-582.

184. Kumar A, Vishwakarma HS, Singh J, Dwivedi S, Kumar M (2015): Microbial pigments: Production and their applications in various industries. International Journal of Pharmaceutical, Chemical & Biological Sciences. 5(1): 203-212.

185. Kumar P, Gupta P, Sharma C (2021b): Surface modified novel magnetically tuned halloysite functionalized sulfonic acid: synthesis, characterization and catalytic activity. Catalysis Science & Technology. 11(11): 3775-3786.

186. Kumar PS, Ramakrishnan K, Kirupha SD, Sivanesan S (2010): Thermodynamic and kinetic studies of cadmium adsorption from aqueous solution onto rice husk. Brazilian Journal of Chemical Engineering. 27: 347-355.

187. Kumar V, Yadav SK, Patel AK, Mishra BB, Ahluwalia V, Thakur LK, Kumar J (2022): Bioprocessing of agri-food processing residues into nutraceuticals and bioproducts. In: Current Developments in Biotechnology and Bioengineering. Elsevier, pp 301-322

188. Kupina S, Fields C, Roman MC, Brunelle SL (2018): Determination of total phenolic content using the Folin-C assay: single-laboratory validation, first action 2017.13. Journal of AOAC International. 101(5): 1466-1472.

189. Kute AB, Mohapatra D, Kotwaliwale N, Giri SK, Sawant B (2020): Characterization of pectin extracted from orange peel powder using microwave-assisted and acid extraction methods. Agricultural Research. 9(2): 241-248.

190. Ladeira-Ázar RI, Morgan T, Maitan-Alfenas GP, Guimarães VM (2019): Inhibitors compounds on sugarcane bagasse saccharification: effects of pretreatment methods and alternatives to decrease inhibition. Applied Biochemistry and Biotechnology. 188(1): 29-42.

191. Laluce C, Roldan IU, Pecoraro E, Igbojionu LI, Ribeiro CA (2019): Effects of pretreatment applied to sugarcane bagasse on composition and morphology of cellulosic fractions. Biomass and Bioenergy. 126: 231-238.

192. Larsson S, Palmqvist E, Hahn-Hägerdal B, Tengborg C, Stenberg K, Zacchi G, Nilvebrant N-O (1999): The generation of fermentation inhibitors during dilute acid hydrolysis of softwood. Enzyme and Microbial Technology. 24(3-4): 151-159.

193. Lecouvet B, Horion J, D'Haese C, Bailly C, Nysten B (2013): Elastic modulus of halloysite nanotubes. Nanotechnology. 24(10): 1-9.

194. Lee K, Jing Y, Wang Y, Yan N (2022): A unified view on catalytic conversion of biomass and waste plastics. Nature Reviews Chemistry. 6: 635-652.

195. Levis S, Deasy P (2002): Characterisation of halloysite for use as a microtubular drug delivery system. International Journal of Pharmaceutics. 243(1-2): 125-134.

196. Li X, Shu F, He C, Liu S, Leksawasdi N, Wang Q, Qi W, Alam MA, Yuan Z, Gao Y (2018): Preparation and investigation of highly selective solid acid catalysts with sodium lignosulfonate for hydrolysis of hemicellulose in corncob. RSC Advances. 8(20): 10922-10929.

197. Liang YR, Wu Q, Lin XF (2017): Effect of additives on the selectivity and reactivity of enzymes. The Chemical Record. 17(1): 90-121.

198. Libertino S, Aiello V, Scandurra A, Renis M, Sinatra F (2008): Immobilization of the enzyme glucose oxidase on both bulk and porous SiO2 surfaces. Sensors. 8(9): 5637-5648.

199. Liu D-M, Chen J, Shi Y-P (2018a): Advances on methods and easy separated support materials for enzymes immobilization. TrAC Trends in Analytical Chemistry. 102: 332-342.

200. Liu D-M, Dong C (2020): Recent advances in nano-carrier immobilized enzymes and their applications. Process Biochemistry. 92: 464-475.

201. Liu F, Huang K, Zheng A, Xiao F-S, Dai S (2018b): Hydrophobic solid acids and their catalytic applications in green and sustainable chemistry. ACS Catalysis. 8(1): 372-391.

202. Liu R, Sarker M, Rahman MM, Li C, Chai M, Cotillon R, Scott NR (2020): Multi-scale complexities of solid acid catalysts in the catalytic fast pyrolysis of biomass for bio-oil production–A review. Progress in Energy and Combustion Science. 80: 1-34.

203. Liu Z-H, Qin L, Li B-Z, Yuan Y-J (2015): Physical and chemical characterizations of corn stover from leading pretreatment methods and effects on enzymatic hydrolysis. ACS Sustainable Chemistry & Engineering. 3(1): 140-146.

204. Lowry OH (1951): Protein measurement with the Folin phenol reagent. Journal of Biological Chemistry. 193: 265-275.

205. Lu F, Rodriguez-Garcia J, Van Damme I, Westwood NJ, Shaw L, Robinson JS, Warren G, Chatzifragkou A, Mason SM, Gomez L (2018): Valorisation strategies for cocoa pod husk and its fractions. Current Opinion in Green and Sustainable Chemistry. 14: 80-88.

206. Lu M, Li J, Han L, Xiao W (2019): An aggregated understanding of cellulase adsorption and hydrolysis for ball-milled cellulose. Bioresource Technology. 273: 1-7.

207. Lu S, Wang Q, Liang Z, Wang W, Liang C, Wang Z, Yuan Z, Lan P, Qi W (2021): Saccharification of sugarcane bagasse by magnetic carbon-based solid acid pretreatment and enzymatic hydrolysis. Industrial Crops and Products. 160: 1-7.

208. Lun H, Ouyang J, Yang H (2014): Natural halloysite nanotubes modified as an aspirin carrier. RSC Advances. 4(83): 44197-44202.

209. Luo P, Zhao Y, Zhang B, Liu J, Yang Y, Liu J (2010): Study on the adsorption of Neutral Red from aqueous solution onto halloysite nanotubes. Water Research. 44(5): 1489-1497.

210. Lupoi JS, Smith EA (2011): Evaluation of nanoparticle-immobilized cellulase for improved ethanol yield in simultaneous saccharification and fermentation reactions. Biotechnology and Bioengineering. 108(12): 2835-2843.

211. Lvov YM, Shchukin DG, Mohwald H, Price RR (2008): Halloysite clay nanotubes for controlled release of protective agents. ACS Nano. 2(5): 814-820.

212. Mahajan A, Gupta P (2020): Halloysite nanotubes based heterogeneous solid acid catalysts. New Journal of Chemistry. 44(30): 12897-12908.

213. Makanjuola O, Arowosola T, Chenyu D (2020a): The utilization of food waste: Challenges and opportunities. Journal of Food Chemistry and Nanotechnology. 6: 182-188.

214. Makov T, Shepon A, Krones J, Gupta C, Chertow M (2020): Social and environmental analysis of food waste abatement via the peer-to-peer sharing economy. Nature Communications. 11(1): 1-8.

215. Maksym P, Tarnacka M, Dzienia A, Matuszek K, Chrobok A, Kaminski K, Paluch M (2017): Enhanced polymerization rate and conductivity of ionic liquid-based epoxy resin. Macromolecules. 50(8): 3262-3272.

216. Mankar AR, Pandey A, Modak A, Pant K (2021): Pretreatment of lignocellulosic biomass: A review on recent advances. Bioresource Technology. 334: 1-12.

217. Mardani T, Khiabani MS, Mokarram RR, Hamishehkar H (2018): Immobilization of α-amylase on chitosan-montmorillonite nanocomposite beads. International Journal of Biological Macromolecules. 120: 354-360.

218. Mariño MA, Moretti P, Tasic L (2021): Immobilized commercial cellulases onto amino-functionalized magnetic beads for biomass hydrolysis: enhanced stability by non-polar silanization. Biomass Conversion and Biorefinery: 1-11.

219. Markande AR, Patel D, Varjani S (2021): A review on biosurfactants: properties, applications and current developments. Bioresource Technology. 330: 1-11.

220. Marques S, Moreno AD, Ballesteros M, Gírio F (2018): Starch biomass for biofuels, biomaterials, and chemicals. In: Biomass and Green Chemistry. Springer, pp 69-94

221. Massaro M, Lazzara G, Milioto S, Noto R, Riela S (2017): Covalently modified halloysite clay nanotubes: synthesis, properties, biological and medical applications. Journal of Materials Chemistry B. 5(16): 2867-2882.

222. Massaro M, Noto R, Riela S (2020): Past, present and future perspectives on halloysite clay minerals. Molecules. 25(20): 1-44.

223. Mata R, Rivero-Cruz JF, Rojas A (2018): Bioactive natural products of medicinal and agrochemical interest from selected Mexican medicinal plants. In: Chemistry, Biological and Pharmacological Properties of Medicinal Plants from the Americas. Routledge, pp 161-183

224. Matassa S, Boon N, Pikaar I, Verstraete W (2016): Microbial protein: future sustainable food supply route with low environmental footprint. Microbial Biotechnology. 9(5): 568-575.

225. Matei E, Râpă M, Predescu AM, Țurcanu AA, Vidu R, Predescu C, Bobirica C, Bobirica L, Orbeci C (2021): Valorization of Agri-Food Wastes as Sustainable Eco-Materials for Wastewater Treatment: Current State and New Perspectives. Materials. 14(16): 1-27.

226. Mazzotta E, Rella S, Turco A, Malitesta C (2015): XPS in development of chemical sensors. RSC Advances. 5(101): 83164-83186.

227. McNutt J, He QS (2019): Spent coffee grounds: A review on current utilization. Journal of Industrial and Engineering Chemistry. 71: 78-88.

228. Medina-Morales MA, Gómez-García R, Cruz-Requena M, Aguilar CN (2021): Dual-Purpose Bioprocesses: Biotransformation of Agri-Food Residues and High Added-Value Bioproducts Recovery. In: Bioprocessing of Agri-Food Residues for Production of Bioproducts. Apple Academic Press, pp 1-31

229. Meng X, Foston M, Leisen J, DeMartini J, Wyman CE, Ragauskas AJ (2013): Determination of porosity of lignocellulosic biomass before and after pretreatment by using Simons' stain and NMR techniques. Bioresource Technology. 144: 467-476.

230. Meng X, Pu Y, Yoo CG, Li M, Bali G, Park DY, Gjersing E, Davis MF, Muchero W, Tuskan GA (2017): An in-depth understanding of biomass recalcitrance using natural poplar variants as the feedstock. ChemSusChem. 10(1): 139-150.

231. Mhlongo SI, den Haan R, Viljoen-Bloom M, van Zyl WH (2015): Lignocellulosic hydrolysate inhibitors selectively inhibit/deactivate cellulase performance. Enzyme and Microbial Technology. 81: 16-22.

232. Miller GL (1959): Use of dinitrosalicylic acid reagent for determination of reducing sugar. Analytical Chemistry. 31(3): 426-428.

233. Mohamed SA, Al-Harbi MH, Almulaiky YQ, Ibrahim IH, Salah HA, El-Badry MO, Abdel-Aty AM, Fahmy AS, El-Shishtawy RM (2018): Immobilization of Trichoderma harzianum α-amylase on PPyAgNp/Fe3O4-nanocomposite: chemical and physical properties. Artificial Cells, Nanomedicine, and Biotechnology. 46(sup2): 201-206.

234. Mohammadi NS, Khiabani MS, Ghanbarzadeh B, Mokarram RR (2020): Enhancement of biochemical aspects of lipase adsorbed on halloysite nanotubes and entrapped in a polyvinyl alcohol/alginate hydrogel: strategies to reuse the most stable lipase. World Journal of Microbiology and Biotechnology. 36(3): 1-15.

235. Mohammadi ZB, Zhang F, Kharazmi MS, Jafari SM (2022): Nano-biocatalysts for food applications; immobilized enzymes within different nanostructures. Critical Reviews in Food Science and Nutrition. 1: 1-19.

236. Molaverdi M, Karimi K, Mirmohamadsadeghi S, Galbe M (2019): High titer ethanol production from rice straw via solid-state simultaneous saccharification and fermentation by Mucor indicus at low enzyme loading. Energy Conversion and Management. 182: 520-529.

237. Monteiro RR, de Oliveira ALB, de Menezes FL, de Souza MCM, Fechine PB, dos Santos JC (2022): Improvement of enzymatic activity and stability of lipase A from Candida antartica onto halloysite nanotubes with Taguchi method for optimized immobilization. Applied Clay Science. 228: 1-12.

238. Mood SH, Golfeshan AH, Tabatabaei M, Jouzani GS, Najafi GH, Gholami M, Ardjmand M (2013): Lignocellulosic biomass to bioethanol, a comprehensive review with a focus on pretreatment. Renewable and Sustainable Energy Reviews. 27: 77-93.

239. Moradali MF, Rehm BH (2020): Bacterial biopolymers: from pathogenesis to advanced materials. Nature Reviews Microbiology. 18(4): 195-210.

240. Morellon-Sterling R, Carballares D, Arana-Peña S, Siar E-H, Braham SA, Fernandez-Lafuente R (2021): Advantages of supports activated with divinyl sulfone in enzyme coimmobilization: Possibility of multipoint covalent immobilization of the most stable enzyme and immobilization via ion exchange of the least stable enzyme. ACS Sustainable Chemistry & Engineering. 9(22): 7508-7518.

241. Morone P, Koutinas A, Gathergood N, Arshadi M, Matharu A (2019): Food waste: Challenges and opportunities for enhancing the emerging bio-economy. Journal of Cleaner Production. 221: 10-16.

242. Mortazavi S, Aghaei H (2020): Make proper surfaces for immobilization of enzymes: immobilization of lipase and α-amylase on modified Na-sepiolite. International Journal of Biological Macromolecules. 164: 1-12.

243. Mulko L, Pereyra JY, Rivarola CR, Barbero CA, Acevedo DF (2019): Improving the retention and reusability of Alpha-amylase by immobilization in nanoporous polyacrylamide-graphene oxide nanocomposites. International Journal of Biological Macromolecules. 122: 1253-1261.

244. Munyentwali A, Li H, Yang Q (2022): Review of advances in bifunctional solid acid/base catalysts for sustainable biodiesel production. Applied Catalysis A: General. 633. doi:https://doi.org/10.1016/j.apcata.2022.118525

245. Najeeb J, Akram S, Mumtaz MW, Danish M, Irfan A, Touqeer T, Rashid U, Ghani WAWAK, Choong TSY (2021): Nanobiocatalysts for biodiesel synthesis through transesterification—a review. Catalysts. 11(2): 1-40.

246. Ng HS, Kee PE, Yim HS, Chen P-T, Wei Y-H, Lan JC-W (2020): Recent advances on the sustainable approaches for conversion and reutilization of food wastes to valuable bioproducts. Bioresource Technology. 302: 1-8.

247. Niju S, Swathika M (2019): Delignification of sugarcane bagasse using pretreatment strategies for bioethanol production. Biocatalysis and Agricultural Biotechnology. 20: 1-9.

248. Okwuenu P, Agbo K, Ezugwu A, Eze S, Chilaka F (2017): Effect of divalent metal ions on glucoamylase activity of glucoamylase isolated from Aspergillus niger. Fermentation Technology. 6(141): 1-6.

249. Osbon Y, Kumar M (2019): Biocatalysis and strategies for enzyme improvement. In: Biophysical chemistry-advance applications. IntechOpen, pp 27-40

250. Osorio LLDR, Flórez-López E, Grande-Tovar CD (2021): The potential of selected agri-food loss and waste to contribute to a circular economy: Applications in the food, cosmetic and pharmaceutical industries. Molecules. 26(2): 1-42.

251. Ozyilmaz E, Alhiali A, Caglar O, Yilmaz M (2021): Preparation of regenerable magnetic nanoparticles for cellulase immobilization: Improvement of enzymatic activity and stability. Biotechnology Progress. 37(4): 1-12.

252. Pan X, Gilkes N, Saddler JN (2006): Effect of acetyl groups on enzymatic hydrolysis of cellulosic substrates. Holzforschung. 60: 398-401.

253. Panakkal EJ, Sriariyanun M, Ratanapoompinyo J, Yasurin P, Cheenkachorn K, Rodiahwati W, Tantayotai P (2022): Influence of sulfuric acid pretreatment and inhibitor of sugarcane bagasse on the production of fermentable sugar and ethanol. Applied Science and Engineering Progress. 15(1): 1-13.

254. Panda SK, Sahu L, Behera SK, Ray RC (2019): Research and production of organic acids and industrial potential. Bioprocessing for Biomolecules Production: 195-209.

255. Pandey G, Munguambe DM, Tharmavaram M, Rawtani D, Agrawal Y (2017): Halloysite nanotubes-An efficient 'nano-support'for the immobilization of α-amylase. Applied Clay Science. 136: 184-191.

256. Panesar R, Kaur S, Panesar PS (2015): Production of microbial pigments utilizing agro-industrial waste: a review. Current Opinion in Food Science. 1: 70-76.

257. Panzella L, Moccia F, Nasti R, Marzorati S, Verotta L, Napolitano A (2020): Bioactive phenolic compounds from agri-food wastes: An update on green and sustainable extraction methodologies. Frontiers in Nutrition. 7: 1-27.

258. Papaioannou EH, Mazzei R, Bazzarelli F, Piacentini E, Giannakopoulos V, Roberts MR, Giorno L (2022): Agri-Food Industry Waste as Resource of Chemicals: The Role of Membrane Technology in Their Sustainable Recycling. Sustainability. 14(3): 1-21.

259. Papathoti NK, Laemchiab K, Megavath VS, Keshav PK, Numparditsub P, Le Thanh T, Buensanteai N (2021): Augmented ethanol production from alkali-assisted hydrothermal pretreated cassava peel waste. Energy Sources, Part A: Recovery, Utilization, and Environmental Effects: 1-11.

260. Park EJ, Jin J-H, Kim JH, Min NK (2011): Surface activation of plasma-patterned carbon nanotube based DNA sensing electrodes. Microchimica Acta. 174(3): 231-238.

261. Pascoal AM, Mitidieri S, Fernandes KF (2011): Immobilisation of α-amylase from Aspergillus niger onto polyaniline. Food and Bioproducts Processing. 89(4): 300-306.

262. Patel A, Arora N, Sartaj K, Pruthi V, Pruthi PA (2016): Sustainable biodiesel production from oleaginous yeasts utilizing hydrolysates of various non-edible lignocellulosic biomasses. Renewable and Sustainable Energy Reviews. 62: 836-855.

263. Patel H, Royall PG, Gaisford S, Williams GR, Edwards CH, Warren FJ, Flanagan BM, Ellis PR, Butterworth PJ (2017): Structural and enzyme kinetic studies of retrograded starch: Inhibition of α-amylase and consequences for intestinal digestion of starch. Carbohydrate Polymers. 164: 154-161.

264. Paul V, Rai S, Tripathi AD, Rai DC, Agarwal A (2021): Impact of fermentation types on enzymes used for biofuels production. In: Bioprocessing for Biofuel Production. Springer, pp 1-27

265. Payan F, Haser R, Pierrot M, Frey M, Astier J, Abadie B, Duée B, Buisson G (1980): The three-dimensional structure of α-amylase from porcine pancreas at 5 Å resolution–the active-site location. Acta Crystallographica Section B: Structural Crystallography and Crystal Chemistry. 36(2): 416-421.

266. Payne CM, Knott BC, Mayes HB, Hansson H, Himmel ME, Sandgren M, Stahlberg J, Beckham GT (2015): Fungal cellulases. Chemical Reviews. 115(3): 1308-1448.

267. Paz-Cedeno FR, Carceller JM, Iborra S, Donato RK, Godoy AP, de Paula AV, Monti R, Corma A, Masarin F (2021): Magnetic graphene oxide as a platform for the

immobilization of cellulases and xylanases: Ultrastructural characterization and assessment of lignocellulosic biomass hydrolysis. Renewable Energy. 164: 491-501.

268. Peciulyte A, Karlström K, Larsson PT, Olsson L (2015): Impact of the supramolecular structure of cellulose on the efficiency of enzymatic hydrolysis. Biotechnology for Biofuels. 8(1): 1-13.

269. Peguero DA, Gold M, Vandeweyer D, Zurbrügg C, Mathys A (2021): A review of pretreatment methods to improve agri-food waste bioconversion by black soldier fly larvae. Frontiers in Sustainable Food Systems. 5: 1-9.

270. Peña Duque LE (2009) Acid-functionalized nanoparticles for hydrolysis of lignocellulosic feedstocks. Master of Science, Kansas State University, Kansas, USA

271. Peña L, Ikenberry M, Hohn K, Wang D (2012): Acid-functionalized nanoparticles for pretreatment of wheat straw. Journal of Biomaterials and Nanobiotechnology. 3(3): 1-11.

272. Peña L, Xu F, Hohn KL, Li J, Wang D (2014): Propyl-sulfonic acid functionalized nanoparticles as catalyst for pretreatment of corn stover. Journal of Biomaterials and Nanobiotechnology. 2014: 1-9.

273. Pereira PHF, Voorwald HCJ, Cioffi MOH, Mullinari DR, Da Luz SM, Da Silva MLCP (2011): Sugarcane bagasse pulping and bleaching: Thermal and chemical characterization. BioResources. 6(3): 2471-2482.

274. Philippini RR, Martiniano SE, Chandel AK, de Carvalho W, da Silva SS (2019): Pretreatment of sugarcane bagasse from cane hybrids: effects on chemical composition and 2G sugars recovery. Waste and Biomass Valorization. 10(6): 1561-1570.

275. Piechowiak T, Grzelak-Błaszczyk K, Bonikowski R, Balawejder M (2020): Optimization of extraction process of antioxidant compounds from yellow onion skin and their use in functional bread production. LWT-Food Sciences and Technology. 117: 1-7.

276. Pietraszek A, Karewicz A, Widnic M, Lachowicz D, Gajewska M, Bernasik A, Nowakowska M (2019): Halloysite-alkaline phosphatase system—A potential bioactive component of scaffold for bone tissue engineering. Colloids and Surfaces B: Biointerfaces. 173: 1-8.

277. Pinto ÉSM, Dorn M, Feltes BC (2020): The tale of a versatile enzyme: Alpha-amylase evolution, structure, and potential biotechnological applications for the bioremediation of n-alkanes. Chemosphere. 250: 1-18.

278. Poorakbar E, Saboury AA, Laame Rad B, Khoshnevisan K (2020): Immobilization of cellulase onto core-shell magnetic gold nanoparticles functionalized by aspartic acid and determination of its activity. The Protein Journal. 39(4): 328-336.

279. Pota G, Sapienza Salerno A, Costantini A, Silvestri B, Passaro J, Califano V (2022): Co-immobilization of Cellulase and β-Glucosidase into Mesoporous Silica Nanoparticles for the Hydrolysis of Cellulose Extracted from Eriobotrya japonica Leaves. Langmuir. 38(18): 5481-5493.

280. Pozo C, Rodríguez-Llamazares S, Bouza R, Barral L, Castaño J, Müller N, Restrepo I (2018): Study of the structural order of native starch granules using combined FTIR and XRD analysis. Journal of Polymer Research. 25(12): 1-8.

281. Premjit Y, Pandhi S, Kumar A, Rai DC, Duary RK, Mahato DK (2021): Current trends in flavor encapsulation: A comprehensive review of emerging encapsulation techniques, flavour release, and mathematical modelling. Food Research International. 151: 1-15.

282. Qi W, He C, Wang Q, Liu S, Yu Q, Wang W, Leksawasdi N, Wang C, Yuan Z (2018): Carbon-based solid acid pretreatment in corncob saccharification: specific xylose production and efficient enzymatic hydrolysis. ACS Sustainable Chemistry & Engineering. 6(3): 3640-3648.

283. Qi W, Liu G, He C, Liu S, Lu S, Yue J, Wang Q, Wang Z, Yuan Z, Hu J (2019): An efficient magnetic carbon-based solid acid treatment for corncob saccharification with high selectivity for xylose and enhanced enzymatic digestibility. Green Chemistry. 21(6): 1292-1304.

284. Rai M, Ingle AP, Pandit R, Paralikar P, Biswas JK, da Silva SS (2019): Emerging role of nanobiocatalysts in hydrolysis of lignocellulosic biomass leading to sustainable bioethanol production. Catalysis Reviews. 61(1): 1-26.

285. Rashid SS, Mustafa AH, Ab Rahim MH, Gunes B (2022): Magnetic nickel nanostructure as cellulase immobilization surface for the hydrolysis of lignocellulosic biomass. International Journal of Biological Macromolecules. 209: 1048-1053.

286. Raud M, Tutt M, Olt J, Kikas T (2016): Dependence of the hydrolysis efficiency on the lignin content in lignocellulosic material. International Journal of Hydrogen Energy. 41(37): 16338-16343.

287. Ravindra P (2000): Value-added food:: Single cell protein. Biotechnology Advances. 18(6): 459-479.

288. Ravindran R, Jaiswal AK (2016): Microbial enzyme production using lignocellulosic food industry wastes as feedstock: a review. Bioengineering. 3(4): 1-22.

289. Razzaghi M, Homaei A, Vianello F, Azad T, Sharma T, Nadda AK, Stevanato R, Bilal M, Iqbal H (2021): Industrial applications of immobilized nano-biocatalysts. Bioprocess and Biosystems Engineering. 45: 237-256.

290. Ren J, Huo J, Wang Q, Liu Z, Li S, Wang S, Guo W, Li H (2022): Characteristics of immobilized dye-decolorizing peroxidase from Bacillus amyloliquefaciens and application to the bioremediation of dyeing effluent. Biochemical Engineering Journal. 182: 1-9.

291. Reshmy R, Philip E, Sirohi R, Tarafdar A, Arun K, Madhavan A, Binod P, Awasthi MK, Varjani S, Szakacs G (2021): Nanobiocatalysts: advancements and applications in enzyme technology. Bioresource Technology. 337: 1-11.

292. Rivero-Cruz JF, Granados-Pineda J, Pedraza-Chaverri J, Pérez-Rojas JM, Kumar-Passari A, Diaz-Ruiz G, Rivero-Cruz BE (2020): Phytochemical constituents, antioxidant,

cytotoxic, and antimicrobial activities of the ethanolic extract of Mexican brown propolis. Antioxidants. 9(1): 1-11.

293. Robak K, Balcerek M (2018): Review of second generation bioethanol production from residual biomass. Food Technology and Biotechnology. 56(2): 174-187.

294. Rodrigues de Melo R, Alnoch RC, Vilela AFL, Maltempi de Souza E, Krieger N, Ruller R, Harumi Sato H, Mateo C (2017): New heterofunctional supports based on glutaraldehyde-activation: A tool for enzyme immobilization at neutral pH. Molecules. 22(7): 1-18.

295. Rodrigues RC, Berenguer-Murcia Á, Carballares D, Morellon-Sterling R, Fernandez-Lafuente R (2021): Stabilization of enzymes via immobilization: Multipoint covalent attachment and other stabilization strategies. Biotechnology Advances. 52: 1-37.

296. Rodrigues RC, Ortiz C, Berenguer-Murcia Á, Torres R, Fernández-Lafuente R (2013): Modifying enzyme activity and selectivity by immobilization. Chemical Society Reviews. 42(15): 6290-6307.

297. Rouster P, Dondelinger M, Galleni M, Nysten B, Jonas AM, Glinel K (2019): Layer-by-layer assembly of enzyme-loaded halloysite nanotubes for the fabrication of highly active coatings. Colloids and Surfaces B: Biointerfaces. 178: 508-514.

298. Roy S, Dikshit PK, Sherpa KC, Singh A, Jacob S, Rajak RC (2021): Recent nanobiotechnological advancements in lignocellulosic biomass valorization: a review. Journal of Environmental Management. 297: 1-14.

299. Russo T, Fucile P, Giacometti R, Sannino F (2021): Sustainable removal of contaminants by biopolymers: a novel approach for wastewater treatment. Current state and future perspectives. Processes. 9(4): 1-20.

300. Saadoun JH, Bertani G, Levante A, Vezzosi F, Ricci A, Bernini V, Lazzi C (2021): Fermentation of agri-food waste: A promising route for the production of aroma compounds. Foods. 10(4): 1-14.

301. Saha K, Verma P, Sikder J, Chakraborty S, Curcio S (2019): Synthesis of chitosan-cellulase nanohybrid and immobilization on alginate beads for hydrolysis of ionic liquid pretreated sugarcane bagasse. Renewable Energy. 133: 66-76.

302. Salehi Jouzani G, Aghbashlo M, Tabatabaei M (2020): Biofuels: types, promises, challenges, and role of fungi. In: Fungi in Fuel Biotechnology. Springer, pp 1-14

303. Salem K, Jabalera Y, Puentes-Pardo JD, Vilchez-Garcia J, Sayari A, Hmida-Sayari A, Jimenez-Lopez C, Perduca M (2021): Enzyme storage and recycling: Nanoassemblies of α-Amylase and xylanase immobilized on biomimetic magnetic nanoparticles. ACS Sustainable Chemistry & Engineering. 9(11): 4054-4063.

304. Sánchez A, Valero F, Lafuente J, Solà C (2000): Highly enantioselective esterification of racemic ibuprofen in a packed bed reactor using immobilised Rhizomucor miehei lipase. Enzyme and Microbial Technology. 27(1-2): 157-166.

305. Schwiderski M, Kruse A, Grandl R, Dockendorf D (2014): Comparison of the influence of a Lewis acid AlCl3 and a Brønsted acid HCl on the organosolv pulping of beech wood. Green Chemistry. 16(3): 1569-1578.

306. Seenuvasan M, Kumar KS, Kumar A, Parthiban R (2020): Review on surface modification of nanocarriers to overcome diffusion limitations: An enzyme immobilization aspect. Biochemical Engineering Journal. 158: 1-8.

307. Segal L, Creely JJ, Martin Jr A, Conrad C (1959): An empirical method for estimating the degree of crystallinity of native cellulose using the X-ray diffractometer. Textile Research Journal. 29(10): 786-794.

308. Sen T, Barrow CJ, Deshmukh SK (2019): Microbial pigments in the food industry—challenges and the way forward. Frontiers in Nutrition. 6: 1-14.

309. Sethy K, Dass R, Garg A, Sahu S, Gogoi S (2015): Effect of different selenium sources (Selenium yeast and Sodium selenite) on haematology, blood chemistry and thyroid hormones in male goats (Capra hircus). Indian Journal of Animal Research. 49(6): 788-792.

310. Setter OP, Segal E (2020): Halloysite nanotubes–the nano-bio interface. Nanoscale. 12(46): 23444-23460.

311. Sharma HK, Xu C, Qin W (2019a): Biological pretreatment of lignocellulosic biomass for biofuels and bioproducts: an overview. Waste and Biomass Valorization. 10(2): 235-251.

312. Sharma P, Gaur VK, Sirohi R, Varjani S, Kim SH, Wong JW (2021): Sustainable processing of food waste for production of bio-based products for circular bioeconomy. Bioresource Technology. 325: 1-12.

313. Sharma V, Nargotra P, Bajaj BK (2019b): Ultrasound and surfactant assisted ionic liquid pretreatment of sugarcane bagasse for enhancing saccharification using enzymes from an ionic liquid tolerant Aspergillus assiutensis VS34. Bioresource Technology. 285: 1-12.

314. Sheldon RA, Woodley JM (2018): Role of biocatalysis in sustainable chemistry. Chemical Reviews. 118(2): 801-838.

315. Sillu D, Agnihotri S (2020): Cellulase immobilization onto magnetic halloysite nanotubes: enhanced enzyme activity and stability with high cellulose saccharification. ACS Sustainable Chemistry & Engineering. 8(2): 900-913.

316. Sillu D, Agnihotri S, Reddy MS (2022): Magnetic Halloysite Nanotube/α-Amylase Based Nanobiocatalytic Transformation of Food Processing Waste into an Active Fermentation Ingredient. ACS Sustainable Chemistry & Engineering. 10(31): 10169–10180.

317. Silva SM, Peixoto AF, Freire C (2018): HSO3-functionalized halloysite nanotubes: New acid catalysts for esterification of free fatty acid mixture as hybrid feedstock model for biodiesel production. Applied Catalysis A: General. 568: 221-230.

318. Sindhu R, Binod P, Pandey A (2016): Biological pretreatment of lignocellulosic biomass–an overview. Bioresource Technology. 199: 76-82.

319. Singh B (1996): Why does halloysite roll?—A new model. Clays and Clay Minerals. 44(2): 191-196.

320. Singh B (2020): Enhanced production of bacterial xylanase and its utility in saccharification of sugarcane bagasse. Bioprocess and Biosystems Engineering. 43(6): 1081-1091.

321. Singh R, Singh T (2022a): Fructooligosaccharides Production from Inulin by Immobilized Endoinulinase on 3-Aminopropyltriethoxysilane Functionalized Halloysite Nanoclay. Catalysis Letters. 152(7): 1927-1949.

322. Singh R, Singh T (2022b): Glutaraldehyde functionalization of halloysite nanoclay enhances immobilization efficacy of endoinulinase for fructooligosaccharides production from inulin. Food Chemistry. 381: 132253.

323. Singh R, Singh T (2022c): Hetero-modification of halloysite nanoclay to immobilize endoinulinase for the preparation of fructooligosaccharides. Food Research International. 159: 1-12.

324. Singh RV, Sharma P, Sambyal K (2022): Application of Sugarcane Bagasse in Chemicals and Food Packaging Industry: Potential and Challenges. Circular Economy and Sustainability: 1-22.

325. Sinha S, Tripathi P (2021): Trends and challenges in valorisation of food waste in developing economies: A case study of India. Case Studies in Chemical and Environmental Engineering. 4: 1-5.

326. Sluiter A, Hames B, Ruiz R, Scarlata C, Sluiter J, Templeton D, Crocker D (2008) Determination of structural carbohydrates and lignin in biomass. National Renewable Energy Laboratory, Colorado, USA

327. Sodhi AS, Sharma N, Bhatia S, Verma A, Soni S, Batra N (2022): Insights on sustainable approaches for production and applications of value added products. Chemosphere. 286: 1-21.

328. Soltaninejad A, Jazini M, Karimi K (2022): Sustainable bioconversion of potato peel wastes into ethanol and biogas using organosolv pretreatment. Chemosphere. 291. doi:https://doi.org/10.1016/j.chemosphere.2021.133003

329. Sriwong KT, Matsuda T (2022): Recent Advances in Enzyme Immobilization Utilizing Nanotechnology for Biocatalysis. Organic Process Research & Development. 26(7): 1857-1877.

330. Sun P, Liu G, Lv D, Dong X, Wu J, Wang D (2015): Effective activation of halloysite nanotubes by piranha solution for amine modification via silane coupling chemistry. RSC Advances. 5(65): 52916-52925.

331. Sun Z, Bottari G, Afanasenko A, Stuart MC, Deuss PJ, Fridrich B, Barta K (2018): Complete lignocellulose conversion with integrated catalyst recycling yielding valuable aromatics and fuels. Nature Catalysis. 1(1): 82-92.

332. Talan A, Tiwari B, Yadav B, Tyagi RD, Wong JW-C, Drogui P (2021): Food waste valorization: Energy production using novel integrated systems. Bioresource Technology. 322: 1-12.

333. Tamburini E, Gaglio M, Castaldelli G, Fano EA (2020): Biogas from agri-food and agricultural waste can appreciate agro-ecosystem services: The case study of Emilia Romagna region. Sustainability. 12(20): 1-15.

334. Testa ML, La Parola V (2021): Sulfonic acid-functionalized inorganic materials as efficient catalysts in various applications: A minireview. Catalysts. 11(10): 1-26.

335. Tharmavaram M, Pandey G, Bhatt P, Prajapati P, Rawtani D, Sooraj K, Ranjan M (2021): Chitosan functionalized halloysite nanotubes as a receptive surface for laccase and copper to perform degradation of chlorpyrifos in aqueous environment. International Journal of Biological Macromolecules. 191: 1046-1055.

336. Tharmavaram M, Pandey G, Rawtani D (2018): Surface modified halloysite nanotubes: a flexible interface for biological, environmental and catalytic applications. Advances in Colloid and Interface Science. 261: 82-101.

337. Thielemans K, De Bondt Y, Van den Bosch S, Bautil A, Roye C, Deneyer A, Courtin CM, Sels BF (2022): Decreasing the degree of polymerization of microcrystalline cellulose by mechanical impact and acid hydrolysis. Carbohydrate Polymers. 294: 1-8.

338. Tian D, Chandra RP, Lee J-S, Lu C, Saddler JN (2017): A comparison of various lignin-extraction methods to enhance the accessibility and ease of enzymatic hydrolysis of the cellulosic component of steam-pretreated poplar. Biotechnology for Biofuels. 10(1): 1-10.

339. Tian Y, Zhang F, Wang J, Cao L, Han Q (2021): A review on solid acid catalysis for sustainable production of levulinic acid and levulinate esters from biomass derivatives. Bioresource Technology. 342: 1-16.

340. Tibolla H, Pelissari FM, Martins JT, Vicente A, Menegalli FC (2018): Cellulose nanofibers produced from banana peel by chemical and mechanical treatments: characterization and cytotoxicity assessment. Food Hydrocolloids. 75: 192-201.

341. Tierrablanca E, Romero-García J, Roman P, Cruz-Silva R (2010): Biomimetic polymerization of aniline using hematin supported on halloysite nanotubes. Applied Catalysis A: General. 381(1-2): 267-273.

342. Tizchang S, Khiabani MS, Mokarram RR, Hamishehkar H, Mohammadi NS, Chisti Y (2021): Immobilization of β-galactosidase by halloysite-adsorption and entrapment in a cellulose nanocrystals matrix. Biochimica et Biophysica Acta (BBA)-General Subjects. 1865(6): 1-10.

343. Torabizadeh H, Montazeri E (2020): Nano co-immobilization of α-amylase and maltogenic amylase by nanomagnetic combi-cross-linked enzyme aggregates method for maltose production from corn starch. Carbohydrate Research. 488: 1-11.

344. Torgbo S, Quan VM, Sukyai P (2021): Cellulosic value-added products from sugarcane bagasse. Cellulose. 28(9): 5219-5240.

345. Torr KM, Love KT, Simmons BA, Hill SJ (2016): Structural features affecting the enzymatic digestibility of pine wood pretreated with ionic liquids. Biotechnology and Bioengineering. 113(3): 540-549.

346. Torres-León C, Chávez-González ML, Hernández-Almanza A, Martínez-Medina GA, Ramírez-Guzmán N, Londoño-Hernández L, Aguilar CN (2021): Recent advances on the microbiological and enzymatic processing for conversion of food wastes to valuable bioproducts. Current Opinion in Food Science. 38: 40-45.

347. Torres-Valenzuela LS, Ballesteros-Gómez A, Rubio S (2020): Green solvents for the extraction of high added-value compounds from agri-food waste. Food Engineering Reviews. 12(1): 83-100.

348. Tsouko E, Maina S, Ladakis D, Kookos IK, Koutinas A (2020): Integrated biorefinery development for the extraction of value-added components and bacterial cellulose production from orange peel waste streams. Renewable Energy. 160: 944-954.

349. Tu W-C, Hallett JP (2019): Recent advances in the pretreatment of lignocellulosic biomass. Current Opinion in Green and Sustainable Chemistry. 20: 11-17.

350. Tuli HS, Chaudhary P, Beniwal V, Sharma AK (2015): Microbial pigments as natural color sources: current trends and future perspectives. Journal of Food Science and Technology. 52(8): 4669-4678.

351. Tully J, Yendluri R, Lvov Y (2016): Halloysite clay nanotubes for enzyme immobilization. Biomacromolecules. 17(2): 615-621.

352. Tuñón I, Moliner V (2016): Simulating enzyme reactivity: computational methods in enzyme catalysis. Royal Society of Chemistry,

353. UNEP (2021) Food Waste Index Report 2021. UNEP. https://www.unep.org/resources/report/unep-food-waste-index-report-2021. Accessed 08 September 2022

354. Unniganapathi BV, Mohanan Puzhavoorparambil V (2021): Development of PAMAM dendrimer-modified magnetic chitosan: a novel platform for α-amylase immobilization. Polymer Bulletin: 1-18.

355. Usmani Z, Sharma M, Awasthi AK, Sivakumar N, Lukk T, Pecoraro L, Thakur VK, Roberts D, Newbold J, Gupta VK (2021): Bioprocessing of waste biomass for sustainable product development and minimizing environmental impact. Bioresource Technology. 322: 1-12.

356. Vaidya AA, Donaldson LA, Newman RH, Suckling ID, Campion SH, Lloyd JA, Murton KD (2016): Micromorphological changes and mechanism associated with wet ball

milling of Pinus radiata substrate and consequences for saccharification at low enzyme loading. Bioresource Technology. 214: 132-137.

357. Valladares-Diestra KK, de Souza Vandenberghe LP, Torres LAZ, Nishida VS, Zandoná Filho A, Woiciechowski AL, Soccol CR (2021): Imidazole green solvent pre-treatment as a strategy for second-generation bioethanol production from sugarcane bagasse. Chemical Engineering Journal. 420. doi:https://doi.org/10.1016/j.cej.2020.127708

358. Van Soest JJ, Tournois H, de Wit D, Vliegenthart JF (1995): Short-range structure in (partially) crystalline potato starch determined with attenuated total reflectance Fourier-transform IR spectroscopy. Carbohydrate Research. 279: 201-214.

359. Veerabadran NG, Price RR, Lvov YM (2007): Clay nanotubes for encapsulation and sustained release of drugs. Nano. 2(02): 115-120.

360. Verma NK, Raghav N (2021): Comparative study of covalent and hydrophobic interactions for α-amylase immobilization on cellulose derivatives. International Journal of Biological Macromolecules. 174: 134-143.

361. Verma R, Sharma S, Kundu LM, Pandey LM (2020): Experimental investigation of molasses as a sole nutrient for the production of an alternative metabolite biosurfactant. Journal of Water Process Engineering. 38. doi:https://doi.org/10.1016/j.jwpe.2020.101632

362. Vijayalakshmi S, Govindarajan M, Al-Mulahim N, Ahmed Z, Mahboob S (2021): Cellulase immobilized magnetic nanoparticles for green energy production from Allamanda schottii L: Sustainability research in waste recycling. Saudi Journal of Biological Sciences. 28(1): 901-910.

363. Wang D, Hu Y, Zhao J, Zeng L, Tao X, Chen W (2014): Holey reduced graphene oxide nanosheets for high performance room temperature gas sensing. Journal of Materials Chemistry A. 2(41): 17415-17420.

364. Wang L, Zhang L, Li H, Ma Y, Zhang R (2019a): High selective production of 5-hydroxymethylfurfural from fructose by sulfonic acid functionalized SBA-15 catalyst. Composites Part B: Engineering. 156: 88-94.

365. Wang Q, Liu Y, Zhang Y, Chen Y, Feng Q, Wang W, Liang C, Hu Y, Qi W (2022a): Enhanced enzymatic hydrolysis of poplar cellulosic residue fractionated by a magnetic carbon-based solid-acid catalyst in the γ-valerolactone–water system. Industrial Crops and Products. 176: 1-9.

366. Wang Y-T, Yang X-X, Xu J, Wang H-L, Wang Z-B, Zhang L, Wang S-L, Liang J-L (2019b): Biodiesel production from esterification of oleic acid by a sulfonated magnetic solid acid catalyst. Renewable Energy. 139: 688-695.

367. Wang Y, Chen D, Wang G, Zhao C, Ma Y, Yang W (2018): Immobilization of cellulase on styrene/maleic anhydride copolymer nanoparticles with improved stability against pH changes. Chemical Engineering Journal. 336: 152-159.

368. Wang Y, Qi Y, Chen C, Zhao C, Ma Y, Yang W (2019c): Layered co-immobilization of β-glucosidase and cellulase on polymer film by visible-light-induced graft polymerization. ACS Applied Materials & Interfaces. 11(47): 44913-44921.

369. Wang Y, Radosevich M, Hayes D, Labbé N (2011): Compatible Ionic liquid-cellulases system for hydrolysis of lignocellulosic biomass. Biotechnology and Bioengineering. 108(5): 1042-1048.

370. Wang Z, Ren D, Cheng Y, Zhang X, Zhang S, Chen W (2022b): Immobilization of laccase on chitosan functionalized halloysite nanotubes for degradation of Bisphenol A in aqueous solution: degradation mechanism and mineralization pathway. Heliyon. 8(7): 1-10.

371. Wilson D, Langell M (2014): XPS analysis of oleylamine/oleic acid capped Fe3O4 nanoparticles as a function of temperature. Applied Surface Science. 303: 6-13.

372. Woodley JM (2013): Protein engineering of enzymes for process applications. Current Opinion in Chemical Biology. 17(2): 310-316.

373. Wu L, Yuan X, Sheng J (2005): Immobilization of cellulase in nanofibrous PVA membranes by electrospinning. Journal of Membrane Science. 250(1-2): 167-173.

374. Xiang Y, Zhao K, Zhou S, Zhao W, Zeng Z, Zhu X, Liu X (2022): Sulfonic acid covalently grafted halloysite nanotubes for highly efficient synthesis of biofuel 5-ethoxymethylfurfural. Sustainable Energy & Fuels. 6(9): 2368-2376.

375. Xiao Z, Zhang X, Gregg DJ, Saddler JN Effects of sugar inhibition on cellulases and β-glucosidase during enzymatic hydrolysis of softwood substrates. In: Proceedings of the twenty-fifth symposium on biotechnology for fuels and chemicals held May 4–7, 2003, in Breckenridge, CO, 2004. Springer, pp 1115-1126

376. Xie Y, Qian D, Wu D, Ma X (2011): Magnetic halloysite nanotubes/iron oxide composites for the adsorption of dyes. Chemical Engineering Journal. 168(2): 959-963.

377. Ximenes E, Kim Y, Mosier N, Dien B, Ladisch M (2011): Deactivation of cellulases by phenols. Enzyme and Microbial Technology. 48(1): 54-60.

378. Xiong S, Guan Y, Luo C, Zhu L, Wang S (2021): Critical review on the preparation of platform compounds from biomass or saccharides via hydrothermal conversion over carbon-based solid acid catalysts. Energy & Fuels. 35(18): 14462-14483.

379. Xu J, Huo S, Yuan Z, Zhang Y, Xu H, Guo Y, Liang C, Zhuang X (2011): Characterization of direct cellulase immobilization with superparamagnetic nanoparticles. Biocatalysis and Biotransformation. 29(2-3): 71-76.

380. Xu Q, Yang W, Liu G, Liang C, Lu S, Qi Z, Hu J, Wang Q, Qi W (2019): Enhanced enzymatic hydrolysis of corncob by synthesized enzyme-mimetic magnetic solid acid pretreatment in an aqueous phase. ACS Omega. 4(18): 17864-17873.

381. Xue Y-P, Jiang T, Liu X, Zheng Y-G (2013): Efficient production of S-(+)-2-chlorophenylglycine by immobilized penicillin G acylase in a recirculating packed bed reactor. Biochemical Engineering Journal. 74: 88-94.

382. Yang J, Chen H, Niu H, McNutt J, He Q (2021): A Comparative Study on Thermochemical Valorization Routes for Spent Coffee Grounds. Energies. 14(13): 1-10.

383. Yasmin HAN, Naresh S, Kunasundari B, Shuit SH (2022): Immobilization of cellulase on magnetized multiwall carbon nanotubes (m-MWCNTs) synthesized via eco-friendly (water-based) method. Chemical Papers. 76(1): 453-464.

384. Yoshida M, Liu Y, Uchida S, Kawarada K, Ukagami Y, Ichinose H, Kaneko S, Fukuda K (2008): Effects of cellulose crystallinity, hemicellulose, and lignin on the enzymatic hydrolysis of Miscanthus sinensis to monosaccharides. Bioscience, Biotechnology, and Biochemistry. 72(3): 805-810.

385. Yu H, Cheng L, Yin J, Yan S, Liu K, Zhang F, Xu B, Li L (2013): Structure and physicochemical properties of starches in lotus (N elumbo nucifera Gaertn.) rhizome. Food Science & Nutrition. 1(4): 273-283.

386. Yuan P, Southon PD, Liu Z, Green ME, Hook JM, Antill SJ, Kepert CJ (2008): Functionalization of halloysite clay nanotubes by grafting with γ-aminopropyltriethoxysilane. The Journal of Physical Chemistry C. 112(40): 15742-15751.

387. Yuan P, Tan D, Annabi-Bergaya F (2015): Properties and applications of halloysite nanotubes: recent research advances and future prospects. Applied Clay Science. 112: 75-93.

388. Zabed HM, Akter S, Yun J, Zhang G, Awad FN, Qi X, Sahu J (2019): Recent advances in biological pretreatment of microalgae and lignocellulosic biomass for biofuel production. Renewable and Sustainable Energy Reviews. 105: 105-128.

389. Zakaria N, Rahman R, Zaidel D, Dailin D, Jusoh M (2021): Microwave-assisted extraction of pectin from pineapple pee. Malaysian Journal of Fundamental and Applied Science. 17(1): 33-38.

390. Zarei A, Alihosseini F, Parida D, Nazir R, Gaan S (2021): Fabrication of Cellulase Catalysts Immobilized on a Nanoscale Hybrid Polyaniline/Cationic Hydrogel Support for the Highly Efficient Catalytic Conversion of Cellulose. ACS Applied Materials & Interfaces. 13(42): 49816-49827.

391. Zdarta J, Meyer AS, Jesionowski T, Pinelo M (2018): A general overview of support materials for enzyme immobilization: characteristics, properties, practical utility. Catalysts. 8(2): 1-27.

392. Zeng M, Pan X (2022): Insights into solid acid catalysts for efficient cellulose hydrolysis to glucose: progress, challenges, and future opportunities. Catalysis Reviews. 64(3): 445-490.

393. Zeng S, Reyes C, Liu J, Rodgers PA, Wentworth SH, Sun L (2014): Facile hydroxylation of halloysite nanotubes for epoxy nanocomposite applications. Polymer. 55(25): 6519-6528.

394. Zhai R, Zhang B, Liu L, Xie Y, Zhang H, Liu J (2010): Immobilization of enzyme biocatalyst on natural halloysite nanotubes. Catalysis Communications. 12(4): 259-263.

395. Zhang H, Jiang Z, Xia Q, Zhou D (2021): Progress and perspective of enzyme immobilization on zeolite crystal materials. Biochemical Engineering Journal. 172: 1-11.

396. Zhang H, Li J, Huang G, Yang Z, Han L (2018): Understanding the synergistic effect and the main factors influencing the enzymatic hydrolyzability of corn stover at low enzyme loading by hydrothermal and/or ultrafine grinding pretreatment. Bioresource Technology. 264: 327-334.

397. Zhang L, Tang W, Ma T, Zhou L, Hui C, Wang X, Wang P, Zhang C, Chen C (2019a): Laccase-immobilized tannic acid-mediated surface modification of halloysite nanotubes for efficient bisphenol-A degradation. RSC Advances. 9(67): 38935-38942.

398. Zhang Y-HP, Lynd LR (2005): Determination of the number-average degree of polymerization of cellodextrins and cellulose with application to enzymatic hydrolysis. Biomacromolecules. 6(3): 1510-1515.

399. Zhang Y, He X, Ouyang J, Yang H (2013): Palladium nanoparticles deposited on silanized halloysite nanotubes: synthesis, characterization and enhanced catalytic property. Scientific Reports. 3(1): 1-6.

400. Zhang Y, Li Y, Zhang Y, Ding D, Wang L, Liu M, Zhang F (2019b): Thermal behavior and kinetic analysis of halloysite–stearic acid complex. Journal of Thermal Analysis and Calorimetry. 135(4): 2429-2436.

401. Zhao X, Zhang L, Liu D (2012): Biomass recalcitrance. Part I: the chemical compositions and physical structures affecting the enzymatic hydrolysis of lignocellulose. Biofuels, Bioproducts and Biorefining. 6(4): 465-482.

402. Zhao Y, Damgaard A, Christensen TH (2018): Bioethanol from corn stover–a review and technical assessment of alternative biotechnologies. Progress in Energy and Combustion Science. 67: 275-291.

403. Zhong C, Wang C, Huang F, Wang F, Jia H, Zhou H, Wei P (2015): Selective hydrolysis of hemicellulose from wheat straw by a nanoscale solid acid catalyst. Carbohydrate Polymers. 131: 384-391.

404. Zhong S, Zhou C, Zhang X, Zhou H, Li H, Zhu X, Wang Y (2014): A novel molecularly imprinted material based on magnetic halloysite nanotubes for rapid enrichment of 2, 4-dichlorophenoxyacetic acid in water. Journal of Hazardous Materials. 276: 58-65.

405. Zhou F, Tang J, Fei Z, Zhou X, Chen X, Cui M, Qiao X (2014): Efficient cyclohexyl acrylate production by direct addition of acrylic acid and cyclohexene over SBA-15-SO3H. Journal of Porous Materials. 21(2): 149-155.

406. Zhou M, Ju X, Zhou Z, Yan L, Chen J, Yao X, Xu X, Li L-Z (2019): Development of an immobilized cellulase system based on metal–organic frameworks for improving ionic liquid tolerance and in situ saccharification of bagasse. ACS Sustainable Chemistry & Engineering. 7(23): 19185-19193.

407. Zhou Z, Liu D, Zhao X (2021): Conversion of lignocellulose to biofuels and chemicals via sugar platform: an updated review on chemistry and mechanisms of acid hydrolysis of lignocellulose. Renewable and Sustainable Energy Reviews. 146: 1-24.

408. Zhu X, Fan X, Wang Y, Zhai Q, Hu M, Li S, Jiang Y (2021): Amino modified magnetic halloysite nanotube supporting chloroperoxidase immobilization: enhanced stability, reusability, and efficient degradation of pesticide residue in wastewater. Bioprocess and Biosystems Engineering. 44(3): 483-493.

409. Zoghlami A, Paës G (2019): Lignocellulosic biomass: understanding recalcitrance and predicting hydrolysis. Frontiers in Chemistry. 7: 1-11.

410. Zykova AK, Pantyukhov PV, Mastalygina EE, Chaverri-Ramos C, Nikolaeva SG, Saavedra-Arias JJ, Popov AA, Wortman SE, Poletto M (2021): Biocomposites of low-density polyethylene plus wood flour or flax straw: Biodegradation kinetics across three environments. Polymers. 13(13): 1-15.

Appendix

Appendix-A

Details of instruments used

- **Autoclave:** Equitron, India.
- **Centrifuge:** Himac 22G, Hitachi, Japan; Sorvall Legend XFR, Thermo Scientific, USA.
- **ELISA plate reader:** Multiskan Spectrum, Thermo Scientific, USA.
- **Field emission-scanning electron microscopy:** Hitachi SU8010, Japan; Carl-Zeiss Sigma 500 FEG-SEM, Germany.
- **Fourier Transform Infrared Spectroscopy:** Cary 630 FTIR, Agilent Technologies, USA; IRTracer-100, Shimadzu Corp., Japan.
- **Furnace:** Lenton furnace, UK.
- **High Performance Liquid Chromatography:** Waters 515, Waters, USA; UFLC HPLC System, Shimazdu Corp., Japan.
- **High resolution transmission electron microscopy:** Jeol JEM-2100, Japan.
- **Incubator:** Calton BOD incubator, NSW India.
- **Laminar flow cabinet:** Thermadyne Biosafety Cabinet Class-I, India.
- **Oven:** NSW India;
- **pH meter:** Adwa AD1030, Hungary.
- **Rotary evaporator:** RVE(1DX), Macro Scientific Works Pvt. Ltd., Delhi, India.
- **Scanning electron microscopy:** JSM-6510LV, JEOL, Japan.
- **Shaking incubator:** Excella E25 Incubator shaker,, New Brunswick Scientific, USA.
- **ThermoGravimetric Analyzer:** EXSTAR TG/DTA 6300, Seiko Instruments Inc., Japan.
- **Ultrasonic bath:** PCI analytics-9L, India.
- **UV-Viz spectrophotometer:** UV-2600, Shimadzu Corp., Japan.
- **Vibrating Sample Magnetometer:** 7407 Lake Shore Cryotronics Inc., USA.
- **Vortex:** Tarson Spinix 3002, India.
- **Water bath:** Precision Reciprocal Shaking Bath, Thermo Scientific, USA; NSW India.
- **Weighing balance:** ME 104 Mettler Toledo, USA.
- **X-ray diffractometer**: PANalytical X-pert Pro, The Netherlands.
- **X-ray photoelectron spectroscopy:** ESCALAB, Thermo Fischer Scientific, USA.

Appendix-B

List of chemicals

All chemicals and reagents used for the experiments were of the highest analytical grade and purchased from Loba-Chemie Pvt. Ltd, India unless otherwise specified. Sterilization of the media components were done in an autoclave at 121°C (15 psi) for 15 min unless otherwise specified.

Hi Media Laboratories Pvt. Ltd. (Mumbai, India): Bovine serum albumin, glutaraldehyde, nutrient agar, nutrient broth, potato dextrose broth, starch, and tris Buffer.

Merck, USA: Acetic acid**,** ethanol**,** hydrochloric acid**,** nitric acid, and sodium hydroxide.

MP Biomedicals, USA: α-amylase.

Sigam Aldrich (USA): (3-aminopropyl)triethoxysilane, 1-butyl-3-methylimidazolium chloride ([bmim][Cl] ≥98.0% purity), 3-mercaptopropyl(trimethoxy)silane, cellulase, dopamine hydrochloride, ferric chloride hexahydrate, ferrous chloride tetrahydrate, fructose assay kit, glucose assay kit (GAGO20), glucose isomerase, halloysite nanotubes, sodium carboxymethyl cellulose.

Sisco Research Laboratories Pvt. Ltd. (Mumbai, India): Folin & Ciocalteus Phenol (FCP) Reagent.

Appendix-C

Details of reagents prepared

1. Citrate buffer

Designated amount of Sodium citrate dihydrate and citric acid were mixed in 80 mL distilled water, and final volume was made 100 mL with addition of distilled water.

Sodium citrate dihydrate	Citric acid	pH
For 50 mM		
675.6 mg	519.2 mg	4.5
854.9 mg	402.1 mg	5
1.034 g	285 mg	5.5
For 100 mM		
275.8 mg	1.741 g	3
992.8 mg	1.273 g	4
1.351 g	1.038 g	4.5
1.566 g	897.9 mg	4.8
1.71 g	804.2 mg	5
2.068 g	570 mg	5.5

2. Phosphate buffer

Designated amount of potassium phosphate dibasic and potassium phosphate monobasic were mixed in 80 mL distilled water, and final volume was made 100 mL with addition of distilled water.

Potassium phosphate dibasic	Potassium phosphate monobasic	pH
For 50 mM		
120.2 mg	586.5 mg	6
293.7 mg	451 mg	6.5
467.1 mg	315.4 mg	7
640.6 mg	179.9 mg	7.5
814.0 mg	44.3 mg	8
For 100 mM		
240.5 mg	1.173 g	6
587.4 mg	901.9 mg	6.5
934.3 mg	630.9 mg	7

3. ***Dinitrosalicyclic acid (DNSA) reagent***

   In 50 mL distilled water 2.5 g DNS and 4 g NaOH were slowly dissolve by heating and stirring at 70 °C. Then, 75 g disodium tartarate was added and stirred until complete dissolution. Final volume was made up to 250 mL with addition of distilled water.

4. ***Analytical reagent for Lowry method***

   Solution A: 2% Na_2CO_3 in 0.1 N NaOH

   Solution B: 1% NaK Tartrate in distilled water

   Solution C: 0.5% $CuSO_4$.5 H_2O in distilled water

   Reagent preparation: 48 mL of solution A, 1 mL of solution B, and 1 mL of solution

5. ***Bradford reagent***

   Reagent was prepared by adding 0.01% (w/v) Coomassie Brilliant Blue G-250, 4.7% (w/v) ethanol, and 8.5% (w/v) phosphoric acid.

Appendix-D

Standard Curves

1. *Standard curve of Bovine Serum Albumin (BSA) using Bradford method*

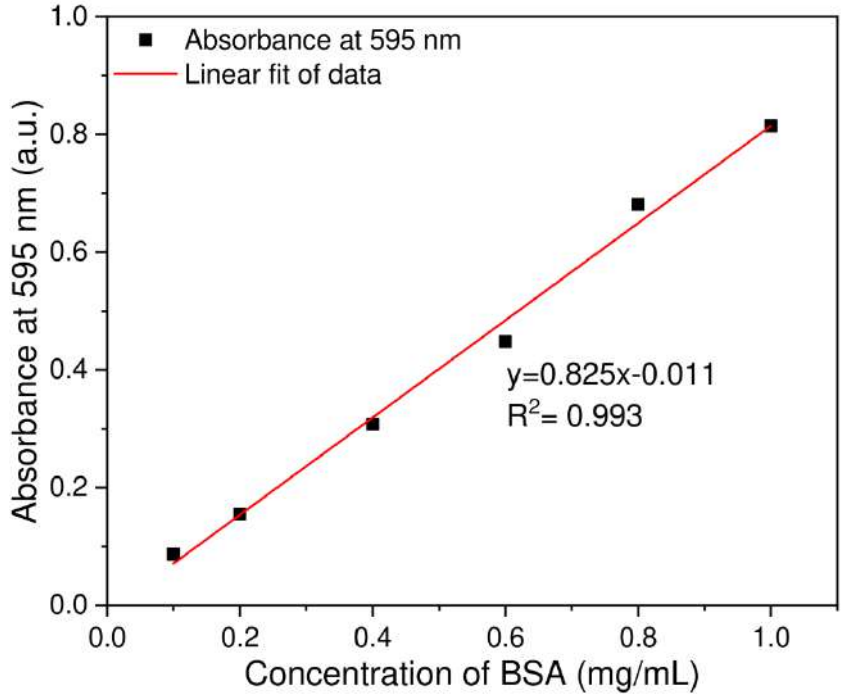

2. *Standard curve of Bovine Serum Albumin (BSA) using Lowry method*

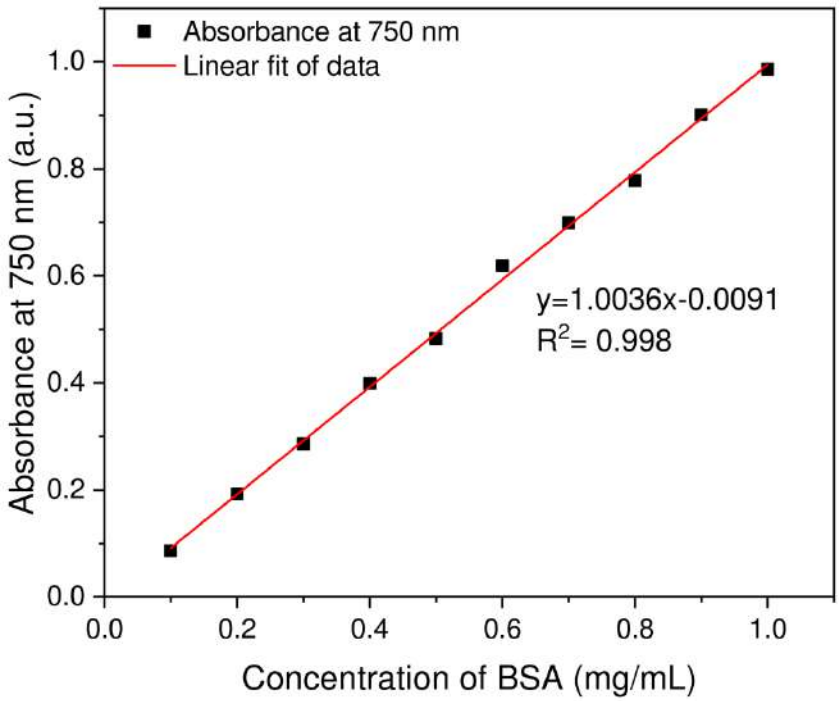

3. *Standard curve of ethanol*

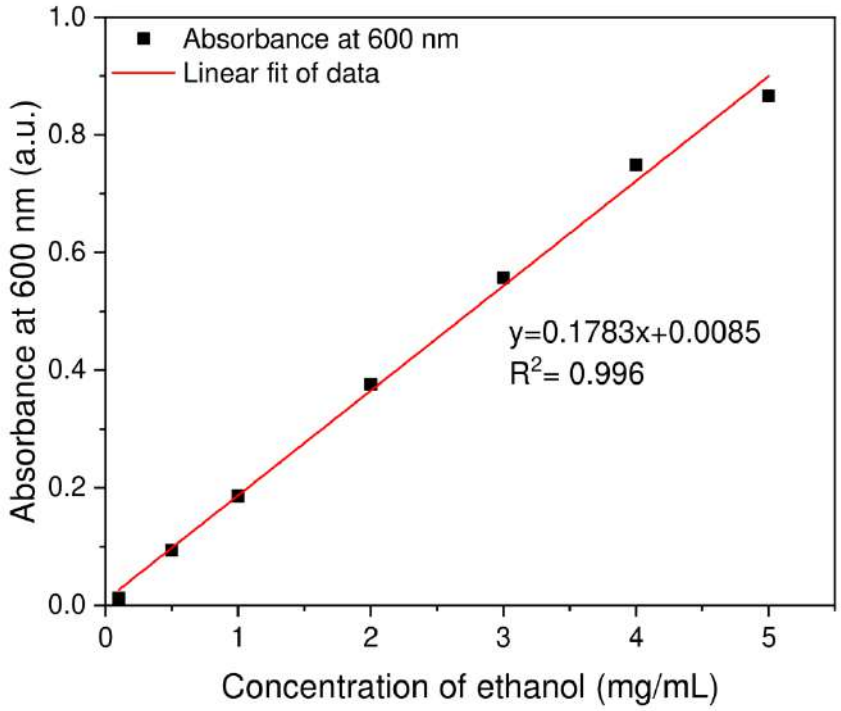

4. *Standard curve of gallic acid*

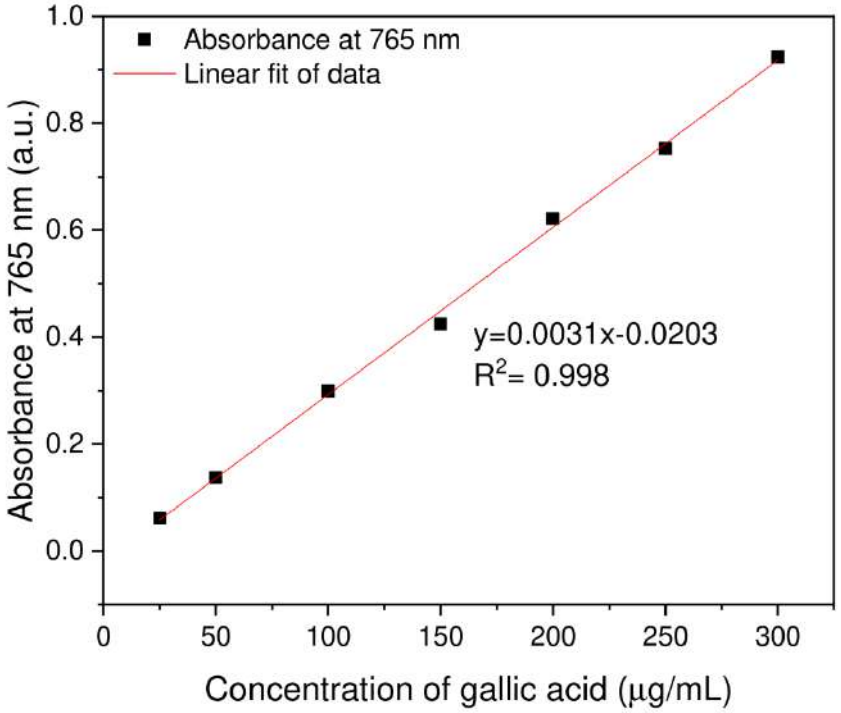

5. *Standard curve of reducing sugar (glucose) using DNSA method*

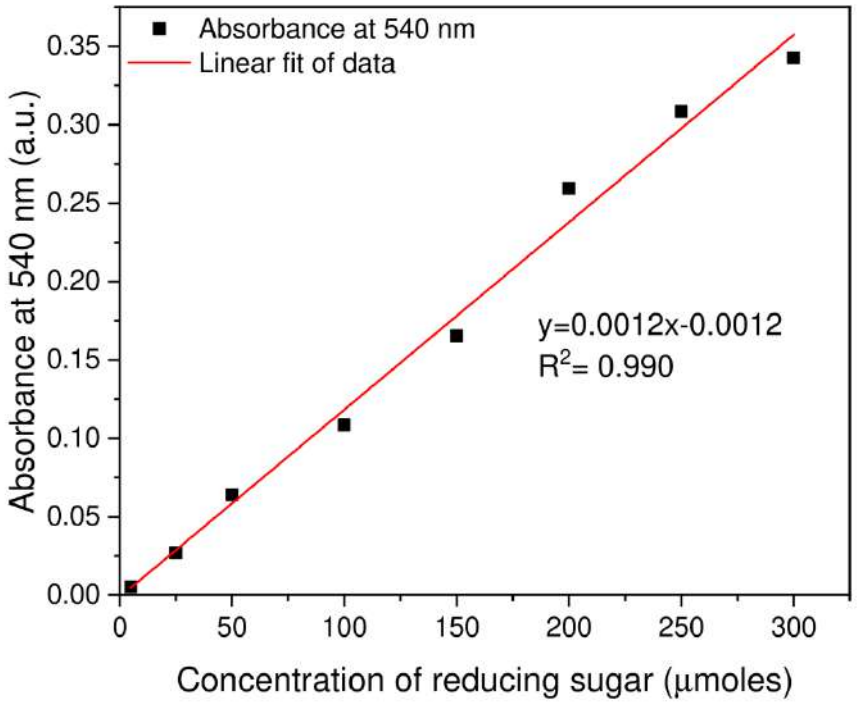

6. *HPLC chromatograms*

Peak of Furfural (retention time=4.612 min) and HMF (retention time=3.668 min)

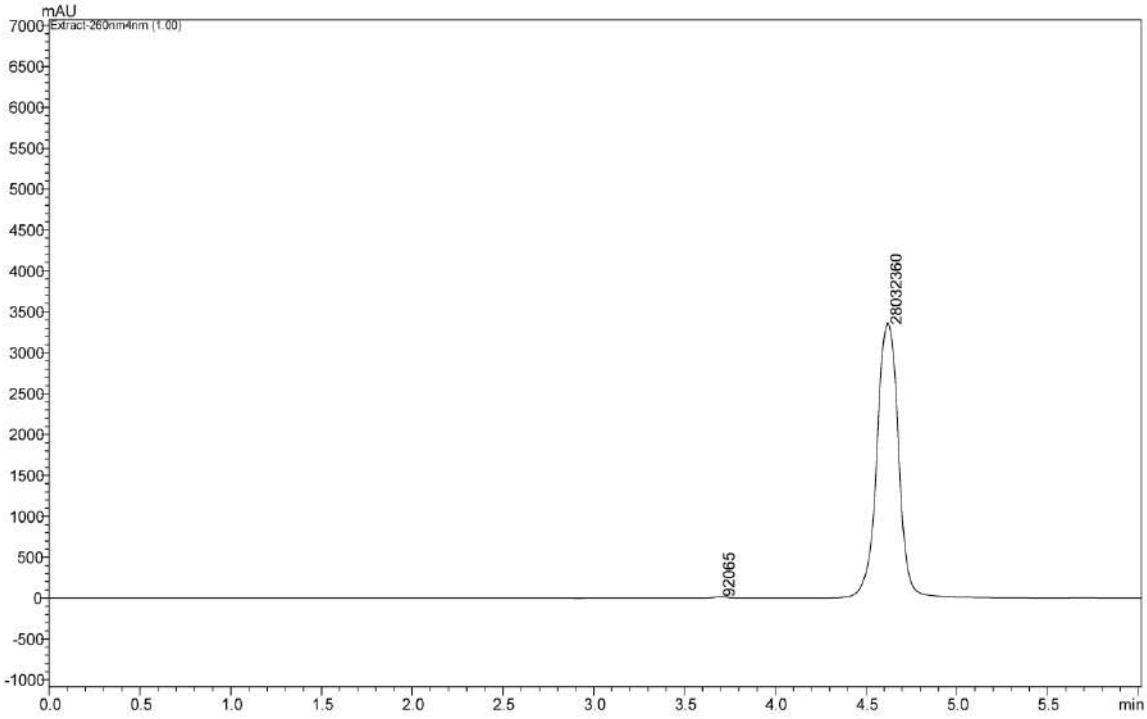

Peaks of different component with retention time (RT) of sugarcane bagasse

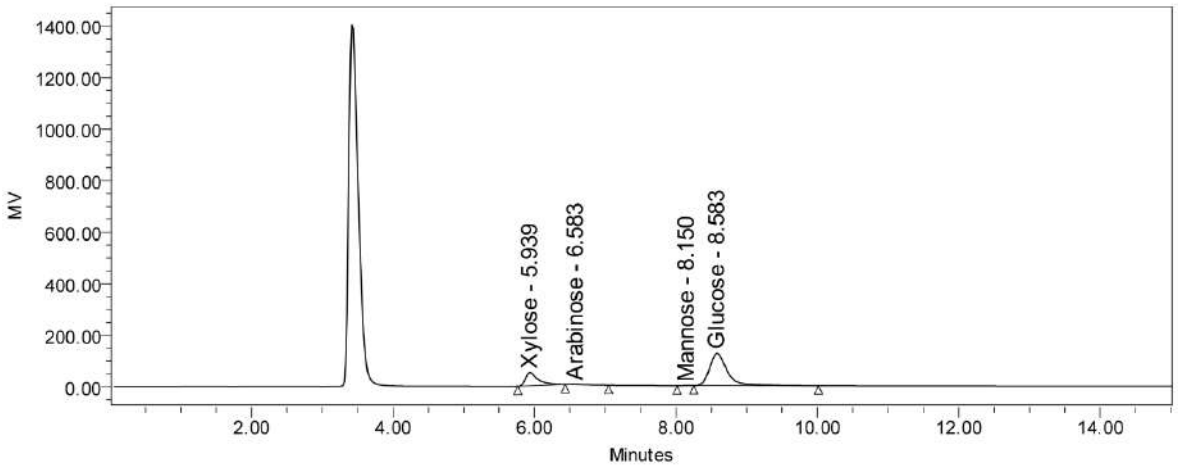

Peaks of glucose and fructose with retention time (RT) during isomerisation reaction

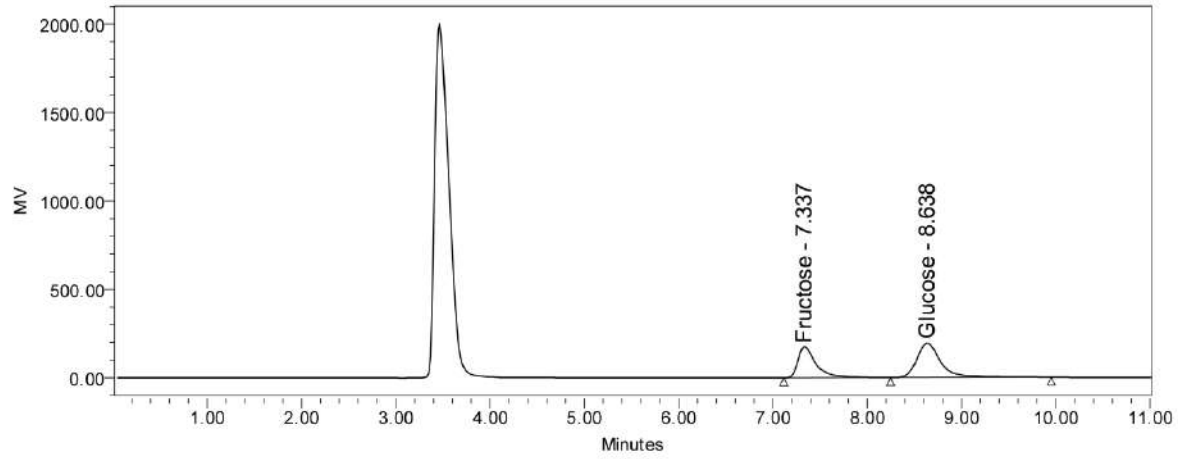

Copyright permission figure 2.5

This Agreement between Mr. Devendra Sillu ("You") and Elsevier ("Elsevier") consists of your license details and the terms and conditions provided by Elsevier and Copyright Clearance Center.

License Number	5386501495288
License date	Sep 12, 2022
Licensed Content Publisher	Elsevier
Licensed Content Publication	Advances in Colloid and Interface Science
Licensed Content Title	Surface modified halloysite nanotubes: A flexible interface for biological, environmental and catalytic applications
Licensed Content Author	Maithri Tharmavaram,Gaurav Pandey,Deepak Rawtani
Licensed Content Date	Nov 1, 2018
Licensed Content	Volume 261
Licensed Content Issue	n/a
Licensed Content Pages	20
Start Page	82
End Page	101
Type of Use	reuse in a thesis/dissertation
Portion	figures/tables/illustrations
Number of figures/tables/illustrations	1
Format	both print and electronic
Are you the author of this Elsevier article?	No
Will you be translating?	No
Title	Nanobiocatalytic Conversion of Agri-Food Waste into Biochemical Products
Institution name	Thapar Institute of Engineering and Technology
Expected presentation date	Jan 2023
Portions	Fig. 2
Requestor Location	Mr. Devendra Sillu C/o Ranjeet Sillu ,Ward No 23, Bhabhuta Siddh Colony, Hanumangarh Town HANUMANGARH, Rajasthan 335513 India
Publisher Tax ID	GB 494 6272 12
Total	0.00 USD

ACS Sustainable Chemistry & Engineering

Research Article

Cite This: ACS Sustainable Chem. Eng. 2020, 8, 900−913

pubs.acs.org/journal/ascecg

Cellulase Immobilization onto Magnetic Halloysite Nanotubes: Enhanced Enzyme Activity and Stability with High Cellulose Saccharification

Devendra Sillu[†] and Shekhar Agnihotri*[,†,‡]

[†]Department of Biotechnology, Thapar Institute of Engineering and Technology, Bhadson Road, Patiala 147004, Punjab, India

[‡]TIFAC Centre of Relevance and Excellence (CORE) in Agro and Industrial Biotechnology, Thapar Institute of Engineering and Technology, Bhadson Road, Patiala 147004, Punjab, India

Supporting Information

ABSTRACT: A quest for efficient biotransformation of cellulosic material into sustainable biochemical products for recent biotechnological interventions is currently under way. Herein, we report the fabrication of nanobiocatalyst (NBC) employing halloysite nanotubes (HNTs) as a template for immobilizing cellulase enzyme, which catalyzed the hydrolysis of cellulose into glucose. Magnetic character was imported to HNTs by *in situ* anchoring of iron oxide nanoparticles, onto which cellulase was immobilized using aminosilane surface-functional chemistry. Characterization studies revealed nanobiocatalyst to be extremely stable during heterogeneous catalysis without compromising their catalytic activity. The optimization of process parameters yielded ∼93.5% activity of cellulase with high enzyme loading (111.6 mg·g^{-1} HNTs) after immobilization. Immobilized cellulase displayed superior stability at elevated temperatures (≥60°C) and storage capability compared with their free forms. The NBC even retained ∼68.2% of its original activity after seven consecutive uses with a minimum yield of 25.4 mg glucose·g^{-1} cellulose and was 100% recoverable using a magnet. Displaying a high ionic-liquid tolerance ability is concurrent with superior catalytic potential against CMC and extracted cellulose (bagasse), and achieving ∼50.2% saccharification and 0.56 g glucose·g^{-1} cellulose within 48 h of continuous operation establishes the commercial viability of using cellulase-immobilized HNTs for efficient cellulose hydrolysis. The sustainability and eco-friendly endeavors in this approach would pave the way toward valorization and consolidated bioprocessing of cellulose materials.

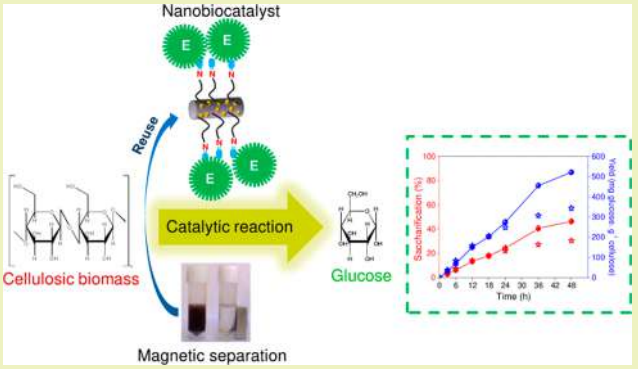

KEYWORDS: *cellulose hydrolysis, lignocellulosic biomass, ionic liquid tolerance, surface functionalization, magnetic recovery, thermal stability, response surface methodology*

INTRODUCTION

The abundance of lignocellulosic biomass and its potential bioconversion into sustainable products has demanded new innovations in biotechnological processing strategies for maximum utilization of cellulose. Almost all industrial sectors involving cellulose processing such as chemicals, biofuels, brewery/distilleries, and food industries require the inevitable step of hydrolysis of cellulose into glucose for its utilization.[1,2] However, the conventional hydrolysis treatments of cellulose involve the use of corrosive and harsh chemicals, which have raised serious environmental concerns due to the formation of toxic byproducts.[3] These chemical treatments may further affect the purity and stability of reaction components, making sequential extraction of the final product difficult. On the contrary, enzyme catalyzed reactions are well-known for their high regioselectivity, chemoselectivity, and catalytic efficiency and for working under mild operational conditions.[4] Particularly, cellulase enzyme has been widely employed to hydrolyze cellulosic biomass into glucose for industrial bioconversions. In biotechnology relevant industries, cellulase has recently witnessed a few notable developments in food and beverages, cosmetics, pharmaceuticals, and chemical detergents.

Despite the aforementioned benefits, the catalytic transformation of cellulosic biomass using cellulase still exists in naive stages and faces key challenges for strategy implementation in the bioprocessing sector.[5] Particularly, the use of free enzymes (i.e., colloidal form) exhibit many limitations, viz., high production cost, low recovery of biocatalyst from the reaction mixture, and extremely low stability of enzymes after every use, eventually making this approach nonsustainable over longer runs.[6,7] Although enzyme immobilization has been

Received: September 11, 2019
Revised: December 8, 2019
Published: December 12, 2019

DOI: 10.1021/acssuschemeng.9b05400
ACS Sustainable Chem. Eng. 2020, 8, 900−913

considered as an effective tool to overcome the above limitations, some major drawbacks coexist under practically relevant conditions. For instance, the entrapment of enzymes within a porous material suffers with diffusional limitations and poor accessibility of substrate from the bulk phase.[8] The other two strategies, i.e., cross-linking and covalent immobilization, often change the intrinsic properties of enzymes (structural confirmation and substrate selectivity) and eventually lead to steric hindrance of active sites.[9] Since the hydrolysis of cellulose using cellulase involves heterogeneous catalysis, the selection of an effective immobilization support becomes an aspect of utmost importance for assessing the commercial feasibility of immobilized cellulase.

The integration of nanoscience with biotechnology has received due consideration in recent years where functional nanomaterials are being extensively studied for water disinfection, photocatalysis, drug delivery, biosensing, and biomedical applications.[10−14] The use of functionalized inorganic nanomaterials as a support matrix for immobilizing enzymes has also been documented recently.[8,15] A high aspect ratio (surface area/volume) of nanostructures provides larger surface area for high enzyme loading concurrently reducing diffusional limitations which results in high catalytic efficiency, better conversion yield, and an improved interaction between substrate and enzyme.[16] Naturally occurring clay materials such as montmorillonite, bentonite, double-layered hydroxides, and zeolites have been investigated as a potential substitute of conventional nanomaterials for biological applications.[17,18] Being abundant, porous, chemically inert, and mechanically and thermally stable, clay materials can be established as an immobilizing template.[19] That is why halloysite nanotubes (HNTs, $Al_2Si_2O_5(OH)_4{\cdot}2H_2O$) are increasingly gaining importance in biocatalytic applications.[20] Similar to other silica-based materials, the presence of siloxane (−Si−O−Si−) and silanol groups (−Si−OH) at the outer surface of HNTs make them versatile to be modified, undergoing specific surface functionalization for intended applications.[21] Amino-silanization is one of those strategies where a uniform self-assembled layer of functional groups can be created over HNTs for dense immobilization of enzymes, which remain unexplored to date.

It is evident from recent literature that most of the studies claiming the use of cellulase immobilized nanomaterials were inclined toward fermentative biofuels production (ethanol and butanol),[3,22−24] and the biochemical conversion of cellulosic biomass into reducing sugars and other valuable bioproducts is yet another sector, which will have even greater commercial significance. The current study would probably be one of those rare studies where cellulose hydrolysis was achieved with high saccharification concurrent with a high yield of glucose production. We aimed to synthesize a nanobiocatalyst (NBC) with high payload of enzymes, which transformed the insoluble cellulose substrates into glucose with enhanced catalytic activity and reusability. The morphology, composition, and surface chemistry of NBC were thoroughly analyzed and correlated with its biocatalytic characteristics. The kinetics, thermodynamic characteristics, and ionic-liquid tolerance capabilities further established an improved performance of cellulase enzyme after immobilizing over magnetic HNTs. Thus, the naturally occurring HNTs coupled with ease in surface functionalization emerged as a versatile template/matrix for immobilizing enzymes, not limited to only cellulase. The outcome of the work would critically enhance our understandings in development, process optimization, and utilization of immobilized enzymes using nanomaterials. From a sustainable bioprocessing viewpoint, this approach would pave new pathways in an efficient utilization of lignocellulosic biomass into biochemical products via nanobiocatalyst.

EXPERIMENTAL SECTION

All details regarding materials involved and analytical characterizations are provided in the Supporting Information.

Synthesis of Magnetic Halloysite Nanotubes (MHNTs). A total of 0.5 g of HNT powder was dispersed in 100 mL of deionized water undergoing ultrasonication for 5 min. A binary mixture of $FeCl_3{\cdot}6H_2O$ and $FeCl_2{\cdot}4H_2O$ having molar ratios of 2:1 was introduced into the HNTs suspension under vigorous stirring at 60 °C with nitrogen purging. Ammonia solution (25%, v/v) was added dropwise to adjust the final pH of the resulting suspension within the range of 9−10. The formation of black color indicated the successful synthesis of magnetic nanoparticles over HNTs. The mixture was further aged at 60 °C over 4 h and then washed three times with deionized water until the final pH of the suspension became 7. The solution was separated using a magnet in order to remove the unbound/loosely bound HNTs from the reaction mixture. The as obtained material was dried at 60 °C for 24 h and kept in sealed plastic bags until further use.

Surface Functionalization of MHNTs. The introduction of amine functional groups onto the surface of MHNTs was done by an established protocol with slight modifications.[14,21] Uniform silanol (Si−OH) sites over MHNTs were generated using sulfochromic acid treatment for 30 min followed by vacuum drying at 120 °C over 90 min. Afterward, 1 g of MHNTs was introduced into a 2% APTES ((3-aminopropyl)triethoxysilane) solution (using absolute ethanol and acetic acid (5:3, v/v) as cosolvent) under inert atmosphere. The mixture was sonicated for 20 min, followed by heating the substrates at 120 °C and 60 min for the condensation of siloxane bonds. Resultant amine-modified MHNTs were separated using a magnet, washed thoroughly with ethanol/acetic acid solution to remove the excess aminosilane, and finally dried overnight at 60 °C.

Immobilization of Cellulase over Amine-Grafted MHNTs. Amine-modified MHNTs were first mixed with 2.5% (v/v) of glutaraldehyde solution, and the solution was left to shake at 120 rpm for 24 h. The resultant solid was separated magnetically and rinsed several times to remove loosely bounded glutaraldehyde. As per the optimized conditions, 20 mg of MHNTs were introduced in 1.44 mg·mL^{-1} cellulase suspension (citrate buffer, 4.8 pH) and were shaken (120 rpm) continuously at 4 °C for 6 h. The cellulase loaded HNTs were recovered with the help of a magnet followed by washing in buffer solution in order to remove any unbound enzyme and were finally stored in citrate buffer (pH 5) at 4 °C until further use. The residual enzyme concentration in the supernatant was used to determine the extent of enzyme loading.

Experimental Design, Optimization, and Statistical Analysis. Experiment design and statistical analysis were done using "Design Expert" (version 6.0.8, Stat-Ease Inc., Minneapolis, MN, U.S.A.) for evaluating the correlation between process parameters and cellulase loading (%) onto MHNTs as dependent and independent variables, respectively. The effect of selected parameters on final outcome, i.e., cellulase loading (%), was determined using Box-Behnken design (BBD) of the response surface methodology (RSM). The design was simplified by eliminating parameters that were not regarded as statistically significant ($P > 0.05$) by the analysis of variance (ANOVA). Based on preliminary experiments, three parameters, namely, amount of MHNTs, conc. of enzyme, and the pH of immobilization solution, were chosen as dependent variables (Supporting Information). The optimization studies for enzyme immobilization were performed by adding varied amounts of MHNTs (20−30 mg) and cellulase concentrations (1.25−1.75 mg·mL^{-1}) prepared in citrate buffer and maintaining at varied pH (4.5−5.5) as per the BBD experimental design (Table 1).

DOI: 10.1021/acssuschemeng.9b05400
ACS Sustainable Chem. Eng. 2020, 8, 900−913

Table 1. RSM Based Box-Behnken Experimental Design for Independent Variables and Their Corresponding Responses (% Enzyme Loading) for Cellulase Immobilization

run	amount of MHNTs (mg)	cellulase conc. (mg·mL^{-1})	solution pH	loading (%) actual	loading (%) predicted
1	25.00	1.25	5.50	72.82	72.04
2	25.00	1.50	5.00	79.82	78.14
3	20.00	1.50	4.50	77.35	76.38
4	25.00	1.25	4.50	70.31	70.34
5	25.00	1.50	5.00	78.64	78.14
6	20.00	1.50	5.50	72.38	72.19
7	25.00	1.50	5.00	77.97	78.14
8	25.00	1.75	4.50	67.78	68.57
9	20.00	1.25	5.00	74.83	75.81
10	25.00	1.50	5.00	78.02	78.14
11	25.00	1.75	5.50	65.68	65.71
12	25.00	1.50	5.00	76.27	78.14
13	30.00	1.50	5.50	80.48	81.45
14	30.00	1.25	5.00	79.87	79.68
15	20.00	1.75	5.00	69.78	69.97
16	30.00	1.50	4.50	78.24	78.43
17	30.00	1.75	5.00	78.39	77.42

Determining Enzyme Loading and Activity. The following equation was used to calculation the enzyme loading on the support matrix through the Bradford assay:[25]

$$\text{Enzyme loading (\%)} = \frac{C_0 - C}{C_0} \times 100 \quad (1)$$

$$\text{Enzyme loading (mg·g}^{-1}) = \frac{(C_0 - C)V}{W} \times 100 \quad (2)$$

Enzyme activity was calculated by measuring the endoglucanase activity of cellulase employing carboxymethyl cellulose (CMC) as substrate. The amount of reducing sugar released was determined spectrophotometrically at 540 nm using the dinitrosalicylic acid (DNSA) method as per standard protocol. One international unit (IU) of enzyme activity is defined as the amount of cellulase that hydrolyzes CMC to produce 1 μmol of glucose equivalents per minute under standard assay conditions. The catalytic activities of both free and immobilized enzymes carrying equivalent units (2.43 IU) were determined under an identical set of experimental conditions. For determining the effectiveness of immobilization, the release profile of cellulase from HNTs was continuously monitored over a period of 48 h, taking aliquots after predefined time intervals, and the amount of cellulase released was calculated.

Catalytic Activity: Impact of Process Parameters. A wide pH range (3−7) was selected to determine its impact on the catalytic potential of free and immobilized cellulase. Both enzyme forms were soaked separately in different pH buffers (0.1 M citrate buffer for pH range 3−5, 0.1 M phosphate buffer for pH 6−7) while stirring over the 30 min incubation period. Required aliquots were taken after a specific time duration, and their respective catalytic activities were calculated by the DNSA method as described earlier. Similarly, the effect of temperature (30−70 °C) on the activity of immobilized and free enzymes was also determined, keeping other conditions constant, i.e., citrate buffer, pH 5, and an incubation time of 30 min.

Thermal stability was evaluated by incubating an equal amount of free and immobilized enzyme to elevated temperatures (50−70 °C) while sample aliquots were withdrawn after different time intervals for the residual activity calculation. The storage abilities of the two forms of enzymes, free and immobilized (NBC), were determined by assessing their residual activity over 20 days of storage at 4 °C. Required aliquots were taken at specific intervals of time, and the activity assays were carried out. The activity during the first catalytic reaction was considered as 100%. The reuse potential of immobilized cellulase was determined under standard assay conditions. In brief, the equivalent units (6.07 IU) of cellulase enzyme, both in the free and in the immobilized form, were added separately to 50 mL of 1% (w/v) CMC solution for 6 h at 50 °C under continuous stirring at 120 rpm. After each cycle, the NBC was separated using a magnet, washed twice with storage buffer, and then resuspended in fresh CMC solution. The residual activity was determined after each cycle considering the catalytic activity to be 100% after the first cycle.

Kinetics and Thermodynamic Parameters of Cellulase Activity. The kinetic parameters of free and immobilized cellulase were determined by measuring the initial rate with varying substrate concentration (100−5000 μM). The k_M, V_{max}, and catalytic efficiency (V_{max}/k_M) values of free and immobilized cellulase were obtained from nonlinear regression fitting. For the estimation of thermodynamic parameters, thermal inactivation of cellulase was done by exposing the enzyme solution (both free and immobilized) in citrate buffer (100 mM, pH 5) at various temperatures i.e., 30 °C, 40 °C, 50 °C, 60 °C, and 70 °C, without adding substrate. Required aliquots were taken after desired time intervals, cooled on ice for 30 min, and were assayed for cellulase activity at 50 °C. The data fitted to first-order plot and thermodynamic characteristics (inactivation rate constants, half-life, and activation energy) of free and immobilized cellulase were calculated as given below:

$$\ln\left[\frac{A}{A_0}\right] = -k_d t \quad (3)$$

$$t_{1/2} = \frac{0.693}{k_d} \quad (4)$$

$$-\ln k_d = \frac{E_a}{R}\left[\frac{1}{T}\right] - \ln A \quad (5)$$

Based on the transition energy state model, the Eyring equation correlates enzyme catalysis with temperature for calculating Gibbs free energy, enthalpy, and entropy;

$$\Delta G = -RT \ln\left[\frac{hk_d}{k_B T}\right] \quad (6)$$

$$\Delta H = E_a - RT \quad (7)$$

$$\Delta S = \frac{\Delta H - \Delta G}{T} \quad (8)$$

Impact of the Ionic Liquid on Enzyme Inactivation. The impact of the ionic liquid (IL) on catalytic activity of both free and immobilized cellulase was investigated. 1-Butyl-3-methylimidazolium chloride ([bmim][Cl] was taken as the representative ionic liquid, well-known for lignocellulosic biomass pretreatments. [bmim][Cl] of various concentrations (5%, 10%, 20%, 30%, v/v) were prepared, onto which ∼6.07 equiv units of both free and immobilized cellulase were added separately and incubated for 3 h. The pH of the ionic liquid−enzyme suspension was maintained at 5 using citrate buffer. After the required incubation, the catalytic activities of both free cellulase and cellulase-MHNTs were evaluated. The residual activities (%) were reported considering the activities of free cellulase and the nanobiocatalyst (equivalent units) in the IL-free suspension to be 100%. Exhaustive studies were conducted against two substrates, CMC and extracted cellulose (sugar cane bagasse), under the tested conditions.

Analysis of Cellulose Saccharification. A 100 mL, 1% (w/v) CMC and cellulose extracted from bagasse were incubated separately with 12.14 equiv IU of free and immobilized cellulase preparations for 48 h at 50 °C with continuous shaking (120 rpm). The hydrolysis reactions using free enzyme under identical conditions were taken as the control. The amount of glucose produced after required time intervals was monitored using a glucose assay kit, and the cellulose saccharification (%) was calculated using the following equation:

DOI: 10.1021/acssuschemeng.9b05400
ACS Sustainable Chem. Eng. 2020, 8, 900−913

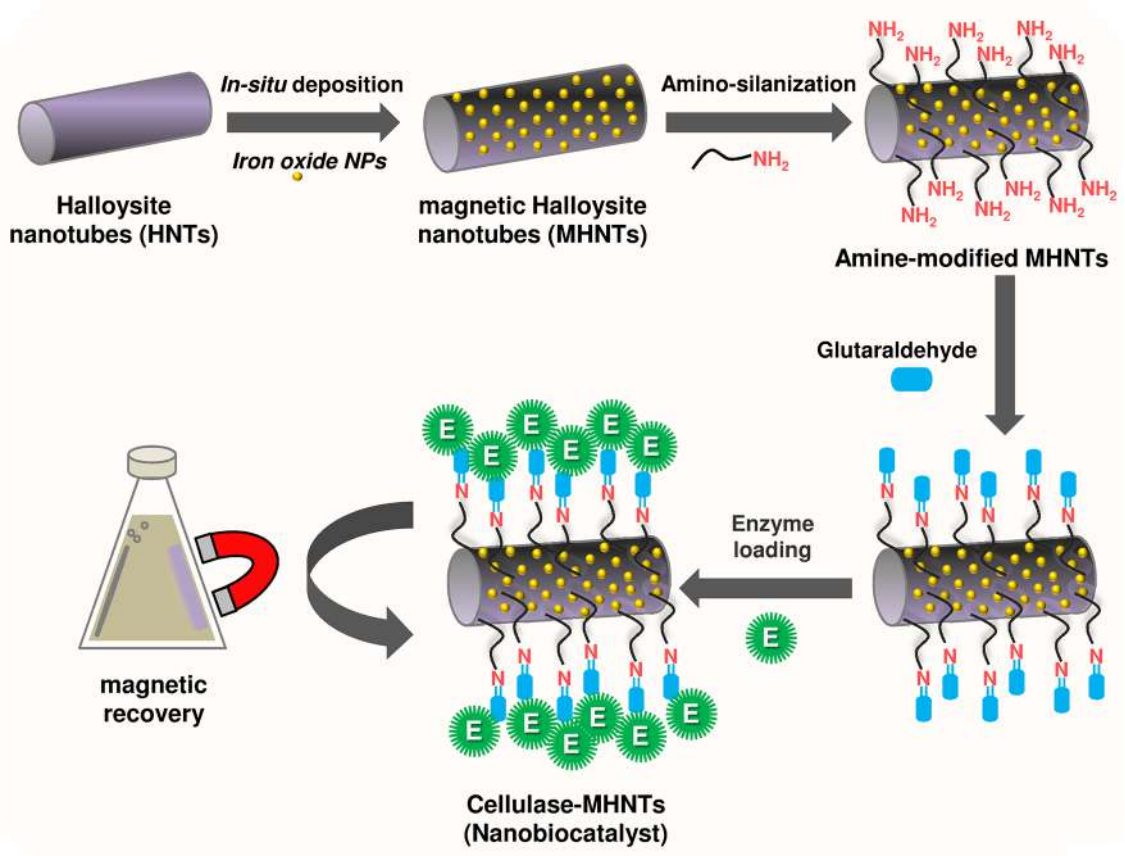

Figure 1. Representative illustration for immobilizing cellulase enzyme on to halloysite nanotubes as a template/matrix using aminosilane as a cross-linker. Prior to this, iron oxide nanoparticles were synthesized over halloysite nanotubes in concurrent with their deposition, rendering the nanobiocatalyst recoverable using a magnet.

$$\text{Saccharification (\%)} = \frac{\text{Sugar (g)} \times 0.89}{\text{Cellulose (g)}} \times 100\% \quad (9)$$

The hydrolyzed products of cellulose (20 μL injection volume) were also analyzed using high performance liquid chromatography (HPLC) equipped with an Aminex HPX-87H ion exclusion column (Bio-Rad Laboratories, U.S.A.) and a refractive index detector (PerkinElmer Series-200). Samples were eluted using a 0.6 mL·min^{-1} flow rate of 80% acetonitrile as the mobile phase. The chromatograms were fitted to an exponentially modified Gaussian function (TotalChrom Workstation) to obtain peak areas. Calibration curves were constructed from the peak areas of the standard solution.

RESULTS AND DISCUSSION

Development of Nanobiocatalyst (NBC). A schematic representation for developing a novel nanobiocatalyst via surface functionalization employing magnetic halloysite nanotubes (MHNTs) is shown in Figure 1. Interestingly, the choice of selecting nonporous HNTs as an immobilizing template warrants two important considerations. First, the exterior surface of HNTs offers a large surface area which can be modified undergoing specific surface chemistry. We have evidenced that uniform silanol (Si−OH) sites over silica-based materials can be transformed into much stronger siloxane (Si−O−Si) bonds through aminosilanization causing orientation of amine groups away from the surface.[21] In addition to this, a strong hydrogen bonding might also occur between amino groups of the organosilanes and silanol groups. Second, the nonporous nature of HNTs also ensures maximum interaction between the substrate (CMC) and immobilized enzyme, overcoming external mass transfer limitations in a manner its catalytic behavior would not be compromised. We also employed extracted cellulose (from sugar cane bagasse) as another substrate, though at a very low concentration of 1% (w/v). It is evidenced through this study that such a diluted cellulose suspension behaved similar to CMC in terms of its aqueous solubility. As a combined effect, the aminosilanization of magnetic HNTs facilitated a dense, multipoint anchoring of the enzyme that existed on their surface residues. The multipoint anchoring of the enzyme indicates a stronger interaction between the enzyme and the support matrix via cross-linking than its restriction, where the use of cross-linker can offer two basic advantages for immobilization. First, it may improve the stable anchoring of enzymes over a solid support while the arm space of a cross-linker would govern the mobility of the enzyme with the required flexibility to interact with the substrate molecules. The as developed nanobiocatalyst, i.e., cellulase immobilized MHNTs, was analyzed further through several characterization studies before employing it for biocatalytic experiments.

Analytical Characterizations. The variation in surface characteristics of HNTs after in situ anchoring of magnetic nanoparticles, APTES functionalization, and cellulase immobilization were initially assessed using FTIR spectroscopy over the range of 4000−400 cm^{-1} (Figure 2a). Peaks at 3701, 3623, 1032, and 911 cm^{-1} correspond to the characteristic vibrations of HNTs[26] where vibrational band near-infrared regions (<800) were ascribed to the Fe−O bond of iron oxide nanoparticles.[27] Grafting of APTES over MHNTs was

DOI: 10.1021/acssuschemeng.9b05400
ACS Sustainable Chem. Eng. 2020, 8, 900−913

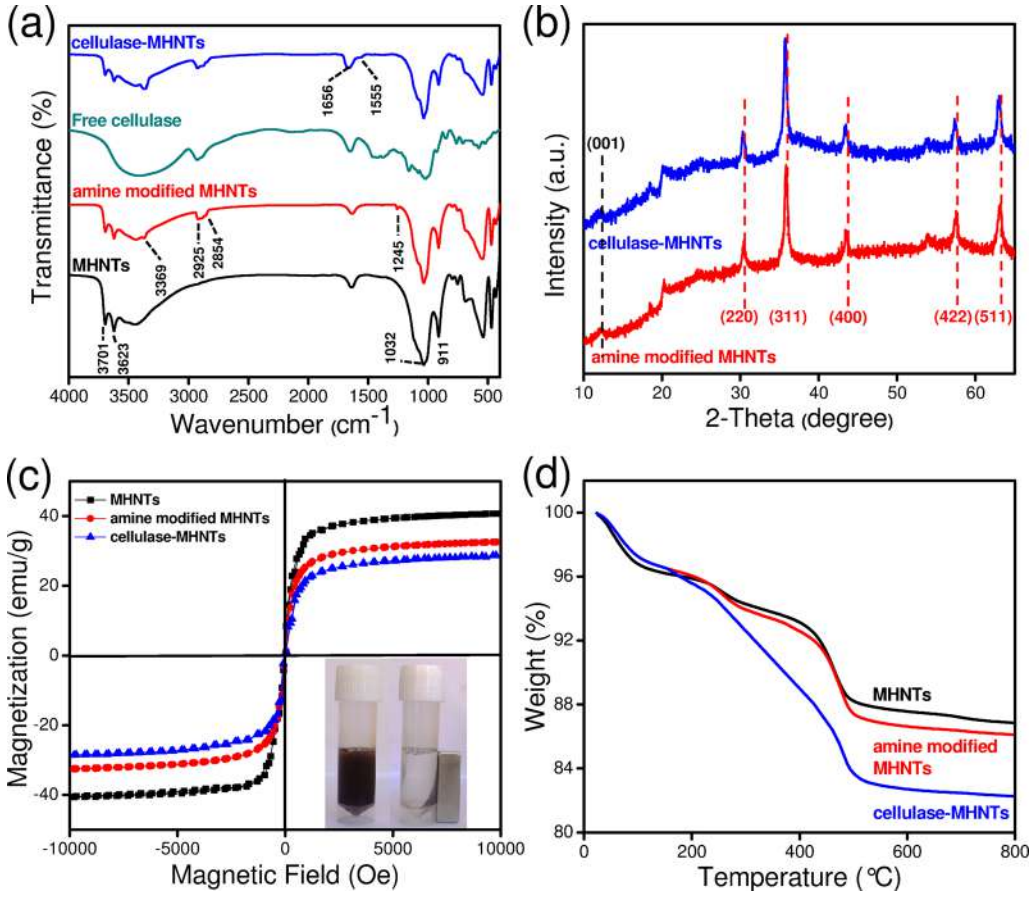

Figure 2. Characterization of various samples, i.e., magnetic HNTs before and after amine group modifications and after enzyme immobilization through (a) FTIR spectroscopy and (b) XRD analyses demonstrating its characteristic peaks and crystalline planes. (c) Magnetic hysteresis loops demonstrating the magnetization potential and (d) thermogravimetric analysis (TGA). Inset photographic image shows ease in separating the nanobiocatalyst from a colloidal suspension.

confirmed with peaks at 3369, 2925, 2854, and 1245 cm^{-1}, assigned to symmetric and asymmetric vibrations of N−H_2, C−H_2, C−H_2, and C−N bonds, respectively.[26] The FTIR spectra of the free cellulase enzyme depicted two characteristic peaks at 1600 and 3430 cm^{-1} due to the stretching vibrations of amide-I bands and amine groups, respectively.[3] The corresponding spectral vibrations of cellulase-MHNTs demonstrated hybrid characteristics of both cellulase and MHNTs, which is indicative of the successful anchoring of enzymes over MHNTs. It validates not only the fact that MHNTs retained their inherent structural integrity after immobilization but also that a stable binding of cellulase over the functionalized MHNTs matrix was also conferred in the resulting nanobiocatalytic system.[3]

To determine any changes either in the backbone structure or in the crystalline nature of the synthesized materials, XRD analyses were performed. As shown in Figure 2b, a 2θ peak at 12.21° was observed in functionalized MHNTs, before and after cellulase immobilization, which confirmed the existence of the nanotubular structure of the HNTs matrix. This peak is attributed to the (001) plane of the HNTs with basal spacing 0.724 nm (JCPDS Card No. 29-1487).[28,29] The incorporation of iron oxide nanoparticles was established by the presence of intrinsic peaks at 2θ = 30.43°, 35.78°, 43.47°, 57.46°, and 63.09°, which are attributed to (220), (311), (400), (422), and (511) planes of the magnetite Fe_3O_4 (JCPDS Card No. 01-075-0449). These observations confirm the presence of magnetic nanoparticles over the HNTs surface even after immobilizing the cellulase enzyme.[30] Nevertheless, the absence of any new peak in the spectra concludes that the loading of cellulase onto MHNTs did not alter the physicochemical characteristics of the HNTs matrix.

The magnetic behavior of all forms of MHNTs was investigated using the vibrating sample magnetometer where magnetization curves indicate sample magnetization in response to the applied magnetic field (Figure 2c). The amine-modified MHNTs, before and after enzyme immobilization, demonstrated the saturated values of magnetization as 32.54 and 28.68 emu·g^{-1}, respectively. This value along with zero coercivity and remanence represents their superparamagnetic nature. The unmodified MHNTs, however, showed a slightly higher saturated value of magnetization (40.68 emu·g^{-1}), which occurred due to the absence of nonmagnetic materials, i.e., aminosilane and cellulase enzyme. Despite this, the magnetic recovery of NBC was not at all compromised. Regardless of MHNTs forms, all samples were able to get separated from the reaction mixture using a simple magnet, as evident from the photographic image (inset). The relative proportion of iron oxide:HNTs was optimized in a way that the magnetic properties could be imported to HNTs just sufficient for their recovery, yet retaining the maximum surface area available for enzyme immobilization.

Thermogravimetric analyses (TGA) were performed to confirm the immobilization of cellulase over amine-modified

DOI: 10.1021/acssuschemeng.9b05400
ACS Sustainable Chem. Eng. 2020, 8, 900−913

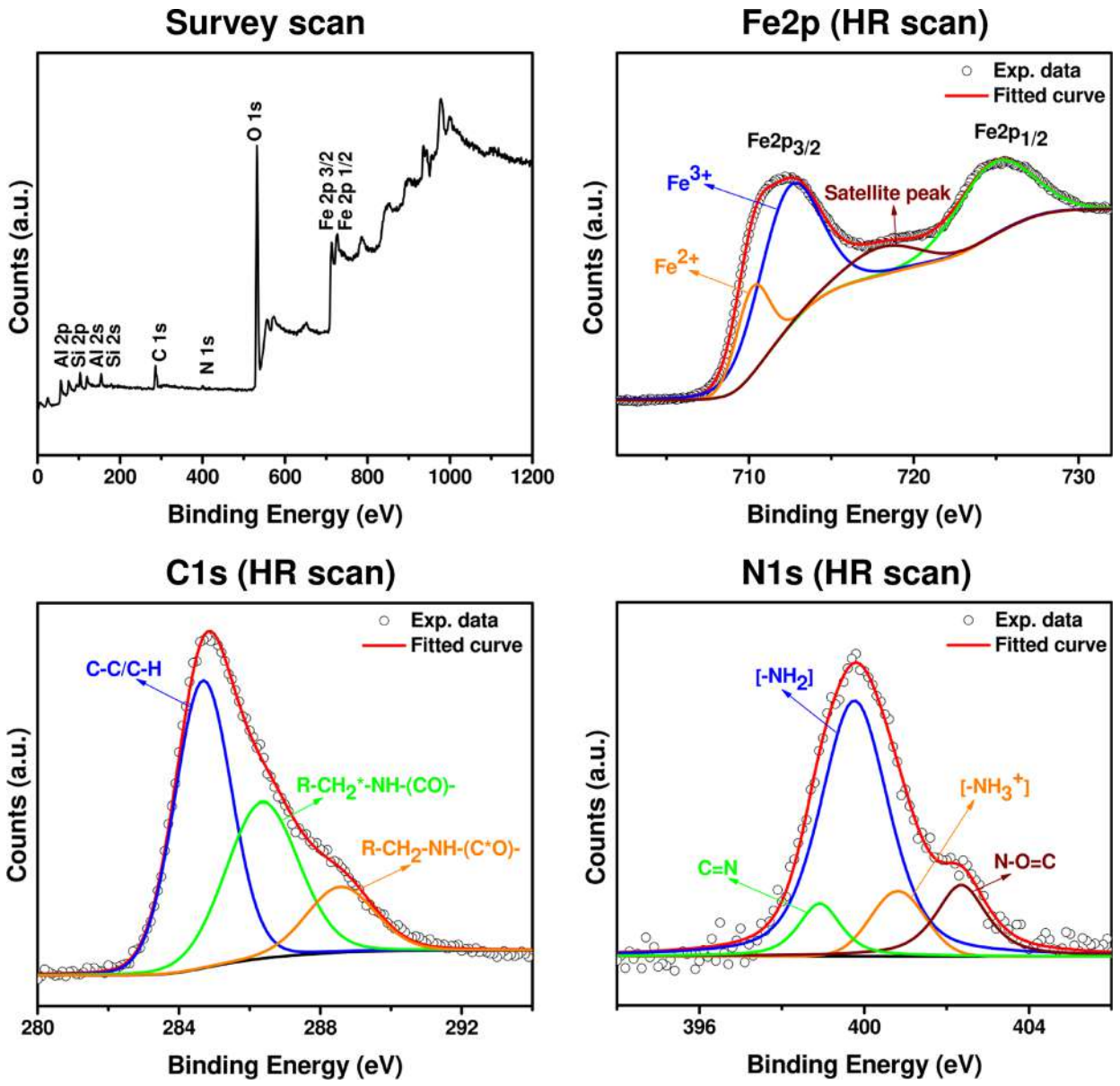

Figure 3. XPS spectral analysis of nanobiocatalyst, i.e., cellulase-MHNTs showing the survey scan and corresponding deconvoluted peaks in the high resolution (HR) spectra of the respective elements present, i.e., Fe (2p), C (1s), and N (1s).

MHNTs via glutaraldehyde cross-linking (Figure 2d). Pristine MHNTs sample (without amine-functionalization) was taken as a negative control. The thermogram profile of pristine MHNTs and amine-functionalized MHNTs exhibited almost a similar trend in weight loss until 480 °C, validating our FTIR and XRD analyses that the adopted immobilization protocol did not affect the overall structural integrity of MHNTs. A further increase in temperature up to 800 °C resulted in only 0.73% higher weight loss in amine-functionalized MHNTs as compared to its pristine counterpart, which is ascribed to the organosilane coating over MHNTs. On the contrary, the cellulase immobilized MHNTs depicted an ∼12.82% weight loss within the 150−500 °C temperature, which confirms the presence of cellulase binding over MHNTs.[30,31] A simple mass balance was applied for determining the immobilization efficiency of cellulase through UV−vis spectroscopy (Bradford assay), which matched well with that of TGA data.

X-ray photoelectron spectroscopy (XPS) is considered as one of the most sensitive techniques for evaluating the surface chemistry of nanomaterials. Figure 3 depicts a wide scan spectrum of the nanobiocatalyst (i.e., cellulose immobilized MHNTs), where the existence of binding energy peaks of Al (2s, 2p), Si (2s, 2p), C 1s, O 1s, Fe 2p, and N 1s are indicative of the successful anchoring of iron oxide NPs over HNTs, amine functionalization, and subsequent loading of cellulase enzyme. A high resolution spectrum of Fe,2p exhibits as two spin−orbit doublets at 712.18 eV (Fe $2p_{3/2}$) and 725.51 eV (Fe $2p_{1/2}$). The energy separation of 13.4 eV is a characteristics marker for a chemical shift difference between the Fe^{2+} and Fe^{3+} states present in Fe_3O_4 NPs.[32] A further deconvolution of the Fe spectra gave rise to two peaks in the Fe $2p_{3/2}$ spin orbit peak which are attributed to the existence of Fe^{2+} and Fe^{3+}. On the other side, the existence of a satellite peak between the Fe $2p_{3/2}$ and Fe $2p_{1/2}$ peaks is credited to the presence of a small amount of Fe_2O_3.[32] The obtained results are in good accord

DOI: 10.1021/acssuschemeng.9b05400
ACS Sustainable Chem. Eng. 2020, 8, 900−913

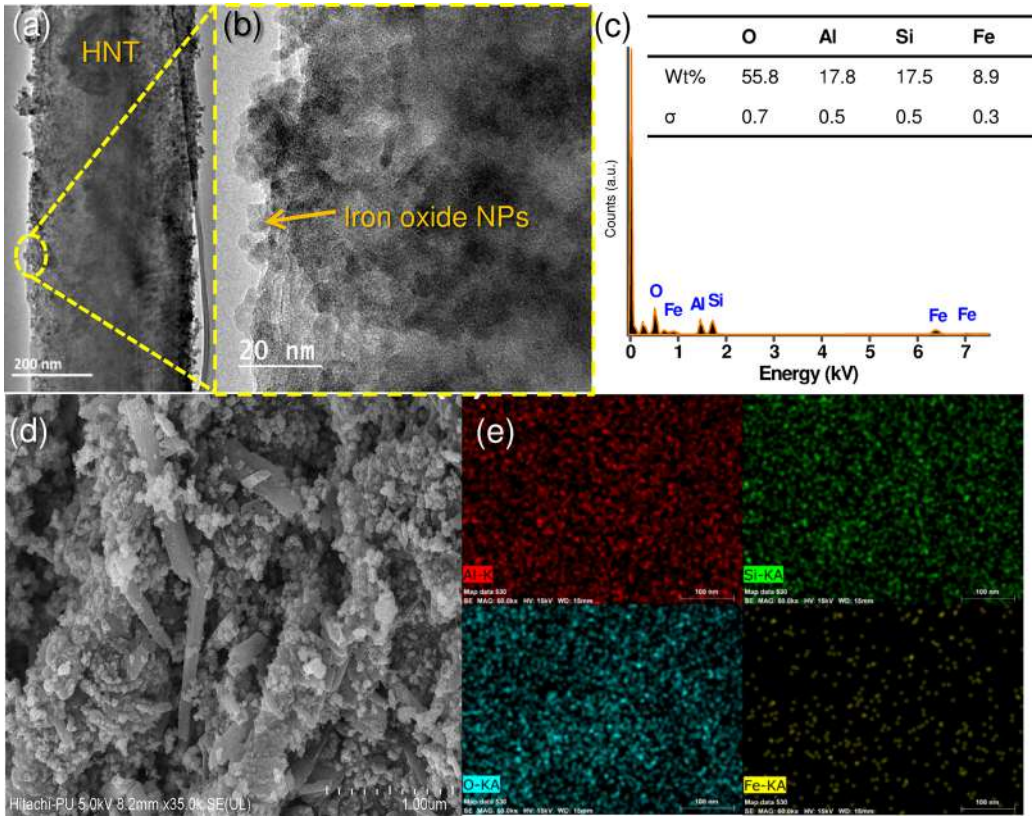

Figure 4. (a) TEM micrograph of a single halloysite nanotube showing densely decorated iron-oxide nanoparticles. (b) Corresponding high resolution TEM image evidenced a clear interface between iron oxide and HNTs. (c) EDS spectra confirming the existence of iron (Fe) in the nanobiocatalyst as demonstrated through its characteristic peaks along with other elements. (d) SEM micrograph of as synthesized cellulase-MHNTs nanobiocatalyst used for the cellulose hydrolysis. (e) Elemental mapping of the selected region confirms a uniform distribution of iron nanoparticles (Fe), while the presence of aluminum (Al), silicon (Si), and oxygen (O) was attributed to the inherent elemental composition of halloysite nanotubes.

with the previous reports, confirming the presence of Fe_3O_4 in the nanobiocatalyst.

In C 1s high resolution spectra, a peak centered at 284.6 eV is assigned to sp^2 hybridized carbon (C−C and C−H bonds).[33] This was further deconvoluted into two peaks at 286.3 and 288.5 eV, which can be ascribed to either R−CH_2*−NH−(CO)−/R−CH_2−NH−(C*O)− or the amide bonding (R−CONH−) group, respectively.[34] Since these functional moieties are the characteristic features of a protein's structures, we may confirm the loading of cellulase enzyme onto MHNTs matrices. In addition to this, a high resolution N 1s spectrum was deconvoluted into four distinct peaks that correspond to the C═N bond (398.9 eV),[35] amine group from APTES and cellulase (399.7 eV), hydrogen-bonded amine (H−NH_2) or protonated amine (400.8 eV), and N−O═C (402.3 eV).[36,37] The lower intensity of the protonated amine and high intensity of the NH_2 group peak endorses the high loading of cellulase, as the amine groups are pointing away from the substrate. The obtained data confirms the covalent immobilization of cellulase onto APTES functional groups via cross-linking with glutaraldehyde.

The structural morphology of functionalized MHNTs and enzyme loaded MHNTs was investigated by transmission electron microscopy. The HR-TEM image confirms the successful loading of iron oxide nanoparticles on the surface of HNTs, where a distinct interface between two nanoscale structures was observed (Figure 4a). This validates the fact that an in situ synthesis of magnetic nanoparticles and their subsequent immobilization was facilitated through a one-step protocol rendering the inherent morphology of HNTs intact even after loading iron oxide nanoparticles (Figure 4b). Energy-dispersive X-ray spectra confirmed the presence of iron along with the characteristic elements of HNTs (Figure 4c). The cellulase-MHNTs were investigated through FE-SEM where the cellulase enzyme was found to be densely anchored over amine-modified MHNTs with a high payload (Figure 4d). The intact morphology of HNTs was corroborated with the results obtained through XRD analyses. The corresponding elemental mapping further confirms the effective distribution of iron oxide nanoparticles throughout the sample (Figure 4e).

Optimization of Immobilization Parameters. Three independent factors, i.e., amount of MHNTs (mg), enzyme concentration (mg·mL^{-1}), and solution pH, which might affect the enzyme loading, were investigated as a prerequisite for process optimization. Single factor studies (Supplementary Information, Figure S1) depict that the loading (%) of enzyme was increased with increasing the amount of MHNTs since the availability of multiple anchoring sites over MHNTs facilitated more loading of enzymes. The enzyme loading (%) reached to its maximum value when the amount of MHNTs was increased to 30 mg. A significant reduction in catalytic activity of the cellulase was also manifested when the amount of MHNTs was increased beyond this value (Figure S2). Out of the selected parameters, solution pH showed the least impact on enzyme loading. However, the combinational influence of pH with other factors could not be predicted solely using single factor

DOI: 10.1021/acssuschemeng.9b05400
ACS Sustainable Chem. Eng. 2020, 8, 900−913

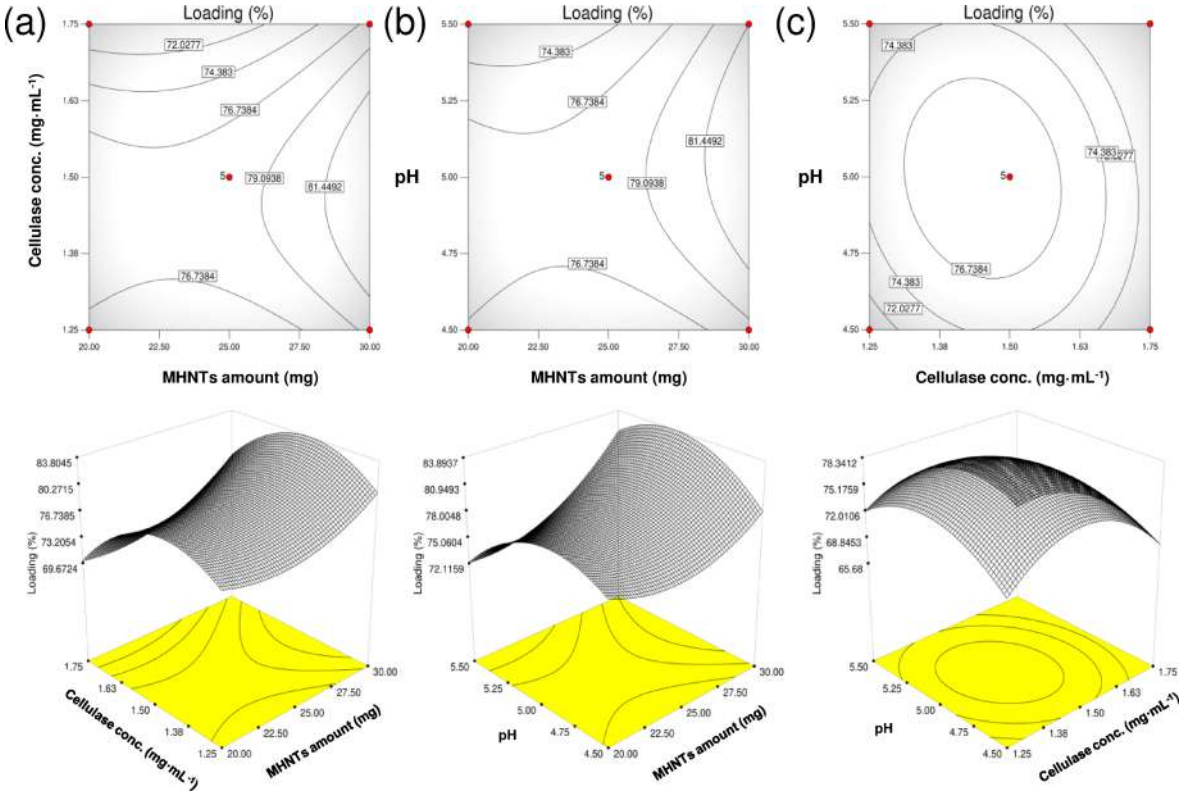

Figure 5. 3D response surface plots and 2D contour plots for analyzing the interaction effects between (a) cellulase conc. and amount of MHNTs (at constant 4.8 pH), (b) pH and amount of MHNTs (at constant 1.44 mg·mL^{-1} cellulase conc.), and (c) pH and cellulase conc. (at constant 20 mg of MHNTs amount).

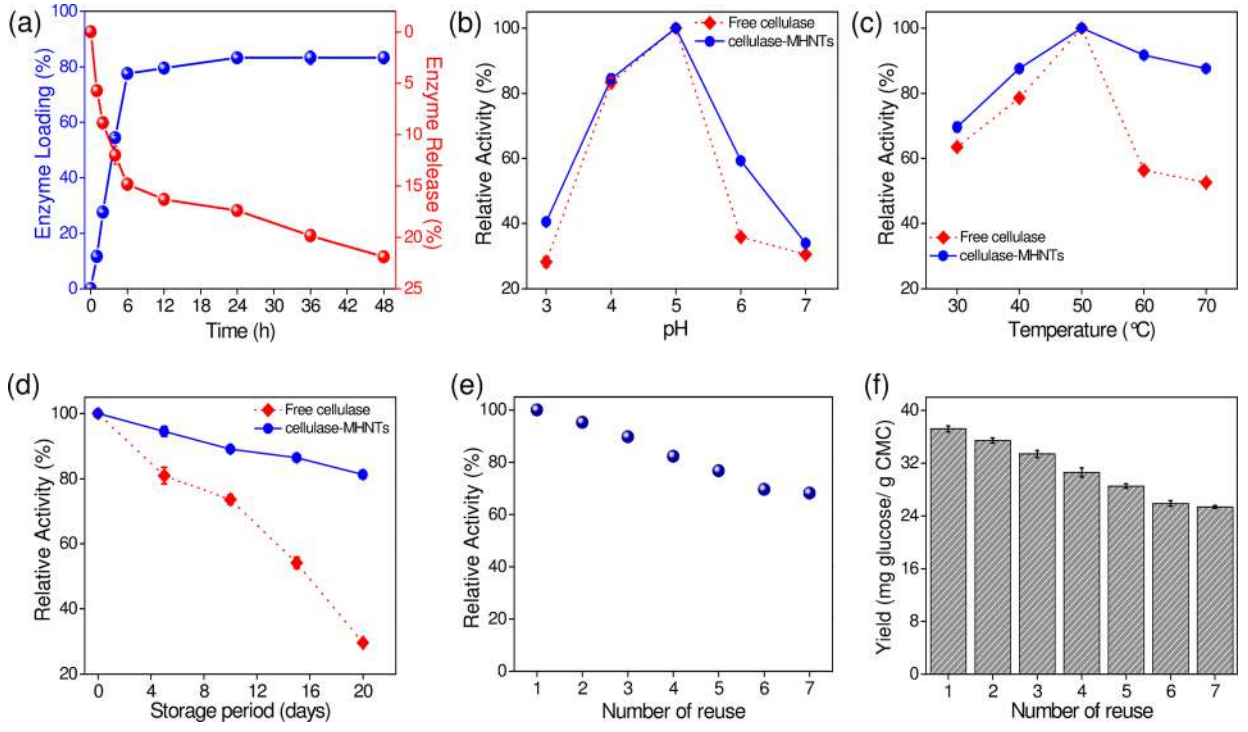

Figure 6. (a) Extent of enzyme loading and its subsequent release kinetics withstanding harsh process conditions over a 2 day period. The impact of two important factors, i.e., (b) solution pH and (c) working temperature, over a broad range of 30−70 °C, on catalytic activity was determined under optimized conditions. (d) The storage ability of cellulase at 4 °C (suspended in buffer) was tested over a three week period. (e) The variation in catalytic activity after every reuse over seven cycles and (f) corresponding yield of production of glucose (mg glucose·g^{-1} substrate) was evaluated. It is worth noting that the duration for each batch of biocatalytic reactions was of 6 h. All studies were performed in triplicate, and the mean value along with standard errors value are presented.

DOI: 10.1021/acssuschemeng.9b05400
ACS Sustainable Chem. Eng. 2020, 8, 900−913

studies. Therefore, a pH range from 4.50 to 5.50 was chosen to study the overall impact of pH along with other parameters on enzyme loading (%).

The operational ranges of independent parameters having a positive effect on the response, as obtained by single-factor studies, were statistically optimized employing response surface methodology, using Box-Behnken design (Table 1). Multiple regression analysis was done to resolve the polynomial coefficients for each term of the equation. The actual factors controlling the immobilization efficiency of cellulase over MHNTs and their combinational impact is represented in form of a regression equation as the following:

$$Y = -371.09675 - 9.64850A + 269.54600B + 147.25500C + 0.11077A^2 - 83.13200B^2 - 15.20300C^2 + 0.71400AB + 0.72100AC - 9.22000BC \quad (10)$$

where Y is enzyme loading(%) and A, B, and C are the amount of MHNTs (mg), conc. of cellulase enzyme (mg·mL^{-1}), and solution pH, respectively.

The significance of the predicted model was evaluated using Analysis of variance (ANOVA), which indicated this model to be highly significant (Table S2 and S3, Supporting Information). The model F-value (21.41) observed in Fisher's F-test confirmed the adequacy of the model for the selected parameters. A p-value of 0.0003 also signifies that the model accurately summarizes the relationship between selected factors and the response. The probability of error because of the noise was only 0.03%. The lack of fit of the F-value of 1.04 indicates this value to be insignificant relative to pure error. The multiple correlation coefficients (R^2), which measure the extent of variance from the model's mean value, indicated a close proximity among independent variables, viz., the amount of MHNTs, conc. of enzyme, and solution pH. R^2 value obtained from ANOVA was in accordance with the defined limit for the model to be effective.

Figure 5 demonstrates contour plots and 3-D surface graphical representations for the response generated, i.e., % enzyme loading. The response is represented as height in each of the 3D surface plots. The optimum conditions contributing toward maximum loading of enzyme onto MHNTs were as follows: 20 mg of NBC, 1.44 mg·mL^{-1} cellulase concentration, and 4.8 solution pH. The predicted model was validated by conducting the experiment at the optimum levels obtained from the BBD model. The model was further validated by carrying out the immobilization procedure under the optimized conditions, where a maximum immobilization of 77.52% was obtained, which was in good agreement with the model's predicted value (78.70%). The averages of three replicates were tested, and the mean values are reported.

Evaluation of Biocatalytic Characteristics. The impact of the amine functionalization of MHNTs over cellulase immobilization and its biocatalytic activity was correlated using release profile studies (Figure 6a). Under the given set of conditions, enzyme loading significantly increased with time until 6 h (77.5 ± 1.1%) and attained a maximum value of 83.2 ± 2.3% in 48 h. Interestingly, the biocatalytic activity of cellulase-MHNTs was marginally decreased to only 93.4% as compared to free cellulase. The corresponding release kinetics further revealed that ∼21.9% of total immobilized cellulase was released in the reaction system over a period of 48 h. Both results clearly show the effectiveness of the surface immobilization strategy without compromising its activity much. In fact, after immobilizing cellulase onto MHNTs, the nanobiocatalyst demonstrated heterogeneous catalysis, where the CMC substrate was easily accessible to the enzyme catalytic sites with insignificant external mass transfer limitations. After the enzymatic reaction, the resultant molecules rediffuse out of the catalytic templates as reaction products, i.e., glucose.

The influence of various process parameters on the catalytic performance of cellulase-MHNTs was determined and compared with free cellulase. Both free and immobilized cellulase showed distinct residual activities over a broad pH range (3−7) and the best activities at an optimal pH of 5. Varying pH from its optimum value, i.e., 6, adversely affected the activity of free cellulase (65% activity lost) while the nanobiocatalyst could be able to retain 60% of its catalytic activity under similar test conditions (Figure 6b). In a few recent reports, cellulase immobilization over styrene/maleic anhydride nanoparticles[38] and magnetic nanocomposites[39,40] has also witnessed a significant improvement in their pH dependent stability, similar to our work.

Similarly, the activity assays at varying temperatures (30−70 °C) revealed 50 °C as an optimal temperature for both forms of cellulase.[41] Increasing temperature to 60 °C lead to only 56.33% activity of free enzyme, whereas, the activity of immobilized cellulase was marginally reduced to 91.67% (Figure 6c). The cellulase-MHNTs could retain a minimum of ∼70% residual activity regardless of temperature variations (30−70 °C) which was likely due to the immobilization-induced heat resistance of enzymes. This was further verified by exposing both free cellulase and cellulase-MHNTs to 70 °C at pH 5 for 6 h. As expected, the residual activity of free cellulase was severely affected and reached to ∼12.63 ± 0.7% after 6 h. Whereas, immobilized cellulase could manage to retain ∼76.6 ± 0.5% activity within the similar time period. An improved thermal resistance of immobilized cellulase confirmed their stability under high temperature, which can be exploited for utilization under harsh processing conditions.

Considering the fact that the majority of free enzymes fail to retain their catalytic activity after being stored for long durations, it would be interesting to compare the residual activities of cellulase existing in different states by storing it at 4 °C for 20 days. As depicted from Figure 6d, while free cellulase could retain only 29.6% of its initial activity, the NBC retained 81.2% activity even after 20 days of storage. Interestingly, the activity of free cellulase decreased sharply after 10 days and became even lower in the following days while cellulase-HNTs displayed a linear trend in % activity loss, much lower than the former one. These observations again supported our hypothesis that a multipoint anchoring of enzymes with amine-modified HNTs surface not only allowed an easy access of substrate to the active sites of immobilized enzyme but also offered them even more flexibility and robustness to withstand harsh processing conditions. Even if the covalent binding of cellulase causes lowering in their kinetic values (k_M and V_{max}), immobilized cellulase would still be advantageous in terms of its affordability, reusability, and potential efficiency.

Reusability performance of the NBC was tested over seven repeated cycles under the optimized conditions. A total of 216.34 mg glucose·g^{-1} CMC was produced using the nanobiocatalyst over seven batches which is ∼5.8 fold as obtained through unsupported cellulase. Although results

DOI: 10.1021/acssuschemeng.9b05400
ACS Sustainable Chem. Eng. 2020, 8, 900−913

suggest a loss in catalytic performance of the NBC after every usage, still ~68.2% of the initial activity could be retained after the seventh cycle (Figure 6e). Corresponding glucose production also depicted a marginal reduction from 37.2 to 25.4 mg glucose·g^{-1} CMC after the first to seventh uses (Figure 6f). Although, the loss of material could be a major cause for lowering in the biocatalytic activity of the enzyme over repeated usage, we were able to recover the nanobiocatalyst over 99% on a mass balance basis. Further, no significant release of cellulase enzyme was detected into the solution within 6 h after repeated use. Hence, a reduction in the catalytic activity of immobilized cellulase was more likely due to the enzyme inactivation mechanisms over repeated cycles, as demonstrated elsewhere.[42]

Kinetic and Thermodynamics Parameters. The kinetic parameters (k_M, V_{max}, and catalytic efficiency) of cellulose hydrolysis employing free cellulase and cellulase-MHNTs were tested separately treating a wide range of substrate concentrations (100−5000 μM). Free and immobilized enzymes both obeyed the Henri−Michaelis−Menten kinetics model (Figure S3). The apparent K_M of cellulase-MHNTs was slightly higher (1423 μM) than that of free cellulase (1288 μM) which is likely due to the lower affinity of enzymes toward the substrate after immobilization (Table 2). It is evidenced that the diffusion limitations of the substrate near close vicinity of the immobilized enzyme and/or localized conformational changes at the active sites of enzyme would be the responsible causes for the increase in the k_M value.[43,44] However, a proportionate increase in k_M values of the enzyme after immobilization onto nanomaterials was found to be much lower as reported in other studies.[3,39,44,45] This can be ascribed to the efficient loading of enzyme and high specific surface area of MHNTs which minimized any changes in structural conformations and/or mass transfer constraints. Similarly, no significant variation in V_{max} values was observed before (10.1 μM·min^{-1}) and after immobilizing cellulase (11.7 μM·min^{-1}). It was established that the microenvironment near immobilized enzymes would have an unnoticeable impact on overall catalytic activity of the NBC. Further, the catalytic efficiency (V_{max}/ k_M) of the nanobiocatalyst was increased by 5% more than that of the free cellulase at 50 °C.

Table 2. Summary of Variation in Kinetics and Thermodynamic Parameters before and after Immobilizing Cellulase Enzyme onto Magnetic HNTs

parameters[a]	free cellulase	cellulase-MHNTs (nanobiocatalyst)
k_M (μM)	1280 (R^2 = 0.9822)	1423 (R^2 = 0.9776)
V_{max} (μM·min^{-1})	10.1	11.7
catalytic efficiency	7.8 × 10^{-3}	8.2 × 10^{-3}
k_d (h^{-1})	0.080	0.025
half-life, $t_{1/2}$ (h)	8.67	26.75
Q_{10}	1.47	1.39
E_a (kJ·mol^{-1})	28.11	28.14
ΔH (kJ·mol^{-1})	25.42	25.45
ΔG (kJ·mol^{-1})	108.14	111.17
ΔS (J·mol^{-1}·K^{-1})	255.98	265.25

[a]All parameters were evaluated at 50 °C, i.e., optimum working temperature.

While analyzing the kinetics−temperature profiles over a broad range (30−70°C), the thermodynamic parameters of irreversible thermal inactivation of both forms of cellulase were monitored (Figure 7a). At optimal temperature (50 °C), the values of activation energy (E_a), enthalpy change (ΔH), Gibbs free energy change (ΔG), and entropy change (ΔS) were obtained as 28.11 kJ·mol^{-1}, 25.42 kJ·mol^{-1}, 108.14 kJ·mol^{-1}, and 255.98 J·mol^{-1}·K^{-1}, respectively for free cellulase, whereas, the corresponding values for immobilized cellulase-MHNTs were found to be 28.14 kJ·mol^{-1}, 25.45 kJ·mol^{-1}, 111.17 kJ·mol^{-1}, and 265.25 J·mol^{-1}·K^{-1} (Table 2). Interestingly, similar E_a and ΔG parameters indicate that cellulase-HNTs requires almost the same amount of free energy (ΔG) to form the transition state as with free cellulase enzyme (Figure 7b). It implies that the immobilized nature of cellulase marked no significant impact in energy requirements by native cellulase to catalyze cellulose saccharification. An increase in the ΔS value after immobilization could be indicative of the increasing order of randomness at the nanobio interface of the nanobiocatalyst.

Ionic Liquid Tolerance Potential of Cellulase Enzyme. Ionic liquid (IL) based pretreatments have been established as an integrated technology in contemporary methods for recovering cellulosic components and their possible conversion into other value-added products.[46] Although such strategies seem effective in solubilizing cellulose to a large extent, the presence of even a trace amount of ILs creates unfavorable conditions for enzymatic hydrolysis, rendering those pretreat-

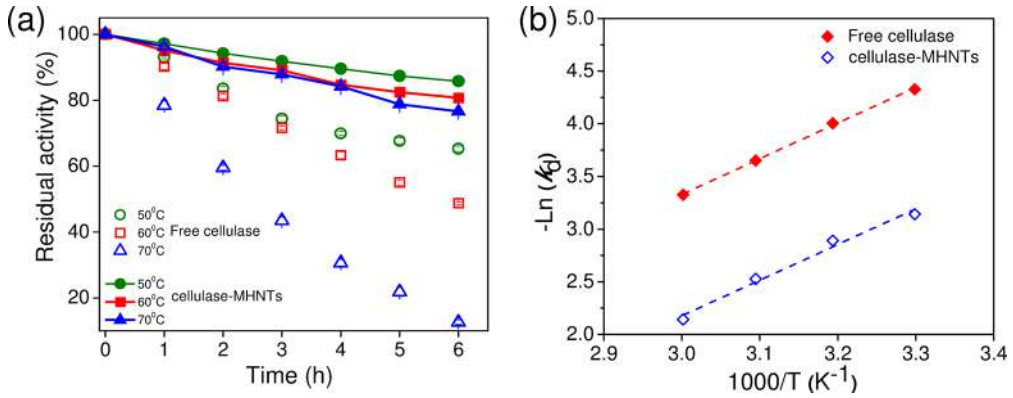

Figure 7. (a) Relative thermal inactivation of two forms of enzyme (free cellulase vs cellulase-MHNTs) when exposed to elevated temperatures 50 °C, 60 °C, and 70 °C. (b) Arrhenius plot to calculate the thermodynamic parameters for irreversible thermal inactivation of cellulase before and after immobilization.

DOI: 10.1021/acssuschemeng.9b05400
ACS Sustainable Chem. Eng. 2020, 8, 900−913

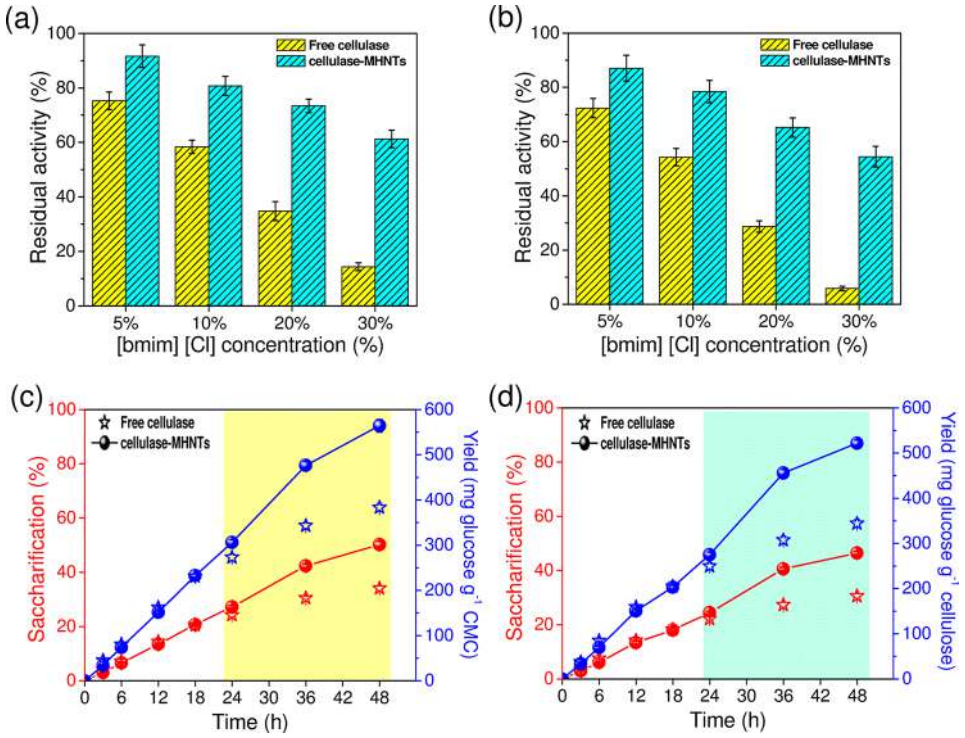

Figure 8. Residual enzyme activities (%) of both free and immobilized cellulase were tested against varying ionic-liquid concentrations ([bmim][Cl], 5−30% (v/v)) using (a) CMC and (b) cellulose extracted from the lignocellulosic biomass (i.e., sugar cane bagasse) as two representative sources of cellulose. Further, the extent of hydrolysis (i.e., saccharification %) and glucose yield were also determined against (c) CMC and (d) extracted cellulose using immobilized cellulase. The shaded portion indicates the time period where cellulase-MHNTs started displaying a predominated impact on both cellulose saccharification and glucose yield compared with its free form during a continuous operation of 48 h. Corresponding data pertaining to free cellulase enzyme is presented as a control in all studies for comparison.

ment strategies incompatible for further downstream processing.[47] Considering this as a challenge, we also tried to elucidate the commercial viability of cellulase-MHNTs in industrial bioprocesses hypothesizing its IL-tolerant ability as compared to free cellulase suspensions. Regardless of the substrate employed, i.e., CMC and cellulose extracted from sugar cane bagasse, the cellulase-MHNTs demonstrated an improved ionic liquid tolerant ability over free cellulase under all the tested conditions. In the case of CMC as a substrate (Figure 8a), free cellulase rapidly lost its residual activity from 75.2 ± 3.2% to 14.3 ± 1.4%, i.e., ∼5.2-fold while increasing the concentration of [bmim][Cl] from 5 to 30% (v/v), whereas, cellulase-MHNTs depicted much higher stability and their residual activity was reduced from 91.6 ± 4.1% to 61.2 ± 3.1% under similar conditions. A similar trend was observed when CMC substrate was replaced with the cellulose extracted from bagasse, where the immobilized enzyme retained half of its activity while the activity of free enzyme was adversely affected and came down to only 5.8% (Figure 8b). It was clearly observed that the cellulase-MHNTs manifested a much superior catalytic activity at higher concentrations of ionic liquid ([bmim][Cl], ≥10% v/v) than free cellulase for hydrolyzing either CMC or the extracted cellulose. The presence of two different sources of cellulose did not affect the hydrolytic potential of cellulase-MHNTs at the corresponding [bmim][Cl] concentrations, which confirms that the catalytic activity of immobilized cellulase was not significantly compromised. Rather, immobilized cellulase appeared to be more shielded than its free form, where the presence of the support matrix, i.e., HNTs, could have contributed to improve its tolerant ability against harsh processing of IL treatments. Based on this study, [bmim][Cl] ionic liquid could be a promising pretreatment solvent for rapid cellulose hydrolysis, which marked less influence on enzyme inactivation, particularly using the cellulase-MHNTs system.

Cellulase Saccharification Using Nanobiocatalyst. To determine the practical affordability utilizing this nanobiocatalyst, an operational study was attempted to evaluate the continuous hydrolysis of CMC, as a model substrate over a long duration. Although an increase in reducing sugars (i.e., product) in the hydrolysate is known to elicit inhibitory effects on cellulase activity,[48] we still could be able to run this saccharification process over 48 h without any adverse response. As shown in Figure 8c, the extent of CMC hydrolysis (% saccharification) could be achieved to nearly 50.2% in 48 h with a glucose yield of 0.56 ± 0.1 g glucose·g^{-1} CMC. The production of glucose was calculated to be 5.64 g·L^{-1} with 1% CMC as substrate. We obtained better results in comparison to an earlier report where cellulase immobilized onto colloidal magnetic nanoparticles catalyzed the hydrolysis of cellulose with 5.5 g·L^{-1} production of glucose with 10% substrate in 24 h.[49] Those authors claimed no further increase in either cellulose hydrolysis or glucose productivity beyond 24 h, thus limiting their long-term applicability. Another study also evidenced that only up to a maximum of 45.3% saccharification could be achieved with ∼2.3 g·L^{-1} glucose production in 24 h, while no change was observed even after introducing another batch of immobilized enzymes in the reaction mixture.[50]

We further evaluated the efficacy of cellulase-MHNTs, the nanobiocatalytic system in converting a nonfeed, lignocellulosic biomass into an edible biochemical product, i.e., glucose. Cellulose, extracted from agro-waste residues (sugar cane

DOI: 10.1021/acssuschemeng.9b05400
ACS Sustainable Chem. Eng. 2020, 8, 900−913

bagasse), was chosen as the substrate, which was hydrolyzed using NBC under identical conditions as mentioned in case with CMC. Figure 8d shows that changing the source of the substrate from CMC to cellulosic biomass did not affect the biocatalytic potential of cellulase-MHNTs where a maximum of 46.5% saccharification with 521.9 mg glucose·g^{-1} cellulose (glucose yield) could be achieved over 48 h of continuous run. As evident from Figure 8d, the glucose yield decreased from 144.24 mg·g^{-1} to 76.21 mg·g^{-1} during the first and the last quarter of reaction time, respectively. A decrease in glucose yield can be attributed to enzyme inactivation due to the prolonged exposure to reaction mixture constituents. Moreover, the impact of other factors such as substrate depletion, product inhibition,[51] and recalcitrant nature of the extracted cellulose[52] cannot be ignored, which could have also contributed toward decline in glucose yield. Since a longer run of the process beyond 48 h might have resulted in even further reduction in glucose yield per unit time, the nanobiocatalyst was recovered after 48 h of continuous run. Together, these findings provide compelling evidence that an improved glucose yield using nanobiocatalyst was an outcome of the enhanced saccharification of insoluble cellulose into soluble glucose, where the impact of enzyme inactivation due to reaction conditions was minimized. This appeared to be a feasible strategy achieving high-cellulose hydrolysis concurrent with yielding high production of glucose, particularly using lignocellulosic biomass. Glucose determination using HPLC and standard assay kits also confirmed the absence of other soluble cellooligomers (i.e., cellobiose/cellotrioses) in hydrolysate. Summarizing this, we validate our hypothesis where a dense immobilization of cellulase on to MHNTs was anticipated to facilitate maximum cellulose−cellulase interactions without mass transfer limitations concurrent with its high conversion into glucose hydrolysate.

CONCLUSIONS

Cellulose hydrolysis is among the most effective strategies for the sustainable biotransformation of lignocellulosic biomass into value added products. We attempted to develop a novel tool for biocatalytically converting cellulose into glucose with high yield and saccharification via magnetically separable halloysite nanotubes (MHNTs) as an immobilization matrix. Statistical optimization of the immobilization process enabled lower enzyme dosage for achieving higher catalytic yield, thereby avoiding the loss of an extra load of enzyme and making the process cost-effective. Structural characterization confirmed the successful loading of cellulase onto MHNTs without losing their biocatalytic activity. Rather, the support matrix imparted enhanced stability, thermal resistance, and activity to immobilized cellulase as compared to its unsupported form. The magnetic nature of NBC enabled separating it from the reaction mixture after completion of the reaction. An excellent catalytic activity at elevated temperatures, ionic liquid-tolerant characteristics, hydrolyzation continuously over longer durations, and eco-friendly attributes make the cellulase-MHNTs amenable for high cellulose conversion. Conclusively, the nanobiocatalytic material developed using magnetic HNTs is highly attractive for immobilizing a variety of other proteins for commercial purposes.

ASSOCIATED CONTENT

Supporting Information

The Supporting Information is available free of charge at https://pubs.acs.org/doi/10.1021/acssuschemeng.9b05400.

Materials required, characterization, statistical optimization using RSM, single factor study (Figure S1), relation between support matrix amount and enzyme activity (Figure S2), Lineweaver−Burk plot (Figure S3), Box−Behnken statistical experiment design (Table S1), ANOVA table of RSM (Table S2), coefficients of determination table of RSM (Table S3), and comparative details of cellulase immobilization on to nanomaterials (Table S4) (PDF)

AUTHOR INFORMATION

Corresponding Author

*(S.A.) E-mail: shekhar.agnihotri@thapar.edu. Tel.: +91-99200-32558.

ORCID

Shekhar Agnihotri: 0000-0003-1156-9369

Funding

This work was financially supported by Department of Science and Technology, India (DST-SERB), under the project Grant YSS/2015/001599, dated March 23, 2016, in Engineering Sciences. D.S. extends his grateful thanks to DST-SERB for the financial assistantship as JRF and SRF.

Notes

The authors declare no competing financial interest.

NOMENCLATURE

A	residual enzymatic activity (μmol glucose min^{-1}·mg^{-1} protein)
A_0	initial enzymatic activity (μmol glucose min^{-1}·mg^{-1} protein)
C_0	concentration of protein in initial suspension (mg·mL^{-1})
C	concentration of protein in final suspension (mg·mL^{-1})
E_a	Energy of thermal inactivation (J·mol^{-1})
H	Plank constant, 6.626×10^{-34} J·s
k_B	Boltzmann's constant, 1.381×10^{-23} J·K^{-1}
k_d	inactivation rate constant (h^{-1})
k_M	Michaelis−Menten constant (μM)
Q_{10}	temperature coefficient
R	universal gas constant (8.314 J·mol^{-1}·K^{-1})
T	absolute temperature (K)
T	time (h)
$t_{1/2}$	enzyme's half-life (h)
V	working volume of reaction (mL)
W	amount of HNTs used (g)
ΔG	Gibbs free energy change
ΔH	enthalpy change
ΔS	entropy change

REFERENCES

(1) Kong-Win Chang, J.; Duret, X.; Berberi, V.; Zahedi-Niaki, H.; Lavoie, J.-M. Two-step thermochemical cellulose hydrolysis with partial neutralization for glucose production. *Front. Chem.* **2018**, *6* (117), 1−11.

(2) Huang, Y.-B.; Fu, Y. Hydrolysis of cellulose to glucose by solid acid catalysts. *Green Chem.* **2013**, *15* (5), 1095−1111.

(3) Khoshnevisan, K.; Bordbar, A.-K.; Zare, D.; Davoodi, D.; Noruzi, M.; Barkhi, M.; Tabatabaei, M. Immobilization of cellulase enzyme on

DOI: 10.1021/acssuschemeng.9b05400
ACS Sustainable Chem. Eng. 2020, 8, 900−913

superparamagnetic nanoparticles and determination of its activity and stability. *Chem. Eng. J.* **2011**, *171* (2), 669−673.
(4) Zang, L.; Qiu, J.; Wu, X.; Zhang, W.; Sakai, E.; Wei, Y. Preparation of magnetic chitosan nanoparticles as support for cellulase immobilization. *Ind. Eng. Chem. Res.* **2014**, *53* (9), 3448−3454.
(5) Yang, B.; Dai, Z.; Ding, S.-Y.; Wyman, C. E. Enzymatic hydrolysis of cellulosic biomass. *Biofuels* **2011**, *2* (4), 421−449.
(6) Hanefeld, U.; Gardossi, L.; Magner, E. Understanding enzyme immobilisation. *Chem. Soc. Rev.* **2009**, *38* (2), 453−468.
(7) Verma, M. L.; Puri, M.; Barrow, C. J. Recent trends in nanomaterials immobilised enzymes for biofuel production. *Crit. Rev. Biotechnol.* **2016**, *36* (1), 108−119.
(8) Cipolatti, E. P.; Valerio, A.; Henriques, R. O.; Moritz, D. E.; Ninow, J. L.; Freire, D. M.; Manoel, E. A.; Fernandez-Lafuente, R.; de Oliveira, D. Nanomaterials for biocatalyst immobilization−state of the art and future trends. *RSC Adv.* **2016**, *6* (106), 104675−104692.
(9) Secundo, F. Conformational changes of enzymes upon immobilisation. *Chem. Soc. Rev.* **2013**, *42* (15), 6250−6261.
(10) Singh, S.; Tuteja, S. K.; Sillu, D.; Deep, A.; Suri, C. R. Gold nanoparticles-reduced graphene oxide based electrochemical immunosensor for the cardiac biomarker myoglobin. *Microchim. Acta* **2016**, *183* (5), 1729−1738.
(11) Agnihotri, S.; Sillu, D.; Sharma, G.; Arya, R. K. Photocatalytic and antibacterial potential of silver nanoparticles derived from pineapple waste: process optimization and modeling kinetics for dye removal. *Appl. Nanosci.* **2018**, *8* (8), 2077−2092.
(12) Agnihotri, S.; Dhiman, N. K., Development of nano-antimicrobial biomaterials for biomedical applications. In *Advances in Biomaterials for Biomedical Applications*; Tripathi, A., Melo, J. S., Eds.; Springer: Singapore, 2017; pp 479−545, DOI: 10.1007/978-981-10-3328-5_12.
(13) Agnihotri, S.; Mukherji, S.; Mukherji, S. Size-controlled silver nanoparticles synthesized over the range 5−100 nm using the same protocol and their antibacterial efficacy. *RSC Adv.* **2014**, *4* (8), 3974−3983.
(14) Agnihotri, S.; Mukherji, S.; Mukherji, S. Impact of background water quality on disinfection performance and silver release of immobilized silver nanoparticles: Modeling disinfection kinetics, bactericidal mechanism and aggregation behavior. *Chem. Eng. J.* **2019**, *372*, 684−696.
(15) Zdarta, J.; Meyer, A. S.; Jesionowski, T.; Pinelo, M. Developments in support materials for immobilization of oxidoreductases: A comprehensive review. *Adv. Colloid Interface Sci.* **2018**, *258*, 1−20.
(16) Ahmad, R.; Sardar, M. Enzyme immobilization: an overview on nanoparticles as immobilization matrix. *Biochem. Anal. Biochem.* **2015**, *4* (2), 1.
(17) Ghadiri, M.; Chrzanowski, W.; Rohanizadeh, R. Biomedical applications of cationic clay minerals. *RSC Adv.* **2015**, *5* (37), 29467−29481.
(18) Chauhan, A.; Sillu, D.; Agnihotri, S. Removal of pharmaceutical contaminants in wastewater using nanomaterials: A comprehensive review. *Curr. Drug Metab.* **2019**, *20* (6), 483−505.
(19) Dhiman, N.; Agnihotri, S.; Shukla, R., Silver-based polymeric nanocomposites as antimicrobial coatings for biomedical applications. In *Nanotechnology in Modern Animal Biotechnology*; Singh, S., Maurya, P., Eds.; Springer: Singapore, 2019; pp 115−171, DOI: 10.1007/978-981-13-6004-6_4.
(20) Tully, J.; Yendluri, R.; Lvov, Y. Halloysite clay nanotubes for enzyme immobilization. *Biomacromolecules* **2016**, *17* (2), 615−621.
(21) Agnihotri, S.; Mukherji, S.; Mukherji, S. Immobilized silver nanoparticles enhance contact killing and show highest efficacy: elucidation of the mechanism of bactericidal action of silver. *Nanoscale* **2013**, *5* (16), 7328−7340.
(22) Gokhale, A. A.; Lu, J.; Lee, I. Immobilization of cellulase on magnetoresponsive graphene nano-supports. *J. Mol. Catal. B: Enzym.* **2013**, *90*, 76−86.
(23) Xu, J.; Sheng, Z.; Wang, X.; Liu, X.; Xia, J.; Xiong, P.; He, B. Enhancement in ionic liquid tolerance of cellulase immobilized on PEGylated graphene oxide nanosheets: application in saccharification of lignocellulose. *Bioresour. Technol.* **2016**, *200*, 1060−1064.
(24) Mubarak, N.; Wong, J.; Tan, K.; Sahu, J.; Abdullah, E.; Jayakumar, N.; Ganesan, P. Immobilization of cellulase enzyme on functionalized multiwall carbon nanotubes. *J. Mol. Catal. B: Enzym.* **2014**, *107*, 124−131.
(25) Bradford, M. M. A rapid and sensitive method for the quantitation of microgram quantities of protein utilizing the principle of protein-dye binding. *Anal. Biochem.* **1976**, *72* (1−2), 248−254.
(26) Yuan, P.; Southon, P. D.; Liu, Z.; Green, M. E.; Hook, J. M.; Antill, S. J.; Kepert, C. J. Functionalization of halloysite clay nanotubes by grafting with γ-aminopropyltriethoxysilane. *J. Phys. Chem. C* **2008**, *112* (40), 15742−15751.
(27) Xie, Y.; Qian, D.; Wu, D.; Ma, X. Magnetic halloysite nanotubes/iron oxide composites for the adsorption of dyes. *Chem. Eng. J.* **2011**, *168* (2), 959−963.
(28) Kumar-Krishnan, S.; Hernandez-Rangel, A.; Pal, U.; Ceballos-Sanchez, O.; Flores-Ruiz, F.; Prokhorov, E.; De Fuentes, O. A.; Esparza, R.; Meyyappan, M. Surface functionalized halloysite nanotubes decorated with silver nanoparticles for enzyme immobilization and biosensing. *J. Mater. Chem. B* **2016**, *4* (15), 2553−2560.
(29) Zhang, Y.; He, X.; Ouyang, J.; Yang, H. Palladium nanoparticles deposited on silanized halloysite nanotubes: synthesis, characterization and enhanced catalytic property. *Sci. Rep.* **2013**, *3* (2948), 1−6.
(30) Kadam, A. A.; Jang, J.; Lee, D. S. Supermagnetically tuned halloysite nanotubes functionalized with aminosilane for covalent laccase immobilization. *ACS Appl. Mater. Interfaces* **2017**, *9* (18), 15492−15501.
(31) Chao, C.; Liu, J.; Wang, J.; Zhang, Y.; Zhang, B.; Zhang, Y.; Xiang, X.; Chen, R. Surface modification of halloysite nanotubes with dopamine for enzyme immobilization. *ACS Appl. Mater. Interfaces* **2013**, *5* (21), 10559−10564.
(32) Yang, J.; Liu, W.; Niu, H.; Cheng, K.; Ye, K.; Zhu, K.; Wang, G.; Cao, D.; Yan, J. Ultrahigh energy density battery-type asymmetric supercapacitors: $NiMoO_4$ nanorod-decorated graphene and graphene/Fe_2O_3 quantum dots. *Nano Res.* **2018**, *11* (9), 4744−4758.
(33) Wang, D.; Hu, Y.; Zhao, J.; Zeng, L.; Tao, X.; Chen, W. Holey reduced graphene oxide nanosheets for high performance room temperature gas sensing. *J. Mater. Chem. A* **2014**, *2* (41), 17415−17420.
(34) Libertino, S.; Aiello, V.; Scandurra, A.; Renis, M.; Sinatra, F. Immobilization of the enzyme glucose oxidase on both bulk and porous SiO_2 surfaces. *Sensors* **2008**, *8* (9), 5637−5648.
(35) Park, E. J.; Jin, J.-H.; Kim, J. H.; Min, N. K. Surface activation of plasma-patterned carbon nanotube based DNA sensing electrodes. *Microchim. Acta* **2011**, *174* (3−4), 231−238.
(36) Mazzotta, E.; Rella, S.; Turco, A.; Malitesta, C. XPS in development of chemical sensors. *RSC Adv.* **2015**, *5* (101), 83164−83186.
(37) Acres, R. G.; Ellis, A. V.; Alvino, J.; Lenahan, C. E.; Khodakov, D. A.; Metha, G. F.; Andersson, G. G. Molecular structure of 3-aminopropyltriethoxysilane layers formed on silanol-terminated silicon surfaces. *J. Phys. Chem. C* **2012**, *116* (10), 6289−6297.
(38) Wang, Y.; Chen, D.; Wang, G.; Zhao, C.; Ma, Y.; Yang, W. Immobilization of cellulase on styrene/maleic anhydride copolymer nanoparticles with improved stability against pH changes. *Chem. Eng. J.* **2018**, *336*, 152−159.
(39) Abraham, R. E.; Verma, M. L.; Barrow, C. J.; Puri, M. Suitability of magnetic nanoparticle immobilised cellulases in enhancing enzymatic saccharification of pretreated hemp biomass. *Biotechnol. Biofuels* **2014**, *7* (1), 90−101.
(40) Hosseini, S. H.; Hosseini, S. A.; Zohreh, N.; Yaghoubi, M.; Pourjavadi, A. Covalent immobilization of cellulase using magnetic poly (ionic liquid) support: improvement of the enzyme activity and stability. *J. Agric. Food Chem.* **2018**, *66* (4), 789−798.

DOI: 10.1021/acssuschemeng.9b05400
ACS Sustainable Chem. Eng. 2020, 8, 900−913

(41) Jordan, J.; Kumar, C. S. S. R.; Theegala, C. Preparation and characterization of cellulase-bound magnetite nanoparticles. *J. Mol. Catal. B: Enzym.* **2011**, *68* (2), 139−146.
(42) Lupoi, J. S.; Smith, E. A. Evaluation of nanoparticle-immobilized cellulase for improved ethanol yield in simultaneous saccharification and fermentation reactions. *Biotechnol. Bioeng.* **2011**, *108* (12), 2835−2843.
(43) Das, R.; Talat, M.; Srivastava, O. N.; Kayastha, A. M. Covalent immobilization of peanut β-amylase for producing industrial nano-biocatalysts: A comparative study of kinetics, stability and reusability of the immobilized enzyme. *Food Chem.* **2018**, *245*, 488−499.
(44) Kadam, A. A.; Jang, J.; Jee, S. C.; Sung, J.-S.; Lee, D. S. Chitosan-functionalized supermagnetic halloysite nanotubes for covalent laccase immobilization. *Carbohydr. Polym.* **2018**, *194*, 208−216.
(45) Wu, L.; Yuan, X.; Sheng, J. Immobilization of cellulase in nanofibrous PVA membranes by electrospinning. *J. Membr. Sci.* **2005**, *250* (1−2), 167−173.
(46) Datta, S.; Holmes, B.; Park, J. I.; Chen, Z.; Dibble, D. C.; Hadi, M.; Blanch, H. W.; Simmons, B. A.; Sapra, R. Ionic liquid tolerant hyperthermophilic cellulases for biomass pretreatment and hydrolysis. *Green Chem.* **2010**, *12* (2), 338−345.
(47) Zhou, M.; Ju, X.; Zhou, Z.; Yan, L.; Chen, J.; Yao, X.; Xu, X.; Li, L.-Z. Development of an immobilized cellulase system based on metal-organic frameworks for improving ionic liquid-tolerance and in situ saccharification of bagasse. *ACS Sustainable Chem. Eng.* **2019**, *7* (23), 19185−19193.
(48) Xiao, Z.; Zhang, X.; Gregg, D. J.; Saddler, J. N. Effects of sugar inhibition on cellulases and β-glucosidase during enzymatic hydrolysis of softwood substrates. *Proceedings of the Twenty-Fifth Symposium on Biotechnology for Fuels and Chemicals*, May 4−7, 2003, Breckenridge, CO; Springer: 2004; pp 1115−1126, DOI: 10.1007/978-1-59259-837-3_90.
(49) Xu, J.; Huo, S.; Yuan, Z.; Zhang, Y.; Xu, H.; Guo, Y.; Liang, C.; Zhuang, X. Characterization of direct cellulase immobilization with superparamagnetic nanoparticles. *Biocatal. Biotransform.* **2011**, *29* (2−3), 71−76.
(50) Wang, Y.; Radosevich, M.; Hayes, D.; Labbe, N. Compatible ionic liquid-cellulases system for hydrolysis of lignocellulosic biomass. *Biotechnol. Bioeng.* **2011**, *108* (5), 1042−1048.
(51) Rodrigues, R. C.; Ortiz, C.; Berenguer-Murcia, Á.; Torres, R.; Fernández-Lafuente, R. Modifying enzyme activity and selectivity by immobilization. *Chem. Soc. Rev.* **2013**, *42* (15), 6290−6307.
(52) Tian, D.; Chandra, R. P.; Lee, J.-S.; Lu, C.; Saddler, J. N. A comparison of various lignin-extraction methods to enhance the accessibility and ease of enzymatic hydrolysis of the cellulosic component of steam-pretreated poplar. *Biotechnol. Biofuels* **2017**, *10* (1), 157−166.

DOI: 10.1021/acssuschemeng.9b05400
ACS Sustainable Chem. Eng. 2020, 8, 900−913

ACS Sustainable Chemistry & Engineering

pubs.acs.org/journal/ascecg

Research Article

Magnetic Halloysite Nanotube/α-Amylase Based Nanobiocatalytic Transformation of Food Processing Waste into an Active Fermentation Ingredient

Devendra Sillu, Shekhar Agnihotri,* and M. Sudhakara Reddy

Cite This: https://doi.org/10.1021/acssuschemeng.2c01547

Read Online

ACCESS | Metrics & More | Article Recommendations | Supporting Information

ABSTRACT: The concept of "nanobiocatalysis" creates exciting opportunities for improving enzyme performance via immobilization onto nanomaterials. A nanobiocatalyst consisting of magnetic halloysite nanotube (MHNT)/α-amylase was evaluated to transform food processing waste into an active fermentation medium formulation for low-cost bioprocessing. A high loading of α-amylase (185.5 mg (g of support)$^{-1}$) was achieved on the surface of MHNTs through polydopamine functionalization. We validated the establishment of an enzyme-support system retaining >89% catalytic activity (27332 IU (g of support)$^{-1}$) with improved enzyme handling (>99.1% recovery) and reusability (>56% activity, 10 cycles). MHNTs remarkably improved the enzyme kinetics and thermodynamic characteristics along with operational and storage stabilities and mitigated the likely inhibitory effects of cellulose/metal ions as contaminants. In addition to facilitating a continuous production of reducing sugars from the extracted starch over 72 h, the nanobiocatalyst was equally effective in preparing a nutritive food waste hydrolysate as a fermentable medium substitute for batch culturing of *E. coli* and a single-cell protein (*A. niger*). The commercial relevance of waste hydrolysate was also investigated to promote calcite precipitation via *Bacillus* sp. induced biocementation. We evidenced that nanobiocatalyst-assisted "starch depolymerization" released more nutritional components into the hydrolysate suspension, easily accessible to growing microbial cultures.

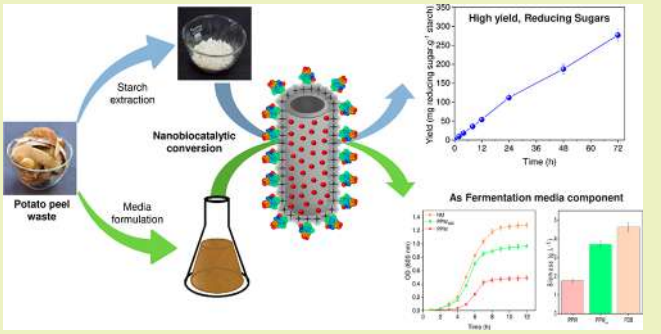

KEYWORDS: *food waste management, enzyme immobilization, nanobiocatalyst, biomass valorization, medium alternative*

INTRODUCTION

The exponential rise in food processing industries has inevitably contributed to the generation of food waste, a top portion of which ends up in landfills, triggering excess emission of greenhouse gases.[1,2] To minimize losses and redistribute resources, the viable conversion alternatives, i.e., biofuel and animal feedstock, were the primary focus under food waste management policies, which incurred a substantial economic loss.[3] Meanwhile, the possibilities of transforming food waste into more value-added biochemical products have been underrated for human consumption or in bioprocessing industries.[4,5] The rising demands for economical yet eco-friendly products have further propelled the scientific communities[5] toward finding novel solutions to food waste valorization. Food waste is a remarkable blend of several organic ingredients, acting as precursors in various biochemical reactions. For instance, potato peel waste, a "zero value" byproduct of the food industries, is generated up to ∼40% of the initial mass during potato processing.[6] Unfortunately, it is rarely utilized to generate valuable biochemicals and nutritional products and thus warrants its significant relevance in our contemporary efforts toward biomass valorization.

Potato peel waste contains sufficient amounts of starch and nonstarch polysaccharides, which can produce bioethanol, biobutanol, lactic acid, and fermentable sugars. Starch hydrolysis is a standard process utilizing enzymatic saccharification, which produces a relatively clean glucose stream for further biotransformations.[7] In contrast to chemical treatments, α-amylase-led starch hydrolysis is an effective strategy to achieve reaction specificity, improved yields, and a critical reduction in energy/water consumption during industrial processing.[8] However, the overall cost of production and mild operating conditions required for enzymes still impede their application on an industrial scale. Enzyme immobilization is a widely accepted approach to overcoming these hurdles.[9] Although immobilization aims to improve the stability and reusability of the biocatalyst, its extent explicitly depends on the intrinsic characteristics of the support matrix employed.[4,10,11]

Received: March 15, 2022
Revised: July 11, 2022

Nanotechnological interventions in biotechnology have forecasted the potential of "nanobiocatalysis" as a sustainable tool in food waste valorization.[12−14] The "waste-to-wealth" concept via an enzyme−nanomaterial system has been synchronized to produce industrially relevant biochemical products, viz. biodiesel,[15,16] bioactive ingredients,[17−20] and hydrolysates,[21,22] from several food residues. Nanosized materials are well suited for immobilizing enzymes due to their high surface area for enzyme binding, quantum size effect, and insignificant mass transfer limitations.[10,13,23,24] Particularly, the immobilization of starch-saccharifying α-amylase enzyme on various nanomaterials has shown numerous benefits in recent times. For instance, a hydroxyapatite-decorated ZrO_2 nanocomposite, used as a support material for α-amylase, yielded >70% residual enzyme activity after 10 repeated cycles and 8 weeks of storage.[25] The authors demonstrated an improved catalytic potential and pH/temperature activity profile of immobilized α-amylase in comparison to those of its free form. Similarly, immobilization of α-amylase on a porous, protein/metal−organic framework nanocomposite[26] exhibited an improved catalytic efficiency, reusability (20 times), and storage stability (>90%, 8 weeks) of immobilized α-amylase, making it amenable for industrial applications. Recently, α-amylase was scrutinized to produce a high-maltose-containing syrup after immobilization onto a graphene oxide/Fe_3O_4 nanocomposite.[27] Under optimal conditions, in addition to higher catalytic activity and half-life values, immobilized α-amylase displayed superior alkali tolerance, thermodynamic features, and reusability (10 cycles) and produced 40% dextrose equivalent values, emphasizing its commercial relevance. The quest for developing a robust, economically viable yet sustainable support matrix for binding α-amylase requires more effort.

Clay materials, for example, halloysite nanotubes (HNTs), have been exhaustively studied for binding biomolecules due to their biocompatible nature and vast availability at a cheap price. Their unique nanotubular structure and ease in undergoing surface functionalization make them a potential candidate to bind enzymes.[28,29] Additionally, the biocompatibility and adhesive nature of the cross-linker are equally crucial for ensuring enzyme anchoring and its stability in an immobilized state. The oxidative polymerization of dopamine is a biomimetic approach for surface modification of inorganic materials, generating complementary sites for enzyme binding.[30,31] Dopamine-inspired immobilization has been reported to improve enzyme stability and reusability for bioprocessing applications.[30,31]

Herein, we report a nanobiocatalytic system for converting a food processing byproduct into an active fermentation medium formulation, which may lead to the development of low-cost bioprocessing toward the bioeconomy. The nanobiocatalyst exhibited good biocompatibility with a high loading of α-amylase and preserved its biocatalytic activity. The immobilization imparted overall enzymatic stability to sustain harsh process conditions, improved reaction kinetics, and superior tolerance to contaminants (cellulose/metal ions) and ensured excellent reusability. The extracted starch from potato peel waste (Figure S1) was efficaciously utilized as the substrate for producing high-maltose syrup using immobilized α-amylase. The nanobiocatalyst-treated potato peel waste was also used as a fermentation medium substitute for *E. coli* and to produce a single-cell protein as a dietary supplement. The waste hydrolysate was also tested to promote microbial-induced calcium carbonate precipitation (MICP), which is of great relevance for the remediation of building structures.[32,33] In all, the potential conversion of waste into industrially relevant products discussed in this article should significantly contribute to the current food waste management strategies.

EXPERIMENTAL SECTION

Preparation of Dopamine-Functionalized MHNTs (*d*-MHNTs). As has been reported previously,[4] magnetic halloysite nanotubes (MHNTs) were synthesized and underwent surface functionalization by adopting an established method[30] with a slight modification. In brief, 300 mg of MHNTs was dispersed in 50 mL of Tris-HCl buffer (0.05 M, pH 8.5) and the mixture sonicated for 60 min. A 0.3 mg portion of dopamine hydrochloride was introduced into the MHNT solution, and the mixture was kept in an orbital shaker for 6 h to obtain polydopamine-coated MHNTs. The solid mass was separated using a magnet and repeatedly washed with Tris-HCl buffer until the filtrate became colorless and transparent. The obtained powder was dried overnight at 40 °C and denoted as *d*-MHNTs.

Immobilization of α-Amylase on Dopamine-Functionalized MHNTs. For immobilization of α-amylase, 62.48 mg of *d*-MHNTs was homogeneously dispersed in 20 mL of phosphate buffer (0.05 M, pH 6.5), and 17.91 mg of α-amylase (165 IU/mg) was introduced into the solution. The solution was left in a shaker (40 °C). The enzyme-loaded *d*-MHNTs were magnetically recovered and washed with buffer solution to remove loosely bound enzymes. The obtained α-amylase immobilized *d*-MHNTs were stored at 4 °C until further use.

Loading, Activity, and Leaching of α-Amylase. The extent of α-amylase loading onto *d*-MHNTs was calculated by measuring the concentration of α-amylase that remained in the suspension after removing immobilized α-amylase using the Bradford assay.[34] Briefly, 5 mL of Bradford reagent (0.01% (w/v) Coomassie Brilliant Blue G-250, 4.7% (w/v) ethanol, and 8.5% (w/v) phosphoric acid) was added to 1 mL of the protein solution. After 3 min, the absorbance of the solution was measured at 595 nm, and the protein concentration was determined using a standard curve of bovine serum albumin (0−1 mg mL^{-1}) (Figure S2).

$$\text{enzyme loading (\%)} = \frac{C_0 - C}{C_0} \times 100 \quad (1)$$

$$\text{enzyme loading (mg } g^{-1}) = \frac{(C_0 - C)V}{W} \times 100 \quad (2)$$

where C_0 and C are the initial and final α-amylase concentrations in the suspension, V is the solution volume in mL, and W is the weight of *d*-MHNTs added in g.

The amylolytic activity of α-amylase was determined through the production of reducing sugars using starch (1% w/v) as the substrate. Fresh stocks of starch and α-amylase were prepared in phosphate buffer (0.05 M, pH 6.5) and incubated at 40 °C for reaction initiation. Aliquots were withdrawn after the required intervals, and the amount of reducing sugars was quantified using the dinitrosalicylic acid (DNS) method. One unit (IU) of enzyme activity is defined as the amount of enzyme required to liberate one micromole of reducing sugar per minute under standard conditions. Free and immobilized α-amylase possessing equivalent units of α-amylase were exposed to identical reaction conditions to determine the retained catalytic activity. The activity of the free enzyme was considered to be 100%.

The leachability of the immobilized enzyme was evaluated by suspending 100 mg of the nanobiocatalyst in 10 mL of phosphate buffer (0.05 M, pH 6.5) supplemented with either 1.0 M NaCl or 1.0% (v/v) Triton X-100 as separate studies. The incubation period was 12 h at room temperature (25 °C) with orbital shaking (250 rpm). Afterward, the nanobiocatalyst was carefully removed using a magnet (Neodymium N42, surface gauss 2980), and the protein concentration in the supernatant was determined using Bradford's method. The protein present as supernatant would be the leached

https://doi.org/10.1021/acssuschemeng.2c01547
ACS Sustainable Chem. Eng. XXXX, XXX, XXX−XXX

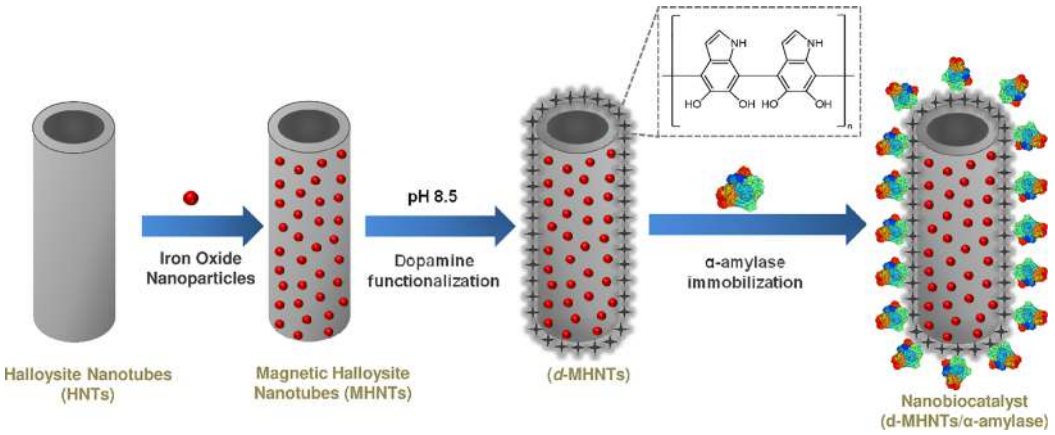

Figure 1. Schematic representation of constructing a magnetically separable nanobiocatalyst by anchoring iron oxide nanoparticles onto halloysite nanotubes followed by dopamine-assisted surface functionalization to immobilize α-amylase enzyme.

enzyme desorbed from the surface, whose proportion (%) relative to the total immobilized enzyme was estimated.

Catalytic Activity: Optimization of Enzyme Activity. To determine the optimum operational pH of free enzyme and the nanobiocatalyst, similar amounts (300 IU) were introduced to different buffers (pH 4.5−8.0) under identical conditions (6 h, 40 °C). Aliquots were withdrawn at predefined time intervals and subjected to starch (1% v/v) hydrolysis, and the catalytic activities were determined. The optimal operational temperature was determined by incubating both forms of the enzyme (300 IU, each) at different temperatures (30−60 °C) at pH 6.5.

The storage potentials of NBC and free α-amylase (300 IU, each) were evaluated for 30 days by storing them at 4 °C. Aliquots were withdrawn periodically to determine the relative catalytic activity, considering the enzyme activity on first day as 100%. To determine the reuse potential of the nanobiocatalyst, 10 mg of the nanobiocatalyst was incubated with 100 mL of a starch (1% w/v) solution for 3 h at 50 °C. After every cycle, the nanobiocatalyst was separated, washed with buffer solution, and reintroduced into fresh starch solution.

Influence of Metal Ions and Cellulose as Contaminants. The catalytic activities of free and immobilized α-amylase in the presence of cellulose were assessed under identical conditions. In brief, equivalent units (300 IU) were incubated to starch (10 mL, 1% w/v) solutions comprising a serial concentration of cellulose (0−1% w/v). To evaluate the effect of metal ions, equivalent units of both forms were incubated separately with 5 mM metal ions (Ca^{2+}, Fe^{2+}, K^{+}, Zn^{2+}, Mg^{2+}, Cu^{2+}, Na^{+}) for 30 min. Subsequently, starch (1% w/v) was introduced into the enzyme−metal ion solution, and the catalytic activities were determined. In the absence of contaminants (cellulose/metal ions), the catalytic activity was considered as 100% and other activities were expressed relatively.

Evaluation of Thermodynamic and Kinetics Parameters. Thermodynamic parameters of free and immobilized α-amylase were assessed by determining their catalytic activities at different temperatures. In brief, both forms (300 IU each) were incubated at predefined temperatures, and aliquots were withdrawn after specific time intervals to analyze the catalytic activity. The relative activity as a function of time was fitted to a first-order plot. The thermodynamic parameters were estimated as described previously (Section S4).[4] The kinetic reaction parameters (K_M, V_{max}) of α-amylase before and after immobilization were compared. The rate of product formation was determined by varying substrate concentrations (1−10 mg mL^{-1}). The kinetic parameters were calculated using a Lineweaver−Burk plot.

Continuous Operation of Nanobiocatalyst and Potential Industrial Application. The nanobiocatalyst was evaluated for the continuous hydrolysis of the starch extracted from potato peel waste. In brief, the substrate solution was prepared by adding 1 g of extracted starch into 90 mL of phosphate buffer (0.05 M, pH 6.5) and was kept at 70 °C for 15 min. The starch suspension and the nanobiocatalyst (10 mg in 10 mL phosphate buffer) were incubated separately at the operating temperature (50 °C). After this temperature was reached, both suspensions were mixed and continuously stirred for 72 h (120 rpm, 50 °C). Aliquots were drawn at a defined interval and analyzed to reduce sugar production.

We mention a new nanobiocatalyst-assisted conversion of potato peel waste (PPW) into a microbial growth medium. To prepare a liquid broth, potato peel waste (5 g) was mixed in phosphate buffer with stirring for 24 h (120 rpm, 50 °C). The suspension was then filtered, and the clear filtrate was used directly as a growth medium, as a PPW medium. Similarly, another growth medium was prepared from the nanobiocatalyst-treated potato peel waste. For this, 5 g of potato peel waste was suspended in 100 mL of phosphate buffer into which 100 mg of the nanobiocatalyst was introduced and the mixture was stirred for 24 h (120 rpm, 50 °C). Afterward, the nanobiocatalyst was recovered using a magnet, and the final suspension was designated as "PPW_{NBC} medium". The pHs of the clear solutions obtained were adjusted to 5 and 7 for fungal and bacterial culture, respectively, and the solutions were autoclaved (121 °C, 15 min). Agar (2% w/v) was used as a solidifying agent for bacterial culture plating. Commercially available nutrient broth/nutrient agar (NM) and potato dextrose broth (PDB) were employed as references for bacterial and fungal cultures. Other details relevant to bacterial and fungal strains and single-cell production are provided in Section S5.

The industrial potential of PPW_{NBC} medium was evaluated and compared with the commercially available nutrient broth (NB) for growing calcifying bacteria *Bacillus* sp. CT5 in biocementation applications.[35] The bacterial culture was grown in autoclaved PPW_{NBC} broth and blend formulations of PPW_{NBC}:NB: i.e., 75:25, 50:50, 25:75, and 0:100% v/v. For precipitation of calcium carbonate (bio cement), the growth media were augmented with filter-sterilized urea (2% w/v) and $CaCl_2$ (25 mM) and were incubated at 37 °C under shaking conditions (120 rpm). The bacterial growth was measured by recording the optical density at 600 nm. Calcium carbonate ($CaCO_3$) precipitation under different growth media was also evaluated by growing bacteria for 96 h. The $CaCO_3$ content was determined by an EDTA titration method.[36]

RESULTS AND DISCUSSION

Formation of Immobilization Matrix. Halloysite nanotubes provide a large specific surface area for high and efficient biomolecule immobilization and other unique physicochemical properties.[37] As reported recently, iron oxide nanoparticles were anchored on the surface of halloysite nanotubes through an *in situ* approach, which served as a primary template for surface modification.[4] Figure 1 illustrates polydopamine functionalization of magnetic halloysite nanotubes (*d*-

https://doi.org/10.1021/acssuschemeng.2c01547
ACS Sustainable Chem. Eng. XXXX, XXX, XXX−XXX

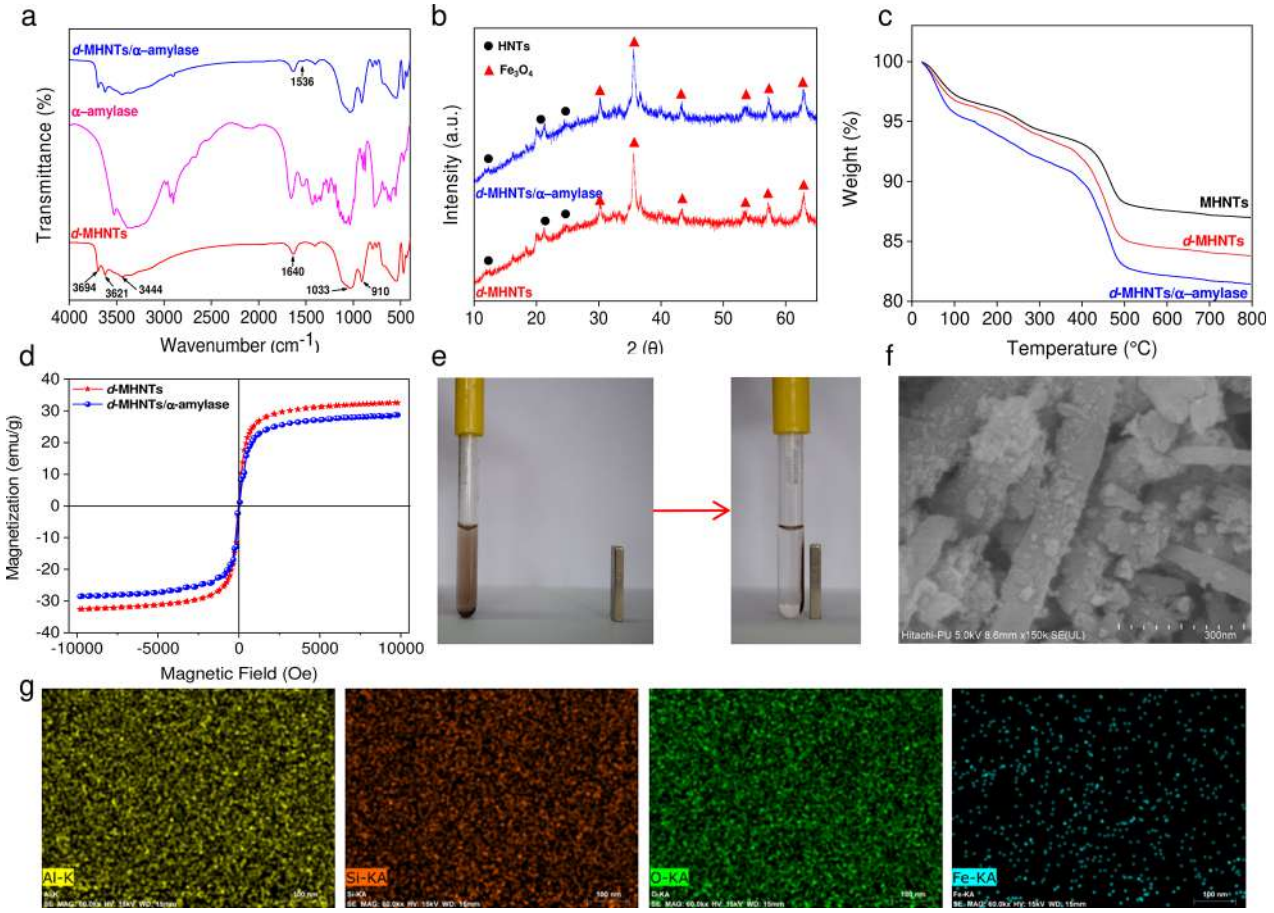

Figure 2. Analytical characterization of MHNTs after dopamine functionalization and α-amylase immobilization through (a) FTIR spectroscopy, (b) XRD analyses, (c) thermogravimetric analyses, and (d) magnetic hysteresis loop. (e) Photographic image showing an easy separation of nanobiocatalyst from the working solution. (f) High-resolution SEM micrograph confirming a high loading of α-amylase corroborated by (g) elemental mapping showing the existence of aluminum (Al), silicon (Si), oxygen (O), and iron (Fe).

MHNTs) and subsequent immobilization of α-amylase. Immersing MHNTs into an alkaline dopamine solution spontaneously generated a thin, surface-adherent polydopamine coating onto MHNTs due to the oxidative self-polymerization of dopamine.[38] The resulting *d*-MHNTs were used for immobilization of α-amylase. Polydopamine acted as a non-specific biomimetic cross-linker to bind enzymes due to quinones, which are reactive toward the nucleophilic groups on enzymes. The covalent coupling between amino groups of enzyme and quinones of polydopamine may occur via Michael addition and/or Schiff base formation.[30,39] The as-synthesized *d*-MHNTs after immobilization of α-amylase, now termed *d*-MHNTs/α-amylase, were evaluated through materialistic characterization and compared to their pristine counterparts before determining their biocatalytic potential.

Material Characterization. The dopamine functionalization of MHNTs and subsequent immobilization of α-amylase on *d*-MHNTs were determined through FTIR spectroscopy (Figure 2a). This also evaluated the variation in functional moieties of *d*-MHNTs, if they occurred, before and after enzyme immobilization. The results indicate that *d*-MHNTs could preserve the inherent absorption peaks at 3694, 3621, 1033, and 910 cm^{-1} ascribed to hydroxyl (−OH) groups, Si−O stretching, and the bending vibrations of Al−OH, respectively, even after immobilizing α-amylase. Both samples showed a characteristic vibrational band in the near-infrared region (<800 cm^{-1}, Fe−O), which established the magnetic nature of MHNTs.[4] The absorption peaks at 3444 and 1640 cm^{-1} are ascribed to the stretching vibrations of amino ($-NH_2$) and carbonyl (−C═O) groups of polydopamine, respectively.[30] The overlapped characteristic peaks of α-amylase with *d*-MHNTs at 1536 and 1426 cm^{-1} further confirm the successful loading of α-amylase and irreversible bonding between enzyme and polydopamine.

XRD analyses were done to evaluate the structural integrity of *d*-MHNTs before and after immobilizing α-amylase (Figure 2b). The presence of characteristic diffraction peaks (JCPDS Card No. 29-1487) in both samples indicated that the crystallinity of HNTs remained intact after polydopamine functionalization, since the attachment of IONPs occurred only on the surface, not in the interlayer. The distinctive peaks of magnetite Fe_3O_4 (JCPDS Card No. 01-075-0449) at 2θ = 30.34, 35.65, 43.33, 53.58, 57.29, and 62.93° can be attributed to the (220), (311), (400), (422), (511), and (440) planes of Fe−O crystals, respectively. It is ascertained that the adopted surface functionalization protocol was efficient in immobilizing α-amylase without adversely affecting the crystallinity of either HNTs or IONPs.[4,29] To further support our hypothesis of achieving stable functionalization followed by enzyme immobilization, thermogravimetric analyses (TGA) were carried out (Figure 2c). While the TGA curve of pristine MHNTs demonstrated a 13.02 wt % weight loss in the 0−800

https://doi.org/10.1021/acssuschemeng.2c01547
ACS Sustainable Chem. Eng. XXXX, XXX, XXX−XXX

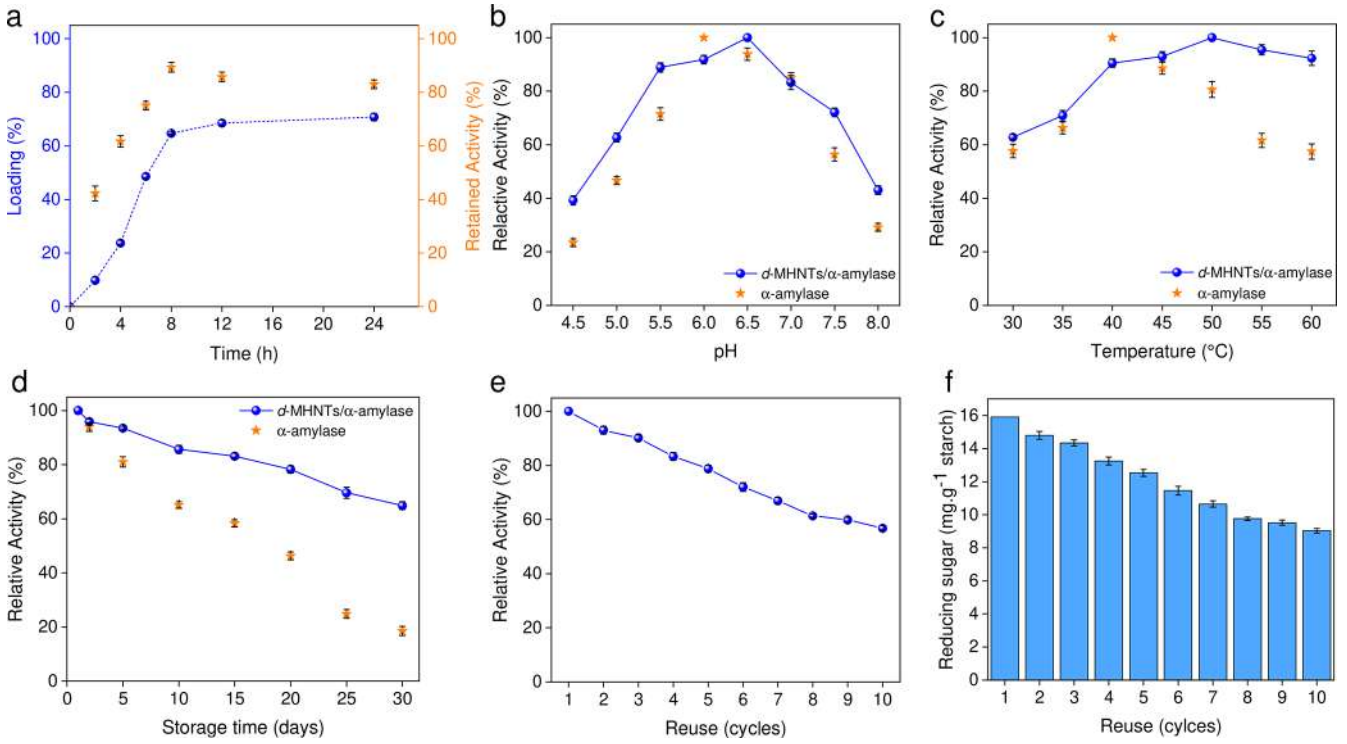

Figure 3. Functional and operational attributes of free enzymes and the nanobiocatalyst evaluated for their relevance to industrial processes: e.g., (a) correlation between the duration of immobilization and the extent of α-amylase loading and the corresponding retained activity, (b) effect of working pH at a constant temperature of 40 °C, (c) influence of working temperature at constant reaction pH of 6.5, (d) storage stability over 30 days at 4 °C, (e) reusability over 10 consecutive reaction cycles, and (f) the obtained yield of reducing sugars per cycle. Experiments were performed in triplicate (technical), and mean ± standard deviation values are presented.

°C temperature range, a more significant weight loss (16.22 wt %) was exhibited in *d*-MHNTs under similar test conditions. Such a minor yet considerable increase (3.2 wt %) in weight loss of *d*-MHNTs occurred due to the presence of polydopamine on its surface, which is corroborated nicely by an earlier report.[30] On a similar note, the TGA curve of d-MHNTs/α-amylase depicted even a greater weight loss of 18.59 wt %, which can occur due to immobilized α-amylase.

Immobilizing enzymes onto a magnetic support is one way to improve their recovery from the reaction mixture, thus promoting its reuse. A vibrating sample magnetometer was employed to assess the impact of enzyme immobilization on *d*-MHNTs (Figure 2d). The magnetization curve revealed that *d*-MHNTs and *d*-MHNTs/α-amylase had a marginal reduction in magnetization saturation values, i.e., 32.5 and 28.7 emu g^{-1} respectively, which occurred solely due to the presence of an additional nonmagnetic content (α-amylase) in the latter. However, such variation did not significantly affect the separation efficiency of the immobilized enzyme (Figure 2e). Since both samples demonstrated superparamagnetism with zero coercivity and remanence, *d*-MHNTs/α-amylase was established as a promising magnetic template, which can easily be removed from the reaction vessel through a simple magnet. Finally, *d*-MHNTs/α-amylase was examined through FEG-SEM to evaluate the morphology of its backbone structure after enzyme loading (Figure 2f). It was evident that the surface topography of HNTs (Figure S3) was significantly changed after incorporating IONPs and enzyme immobilization with the desired surface modifications. The elemental mapping scan further confirmed a homogeneous distribution of all components of HNTs and IONPs, which validates the conclusions derived through XRD, VSM, and TGA analyses (Figure 2g).

Evaluation of Biocatalytic Characteristics. The extent of immobilization was optimized using a response surface methodology to evaluate its effect on enzyme loading and corresponding biocatalytic activity (Figure S4). The results indicate that the enzyme loading increased and reached a plateau after 8 h of incubation (Figure 3a). Possibly, this duration facilitated the required microenvironment over polydopamine-modified HNTs to immobilize α-amylase, resulting in a very high enzyme loading: i.e., 185.5 mg (g of *d*-MHNTs)$^{-1}$. The retained activity of α-amylase in an immobilized state demonstrated a similar trend. The surface anchoring of enzymes onto nonporous halloysite nanotubes reduced the harmful effects of substrate diffusion resistance.[40] However, the retained activity of immobilized α-amylase was drastically reduced by extending the duration beyond 8 h, which was attributed to the dense packing of enzymes.[41] Hence, an optimal reaction time of 8 h was considered for further studies, which possesses the virtue of high enzyme loading (64.7 ± 0.5%) with high retained activity (89.3 ± 1.8%). Further, the leaching of immobilized enzymes in the presence of different desorbant solutions provides critical information regarding the category of immobilization (adsorption, affinity, or covalent attachment). We observed marginal leaching of enzymes in the presence of ionic (2.62%) and detergent (3.87%) solvents. The results indicated hardly any ionic or hydrophobic interactions between the enzyme and support.[42,43] Rather, covalent bonding exists between α-amylase and the dopamine-functionalized MHNTs.

https://doi.org/10.1021/acssuschemeng.2c01547
ACS Sustainable Chem. Eng. XXXX, XXX, XXX−XXX

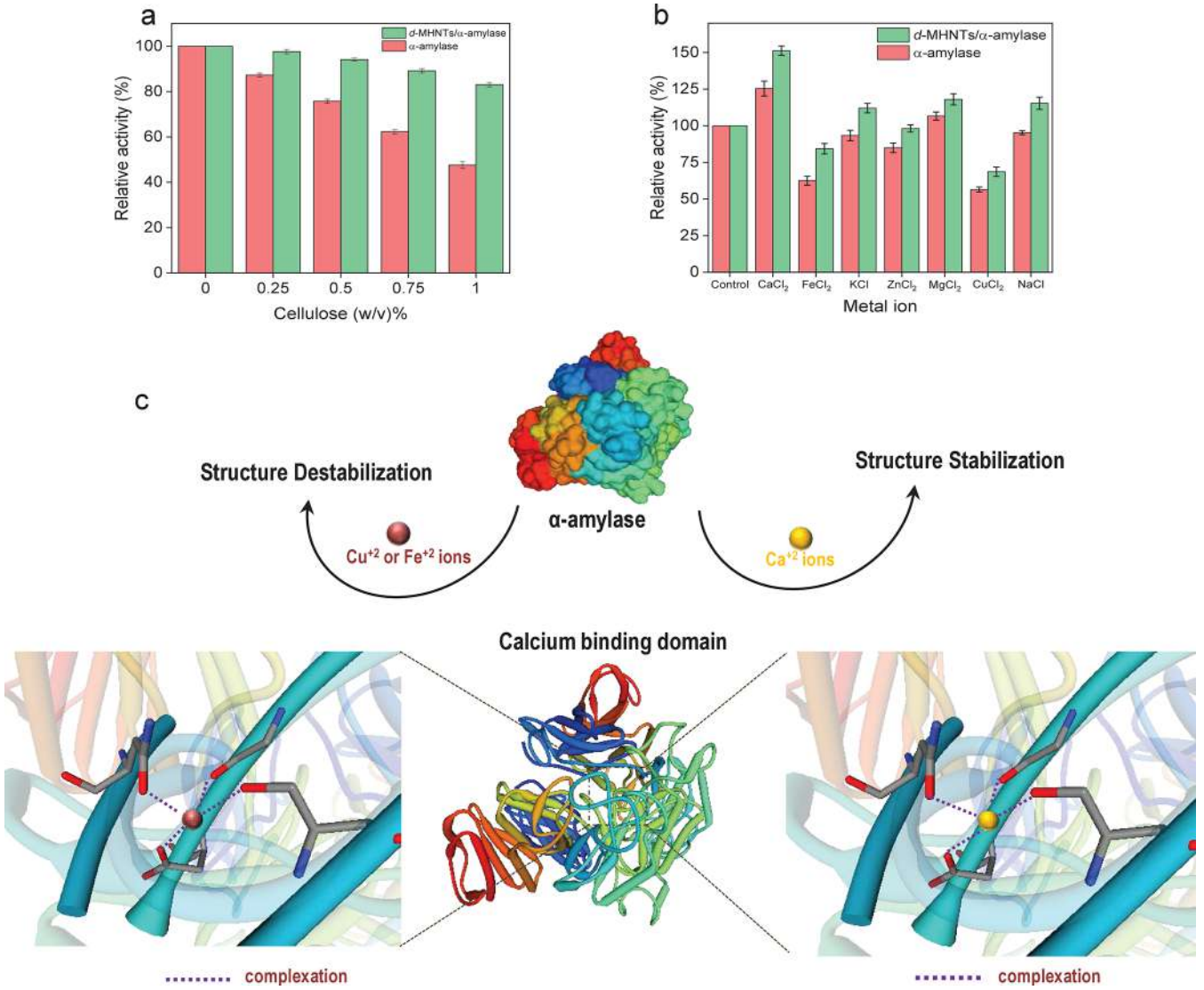

Figure 4. Comparative assessment of the activity of free α-amylase and nanobiocatalyst in the presence of (a) cellulose with varying contents and (b) metal ions. (c) Proposed mechanism of metal ion (Cu^{2+}, Fe^{2+}, Ca^{2+}) interaction with the calcium-binding domain(s) of α-amylase, which may lead either to structure stabilization or destabilization of enzymes in their immobilized state. Experiments were performed in triplicate (technical), and mean ± standard deviation values are presented.

Next, the effect of reaction pH and temperature on the biocatalytic activity of α-amylase in a free versus immobilized state was compared. The initial activities of both free (300 IU, pH 6) and immobilized (268.3 IU, pH 6.5) α-amylase at the corresponding optimal pH values was considered to be 100% while their relative activities were calculated under various conditions of process parameters. The pH of the reaction medium had a more profound effect on the catalytic activity of α-amylase in the free form than in the immobilized form (Figure 3b). At extreme pH values, free α-amylase could retain only 20% (pH 4.5) and 30% (at pH 8.0) of its original activity in comparison to its optimal pH of 6.0. Immobilizing α-amylase, however, significantly broadened its operational pH range from 5 to 7.5, retaining >60% catalytic activity in comparison to its optimum activity (pH 6.5), and the catalyst could withstand harsh process conditions.

In an analysis of the effect of reaction temperature, the activities of free α-amylase (300 IU, 40 °C) and immobilized α-amylase (272.3 IU, 50 °C) at their respective optimal temperatures were considered as 100% (Figure 3c). We observed similar catalytic activity of both forms of α-amylase at a lower temperature range (30−45 °C). Beyond 45 °C, free α-amylase gradually lost its catalytic activity due to thermal degradation of its enzymatic structure and could retain only 42.5% of its original activity at 60 °C in compared to its optimum temperature (40 °C). In contrast, *d*-MHNTs/α-amylase exhibited a superior catalytic potential where 92.3% catalytic activity of α-amylase was retained in comparison to the corresponding optimal activity (50 °C). The reduced temperature sensitivity can be attributed to an increase in the rigidity of the peptide structure of the enzyme after immobilization, which contributed to improved thermal resistance.[44] Overall, the immobilization matrix preserved the structure of α-amylase against any conformational changes prompted by varying reaction conditions and demonstrated a greater utility of dopamine-functionalized MHNTs for enzyme immobilization.

The storage stability of free α-amylase and the nanobiocatalyst was inspected at 4 °C for 30 days (Figure 3d). On day 1, the activity of both free (300 IU) and immobilized

https://doi.org/10.1021/acssuschemeng.2c01547
ACS Sustainable Chem. Eng. XXXX, XXX, XXX−XXX

(269.7 IU) enzymes was considered to be 100%. Free α-amylase, due to the long-term exposure, could retain only 18.5 ± 1.7% of its initial catalytic activity, due to either the instability of the subunits or inactivation at low temperatures, whereas *d*-MHNTs/α-amylase could preserve over 64% of its biocatalytic activity and mitigated the possibilities of activity reduction under the relevant conditions. The improved storage stability is credited to the stiffness brought upon by multipoint attachment between α-amylase and *d*-MHNT, preserving the inherent structure of α-amylase. In addition, curved surface geometries of support matrices have also been reported to suppress lateral interactions between adjacent enzymes, thus improving the enzyme activity by suppressing the steric hindrance.[30]

The reusability potential of the nanobiocatalyst was evaluated by measuring its catalytic activity during starch hydrolysis for 10 consecutive cycles under the optimized process conditions (Figure 3e). The results show that the nanobiocatalyst could retain more than 56% of its initial activity even after 10 cycles. We ruled out enzyme leaching, since the amount of immobilized enzyme recovered after every cycle was always higher than 99%. Since enzyme reutilization is critical for many bioprocesses, the utility of immobilized α-amylase was evaluated in terms of its capacity to produce reducing sugars per cycle (Figure 3f). The production of reducing sugars gradually declined with every reuse, going from 15.9 to 9.03 mg (g od reducing sugar)$^{-1}$ after the 1st and 10th cycles, respectively. However, it is essential to note that the total production of reducing sugar for the entire 10 cycles of nanobiocatalyst was much higher (121.25 mg g^{-1} starch) than that in the continuous reaction of free α-amylase (48.84 mg.g^{-1} starch) over a similar duration.

When enzymes with bulky substrates, viz. α-amylase, are immobilized onto the bulk support materials, their limited surface area creates steric hindrances in binding with the active site of enzymes, leading to a complete loss of catalytic activity. In contrast, nanomaterials with a high surface area/volume ratio (halloysite nanotubes, here) facilitate a better conformational motility of enzymes even after immobilization, thereby inducing a flexible enzyme structure with enhanced protein unfolding. This provides a more favorable reaction condition for maximizing substrate−enzyme interactions at active sites, circumventing steric hindrances and improving catalytic activity. Further, in comparison to the traditional immobilization methods such as entrapment/encapsulation, the surface-bound enzymes offer insignificant mass transfer limitations, resulting in enhanced catalytic activity at a comparatively lower payload level. The biocompatible nanomaterial emerges as an excellent support to improve the catalytic potential of immobilized enzymes and further prevent undesirable changes in the enzyme structure.

Effect of the Presence of Cellulose and Metal Ions on Catalytic Activity. The presence of soluble and insoluble dietary fibers, specifically cellulose in the starch, extracted from potato peel waste could unexpectedly influence the α-amylase activity (Table S5). Hence, the retained catalytic activity of both free and immobilized enzymes was evaluated in the presence of different cellulose concentrations. As expected, a significant deterioration in the activity of α-amylase in both forms was observed for all cellulose concentrations (Figure 4a). Free α-amylase appeared to be extremely sensitive even on introduction of 0.25% (w/v) cellulose, where only 87% activity could be retained with respect to the control. Further, the incremental addition of cellulose (0.5−1% w/v) caused a greater decrease in its catalytic activity from 75.8% to 47.6%, respectively. In contrast, *d*-MHNTs/α-amylase exhibited better biocatalytic power at the similar cellulose concentrations investigated, and it could retain a remarkable 83% activity even at 1% (w/v) concentration. Although the mechanism of inhibitory effects of cellulose on the amylolytic process is still unclear, a decrease in the catalytic activity occurred because of the "adherent" nature of α-amylase toward nonstarch polysaccharides, i.e., cellulose, making them inaccessible to starch due to steric hindrances.[45] The result corroborates a similar fact where cellulose adversely affected amylolysis by impairing the catalytic efficiency of free α-amylase. However, the superior activity of *d*-MHNTs/α-amylase is governed by a more favorable interaction between cellulose−polydopamine (present in the support matrix) and cellulose−amylase so that most of the active sites could remain available for starch molecules.[46]

The presence of metal traces in extracted polysaccharides is a common hurdle for their subsequent hydrolysis, as metal ions might also interfere with the active sites of enzymes. We observed that both Ca^{2+} and Mg^{2+} boosted the relative activities of free α-amylase to 125.4% and 106.6%, respectively (Figure 4b), since these metal ions act as allosteric activators and help in the stabilization of the three-dimensional structure of α-amylase.[47] However, Fe^{2+} and Cu^{2+} ions inhibited the enzyme activity to the greatest extent with catalytic losses of 37% and 43%, respectively, in comparison to the control. This indicates the importance of cysteine residues for the activity of α-amylase, since the sulfhydryl groups of cysteine occasionally act as a ligand of metal ions (Figure 4c). It is also likely that calcium ions between the substrate-binding domains of α-amylase would be replaced by divalent metal ions, leading to structure destabilization. In contrast, immobilized enzymes exhibited a more profound and beneficial effect on their activity in comparison to free enzymes in the presence of metal ions. The most significant effect appeared in Ca^{2+}, where immobilized enzymes could attain 51% more activity incomparison to the control. The superior activity is attributed to the "shielding" and robustness of the enzyme-immobilization matrix, which attenuated the likely replacements of Ca^{2+} ions at the active sites and protected the intrinsic structure of α-amylase.[48] The presence of a biomimetic coating on HNTs proves to be advantageous in both aspects, and the results validate its superiority for immobilizing α-amylase.

Thermodynamics and Kinetic Parameters. Thermodynamic and kinetic parameters provide vital information regarding the thermal behavior of enzymes, rates of reaction, and the reaction mechanism, which are critical for designing a biocatalytic process. Various thermal characteristics of α-amylase in free and immobilized states were monitored over the desired working temperature range (40−60 °C) (Figure S5a). We found the thermal deactivation rate constant (K_d) of nanobiocatalyst to be ∼4.2−4.7-folds lower than that of free α-amylase at 50 and 60 °C. This confirms the much-improved stability and slower denaturation of α-amylase when it is immobilized onto magnetic halloysite nanotubes (Table 1). The half-life of α-amylase in its two states gradually decreased on an increase in the temperature, *d*-MHNTs/α-amylase demonstrated 2.5-, 4.3-, and 4.7-fold higher half-lives in comparison to that of free α-amylase at temperatures of 40, 50, and 60 °C, respectively. The superior half-life and operational stability of enzyme at elevated temperatures indicate that

https://doi.org/10.1021/acssuschemeng.2c01547
ACS Sustainable Chem. Eng. XXXX, XXX, XXX−XXX

Table 1. Comparative Summary of Thermodynamic Parameters before and after Immobilizing α-Amylase onto *d*-MHNTs

	temp (°C)	free enzyme (α-amylase)	nanobiocatalyst (*d*-MHNTs/α-amylase)
k_d (h^{-1})	40	0.019	0.007
	50	0.049	0.011
	60	0.089	0.019
half-life, $t_{1/2}$ (h)	40	34.77	89.10
	50	13.86	59.69
	60	7.74	36.39
D value	40	115.54	296.07
	50	46.05	198.34
	60	25.74	120.92
E_d (kJ mol^{-1})		156.14	165.59
ΔH (kJ mol^{-1})	40	153.54	162.99
	50	153.45	162.91
	60	153.37	162.82
ΔG (kJ mol^{-1})	40	78.41	80.85
	50	78.36	82.29
	60	79.09	83.38
ΔS (J mol^{-1} K)	40	239.91	262.30
	50	232.39	249.49
	60	222.98	238.48

immobilized α-amylase was "more shielded" toward any unforeseen reasons for inactivation.[49] This was well supported by the decimal reduction time (*D* value), which indicated that immobilized α-amylase would take more time to denature than free enzyme. Further, a higher thermal inactivation energy or energy of denaturation (E_d) for the nanobiocatalyst (165.59 kJ mol^{-1}) in comparison to that for the free enzyme (156.14 kJ mol^{-1}) revealed that more energy would be required to denature the immobilized enzyme.

Similarly, immobilized α-amylase exhibited higher values of enthalpy change, ΔH (162.99 kJ mol^{-1}), and Gibbs free energy change, ΔG (80.85 kJ mol^{-1}), in comparison to its free form (Figure S5b). The higher total energy required for enzyme denaturation indicates the superior thermal stability of immobilized enzymes in comparison to free enzymes. Moreover, a higher value of the entropy change (ΔS) in the nanobiocatalyst in comparison to that of its free form is a sign of more disorder at the nanobio interface, which is beneficial for the operational flexibility of enzymes in industrial bioprocessing. The obtained results validate multipoint attachments of α-amylase molecules with dopamine-functionalized MHNTs toward establishing a stable enzyme−support system that enhances the conformational flexibility of immobilized enzymes. The conclusion drawn here is well corroborated by a few recent reports.[49−51]

Kinetic parameters for free α-amylase and the nanobiocatalyst were investigated using a Michaelis−Menten plot (Figure S5c) and a Lineweaver−Burk plot by varying substrate concentrations (Figure S5d). After immobilization, a slight increase in K_M value was observed while the maximum reaction velocities (V_{max}) were estimated to be 67.11 and 64.93 μM min^{-1} for *d*-MHNTs/α-amylase and free α-amylase, respectively (Table S6). Conclusively, no noticeable effect on the enzyme's catalytic efficiency was observed after immobilization. Though "diffusional limitations" is the rationale behind such a minor variation in kinetic parameters, as immobilization inevitably restricts enzyme movement in comparison to its colloidal state, we still could manage to improve other aspects of enzymes that have been limiting their commercial use by promoting reuse, operational stability, and efficiency without altering the inherent kinetics.

Industrial Relevance of Nanobiocatalyst. *d*-MHNTs/α-amylase was evaluated for the continuous production of high-maltose-containing syrups that fermentation industries could use (Figure 5a). We determined that the nanobiocatalyst produced 276.8 mg (g reducing sugar)$^{-1}$ of extracted starch in 72 h of continuous operation without significantly compromising its biocatalytic activity.

Further, it is evident that the organic waste generated in kitchens, food processing plants, and restaurants is enriched with complex nutrients and the hydrolysis of such waste is critical in transforming agro/food waste into a growth medium for microorganisms. We investigated the dual functionality of the nanobiocatalyst to hydrolyze the biopolymeric content in potato peel waste to generate fermentable sugars and liberate soluble proteins/other micronutrients. For this, liquid broth suspensions prepared, i.e., PPW and PPW_{NBC} media, were evaluated for compositional analyses (Table S7). As expected, the amount of reducing/nonreducing sugars obtained after nanobiocatalytic treatment was 3-fold higher (1.328 g·100 mL^{-1}) in comparison to the PPW medium. The protein content was also enhanced from 21 to 123 mg 100 mL^{-1} in the hydrolysate, indicating that the biocatalytic treatment using immobilized α-amylase induced "starch depolymerization", which diminished the recalcitrant nature of potato peel waste, resulting in a greater release of soluble proteins. We envisaged this hydrolysate suspension as a consortium of energy sources along with the presence of other nutrients that can mimic the nutritive complex medium required for microbial/fermentation growth.

To confirm the accessibility of leached nutrients in hydrolysate to microorganisms, the growth characteristics of *E. coli* in PPW- and PPW_{NBC}-based media suspensions were compared to nutrient medium (NM, positive control) broth. The growth curves of the untreated PPW suspension manifested a prolonged lag phase in comparison to PPW_{NBC} and NM (Figure 5b), whereas *E. coli* grown on PPW_{NBC} and NM media showed similar growth kinetics up to the lag phase, which indicates that microbes find no differences while they perform their structural reorganization during adaptation. A noticeable difference was observed in the lag phase, where the specific growth rate (μ) was reduced in the case of untreated PPW (0.13 ± 0.018 h^{-1}) and PPW_{NBC} (0.24 ± 0.009 h^{-1}) in comparison to the NM broth (0.32 ± 0.016 h^{-1}). The overall growth follows the order NM > PPW_{NBC} > PPW. The nutrient broth, being a defined medium, would be best suited for microbial growth in comparison to other complex media sources. However, the inherent richness of PPW_{NBC} (carbon source reducing sugars, nitrogen source proteins, and micronutrients) made it equally capable of supporting fermentation growth in comparison to the untreated species. Thus, PPW_{NBC} can be a feasible alternative to the existing complex media formulations without supplementing any external nutrients. In a solid culture, the growth of *E. coli* exhibited a similar pattern,

https://doi.org/10.1021/acssuschemeng.2c01547
ACS Sustainable Chem. Eng. XXXX, XXX, XXX−XXX

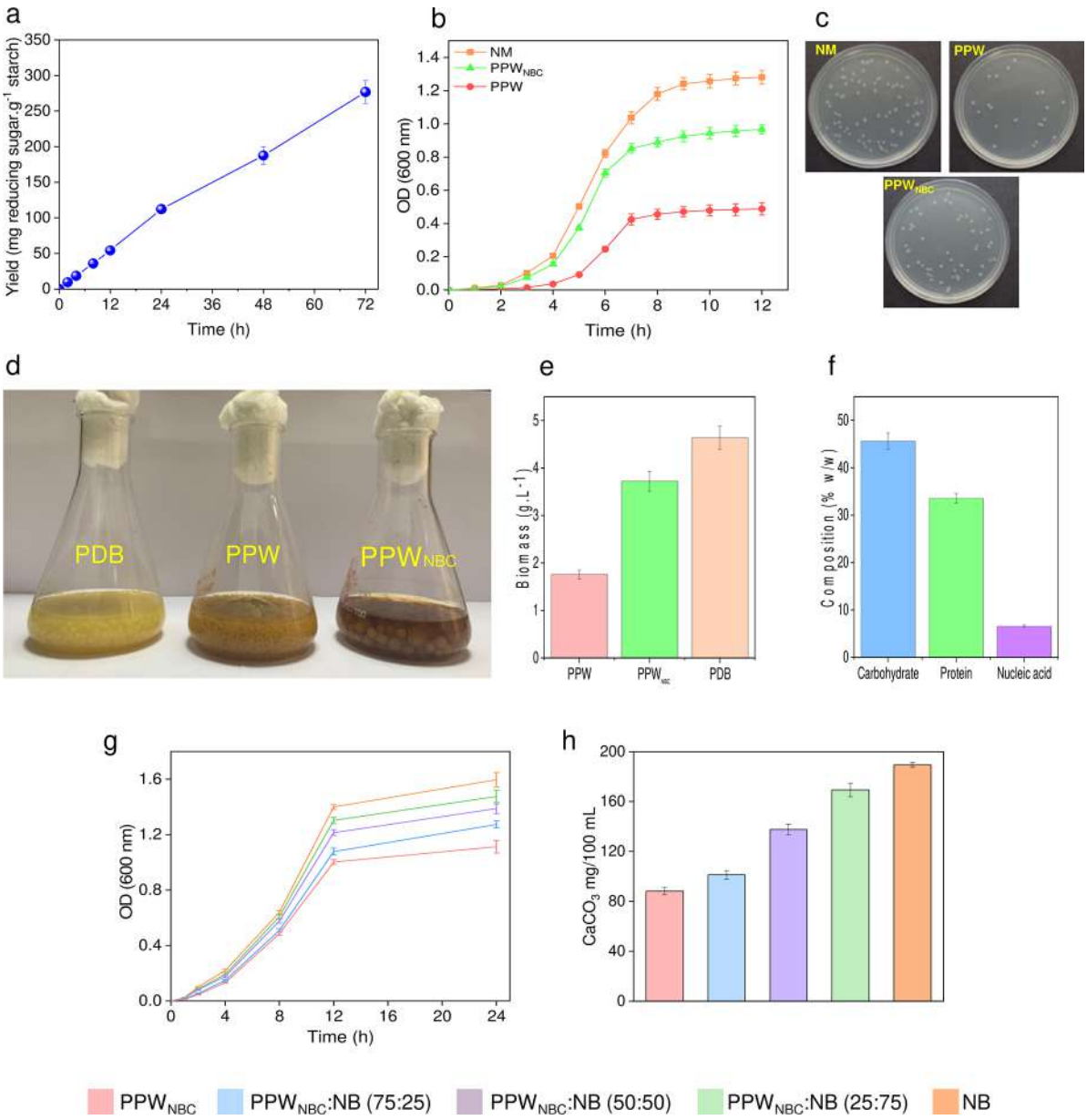

Figure 5. (a) Continuous starch hydrolysis efficiency of the developed nanobiocatalyst against starch extracted from potato peel waste. (b) Bacterial growth curve on all tested media formulations. (c) Photographic image representing the analogous bacterial colony characteristics of different media formulations. (d) Fungal biomass growth on different media. (e) Dry fungal biomass on different media. (f) Compositional analysis of an as-produced single-cell protein, indicating the potency of the as-formulated medium for single-cell protein production. (g) Growth of calcifying bacteria *Bacillus* sp. CT5 on different media. (h) Effect of different media compositions on calcium carbonate precipitation depicting the potential of PPW_{NBC} as a nutrient source for large-scale application. Experiments were performed in triplicate (technical), and of mean ± standard deviation values are presented.

where both NM and PPW_{NBC} were utilized well with no variation in the colony morphology. At the same time, PPW medium appeared to be least suited to the microorganisms (Figure 5c).

The formulated medium was also evaluated for the production of *A. niger* biomass. In comparison to potato dextrose broth (PDB, 100%), PPW and PPW_{NBC} media showed 37% and 80% biomass productions, respectively. A higher amount of nutrient availability in the treated hydrolysate (PPW_{NBC}) could result in better growth (Figure 5d). The quantitative estimation of the single-cell protein (SCP/dried biomass) revealed carbohydrates to be the primary components (45.7% wt/wt), followed by proteins (34.0% wt/wt) and nucleic acids (6.6% wt./wt..) (Figure 5e,f). The biomass with higher nucleic acid content could be used directly as a protein additive in animal feeding.[52] The overall characterization of the produced biomass confirms the acceptable performance of the formulated medium for SCP production.

Finally, we tested the potential industrial relevance of the nanobiocatalyst to enhance the strength and durability of construction materials through biocementation (microbially induced calcium precipitation). The waste hydrolysate (PPW_{NBC}) favored an excellent calcium carbonate precipitation capability of calcifying bacteria, *B. subtilis* CT-5, thus acting as a promising medium alternative. The results indicate

https://doi.org/10.1021/acssuschemeng.2c01547
ACS Sustainable Chem. Eng. XXXX, XXX, XXX−XXX

that, while the maximum growth was observed in nutrient broth, PPW_{NBC} also supported microbial growth (Figure 5g). On a similar note, calcium carbonate precipitation was highest in NB medium (189.4 ± 2.0 mg/100 mL) in comparison to blend formulations (Figure 5h). The $CaCO_3$ precipitations recorded in other media formulations such as PPW_{NBC}:NB (25:75), PPW_{NBC}:NB (50:50), and PPW_{NBC}:NB (75:25) were 169.3 ± 5.5, 137.7 ± 4.2, and 101.3 ± 3.5 mg, respectively. PPW_{NBC} alone had the lowest calcium carbonate precipitation, 88.2 ± 2.9 mg. The accessibility to preferred nitrogen sources has been linked to superior bacterial enzymatic activity.[53] The limited availability of nitrogen sources in PPW_{NBC} might have affected the ureolytic activity and lowered the amount of $CaCO_3$ precipitation. However, the addition of a nitrogen source might further improve the growth and $CaCO_3$ precipitation abilities of PPW_{NBC}. This indicates that the nanobiocatalyst-derived hydrolysate suspension can be used as a substitute for existing media formulations, which may decrease the operational cost of biocementation on a commercial scale.[35]

CONCLUSIONS

We report a viable strategic solution for valorizing potato peel waste as an ingredient of a fermentation medium using a nanobiocatalyst. A systematic material characterization revealed the improved hydrophilicity and aqueous dispersibility of the nanobiocatalyst, which displayed a homogeneous, superior loading of α-amylase along with beneficial catalytic activity under various process conditions. The immobilized α-amylase manifested an improved storage ability, thermal and kinetic activity, and magnet-driven recovery over 10 consecutive reuses, yet it retained >56% activity. Preserving its catalytic power even in the presence of inhibitory components, i.e., metal ions and cellulose, establishes either the "conformational resistance" or "shielding" effect of the enzyme−template system after immobilization. The nanobiocatalyst exhibited continuous starch hydrolysis for 72 h to produce reducing sugars. As a green and sustainable strategy, utilizing all soluble/partially soluble components of potato peel waste in bioprocess applications was also attempted. The waste hydrolysate, produced using the nanobiocatalyst, facilitated the growth of *E. coli*, *B. subtilis*, and *A. niger*. A blend formulation (50%:50% v/v) consisting of a hydrolysate and a commercial growth medium resulted in an ∼73% microbial-induced calcium carbonate precipitation, reducing the overall cost. In addition, the low cost of the backbone structure (HNTs) and simple functionalization procedures provide an opportunity for a viable translation of our technology to a commercial scale to valorize zero-value food waste. In the future, the successful implemenation of this strategy at a larger scale will open up new dimensions in transforming other food waste materials into biochemical products of commercial relevance.

ASSOCIATED CONTENT

Supporting Information

The Supporting Information is available free of charge at https://pubs.acs.org/doi/10.1021/acssuschemeng.2c01547.

Materials, starch extraction from potato peel waste, optimization of process parameters (experimental design and statistical analysis), thermodynamic parameters, microbial cultures and production of SCP, starch extraction and characterization, optimization of immobilization parameters, characterization of extracted starch, BSA standard curve, FE-SEM micrograph of bare halloysite nanotubes, immobilization optimization studies, thermodynamic and kinetic studies, Box−Behnken statistical experiment design, experiments and response, coefficients of the determination table of RSM, ANOVA table of RSM, compositional analysis of PPW and extracted starch, kinetic parameters of free and immobilized enzymes, and compositional analysis of different media formulations (PDF)

AUTHOR INFORMATION

Corresponding Author

Shekhar Agnihotri − *Department of Agriculture and Environmental Sciences and Centre for Advanced Translational Research in Food Nano-Biotechnology (CATR-FNB), National Institute of Food Technology Entrepreneurship and Management, Sonepat 131028 Haryana, India;* orcid.org/0000-0003-1156-9369; Phone: +91-1302281273; Email: agnish@niftem.ac.in

Authors

Devendra Sillu − *Department of Biotechnology, Thapar Institute of Engineering and Technology, Patiala 147004 Punjab, India*

M. Sudhakara Reddy − *Department of Biotechnology, Thapar Institute of Engineering and Technology, Patiala 147004 Punjab, India;* orcid.org/0000-0002-9743-4993

Complete contact information is available at: https://pubs.acs.org/10.1021/acssuschemeng.2c01547

Notes

The authors declare no competing financial interest.

ACKNOWLEDGMENTS

This work was financially supported by the Department of Science and Technology, India (DST-SERB), under project grant No. YSS/2015/001599 in Engineering Sciences. D.S. extends his thanks to the Council of Scientific and Industrial Research (CSIR), India, for SRF (09/677(0045)/2020-EMR-I).

REFERENCES

(1) Morone, P.; Koutinas, A.; Gathergood, N.; Arshadi, M.; Matharu, A. Food waste: challenges and opportunities for enhancing the emerging bio-economy. *J. Clean. Prod.* **2019**, *221*, 10−16.

(2) Gil, J. Going to waste. *Nat. Food.* **2020**, *1* (4), 192−192.

(3) Ebikade, E.; Athaley, A.; Fisher, B.; Yang, K.; Wu, C.; Ierapetritou, M. G.; Vlachos, D. G. The Future is Garbage: Repurposing of food waste to an integrated biorefinery. *ACS Sustain. Chem. Eng.* **2020**, *8*, 8124.

(4) Sillu, D.; Agnihotri, S. Cellulase immobilization onto magnetic halloysite nanotubes: enhanced enzyme activity and stability with high cellulose saccharification. *ACS Sustain. Chem. Eng.* **2020**, *8* (2), 900−913.

(5) Shrestha, S.; Khatiwada, J. R.; Sharma, H. K.; Qin, W. Bioconversion of Fruits and Vegetables Wastes into Value-Added Products. In *Sustainable Bioconversion of Waste to Value Added Products*; Springer: 2021; pp 145−163. DOI: DOI: 10.1007/978-3-030-61837-7_9.

(6) Sepelev, I.; Galoburda, R. Industrial potato peel waste application in food production: a review. *Res. Rural. Dev.* **2015**, *1*, 130−136.

(7) Jagatee, S.; Rout, J. R.; Behera, S.; Ram, S. S.; Sudarshan, M.; Pradhan, C.; Sahoo, S. L.; Mohanty, R. C. Effect of enzymatic hydrolysis on structural, chemical and elemental properties of sweet potato flour. *Waste Biomass Valori.* **2021**, *12* (2), 687−697.
(8) Xia, W.; Zhang, K.; Su, L.; Wu, J. Microbial starch debranching enzymes: Developments and applications. *Biotechnol. Adv.* **2021**, *50*, 107786.
(9) Homaei, A. A.; Sariri, R.; Vianello, F.; Stevanato, R. Enzyme immobilization: an update. *J. Chem. Biol.* **2013**, *6* (4), 185−205.
(10) Defaei, M.; Taheri-Kafrani, A.; Miroliaei, M.; Yaghmaei, P. Improvement of stability and reusability of α-amylase immobilized on naringin functionalized magnetic nanoparticles: A robust nano-biocatalyst. *Int. J. Biol. Macromol.* **2018**, *113*, 354−360.
(11) Torabizadeh, H.; Montazeri, E. Nano co-immobilization of α-amylase and maltogenic amylase by nanomagnetic combi-cross-linked enzyme aggregates method for maltose production from corn starch. *Carbohydr. Res.* **2020**, *488*, 107904.
(12) T.sriwong, K.; Matsuda, T. Recent Advances in Enzyme Immobilization Utilizing Nanotechnology for Biocatalysis. *Org. Process Res. Dev.* **2022**, *26*, 1857−1877.
(13) Bilal, M.; Qamar, S. A.; Ashraf, S. S.; Rodríguez-Couto, S.; Iqbal, H. M. Robust nanocarriers to engineer nanobiocatalysts for bioprocessing applications. *Adv. Colloid Interface Sci.* **2021**, *293*, 102438.
(14) Andler, S. M.; Goddard, J. M. Transforming food waste: how immobilized enzymes can valorize waste streams into revenue streams. *NPJ. Sci. Food* **2018**, *2* (1), 1−11.
(15) Fan, Y.; Wu, G.; Su, F.; Li, K.; Xu, L.; Han, X.; Yan, Y. Lipase oriented-immobilized on dendrimer-coated magnetic multi-walled carbon nanotubes toward catalyzing biodiesel production from waste vegetable oil. *Fuel* **2016**, *178*, 172−178.
(16) Mehrasbi, M. R.; Mohammadi, J.; Peyda, M.; Mohammadi, M. Covalent immobilization of Candida antarctica lipase on core-shell magnetic nanoparticles for production of biodiesel from waste cooking oil. *Renew. Energy* **2017**, *101*, 593−602.
(17) Nadar, S. S.; Patil, P. D.; Rohra, N. M. Magnetic nanobiocatalyst for extraction of bioactive ingredients: A novel approach. *Trends Food Sci. Technol.* **2020**, *103*, 225−238.
(18) Nadar, S. S.; Rathod, V. K. A co-immobilization of pectinase and cellulase onto magnetic nanoparticles for antioxidant extraction from waste fruit peels. *Biocatal. Agric. Biotechnol.* **2019**, *17*, 470−479.
(19) Ladole, M. R.; Nair, R. R.; Bhutada, Y. D.; Amritkar, V. D.; Pandit, A. B. Synergistic effect of ultrasonication and co-immobilized enzymes on tomato peels for lycopene extraction. *Ultrason. Sonochem.* **2018**, *48*, 453−462.
(20) Yuan, B.; Yang, X.-q.; Xue, L.-w.; Feng, Y.-n.; Jiang, J.-h. A novel recycling system for nano-magnetic molecular imprinting immobilised cellulases: Synergistic recovery of anthocyanin from fruit and vegetable waste. *Bioresour. Technol.* **2016**, *222*, 14−23.
(21) Glomm, W. R.; Wubshet, S. G.; Lindberg, D.; Dankel, K. R.; Afseth, N. K.; Stenstad, P. M.; Johnsen, H. Immobilized protease on magnetic particles for enzymatic protein hydrolysis of poultry by-products. *LWT* **2021**, *152*, 112327.
(22) Yazid, N. A.; Barrena, R.; Sánchez, A. The immobilisation of proteases produced by SSF onto functionalized magnetic nano-particles: application in the hydrolysis of different protein sources. *J. Mol. Catal. B Enzym.* **2016**, *133*, S230−S242.
(23) Puri, M.; Barrow, C. J.; Verma, M. L. Enzyme immobilization on nanomaterials for biofuel production. *Trends Biotechnol.* **2013**, *31* (4), 215−216.
(24) Reshmy, R.; Philip, E.; Sirohi, R.; Tarafdar, A.; Arun, K.; Madhavan, A.; Binod, P.; Awasthi, M. K.; Varjani, S.; Szakacs, G. Nanobiocatalysts: advancements and applications in enzyme technology. *Bioresour. Technol.* **2021**, *337*, 125491.
(25) Almulaiky, Y. Q.; Khalil, N.; El-Shishtawy, R. M.; Altalhi, T.; Algamal, Y.; Aldhahri, M.; Al-Harbi, S. A.; Allehyani, E. S.; Bilal, M.; Mohammed, M. M. Hydroxyapatite-decorated ZrO_2 for α-amylase immobilization: Toward the enhancement of enzyme stability and reusability. *Int. J. Biol. Macromol.* **2021**, *167*, 299−308.
(26) Atiroğlu, V.; Atiroğlu, A.; Özacar, M. Immobilization of α-amylase enzyme on a protein@ metal−organic framework nano-composite: A new strategy to develop the reusability and stability of the enzyme. *Food Chem.* **2021**, *349*, 129127.
(27) Desai, R. P.; Dave, D.; Suthar, S. A.; Shah, S.; Ruparelia, N.; Kikani, B. A. Immobilization of α-amylase on GO-magnetite nanoparticles for the production of high maltose containing syrup. *Int. J. Biol. Macromol.* **2021**, *169*, 228−238.
(28) Pandey, G.; Munguambe, D. M.; Tharmavaram, M.; Rawtani, D.; Agrawal, Y. Halloysite nanotubes-An efficient 'nano-support'for the immobilization of α-amylase. *Appl. Clay Sci.* **2017**, *136*, 184−191.
(29) Kadam, A. A.; Jang, J.; Lee, D. S. Supermagnetically tuned halloysite nanotubes functionalized with aminosilane for covalent laccase immobilization. *ACS Appl. Mater. Interfaces* **2017**, *9* (18), 15492−15501.
(30) Chao, C.; Liu, J.; Wang, J.; Zhang, Y.; Zhang, B.; Zhang, Y.; Xiang, X.; Chen, R. Surface modification of halloysite nanotubes with dopamine for enzyme immobilization. *ACS Appl. Mater. Interfaces* **2013**, *5* (21), 10559−10564.
(31) Zhang, D.; Deng, M.; Cao, H.; Zhang, S.; Zhao, H. Laccase immobilized on magnetic nanoparticles by dopamine polymerization for 4-chlorophenol removal. *Green Energy Environ.* **2017**, *2* (4), 393−400.
(32) Dhami, N. K.; Reddy, M. S.; Mukherjee, A. Application of calcifying bacteria for remediation of stones and cultural heritages. *Front. Microbiol.* **2014**, *5*, 304.
(33) Achal, V.; Mukherjee, A.; Reddy, M. S. Effect of calcifying bacteria on permeation properties of concrete structures. *J. Ind. Microbiol. Biotechnol.* **2011**, *38* (9), 1229−1234.
(34) Bradford, M. M. A rapid and sensitive method for the quantitation of microgram quantities of protein utilizing the principle of protein-dye binding. *Anal. Biochem.* **1976**, *72* (1−2), 248−254.
(35) Achal, V.; Mukherjee, A.; Reddy, M. S. Microbial concrete: way to enhance the durability of building structures. *J. Mater. Civ. Eng.* **2011**, *23* (6), 730−734.
(36) Federation, W. E.; Association, A. *Standard methods for the examination of water and wastewater*; American Public Health Association (APHA): 2005; Vol. *21*.
(37) Tully, J.; Yendluri, R.; Lvov, Y. Halloysite clay nanotubes for enzyme immobilization. *Biomacromolecules* **2016**, *17* (2), 615−621.
(38) Ariaeenejad, S.; Motamedi, E.; Salekdeh, G. H. Immobilization of enzyme cocktails on dopamine functionalized magnetic cellulose nanocrystals to enhance sugar bioconversion: A biomass reusing loop. *Carbohydr. Polym.* **2021**, *256*, 117511.
(39) Chao, C.; Zhang, B.; Zhai, R.; Xiang, X.; Liu, J.; Chen, R. Natural nanotube-based biomimetic porous microspheres for significantly enhanced biomolecule immobilization. *ACS Sustain. Chem. Eng.* **2014**, *2* (3), 396−403.
(40) An, J.; Li, G.; Zhang, Y.; Zhang, T.; Liu, X.; Gao, F.; Peng, M.; He, Y.; Fan, H. Recent advances in enzyme-nanostructure biocatalysts with enhanced activity. *Catalysts* **2020**, *10* (3), 338.
(41) Klapiszewski, Ł.; Zdarta, J.; Jesionowski, T. Titania/lignin hybrid materials as a novel support for α-amylase immobilization: A comprehensive study. *Colloids Surf., B* **2018**, *162*, 90−97.
(42) Coutinho, T. C.; Rojas, M. J.; Tardioli, P. W.; Paris, E. C.; Farinas, C. S. Nanoimmobilization of β-glucosidase onto hydroxyapatite. *Int. J. Biol. Macromol.* **2018**, *119*, 1042−1051.
(43) Melo, R. R. d.; Alnoch, R. C.; Vilela, A. F. L.; Souza, E. M. d.; Krieger, N.; Ruller, R.; Sato, H. H.; Mateo, C. New heterofunctional supports based on glutaraldehyde-activation: A tool for enzyme immobilization at neutral pH. *Molecules* **2017**, *22* (7), 1088.
(44) Antony, N.; Balachandran, S.; Mohanan, P. Immobilization of diastase α-amylase on nano zinc oxide. *Food Chem.* **2016**, *211*, 624−630.
(45) Patel, H.; Royall, P. G.; Gaisford, S.; Williams, G. R.; Edwards, C. H.; Warren, F. J.; Flanagan, B. M.; Ellis, P. R.; Butterworth, P. J. Structural and enzyme kinetic studies of retrograded starch: Inhibition of α-amylase and consequences for intestinal digestion of starch. *Carbohydr. Polym.* **2017**, *164*, 154−161.

https://doi.org/10.1021/acssuschemeng.2c01547
ACS Sustainable Chem. Eng. XXXX, XXX, XXX−XXX

(46) Han, Y.; Wu, X.; Zhang, X.; Zhou, Z.; Lu, C. Dual functional biocomposites based on polydopamine modified cellulose nanocrystal for Fe^{3+}-pollutant detecting and autoblocking. *ACS Sustain. Chem. Eng.* **2016**, *4* (10), 5667−5673.
(47) Okwuenu, P.; Agbo, K.; Ezugwu, A.; Eze, S.; Chilaka, F. Effect of divalent metal ions on glucoamylase activity of glucoamylase isolated from *Aspergillus niger*. *Ferment. Technol.* **2017**, *6* (141), 2.
(48) Pascoal, A. M.; Mitidieri, S.; Fernandes, K. F. Immobilisation of α-amylase from *Aspergillus niger* onto polyaniline. *Food Bioprod. Process.* **2011**, *89* (4), 300−306.
(49) Rodrigues, R. C.; Berenguer-Murcia, Á.; Carballares, D.; Morellon-Sterling, R.; Fernandez-Lafuente, R. Stabilization of enzymes via immobilization: Multipoint covalent attachment and other stabilization strategies. *Biotechnol. Adv.* **2021**, *52*, 107821.
(50) Ahmed, I. N.; Chang, R.; Tsai, W.-B. Poly (acrylic acid) nanogel as a substrate for cellulase immobilization for hydrolysis of cellulose. *Colloids Surf., B* **2017**, *152*, 339−343.
(51) Morellon-Sterling, R.; Carballares, D.; Arana-Peña, S.; Siar, E.-H.; Braham, S. A.; Fernandez-Lafuente, R. Advantages of Supports Activated with Divinyl Sulfone in Enzyme Coimmobilization: Possibility of Multipoint Covalent Immobilization of the Most Stable Enzyme and Immobilization via Ion Exchange of the Least Stable Enzyme. *ACS Sustain. Chem. Eng.* **2021**, *9* (22), 7508−7518.
(52) Anupama; Ravindra, P. Value-added food:: Single cell protein. *Biotechnol. Adv.* **2000**, *18* (6), 459−479.
(53) Hammami, A.; Bayoudh, A.; Abdelhedi, O.; Nasri, M. Low-cost culture medium for the production of proteases by *Bacillus mojavensis* SA and their potential use for the preparation of antioxidant protein hydrolysate from meat sausage by-products. *Ann. Microbiol.* **2018**, *68* (8), 473−484.

https://doi.org/10.1021/acssuschemeng.2c01547
ACS Sustainable Chem. Eng. XXXX, XXX, XXX−XXX